Performance Improvement for Robotic Mechanisms by: Synthesis Design, Dynamic Balancing and Adaptive Control Techniques

By

Bin Wei

A Thesis Submitted in Partial Fulfillment
of the Requirements for the Degree of

DOCTOR OF PHILOSOPHY (PhD) in Mechanical Engineering

in

The Faculty of Engineering and Applied Science

Program

University of Ontario Institute of Technology

May 2016

ABSTRACT

Robotics have been used in many arenas, such as manufacturing, medical, and space. Currently, the use of robotics is limited with respect to performance capabilities. Improving the performance of robotic mechanisms is a main research area. In this thesis, performance improvement is achieved through the approaches of robotic mechanism synthesis design, dynamic balance, and adaptive control.

A novel three degrees of freedom hybrid manipulator is designed. After discussing the advantages of this new type of hybrid manipulator, the kinematic and Jacobian matrix of this manipulator are analyzed. The kinematic performances, which include stiffness/compliance and workspace, are then analyzed and optimized, and the multi-objective optimization on the compliance and workspace is subsequently conducted. The dynamics of the proposed manipulator are analyzed based on the Lagrangian method.

When robotic mechanisms move, because the center of mass is not fixed and angular momentum is not constant, vibration is produced in the system. Dynamic balance is normally achieved by using counterweight(s), counter-rotation(s) or damping methods. However, the problem is that the whole system will become heavier and have more inertia. It is here proposed that dynamic balancing can be achieved through reconfiguration, rather than using counter-devices, so that the system will not gain any unwanted weight. After designing a balanced single leg, the legs will be combined to synthesize parallel mechanisms, i.e. first dynamically balance a single leg by the

reconfiguration method (decomposition) and then combine the balanced legs to synthesize the whole parallel mechanism (integration).

As the mechanism is reconfigured, the control system has to be reconfigured accordingly. One way to address the control system reconfiguration is by breaking up the control functions into small functional modules, and from those modules assembling the control system. A hybrid controller for serial robotic manipulators is synthesized by combining a proportional–integral–derivative controller and a model reference adaptive controller in order to further improve the accuracy and joint convergence speed performance. The results show that the convergence speed for the hybrid controller is faster than that of the MRAC controller. The hybrid and MRAC controllers are both better than that of the PID controller. Experimental system is developed to model and verify the correctness of a reconfigured control system.

ACKNOWLEDGEMENT

I would like to thank my supervisor, Professor Dan Zhang, for bringing me to his Canada Research Chair Laboratory of Robotics and Automation (RAL) at the University of Ontario Institute of Technology, and for his invaluable supervision and full support. I learned a great deal through my PhD study under his guidance. His professional experience and motivation in research have greatly influenced me in becoming a research scientist. I would also like to mention the financial support from Professor Zhang under the Natural Sciences and Engineering Research Council of Canada (NSERC) and the Canada Research Chairs program.

Secondly, I would like to thank the examining committee members, Dr. Ibrahim Dincer, Dr. Haoxiang Lang, Dr. Moustafa El-Gindy, and external examiner Dr. Marwan Hassan of the University of Guelph for their input and examination of my thesis. I would also like to thank all my other teachers at this university.

I am deeply indebted to my mother who loves me and has always supported me during my PhD studies in Canada.

TABLE OF CONTENTS

List of Figures

List of Tables

Nomenclature

F_D	Dimension of the characteristics for the end-effector
N	The number of limbs
n	The number of actuated limbs
q_i	The number of actuators of the i^{th} actuated limb
p	The number of passive limbs
$(\,)_o$	The joints axes in the bracket intersect at point o
R_e	Rotation matrix of the moving platform with respect to the base
l_i	Length of the U* link
θ_x	Rotation angle of moving platform with respect to X axis
θ_y	Rotation angle of moving platform with respect to Y axis
θ_z	Rotation angle of moving platform with respect to Z axis
u_i	Actuated input
t	The twist of the moving platform
Q_i	Rotation matrix from the i^{th} frame to the $(i+1)^{th}$ frame
J_{serial}	Jacobian matrix of the central passive leg
$J_{parallel}$	Jacobian matrix of the parallel component
J	Jacobian matrix of the whole mechanism

τ	Vector of actuator forces
w	Force or torque applied to the moving platform
C	Actuator compliance matrix
$\Delta\rho$	Joint displacement
Δc	Vector of small Cartesian displacement and rotation
C_c	Cartesian compliance matrix
R_P	Radius of the moving platform
R_b	Radius of the base
η	Global condition index
n_{total}	The total number of previously selected points
F_j	External applied force
λ_i	Lagrangian multiplier
Δ_i	The i^{th} constraint function
Q_j	Actuator force
K	Total kinetic energy
K_p	Kinetic energy of the moving platform
K_{bi}	Kinetic energy of the U* link of limb i
K_a	Kinetic energy of the middle passive limb
U	Total potential energy
U_p	Potential energy of the moving platform
U_{bi}	Potential energy of the U* link of the i^{th} limb
U_a	Potential energy of the middle passive leg

L	Lagrangian function
m_p	Mass of the moving platform
m_b	Mass of the U* link
m_a	Mass of the middle passive limb
f_i	Actuator forces
r_i	Distance between the center of mass and the end of link i
m_i	Mass of link i
m_{cw1}	Mass of counterweight 1
m_{cw2}	Mass of counterweight 2
S_i	The center of mass of link i
I_i	Axial moment of inertia of link i
I_{cr}	Axial moment of inertia of the counter-rotation
M	Inertia matrix
N	Nonlinear term
rp	Desired input
xp	The output of the plant
Kp	Proportional gain
Ki	Integral gain
Kd	Derivative gain
erp	Position error between reference model and manipulator
erv	Velocity error between reference model and manipulator
e	Error vector between desired input and output of the plant

$\hat{M}$	Estimated values of M
l_i	Length of link i
a_i	Acceleration of joint i
k_m	Adaptation gain
$w(t)$	Output of feedback nonlinear block
$y(t)$	Input of feedback nonlinear block
$u(t)$	New external control input

List of Abbreviations

DOF	Degrees of freedom
Pa	Parallelogram
Pa^2	Double parallelogram
U*	Pure-translational universal joint
R	Revolute joint
P	Prismatic joint
S	Spherical joint
U	Universal joint
ADBU	Active dynamic balancing unit
CoM	Center of mass
CRCM	Counter-rotary counter-mass
ELMS	Equivalent linear momentum system
SCR	Separate counter-rotation
DM	Duplicate mechanism
CM	Counter-mass
CR	Counter-rotation
ACRCM	Actively driven counter-rotary counter-mass
ADBM	Active dynamic balancing mechanism
PID	Proportional-integral-derivative

MRAC	Model reference adaptive control
ECAL	Exact compensation adaptive control law
DCAL	Desired compensation adaptive control law
GF	General function
EE	End-effector
DE	Differential evolution
GA	Genetic algorithm
KCI	Kinematics condition index
PSO	Particle swarm optimization

1

Introduction

1.1. Research Overview and Motivation

Robotic mechanisms have become one of the most important components for driving the advanced manufacturing and automation industries. At present, the use of manufacturing robots is limited with respect to performance capabilities. As such, it is necessary to further investigate new robotic mechanisms and new approaches that can be applied to robotics in order to improve the performance of the overall robotic system. Performance improvement can be achieved in different ways, such as the robotic mechanism structure redesign/synthesis, dynamic characteristic enhancement and control approaches.

The purpose of robotic mechanism structure redesign/synthesis is to propose certain mechanisms that have better kinematic and dynamic performance as compared to the old models. New robotic mechanism design for the purpose of further improving overall performance is still a demanding task. For example, one can add limbs and new joints to the mechanism to improve the stiffness and general accuracy of robotic mechanisms.

When mechanisms and parallel manipulators are in motion, vibration is usually produced in the system due to the fact that the center of mass (CoM) of the system is not fixed and also the angular momentum is not constant. Vibration can substantially affects the accuracy. How to reduce these vibrations has become a common goal. One way to

address this problem is to apply the dynamic balancing approach. Dynamic balance is often achieved by using counterweights and counter-rotations. However, the downside of using those counter-devices is that the whole system will become heavier and have more inertia, which will require more energy to drive the system, which is not cost-effective. Here, dynamic balancing through the reconfiguration concept is proposed. Since the mechanism and its controller make a complete system, with the mechanical reconfiguration, the control laws governing the operation of the mechanism also need to be changed.

Controlling the robot to perform in a certain way is one of the most challenging problems because the robotic manipulator mechanism is highly nonlinear. For the robotic manipulators, the coefficients of the dynamic equations are functions of joint variables and also the function of payload mass, which may be unknown or change throughout the task. When the manipulator moves, the joint variables change, which will cause the robotic manipulator's dynamic equation to change throughout a given task. In order to obtain a high degree of accuracy and repeatability in the manipulator performance, it is necessary to use a control system that will account for the changes in the dynamic characteristics of the manipulator. Although conventional control methods model the manipulator as uncoupled linear subsystems, and these methods can produce satisfactory performance at low speeds, they are no longer efficient when used for high speed and high accuracy operations. In order to address the above problem, adaptive control can be applied.

1.2. Problem Definition

a. Synthesis Design

There are many other kinds of parallel manipulators which have been designed and developed during the past decades, the purpose for which all of them is further improving performance [1-10], e.g. stiffness, workspace, positioning accuracy, acceleration, and dynamic characteristics. In Figure 1.1, a three degrees of freedom (DOF) tripod manipulator was proposed by Zhang [11], and a passive link was added to the system in order to increase the stiffness of the mechanism and eliminate unexpected motion. The Tricept manipulator, as shown in Figure 1.2, has high flexibility and accuracy at its end-effector. In Figure 1.3, a Tau hybrid manipulator [12] was proposed, the advantage of which is that it combines the advantages of a serial manipulator and parallel manipulator, which increases its end-effector workspace while its stiffness remains high.

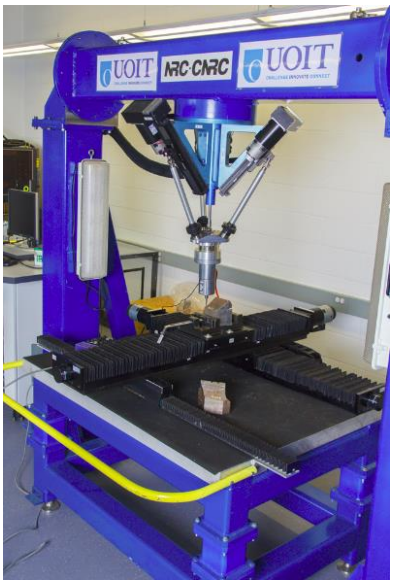

Figure 1.1. 3-DOF high stiffness parallel manipulator (Robotics and Automation Lab at UOIT)

Figure 1.2. Tricept manipulator [13]

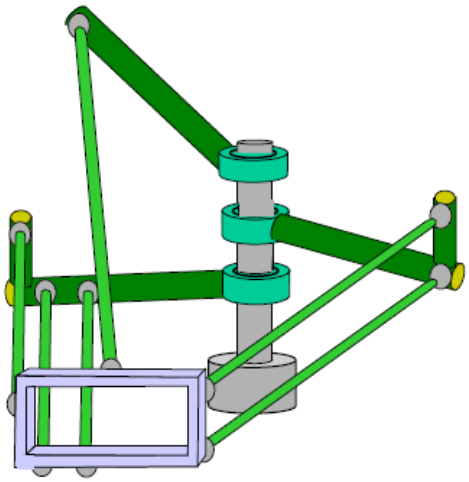

Figure 1.3. Tau hybrid manipulator [12]

b. Dynamic Balancing

In order to reduce or ideally eliminate the vibration of the system when parallel manipulators are in operation, the dynamic balance method can be implemented to achieve the goal. The purpose of dynamic balancing is to make constant the CoM and angular momentum of the system. Normally, dynamic balance is achieved by using counterweights, counter-rotations or damping methods [14-20]. However, the problem with these is that the whole system will become heavier and have more inertia.

Here, in order to achieve the goal, it is proposed to achieve dynamic balance without using counterweights or damping, but through reconfiguration of the system, which can reduce the addition of mass and inertia. When a link rotates around a pivot, because the CoM of the link is not still, the link will have a shaking force, which makes it vibrate. When a counterweight is added to the extended part of that link, the CoM of the whole link is fixed to that revolute joint, then balanced, thus the vibration is eliminated. The purpose of using a counterweight is to move the CoM to the still point. The question is whether it

is possible to achieve the same goal without using a counterweight. This is in fact possible so, for example, a screw link can be used and moved to the point where the CoM moves to the still point, and then balanced. In this method, a counterweight is not used but, through reconfiguring the system by moving the screw link, the system will not become heavy. Based on this idea, a single leg is first dynamically balanced by the reconfiguration method (decomposition) and then the balanced legs are combined to synthesize the whole parallel mechanism (integration); i.e. the decomposition and integration concept.

c. Adaptive Control

The robotic manipulator control problem is generally formulated as follows: given a desired trajectory and a mathematical model of the manipulator, one needs to find the control algorithm which sends torques to the actuators, so that the robotic manipulator achieves the expected motion. The control design for a serial robotic manipulator involves two steps. Firstly, an end-effector motion trajectory is given; i.e. the end-effector is expected to move from point A to point B. From this end-effector motion trajectory, and by using inverse kinematics, the joint motion can be determined so as to produce this desired end-effector motion trajectory. The second step is to determine the joint torque and how much torque one has to apply to the joint so that the joint will have the desired motion. The joint torque can be determined by solving the inverse dynamic equation.

Adaptive control adapts to a controlled system with parameters which vary, or are initially uncertain. For a non-adaptive controller, the controller is designed based on a priori information of the system; i.e. one knows the system and designs the controller

(e.g. PID controller) gears to that system and assumes there is no change in the system. For the adaptive controller, the controller does not necessarily need to depend on the previous information of the system, and if there is a sudden change in the environment, the controller can cope with it to adapt to the changed conditions. If one considers a system where its transfer function is known, one designs a fixed classical controller, which will remain fixed parameter as long as it applies to the system, so one can say that this controller depends on its structure and is designed on a priori information. This is a non-adaptive controller. However, the controller is called adaptive if it depends on posteriori information; for example, if one is changing the parameters of the controller, because of the changes of the parameters of the system or because of the disturbances coming from the environment. If the system is subject to unknown disturbances, or is expected to undergo changes in its parameters in a way which is not pre-determined from the beginning, one uses adaptive control. However, in some cases one knows how the system's operating condition will change. For example, for an aircraft, one knows that the aircraft controller is determined by its altitude and speed, and one expects it to fly at specific value for altitude and speed. In such a case one can design a controller for each expected operating point and switch between the different controllers. This is called gain-scheduling. In other cases, one knows that the parameters of the system change, but one also knows a range for the change of every parameter. In this case, it is possible to design a fixed controller that can cope with different changes of the parameters, and guarantee the stability and performance. This kind of controller is a robust controller.

For non-adaptive control (e.g. fixed-gain control), when one needs to improve performance error, the modelling accuracy will be increased, as illustrated in Figure 1.4. Furthermore, it is assumed that future conditions will be much like present. The controller ignores the environment changes, changes in dynamics and also the structural damage to the system.

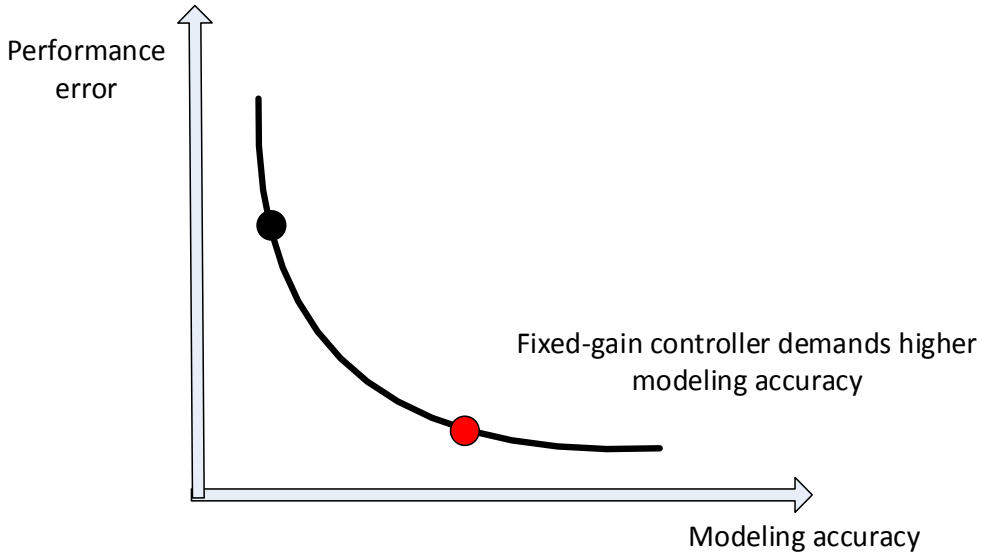

Figure 1.4. Non-adaptive control

Adaptive control obtains a designated system performance asymptotically. It does not trade performance for modelling accuracy, as shown in Figure 1.5, and more importantly, it improves itself under unforeseen and adverse conditions.

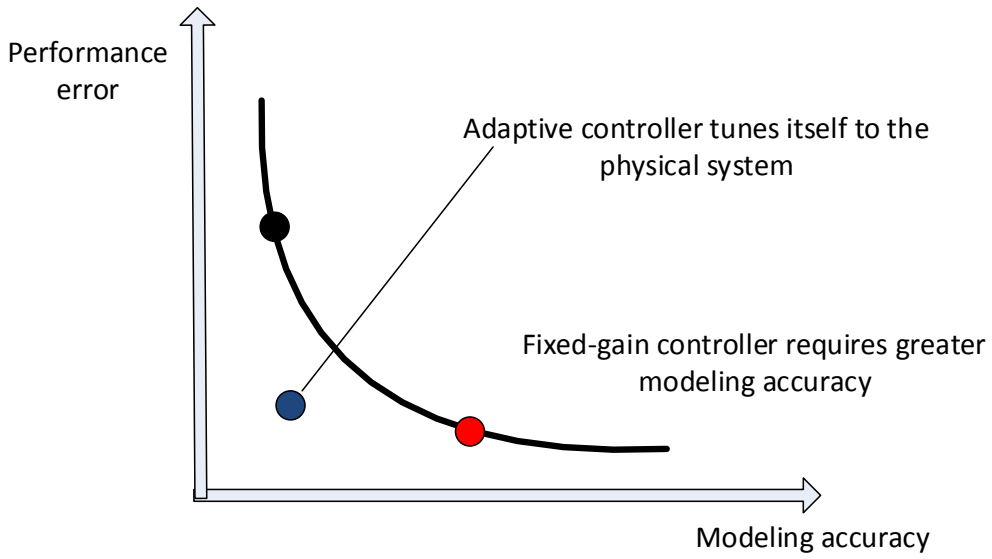

Figure 1.5. Adaptive control

Compared to other control methods, adaptive control can achieve good performance under a wide range of payloads and motions. The advantage of the model reference adaptive control (MRAC) is that the plant parameters need not be fully known. Instead, estimates of the plant parameters are used and the adaptive controller utilizes past input/output information to improve these estimates. However, there are two main issues for designing MRAC. Firstly, stability analysis of the system is critical as it is not easy to design a stable adaptive law. Secondly, MRAC relies on cancellation of the non-linear terms by the reference model [21]. In reality, exact cancellation cannot be expected, but the non-linear terms may be made so small as to be negligible. The model reference adaptive control method was initially introduced in [22], when the authors considered adaptive aircraft flight control systems, using a reference model to obtain error signals between the actual and desired behavior. These error signals were used to modify the controller parameters to attain ideal behavior in spite of uncertainties and varying system

dynamics. The goal of an adaptive control system is to achieve and maintain an acceptable level in the performance of the control system in the presence of plant parameter variations, whereas a conventional feedback control system is mainly dedicated to the elimination of the effect of disturbances upon the controlled variables, also known as manipulated variables. An adaptive control system is mainly dedicated to the elimination of the effect of parameter disturbances/variations upon the performance of the control system.

1.3. Overall Aims and Objectives

A new type of 3-DOF hybrid manipulator is proposed and analyzed. The novelty of this new hybrid mechanism is that by changing the original passive leg to prismatic-universal (PU) type, the manipulator therefore can have the desired three degrees of freedom, and by applying U* joints as three limbs instead of the conventional limbs, the stiffness of this hybrid/parallel manipulator can be greatly improved. The kinematics, Jacobian modelling, stiffness/compliance and workspace performances, multi-objective optimization and dynamics of the hybrid manipulator are analyzed.

Here it is proposed to achieve dynamic balance not by using counterweights or damping, but through designing naturally dynamic balanced mechanisms to achieve the goal. This can be done, for example, by the reconfiguration method that will be proposed. After designing a dynamic balanced single leg, legs will be combined to synthesize parallel mechanisms. This research is important for manufacturing and space areas.

With mechanical reconfiguration, the control laws governing the operation of the mechanism also need to be changed. One way to address control system reconfiguration is by applying “divide and conquer” methodology. A hybrid controller for serial robotic manipulators is synthesized by combining a proportional–integral–derivative controller (PID) and a model reference adaptive controller. The convergence performance of the PID, MRAC, and PID+MRAC hybrid controllers are compared for 1-DOF, 2-DOF and 3-DOF manipulators.

The major contributions of this study are summarized as follows: (1) a new type of 3-DOF high stiffness hybrid manipulator is proposed; (2) dynamic balancing through the reconfiguration concept is proposed, and a spatial dynamic balanced grasper mechanism is designed; (3) a hybrid controller for multi degrees of freedom serial robotic manipulators is synthesized by combining a PID controller and a model reference adaptive controller in order to further improve the accuracy and joint convergence speed performance.

1.4. Structure of the Thesis

Chapter 2 provides a literature review of some of the state of the art regimes in synthesis design, dynamic balancing and adaptive control for robotic mechanisms.

Chapter 3 designs a novel three degrees of freedom hybrid robotic manipulator. After discussing the advantages of this new type of hybrid manipulator, the kinematic and Jacobian matrix of this manipulator are analyzed. The kinematic performances, which include stiffness/compliance and workspace, are studied and optimized. The multi-

objective optimization on the compliance and workspace is conducted, and the dynamics of the manipulator are finally analyzed.

Chapter 4 proposes the concept of dynamic balance through reconfiguration for robotic mechanisms, which can reduce the addition of overall mass and inertia. In this method, reconfiguration of the system is used rather than a counter-device. After designing a dynamic balanced single leg, legs will be combined to synthesize parallel mechanisms, and a spatial dynamic balanced grasper mechanism is designed and studied based on the pantograph and principal vector linkage.

Chapter 5 describes the design for a hybrid controller for multi degrees of freedom serial robotic manipulators by combining a PID controller and a model reference adaptive controller in order to further improve the accuracy and joint convergence speed performance. The convergence performance of the PID controller, the model reference adaptive controller and the PID+MRAC hybrid controller for 1-DOF, 2-DOF and, subsequently 3-DOF manipulators, is compared.

Chapter 6 presents the most important conclusions and observations of the study and suggests the work to be conducted in the future.

2

Literature Review and Analysis

2.1. Robotic Mechanisms

A parallel manipulator, also sometimes called parallel mechanism or parallel robot, is a type of robot which consists of a moving platform, a base and two or more limbs. The whole system forms a closed loop. This type of manipulator was first used in flight simulators, as shown in Figure 2.1. These robots have been developed in numerous ways and are widely used in many different areas, such as conducting manufacturing machining [23-31], picking and placing [32-34], vehicle simulation devices [35], laser cutting [36], medical devices [37-45], space applications [46-48], entertainment equipment [49, 50], underground assembly robots [51-53], sensor applications [54-56] and micro-instruments [57-60], due to their performance characteristics. The most well-known parallel manipulator is the Steward platform, as shown in Figure 2.2. The moving platform is connected to the base by six actuated legs, and the manipulator has six degrees of freedom, i.e. three translational motions along the x, y and z axes, and three rotational motions about the x, y and z axes. The counterpart of parallel manipulators is serial manipulators, as shown in Figures 2.3 and 2.4. The advantages of parallel manipulators compared to serial manipulators are that parallel manipulators possess high levels of

stiffness, rigidity, accuracy, speed and acceleration, and no cumulative joint/link error, due to the parallel structure arrangement.

Figure 2.1. Parallel mechanism used in flight simulator [61]

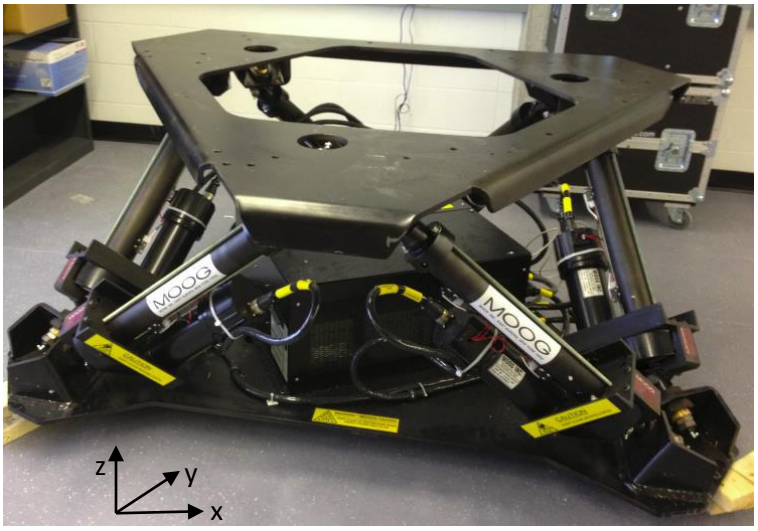

Figure 2.2. Steward platform (Robotics and Automation Lab at UOIT)

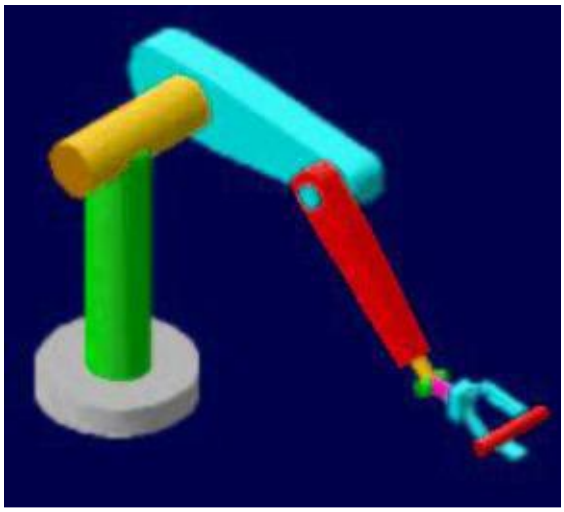

Figure 2.3. Serial manipulator [12]

Figure 2.4. CANADARM - Serial Manipulator Application (Courtesy of NASA) [62]

2.2. Synthesis Design

Nowadays, if one wants to design a new type of parallel manipulator, one cannot just adhere to the conventional joints, i.e. prismatic, revolute, universal and spherical. One can use, for example, a parallelogram (Pa joint), pure-translational universal joint (U*

joint), which can also be seen as a special parallelogram, or the double parallelogram (Pa^2 joint) as a leg or part of a structure instead of a conventional fixed length leg or actuated leg, because the parallelogram structure has a higher levels of stiffness compared to conventional legs. Obviously, a parallelogram has two links acting in parallel, which can distribute the loads, so the stiffness can be improved for the parallelogram structure-based parallel robotics. Furthermore, by using a parallelogram, the tilting angle or rotation capacity can also be improved [63].

Some 4-DOF Schonflies / SCARA motion (three translational DOF and one rotational DOF) parallel manipulators have been proposed by resorting to the parallelograms. In [64], the theory of groups of displacements is used to develop some new architecture of 4-DOF (3T1R) fully-parallel manipulators by resorting to the parallelograms. Each parallelogram based structure is treated as a "motion generator" and, by combining different motion generators, new types of parallel manipulators can be generated. A parallelogram is actually a one degree of freedom parallel structure. If two parallelograms are combined into one, the new structure is called double parallelogram (Pa^2). These parallelograms can also be known as "motion generators" [64]. A parallelogram can generate one translational degree of freedom and Pa^2 can generate two translational degrees of freedom, which is why they are known as motion generators. The following kinematic chains are some examples of parallelogram based structure. Figure 2.5 is a four degrees of freedom motion generator RPa^2R kinematic chain, Figure 2.6 is a four degrees of freedom motion generator PPa^2R kinematic chain, and Figure 2.7 is a five degrees of freedom motion generator PRPaRR kinematic chain. Note that if one removes the last

revolute joint in Figure 2.7, the structure becomes a four degrees of freedom motion generator.

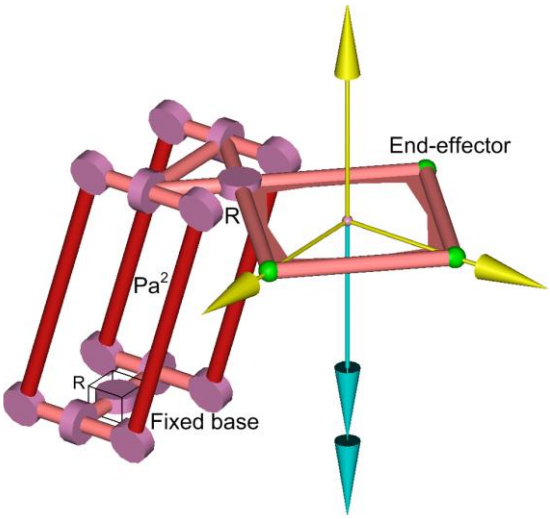

Figure 2.5. RPa^{2}R kinematic chain [65]

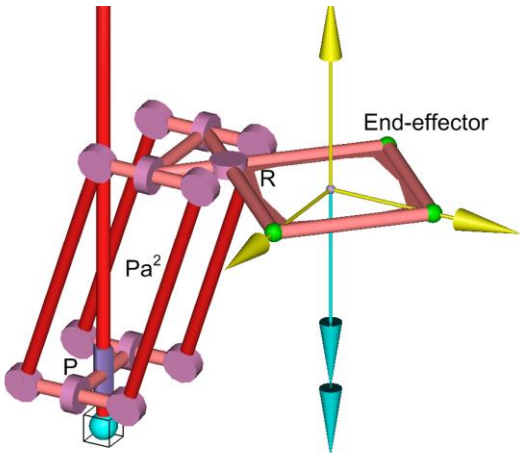

Figure 2.6. PPa^{2}R kinematic chain [65]

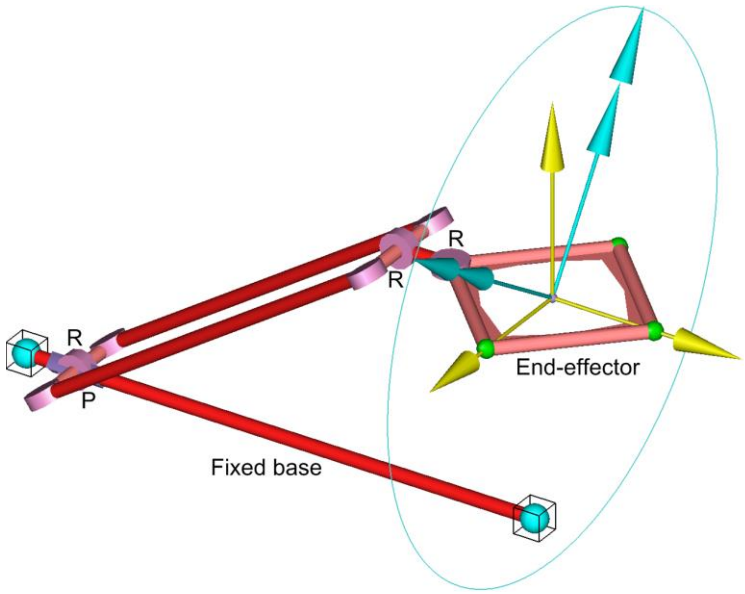

Figure 2.7. PRPaRR kinematic chain [65]

Similarly, in [66], two identical kinematic chains that serve as a Schonflies-Motion Generator is proposed as a kinematic chain for the parallel manipulator. This Schonflies-Motion Generator kinematic chain has four degrees of freedom, and each kinematic chain consists of two parts: one is a proximal module, which is active; the other is a distal module, which is a passive parallelogram, as shown in Figure 2.8. The distal module follows the motions of the proximal module. This parallel manipulator has four degrees of freedom, i.e. three independent translational motions and one rotational motion about an axis of fixed direction, similar to the serial robots SCARA, which is why they are referred to as Schonflies/SCARA-Motion based parallel manipulators.

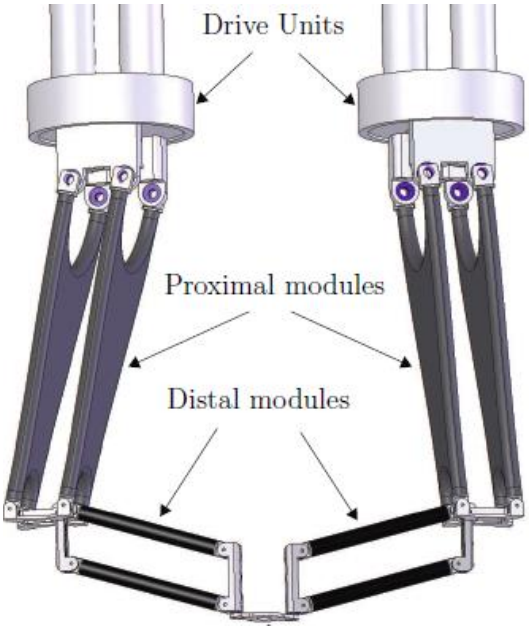

Figure 2.8. Schonflies-Motion based parallel manipulator [66]

Pure-translational universal joint (U* joint) is a type of parallelogram family, with two translational degrees of freedom. It can be seen that U* joint consists of two main parts:

one is two plates; the other is three links which connect the two plates through universal joints. The structure of U* joint is shown in Figure 2.9. This structure can also be seen as a parallel structure. There are two purposes in using a U* joint, one of which is to increase the degrees of stiffness of parallel manipulator. From Figure 2.9, it is obvious that loads on plate 5 can be distributed by three links 2, 3 and 4. Therefore, by using a U* joint, the stiffness of the parallel manipulator is higher than that when using a normal leg. The second purpose is to increase the tilting angle or rotation capacity of the end-effector, because the performance of the U* joint resembles a parallelogram, and the parallelogram can increase the rotation capacity of the parallel manipulator [63].

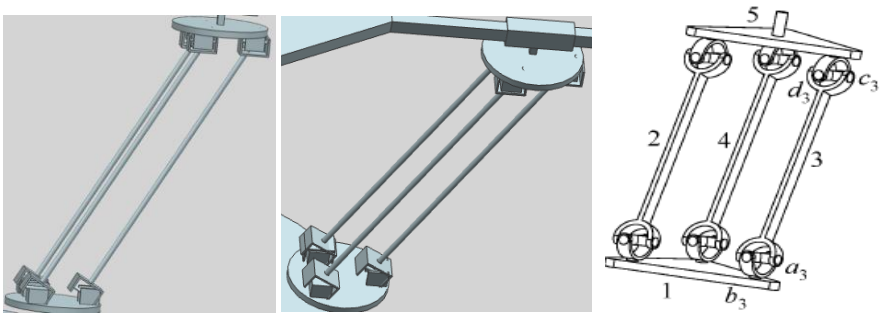

Figure 2.9. Pure-translational universal joint [30]

2.3. Dynamic Balancing

Dynamic balancing for mechanisms has become an important part of mechanism design and development. When mechanisms and parallel manipulators move, due to the fact that the CoM is not fixed and angular momentum is not constant, vibration is often produced in the base. This will deteriorate the accuracy. Dynamic balancing can also be called shaking force balancing and shaking moment balancing. Shaking force balancing

can be achieved by making the center of mass of the mechanism fixed, i.e. linear momentum constant. Normally, the linear momentum is set to zero for the ease of analysis. Shaking moment balancing can be achieved by making the angular momentum constant. Normally, the angular momentum is set to zero. The research for the dynamic balancing of parallel mechanisms is still in its early stage. Since 2000, when Ricard and Gosselin systematically addressed the dynamic balancing of parallel mechanisms [67], dynamic balancing began to increasingly appear in the academic research area. Parallel mechanisms have been used in many areas, such as machine tools, telescopes and space. However, a problem occurs when parallel manipulators are in operation, i.e. not dynamically balanced. This greatly deteriorates the performance of parallel manipulators; e.g., the accuracy is decreased [68]. Dynamic balancing of these parallel manipulators has become an issue for many scholars and industries. In order to achieve dynamic balancing, force balance and moment balance both need to be satisfied at the same time. Traditionally, counterweights are used to achieve force balance, i.e. make the CoM fixed at the (rotation) joint. Counter-rotations are usually used to achieve moment balance, i.e. make the angular momentum equal to zero. Force balancing and moment balancing involves using extra devices (e.g. counterweights, counter-rotations) to counter-balance the shaking force and shaking moment that the original mechanism exerted to the base. However, a problem occurs when using those counter-balancing devices; i.e. the whole mechanism will become heavier and have more inertia. How to design reactionless mechanisms with minimum increase of mass and inertia has become a common goal.

There are generally two main ways for shaking force and shaking moment balancing, i.e. “balancing before kinematic synthesis” and “balancing at the end of the design process”, as summarized in Figure 2.10. Here, the dynamic balancing based on these two main categories will be discussed. Under the category of balancing at the end of the design process, adding counterweights and counter-rotations, active dynamic balancing unit (ADBU) and auxiliary links are the most commonly used methods. Under the category of balancing before kinematic synthesis, Fisher’s method is a typical example.

The problem of shaking force balancing is explained as follows. When a link moves around a hinge, the position of the CoM of the link changes, therefore the link will have a shaking force. When a counterweight is attached to the extended part of the link, the CoM of the system settles to the revolute hinge, then the system is force balanced. If the counterweight is employed, the system will become heavy, which is a drawback of using counterweights. The second method is to use an active dynamic balancing unit (ADBU). This ADBU will create a shaking force and shaking moment, the value of which is equal but has opposite direction to the original shaking force and shaking moment so that it can counter the original shaking force and shaking moment in order to achieve dynamic balancing. The third method is to add auxiliary links; the mass of additional link can be used to force balance the mechanism [68]. In addition, Fisher’s method can also be seen as an adding auxiliary links method. In the next chapter, a new balancing method will be proposed, i.e. balance through reconfiguration. For example, a screw link is used so that the link can be moved, and the CoM of the link can then be moved to the revolute joint, then balanced. In this method, a counterweight is not applied but the system is

reconfigured. For the shaking moment balancing, the “add counter-rotations”, “add counter-rotary counter-mass (CRCM)”, “using inherently dynamic balanced 4-bar linkage” and “add ADBU” methods are the most commonly used principles, which will be discussed in the following sections.

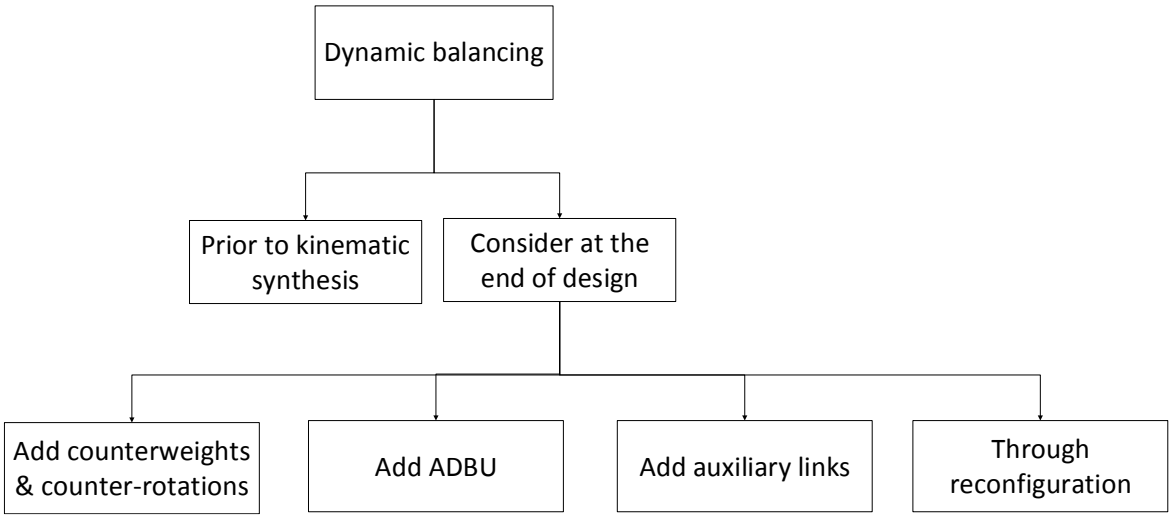

Figure 2.10. Two main categories for dynamic balancing

2.3.1. Balancing Before Kinematic Synthesis

a. Fisher’s method

Fisher’s method is a typical example of balancing before kinematic synthesis. Recently Wijk [69-72] has thoroughly investigated this method. The core content of his work can be concluded as follows: for the shaking force balance, first determine the linear momentum, then determine the force balance condition from the linear momentum, and finally determine the principal dimensions. For the 2-DOF pantograph, first determine linear momentum, then force balance condition, and finally the principal dimensions.

Because the 2-DOF pantograph does not have a middle link, it is easier to solve the principal dimensions without using the equivalent linear momentum systems (ELMS). The 3-DOF and 4-DOF principal vector linkages have middle links, so the ELMS are used for the middle links, which requires a little more effort to calculate the principal dimensions. For the moment balancing, one needs to first write the angular momentum, then substitute the position vectors, position vector derivatives, angle relations and the force balance conditions to the angular momentum equation to obtain the final form of the angular momentum. For linear relations of time dependent parameters, one needs to determine the moment balance condition from the angular momentum. For non-linear relations of time dependent parameters, one also needs to determine the moment balance condition. Finally, reactionless mechanisms are synthesized from the principal vector linkages.

The main content of Fisher's method that Wijk used [69] is to calculate the principal dimensions, and using the auxiliary links/pantograph links to trace the CoM of the whole mechanism. It is shown that the principal vector linkage architecture is force balanced. For the moment balance, the relative motions of the principal vector linkage architecture have to be constrained by additional elements. The moment balance is achieved mainly through the symmetrical design and constraining the DoF of the mechanism, such as adding a slider or similar to reduce the DoF of the mechanism in order to achieve the moment balance. The grasping mechanism [69] is derived from the 4-DOF principal vector linkage with a slider. The motion of the 4-DOF principal vector linkage (grasping mechanism) is reduced in order to achieve the moment balance. Also, the bridge as well as the roof and the wall of the house can be derived from the 2-DOF principal vector

linkage. The above dynamic balanced mechanisms are all synthesized from the principal vector linkages.

In [15], the Dual-V manipulator is derived from two balanced pantographs. By symmetrically designing the structure of the legs of the 4RRR planar parallel manipulator, the shaking moments balanced out each other when moving along the orthogonal axis, so counter-rotations were no longer needed, and only counter-weights were used. The limitation is that the manipulator is dynamically balanced only when the manipulator moves in the orthogonal axis. The idea of the above symmetric design can also be seen as evolving from pantograph arms with a counter-mass (the arm has a parallelogram shape), and the pantograph arms with a counter-mass were evolved from the normal counter-mass adding in each link, as shown in Figure 2.11. Similarly, Wijk [73] derived the general force balancing conditions of the planar 4-RRR parallel manipulator; thus, the different topologies of the 4-RRR manipulator from the force balance condition were obtained.

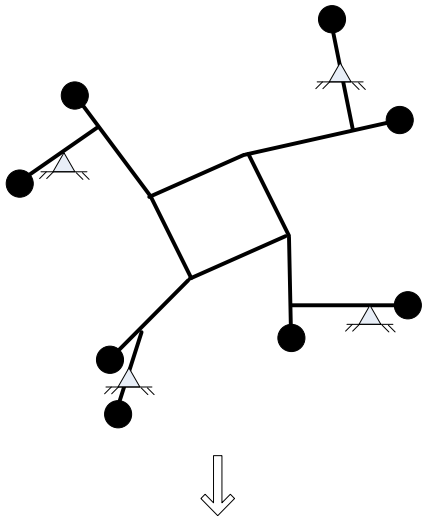

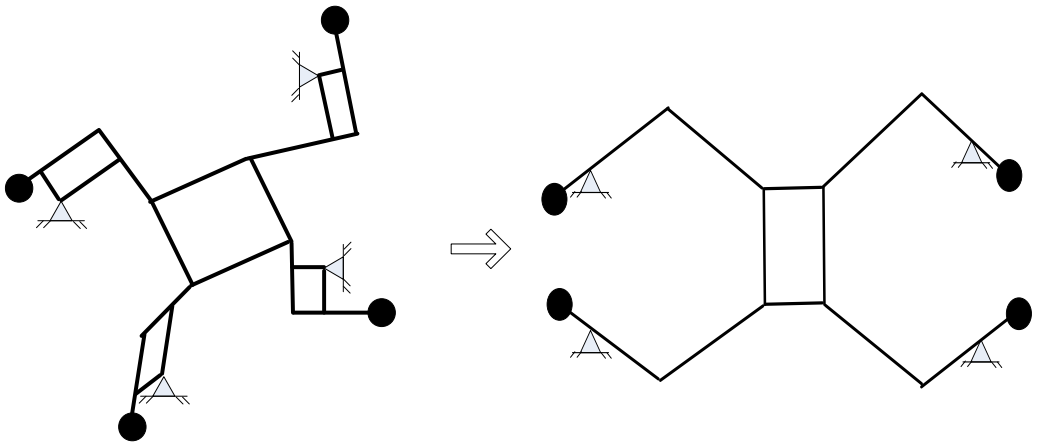

Figure 2.11. Evolving process for the 4-RRR reactionless parallel mechanism [15]

b. Using Naturally Dynamically Balanced 4-bar Linkage

A four-bar linkage was proposed as a building unit to synthesize planar and spatial 3-DOF parallel manipulators [74]. By serially connecting two four-bar linkages, a 2-DOF reactionless serial mechanism was constructed and used to build the 3-DOF parallel manipulators. The advantage of the above mechanism is that it did not employ counter-rotations, but the drawback is that the moving platform was assumed thin, which is not practical. The above four-bar linkage (Gosselin's type II mechanism) is actually derived from the principal vector linkage. The three-serial-chain principal vector linkage is evolved to a four-bar linkage by adding a base link to the ground, as shown in Figure 2.12, and by finding the moment balancing conditions for the four-bar linkage, the Gosselin's type II mechanism can be derived.

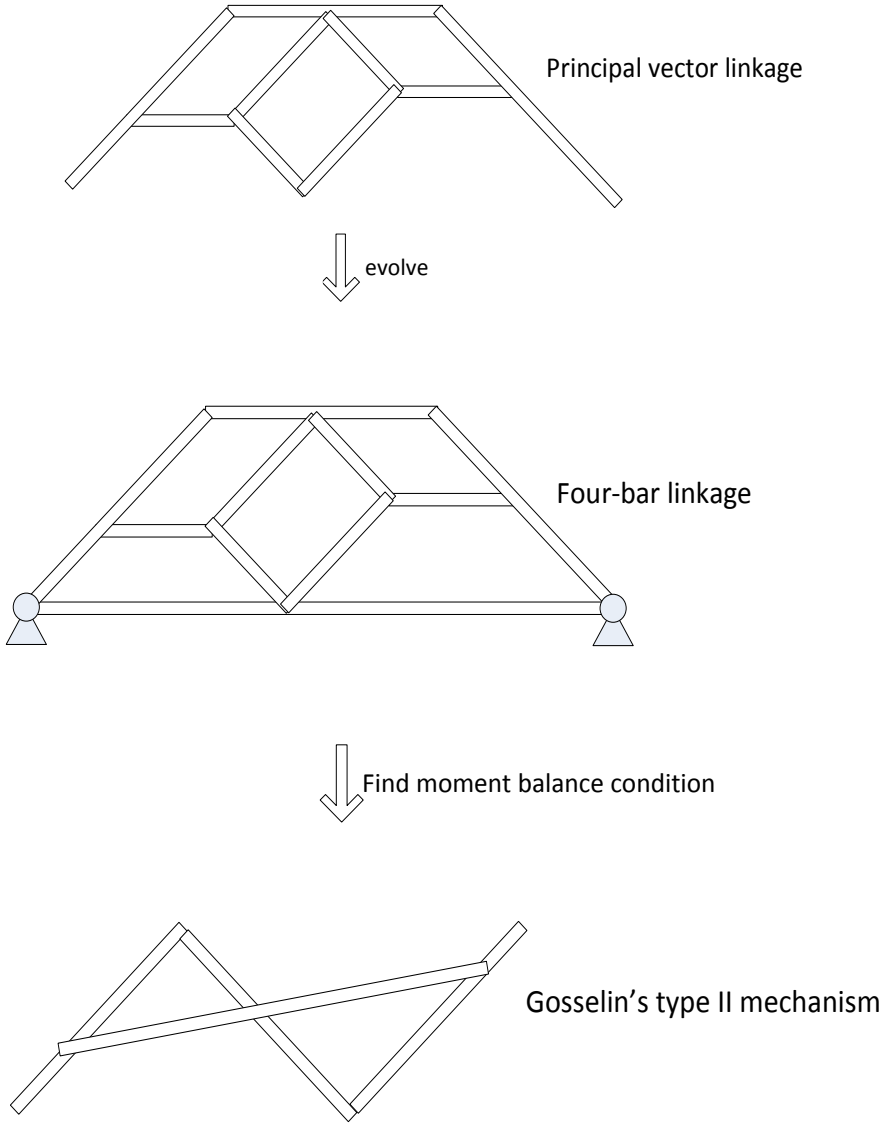

Figure 2.12. Evolving process for deriving Gosselin type II reactionless mechanism [74]

A 3-DOF serially connected mechanism was derived from two four-bar mechanisms and one composite mechanism [75]. This 3-DOF mechanism can be used as a leg to construct the spatial 6-DOF parallel manipulators. The composite mechanism is derived from a pair of four-bar mechanisms that are orthogonally fixed to each other. The author [75] wanted to design a spatial 6-DOF parallel manipulator, which requires the four-bar linkage to move spatially. Due to the fact that the four-bar linkage is not dynamically

balanced when moving spatially, so the composite mechanism is developed. Also the synthesized mechanism, as shown in Figure 2.13, is proposed by connecting the four-bar linkage or composite mechanism to the end bar of the base four-bar linkage. The synthesized mechanism was verified to be dynamically balanced, which is done by the following: if the resulting parameters of the end bar of the base four-bar linkage and attached mechanism (this attached mechanism can be four-bar linkage or composite mechanism) meet the balance condition, then the synthesized mechanism will be dynamically balanced.

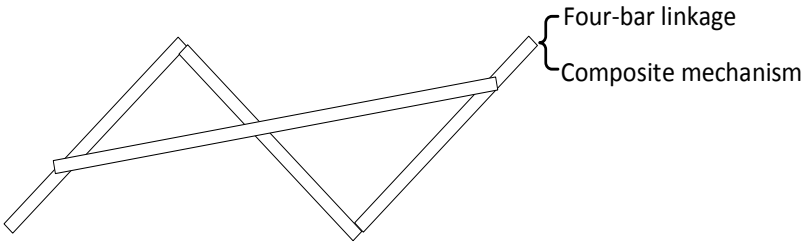

Figure 2.13. Synthesized mechanism [75]

2.3.2. Balancing at End of Design Process

a. Add Normal Counterweights

A parallelogram five-bar linkage (actually it reduced to parallelogram four-bar linkage later) was proposed as a leg for a planar 3-DOF parallel manipulator [14]. This planar 3-DOF parallel manipulator has two of these legs. The moving platform was first replaced by two point masses (because there are two legs) located at the point of attachment of each of the legs to the moving platform. In order to accomplish this, three conditions have

to be satisfied: same mass, same inertia and same CoM. Secondly, for each leg (including the replaced mass), the static balancing has to be first satisfied in order to achieve the dynamic balancing condition. For the static balancing, the CoM equation $\mathrm{Mr} = \sum \mathrm{m}_i \mathrm{r}_i$ (r is the position of CoM) was used and by making the position of CoM equal to 0, two static balance equations (static balance conditions) are obtained. After obtaining the equations, the next step is to solve them. From those two static balancing equations, it can be seen that the masses and length are both positive. The only way to satisfy the equation is to make the position of the CoM of some links to be negative and to do that, counterweights can be added. For the moment balancing, the authors [14] wrote the angular momentum of the five-bar mechanism, and by making the angular momentum equal to zero, three moment balance equations (moment balance conditions) are derived. From the static balancing, two equations were derived, and from the dynamic balancing (angular momentum condition), another three equations were derived; i.e. five equations were provided for the dynamic balancing of the leg (five-bar linkage). The novelty of this study is that the authors proposed the parallelogram five-bar linkage as a leg of a planar 3-DOF parallel mechanism and analyzed the dynamic balancing of the leg. Future wok will employ the proposed leg for other kinds of spatial parallel manipulators. The above method is based on the decomposition and integration method; i.e. first proposing a single linkage (leg), then dynamically balancing a single linkage, and finally combining those linkages to form the whole parallel manipulator. In other words, decompose first and integrate later. However, the disadvantage of the above reactionless mechanism is that counter-weights and counter-rotations were used, which increased the weight,

inertia and complexity. The counterweights are used to keep constant the position of the CoM while the counter-rotations are used to keep constant the angular momentum.

In [76-78], the core idea of dynamic balancing of mechanisms is to use counterweights and counter-rotations (i.e. geared inertia counterweights and planetary-gear-train-inertia counterweight) to force and moment balance linkages, which is straightforward. The CoM formula was used to derive the CoM of the whole mechanism; the CoM was then set to be stationary so that the force balance condition can be obtained. Subsequently, the shaking moment of the linkage was described as the time rate of change of the total angular momentum, and the general formula for the total angular momentum of the linkage $H_o = \sum m_i(x_i \dot{y}_i - y_i \dot{x}_i + K_i^2 \dot{\phi}_i)$ was used. The total angular momentum was subsequently set to zero in order to derive the dynamic balance condition, but later it was found that it was impossible to achieve dynamic balancing unless counter-rotations were added. After adding counter-rotations, the total angular momentum was set to zero and the moment balance condition was obtained. The disadvantage of this balance method is that the planetary-gear-train-inertia counterweight was put on the upper moving link rather than on the ground.

In [16], a double pendulum was dynamically balanced by using two counter-weights and two counter-rotations. The counter-weights are placed at the extension of each link as for the traditional force balance technique to make the CoM fixed at the revolute joint, and shaking moment balancing is achieved by using planetary gear trains that carry out the counter-rotations. Force balancing condition is derived by using the CoM formula and making the position of CoM equal to 0. Two force balance equations are obtained, and

from those two static balancing equations it can be seen that the masses and length are both positive. The only way to satisfy the equation is to make the position of the CoM of some links to be negative. To do that, counterweights were added. The shaking moment of the upper moving link is balanced by a counter-rotation gear, which is mounted on the base, and it is connected to the upper moving link in the following way: two gears at the base joint (one small gear and one large gear) are fixed together; the counter-rotation gear is connected with the large gear, and the small gear is connected to the upper moving link by a belt. In this way, this counter-rotation gear is indirectly connected to the upper moving link and rotates opposite to the upper moving link to achieve moment balancing in order to achieve dynamic balancing. For the moment balancing, the authors [16] wrote the angular momentum of the whole mechanism, and by making the angular momentum equal to 0, two moment balance equations (moment balance conditions) are derived. The disadvantage of the above force balancing and moment balancing methods is that counter-weights and planetary gear trains (counter-rotations) are used, which increase the total mass and complexity. In the second part of the paper, the authors [16] also discussed the shaking moment balancing by using a flywheel. Using this solution is constructively more efficient. The angular momentum of the whole parallel manipulator was first derived. In order to achieve the shaking moment balance condition for this manipulator, the flywheel was used, and this flywheel needed to have the same and opposite shaking moment so that it could moment balance the manipulator. This flywheel is driven by another actuator, which belongs to the active dynamic balancing technique. Finally, the angular acceleration of this flywheel can be obtained by using the moment

formula. However, how to link this flywheel to the parallel manipulator was not mentioned.

In [79], the gear, which is used for balancing the shaking moment, is put on the base so that it can lead to a smaller increase of moving masses. This gear is originally mounted on the moving link, so the mass of the counterweight of the base link is needed to also force balance this gear, but if the gear is put on the mechanism frame, then the counterweight of the base link does not need to force balance the gear, which means the mass of this counterweight of the base link can be decreased. However, the disadvantage is that the number of extra devices increased. This balancing method described above is an extension of Gao's method in [76-78].

In [17], the author derived a 3-DOF parallelepiped mechanism (unit) from the basic 1-DOF pivot link as a leg to synthesize the spatial parallel manipulator, but this parallelepiped mechanism requires three counter-rotations and six counter-weights to achieve the dynamic balance condition, which substantially increases the mass, inertia and complexity of the mechanism. The above parallelepiped mechanism design is not smart because it uses the counter-weights and counter-rotations. The dynamic balancing condition was directly derived from the CoM formula and also the angular momentum was set to zero. Finally, the parallelepiped mechanism was used to construct the spatial parallel manipulators. Future work can focus on how to simplify this mechanism.

b. Add Assur Group

In [19], the authors used the Assur group and three counterweights to achieve dynamic balancing, three counterweights are used to achieve force balancing, and the Assur group and the counterweights are used to achieve the moment balance. In [80], the paper discussed the shaking force balancing and shaking moment balancing for a planar 3-RPR parallel manipulator with prismatic joints. The authors proposed two methods for the balancing: the first is based on the addition of an idler loop between the moving platform and the base. This uses many counter-weights and counter-rotations, which substantially increase the mass and inertia. The second method is based on the addition of a Scott-Russell mechanism (i.e. special crank-slider mechanism, which belongs to the Assur group) to each leg of the 3-RPR parallel manipulator, which can decrease the number of counter-rotations. The second method, which is based on the addition of a Scott-Russell mechanism, belongs to the passive dynamic balancing, and requires 3 counter-rotations. It is expected that if we change the passive balancing to active balancing, the number of counter-rotations can then be reduced.

c. Add CRCM

In [81], the authors mainly presented “shift modification rules”, from which the counter-rotary counterweight was evolved. In [82], the counter-rotary counter-mass (CRCM) was proposed and compared with the separate counter-rotation, with the conclusion that the CRCM principle has reached reduction of added mass and added inertia.

In [18], the total mass (increase) and reduced inertia of a double pendulum were compared within the CRCM, separate counter-rotations (SCR), duplicate mechanisms (DM) and Idler loop. The reduced inertia and total mass of these four balancing principles were first derived, and the mass-inertia factor, which was used for judging the additional mass and additional inertia, was established. The comparison results showed that the DM principle had the lowest values for the mass-inertia factor, which means that the DM principle is the most favorable for low mass and low inertia dynamic balancing, but it requires a larger space. The CMCR principle is the second lowest value for the mass-inertia factor, which means it is the second most favorable for low mass and low inertia dynamic balancing. Since it does not require larger space compared with the DM principle, the CRCM has more potential for use. The general procedure of the above analysis can be concluded as follows:

Step 1: The position vectors of the counter-masses and lump mass were first obtained, then with the derivative of those position vectors, the linear momentum was derived by using the linear momentum formula, which subsequently made the linear momentum equal to zero, and the force balancing condition was derived.

Step 2: The angular momentum about the reference point was obtained by using the angular momentum formula, and the relations between the gears were applied to simplify the angular momentum. By making the angular momentum equal to zero, the moment balancing (dynamic balancing) condition was derived.

Step 3: When deriving the reduced inertia, one can either first determine the kinetic energy and derive the reduced inertia, or directly obtain the reduced inertia by copying

the coefficients of angular velocities in the angular momentum formula, but with the transmission ratios squared.

Step 4: Determine the total mass.

Step 5: The total mass and reduced inertia are compared among those four balancing principles.

For this study, it was not thought necessary to compare the total mass and inertia. Some of the masses and inertia are on the ground, not on the mechanism, so those masses that are on the ground do not really affect the system. The study in [83] has the results same as [18] except that it compared the total mass and reduced inertia among SCR, CRCM and DM for a 1-DOF rotatable link, rather than a double pendulum.

In [84], an additional three CRCM-based balancing principles were derived: low inertia configuration balancing principle; one CRCM balancing principle; and only CRCMs near the base balancing principle. According to the authors, the advantage of the first new balancing principle is its low inertia, while the advantage of the second new balancing principle is that only one CRCM is necessary for the moment balance of the entire mechanism. The advantage of the third new balancing principle is its compact construction. Finally, several CRCM-based 2DOF parallel mechanisms were synthesized by using the CRCM-balanced double pendulum. The 3DOF planar and spatial parallel manipulators were synthesized by using the balanced double pendulum.

The perspective of this study is that the One CRCM Configuration is not a smart balancing principle because there are two gears on the upper moving link rather than the base frame. For the Only CRCMs Near the Base Configuration, the principle is roughly the

same with the Idler loop or the Arakelian and Smith mechanism in [16, 79]; i.e. the moment of the upper moving link is balanced by a CRCM connected to the upper moving link through a gear/belt transmission, and the moment of the base link is balanced by another CRCM connected to a gear attached to the base link. However, the disadvantage of the Only CRCMs Near the Base Configuration is that the CRCM, used for moment balancing the upper moving link, is on the base link, which makes the system heavier. With the Arakelian and Smith mechanism in [16, 79], the gear that is used for moment balancing the upper moving link is on the base/ground, which does not at all affect the system.

d. Add Active Driven CRCM

In [85], by actively driving the CRCM, the double pendulum can be dynamically balanced. The specific angular momentum of the ACRCM was derived, the rotational velocity of the ACRCM was then obtained and the torque of the actuator that actively drove the ACRCM was obtained. Through evaluation, the authors found that the ACRCM principle is better than the passive CRCM or separate counter-rotations mainly in terms of total mass-inertia. A 2-DOF ACRCM-balanced parallel manipulator was derived by combining two CRCM to one ACRCM, as shown in Figure 2.14. The 3-DOF planar and spatial parallel manipulators were synthesized by using the ACRCM-balanced double pendulum. Because the manipulators use the ACRCM, the whole system will still become heavier, and thus belongs to the “consider at the end of the design process” approach.

In [85], a 2-DOF ACRCM-balanced parallel manipulator was derived by combining two CRCM to one ACRCM. Inspired by the above design, new 3-DOF planar 3-2RRR and 4-2RRR reactionless parallel manipulators and spatial 3-DOF 3-2RRR and 4-2RRR reactionless parallel manipulators are derived, as shown in Figure 2.15 by employing a 2-DOF ACRCM-balanced mechanism.

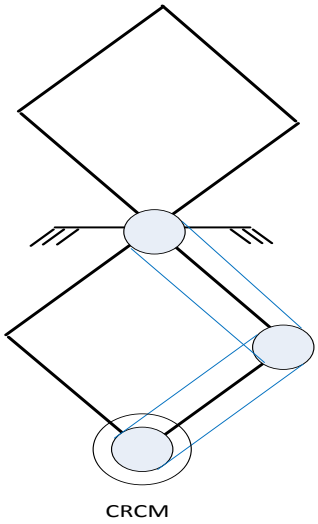

Figure 2.14. ACRCM-balanced manipulator [85]

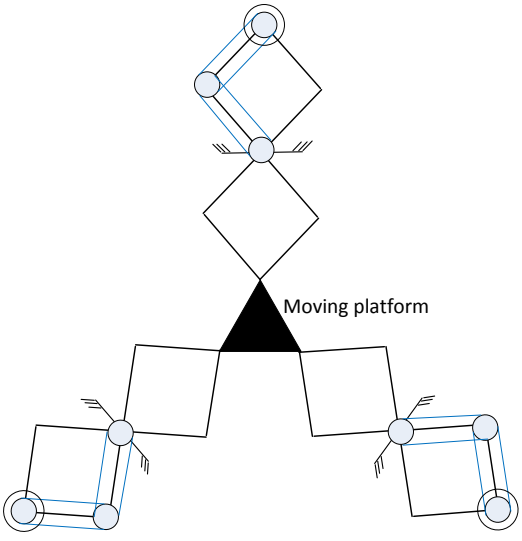

(a) 3DOF planar 3-2RRR reactionless manipulator

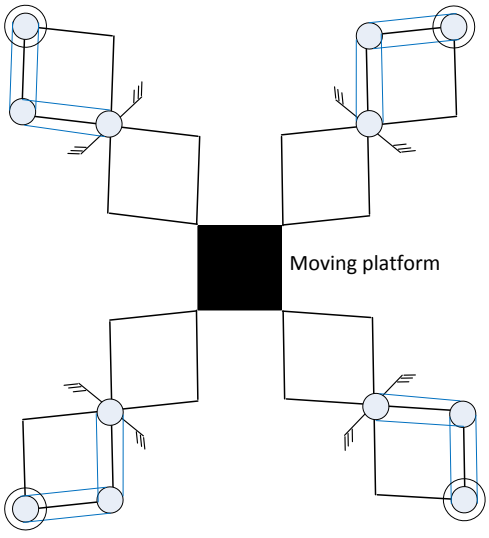

(b) 3DOF planar 4-2RRR reactionless manipulator

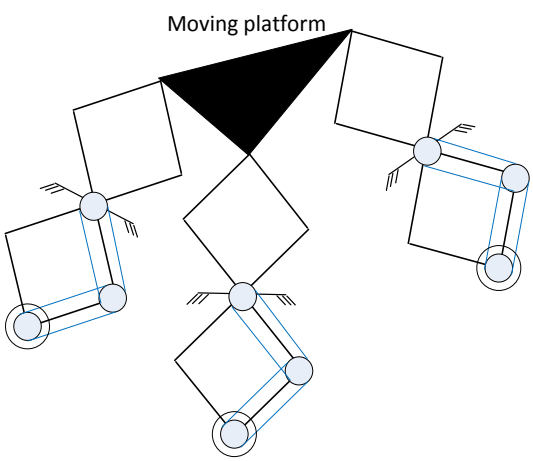

(c) 3DOF spatial 3-2RRR reactionless manipulator

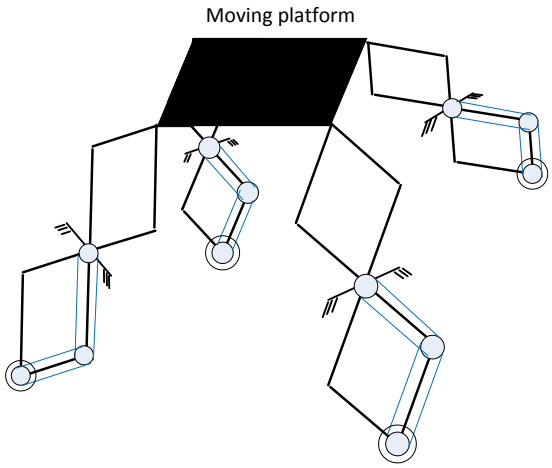

(d) spatial 3DOF 4-2RRR reactionless manipulator

Figure 2.15. 3-DOF planar 3-2RRR and 4-2RRR and spatial 3-2RRR and 4-2RRR reactionless parallel manipulators

e. Active Dynamic Balancing Unit

In [86], the authors focused on active dynamic balancing. The paper presented an active dynamic balancing unit (ADBU), which is a unit that can be mounted on the base of the unbalanced mechanism and controlled such that the complete system is dynamically balanced. The goal of the ADBU is to produce balancing forces and balancing moments that are equal and opposite to the total shaking forces and total shaking moments of the machine. The ADBU constitutes three counter-masses and three counter-rotations. The three counter-masses are used to force balance the shaking force along the x, y and z directions and the three counter-rotations are used to moment balance the shaking moment about the x, y and z directions. Considering the low mass addition aspect, the ADBU is advanced to a new ADBU where the three counter-masses and three counter-rotations are combined. In this study [86], the ADBU needs to balance a xy-robot, which

means this robot has two shaking forces in the plane, i.e. x and y directions and one shaking moment about the z direction, so the ADBU only needs to balance two shaking forces in the x and y directions and one shaking moment in the z direction. Hence, the ADBU is reduced from the original to one that has only two translation motions and one rotation motion. A 2-RRR parallel mechanism is used to move the disc in the x and y directions. The disc can also rotate; i.e. this disc is a CRCM. Future work is to find advanced control strategies for controlling the ADBU.

In [87], a 3-DOF active dynamic balancing mechanism (ADBM), which is attached to the moving platform, was proposed, and it is similar to the ADBU. This mechanism can not only balance the moving platform, but also can actuate the moving platform to move in a certain trajectory. However, the main function of the ADBM is to balance the shaking force and shaking moment of the moving platform. The counter-forces and counter-moments provided by the ADBM are equal to the shaking forces and shaking moments plus the actuated force and actuated moment; i.e. one part of the forces and moments provided by the ADBM is used to balance the shaking force and shaking moment. The other part of the forces and moments provided by the ADBM is used to actuate the moving platform to a certain trajectory.

f. Add Auxiliary Links

Dynamic balancing of Clavel's Delta robot is described in [68]. For force balance, a solution is proposed that each leg and one-third of the moving platform mass are balanced together with one counter-mass plus an additional link; i.e. each leg becomes a 3D-

pantograph. Furthermore, due to the fact that the moving platform of the Delta robot does not rotate, the above force balance method can be simplified to the following: one leg, being a 3D-pantograph, can balance the complete mass of the moving platform and part of the mass of the links that are attached to the moving platform of the other two legs, to which two other counter-masses are also attached. This the complete Delta robot is force balanced by three counter-masses and one additional link. For the moment balance, the author used the active driven method because the velocity of the mechanism cannot be made constant by using passive moment balancing methods. It was found that the mass of the additional link can be used to force balance all of the mass of the moving platform and part of the mass of the links attached to the moving platform. Fisher's method can also be considered as the adding auxiliary links method.

2.4. Adaptive Control of Robotic Manipulators

2.4.1. General Adaptive Control

In a traditional control system, feedback is used to reject the disturbance effect that acts on the controlled variables in order to bring these controlled variables back to their desired value. In order to do so, the variables are measured and compared to the desired values and the difference is fed into the controller. In these feedback systems, the designer adjusts the parameters of the controller so that a desired control performance is achieved. This is done by having a priori knowledge of the plant dynamics. When the parameters of the plant dynamic models change with time due to disturbances, the conventional control can no longer deal with it as the control performance will be

degraded. At this time, one needs to resort to adaptive control. A structured approach for the design of a distributed and reconfigurable control system is presented in [88]. Distributed architectures are conceived as interconnected independent modules, with standard interfaces, which can be modified and reused without affecting the overall control structure, whereas for the centralized control architectures, any change of the machine structure requires an extensive replacement of the control system. In reconfigurable manufacturing systems, modular and distributed architecture is essential to guarantee the capability of each single module or portions of the control to be adapted when a hardware reconfiguration occurs.

In [89], the sustainable manufacturing by reconfiguration of robots through using robot modules was presented. The customized modules are an end-effector, suction pump and adapters, modular frame, steering guide, PLC and robot controller, sensors, power supply and indicators, and a touch screen. In terms of control, there are two different controllers: one is used to control the robot arm and the other is a programmable logic controller that handles user inputs and sensor data. When the robot is reconfigured, the control system needs to be reconfigured to sustain the communication within the system components.

In [90], neural networks are used for control reconfiguration design for a space robot. The traditional controller was presented, and by using the neural networks, the traditional controller is updated to a reconfigurable controller. A fully-connected architecture was employed that was able to combine an a priori approximate linear

solution. The study presents a new reconfigurable neural-network-based adaptive control system for the space robot.

In [91], the authors presented an adaptive reconfigurable flight control system using mode switching of multiple models. The basic idea is to use the on-line estimates of the aircraft parameters to decide which controller to choose in a particular flight condition. This system is related to the multi-mode adaptive control. In [92], the basic concept of adaptive control and several kinds of control categories were introduced, such as open-loop adaptive, direct adaptive, indirect adaptive, robust, and conventional. Adaptive control can be seen as a conventional feedback control system but where the controlled variable is the performance index. Hence there are two loops for the adaptive control: one is the conventional feedback loop and the other is the adaptation loop.

A control development approach is proposed in [93], which consists of three steps: control conceptual design, application development and evaluation of solution robustness. The control system should be conceived as a set of independent and distributed control modules, capable of nesting one to each other. The structuring of control logics is the basis of the entire control development process. In order to enable the control system reconfiguration, an essential feature of the control architecture is the modularity and distribution of the control decisions across the various entities.

2.4.2. Adaptive Control for Robotic Manipulators

Non-adaptive controller designs often ignore the nonlinearities and dynamic couplings between joint motions. When a robot's motions require high speed and accelerations, it

greatly deteriorate its control performance. Furthermore, non-adaptive controller designs require the exact knowledge and explicit use of the complex system dynamics and system parameters. Uncertainties will cause dynamic performance degradation and system instability. There are many uncertainties in all robot dynamic models. Model parameters, such as link length, mass and inertia, variable payloads, elasticities and backlashes of gear trains, are either impossible to know precisely or vary unpredictably. For this reason, adaptive control is needed to address the above problem.

Adaptive control can be categorized into the following: model reference adaptive, self-tuning adaptive and gain-scheduled, as shown in Figure 2.16. Here the model-reference approach will be mainly considered.

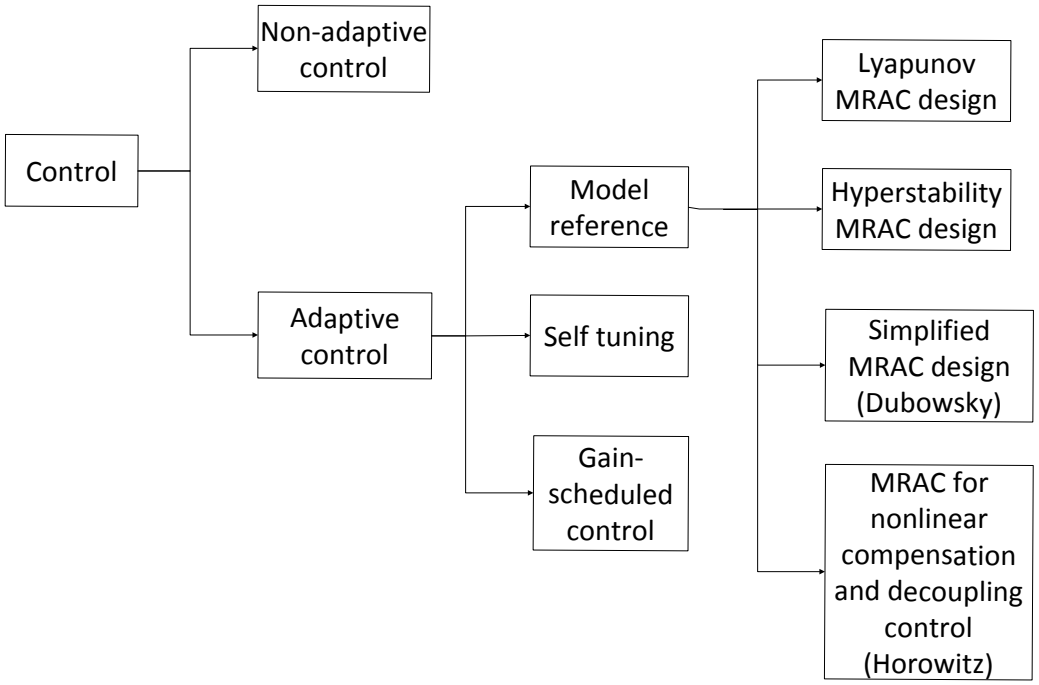

Figure 2.16 Adaptive control categorization

For the model-reference adaptive control, the set value is an input to both the actual and the model systems. The difference between the actual output and the model output can therefore be determined, the result of which is employed to adjust the controller parameters in order to minimize the difference. Figure 2.17 shows such a control system.

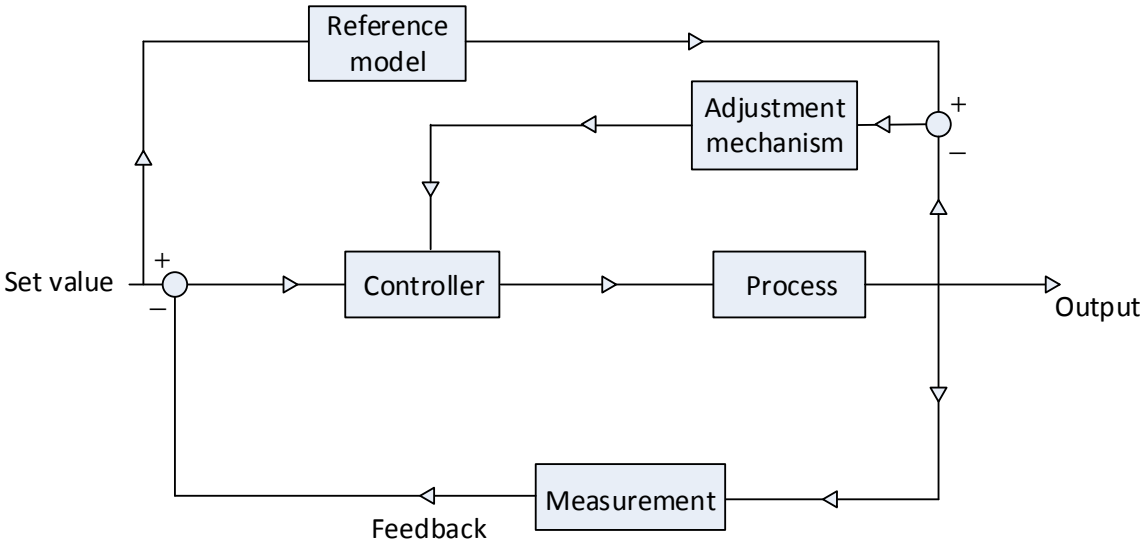

Figure 2.17 Model reference adaptive control [95]

Model reference adaptive control and its usage to robotic arms was introduced in [94] and [95]. Some design problems in adaptive robot control are briefly stated. Dubowsky [96] was the first to apply model reference adaptive control in the robotic manipulator. The approach follows the method in [97]. A linear time-invariant differential equation was used as the reference model for each DOF of the manipulator arm. The arm was manipulated by tuning the position and velocity feedback gains to follow the model. A steepest-descent method was employed for updating the feedback gains. Firstly, the reference model dynamics was written, followed by the nonlinear manipulator (plant)

dynamic equation, but how this equation is related to the Lagrange equation is not clear. Thirdly, an error function was written, which follows the method of steepest-descent. A set of equations was derived for the parameter adjustment mechanism, which will minimize the difference between the actual closed-loop system response and the reference model response.

An adaptive algorithm was developed in [98] for a serial robotic arm for the purpose of compensating nonlinear terms in dynamic equations and decoupling the dynamic interaction among the joints. The adaptive method proposed in this paper is different from Dubowsky's approach [96]. Three main differences are concluded as follows: firstly, in Horowitz's method, the overall control system has an inner loop model reference adaptive system (MRAS) controller and an outer loop PID controller, whereas the control system in Dubowsky's method is entirely based on the model reference adaptive controller. Secondly, in Dubowsky's paper, the coupling among joints and nonlinear terms in the manipulator equations are ignored, whereas this is considered in Horowitz's method. Thirdly, in Horowitz's paper, the design method is based on the hyper-stability method, whereas the adaptive algorithm design in [96] is based on the steepest-descent method. Moreover, in [98], there are some issues as follows. (1) The authors stated in [98] that "The overall control system will have an inner loop MRAS controller and an outer loop PID action controller with fixed gains". This statement is not consistent with Figures 4 and 5 in [98]. According to these figures, the control system has an inner loop MRAS controller, but does not have an outer loop PID action controller. (2) For Figures 4 and 5 in [98], the outer loop controller is not consistent with that in a similar paper [105] by the

same authors. (3) For the equation (13') in [98], the adaptive algorithms are all positive, but in [101] (note that [98] is part of the dissertation [101]), the adaptive algorithms are all negative, which is also not consistent.

Model reference adaptive control, self-tuning adaptive control and linear perturbation adaptive control are briefly reviewed in [99]. For the model reference adaptive control, the main idea is to synthesize/design a control signal to the robot dynamic equation, which will force the robot to behave in a certain manner specified by the reference model, and the adaptive algorithm is designed based on the Lyapunove stability criterion. The MRAC method presented in [100] is based on the theory of partitioning control, which makes them capable of compensating for non-linear terms in the dynamic equations and also of decoupling the dynamic interactions between the links. The method followed and used the method in [101]. Future research would focus on further simplification of MRAC schemes since the implementation of MRAC methods for the real time control of manipulators has proven to be a challenging task.

A MRAC system of a 3-DOF serial robotic manipulator was presented in [101]. The study was concerned with the application of MRAC to mechanical manipulators. Since the dynamic equations of mechanical manipulators are highly nonlinear and complex, and also the payload sometimes varies or is unknown, the MRAC was applied to the mechanical manipulators. An adaptive algorithm was developed for compensating nonlinear terms in dynamic equations and for decoupling the dynamic interactions. Finally, a 3-DOF serial manipulator was used as a computer simulation and the results illustrate that the adaptive control scheme is effective in reducing the sensitivity of the

manipulator's performance to configuration and payload variations. The core content of the method in [101] can be concluded as four steps, the first of which is deterministic nonlinearity compensation and decoupling control. Because one needs to calculate the inertia matrix and nonlinear term, the second step is therefore proposed, i.e. adaptive nonlinearity compensation and decoupling control, which is to adaptively adjust the inertia matrix and nonlinear term instead of calculating them. The final step is to complete the overall control system by adding the feedback gain. In [101], the author did not entirely use the Landau's hyperstability design [102], but used some part of it, and proceeded to develop the adaptive algorithm. According to [99], Horowitz's method was separated from Landau's hyperstability design. In addition, the author in [21] stated that "While Landau's method replied on a pre-specified parameter matrix for a model and continuous adaptation of the plant parameters, it will be seen later that it is possible to estimate the model parameters and adapt them continuously". From this statement, it is clear that Horowitz has his own theory to derive the adaptive algorithm, for which he did not use Landau's method, but how the adaptive algorithm was derived was not explicitly addressed. The author in [21] applied the same approach as Horowitz's [101] to a 2-DOF serial robotic manipulator and a flexible manipulator.

In [103, 104], the experiment on the continuous time and discrete time adaptive control on a 1-DOF test stand robot arm and Toshiba TSR-500V robot were briefly conducted. [105] is the continuation of [106] on a single axis direct drive robotic arm, and applies the method to a two axis direct drive robotic arm. In [107], the authors presented the experiment evaluation of a model reference adaptive controller and robust controller

for the positioning of a robotic arm under variation of payload. The results show that both methods can be insensitive to the payload variation. Four adaptive control methods for the robotic arm were summarized in [108], i.e. the computed torque technique, variable structure systems, adaptive linear model following control, and adaptive perturbation control. The adaptive nonlinear model following control was subsequently proposed, which combines the self-tuning regulator and the model reference adaptive control.

A modified version of the method in [101] was proposed in [109]. The assumption that the inertia matrix and nonlinear term are constant during adaptation can be removed by modifying the control law and parameter adaptation law. It was shown that, through modifying the control law (i.e. modeling the Coriolis and centripetal acceleration compensation controller as a bilinear function of the joint and model reference velocities rather than a quadratic function of the joint velocities) and through modifying the parameter adaptation law (i.e. breaking down the nonlinear parameters in the manipulator dynamic equations into the result of the multiplication of two terms: one constant unknown term, which includes the masses, moments of inertia of the links, payload and link dimensions, and the other a known nonlinear function of the manipulator structural dynamics), the assumption that the inertia matrix and nonlinear term are constant during adaptation is removed. Finally, the stability of the above adaptive control law is proved. The above is called the “exact compensation adaptive control law (ECAL)”. In conclusion, it was found that this procedure is extremely time consuming since computations of highly nonlinear functions of joint positions and velocities are involved. To overcome this difficulty, in [110] and [111], a further modified

version was later proposed. The modification consists of applying the desired joint positions and velocities to the computation of the nonlinearity compensation controller and the parameter adaptation law rather than the actual terms. This is known as the "desired compensation adaptive control law (DCAL)" The above modification process is shown in Figure 2.18.

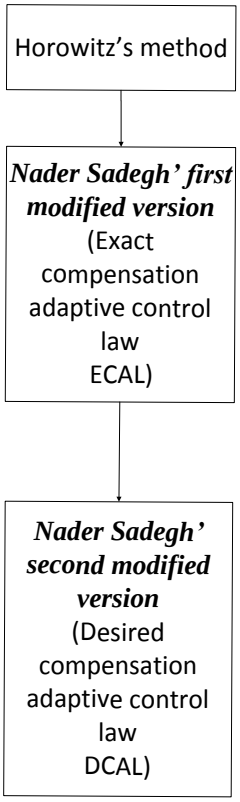

Figure 2.18. Modification process [110]

Nader applied Craig's method [112] to Horowitz's method, so that the condition inertia matrix and nonlinear term assumed constant during adaptation can be removed. Craig's method is re-parametrization; i.e. decompose the nonlinear parameters of the

manipulator’s dynamic equation into the result of the multiplication of two terms: one constant unknown term, which includes the masses, moments of inertia of the links, payload and link dimensions, and a known nonlinear function of the manipulator structural dynamics. The parameter adaptation law is employed to determine the unknown constant terms. One method of reparametrizing the manipulator's dynamic equation consists of breaking down each element of inertia matrix, nonlinear term and gravity term into the result of the multiplication of unknown constant terms and known functions of the joint displacement vector. The second method consists in the re-parametrization of the dynamic equation into the product of the unknown constant vector, and a matrix composed of known functions of the joint positions.

2.5. Conclusions

This chapter provides the state-of-the-art technologies in the field of synthesis design, dynamic balancing and adaptive control for robotic mechanisms. Major synthesis design approaches are presented and analyzed. Dynamic balancing is often accomplished by using counterweights, counter-rotations or damping methods. However, the problem is that the system will become heavier and have more inertia. To address this issue, dynamic balancing through the reconfiguration concept will be proposed in the following chapters. As the mechanism is reconfigured, the control system has to be reconfigured accordingly.

3

Synthesis Design

A novel 3-DOF hybrid manipulator 3PU*S-PU is proposed. The advantages of this new type of hybrid manipulator are first discussed, followed by the kinematics and Jacobian matrix modelling. The stiffness/compliance and workspace are subsequently analyzed and optimized, and the multi-objective optimization on the compliance and workspace is then conducted. Finally, the dynamics of the proposed manipulator are analyzed based on the Lagrangian method.

3.1. Introduction

Type synthesis of parallel manipulators is an important task for future parallel manipulator developments, analysis and applications. The type synthesis of parallel manipulators is and will remain a main issue. Type synthesis is defined as: using various methods to combine the advantages of serial and parallel manipulators to design new application-orientated mechanisms. Furthermore, for the type synthesis of parallel manipulators, it is suggested that one may also consider employing new type of joints (i.e. parallelograms, pure-translational universal joints, and double parallelograms) instead of just adhering to conventional joints (i.e. prismatic, revolute, universal and spherical). A parallelogram has two links acting in parallel, which can distribute the loads. Furthermore,

rotation capacity can be improved by employing parallelograms [63]. Until now, numerous methods have been proposed to provide guidance for designing new types of parallel manipulators for the purpose of further improving the performance. The most common way to design a new parallel manipulator is the one that based on the Chebychev-Grübler-Kutzbach formula and then enumerate all the possibilities, which is cumbersome work. In [64], the systematic enumeration method, which is based on the idea that some of the functional requirements of the desired mechanisms are transformed into structural characteristics, is proposed. In [65], by combining different parallelogram based motion generators, a new 4-DOF (three translations and one rotation) parallel manipulator is designed. Similarly in [66], two identical kinematic chains that serve as Schonflies-Motion Generators are proposed for the parallel manipulator, which employed the parallelograms. The general function (GF) set theory was recently proposed for the type synthesis of parallel manipulators [113].

3.2. Synthesis Design of a New Hybrid Manipulator

A general function set can be categorized into two classes [113]: the first class is $G_F^I(T_a \quad 0 \quad 0; R_\alpha \quad R_\beta \quad 0)$, and the second class is $G_F^{II}(R_\alpha \quad R_\beta \quad 0; T_a \quad 0 \quad 0)$.

For the first class: first of all, we need to determine the number of links, the number of active links, the number of passive links and the number of actuators on the i^{th} active link by using the following formulas (1)-(5) according to the characteristics of the end-effector(EE) [113]:

$$F_D - \sum_{i=1}^{n} q_i = 0 \tag{1}$$

$$N = F_D - \sum_{i=1}^{n} (q_i - 1) + p \tag{2}$$

$$N = n + p \tag{3}$$

$$n \le F_D \tag{4}$$

$$q_i \le F_D (i = 1, 2, 3, ..., n) \tag{5}$$

where F_D is the dimension of the characteristics for the end-effector of parallel topologies, N is the number of limbs, n is the number of actuated limbs, q_i is the number of actuators of the i^{th} actuated limb, and p is the number of passive limbs.

Secondly, according to the intersection algorithms [113], we need to obtain the types of composition of the characteristics of the EE for the class $G_F^I(T_a \quad 0 \quad 0; R_\alpha \quad R_\beta \quad 0)$.

Thirdly, according to the types of composition of the characteristics of the EE just obtained in step two, we can find the required kinematic legs/limbs with the required characteristic of the EE, i.e. all the possibilities of kinematic chains.

Finally, we can synthesize the specific desired parallel manipulator through assembling the kinematic limbs. For the second class $G_F^{II}(R_\alpha \quad R_\beta \quad 0; T_a \quad 0 \quad 0)$, the procedure is the same as the first class, except that in the second step we need to obtain the types of composition of the characteristics of the EE for the class $G_F^{II}(R_\alpha \quad R_\beta \quad 0; T_a \quad 0 \quad 0)$.

Based on the above procedure, a new hybrid 3PU*S-PU manipulator, as shown in Figure 3.1, is derived. 3PU*S-PU means that there are three active PU*S legs and one

passive PU leg, where P represents the prismatic joint, U* represents the pure-translational universal joint, S represents the spherical joint. A large number of three degrees of freedom parallel manipulators can be derived from the GF set theory, but some of them are not at all useful. For example, among them, one is the 3PU*S-$(CR)_o$ parallel manipulator and another is the 3PU*S-$(RC)_o$ parallel manipulator, but these two parallel manipulators have a rotation axis perpendicular to the moving platform; i.e. they have two rotations, one of which is to rotate about the Z axis. The desired outcome is two rotational motions about the X and Y axes, respectively; i.e. two rotation axes parallel to the moving platform. In [114], a hybrid head mechanism 4UPS-PU was proposed to serve as the head section of a groundhog-like mine rescue robot, and the unique feature of that mechanism is that a central passive P-U type limb was incorporated in the mechanism so that it can constrain the whole structure to be three degrees of freedom; i.e. two rotational motions about the X and Y axes and one translational motion along the Z axis. In [115], a comprehensive discussion of hybridization in the context of engineering and a very general idea of hybridization are presented and discussed. Inspired by the design in [114], the middle passive leg is changed from the original to the P-U type. This passive leg consists of a universal joint attached to the moving platform and a passive link fixed to the base, by which the manipulator has the three desired degrees of freedom; i.e. two rotational motions about the X and Y axes, and one translational motion along the Z axis.

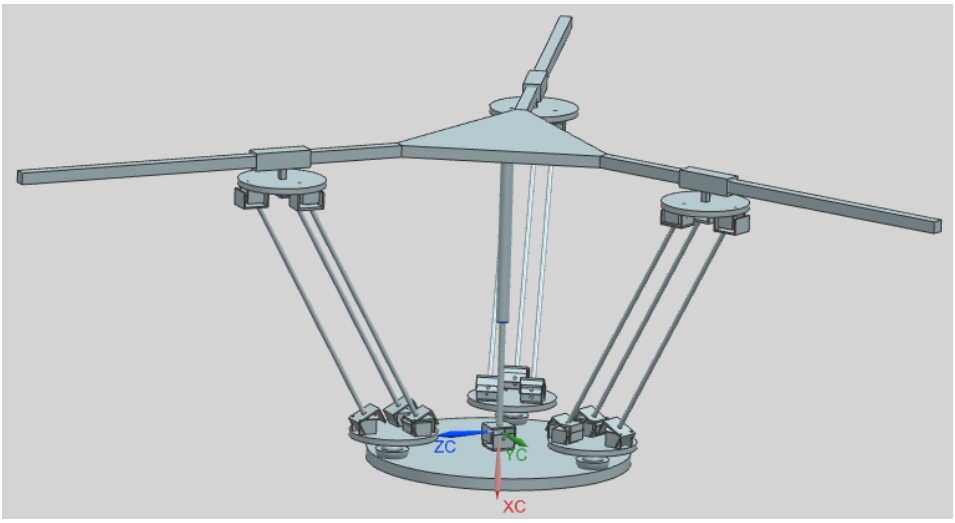

(a). 3-D view

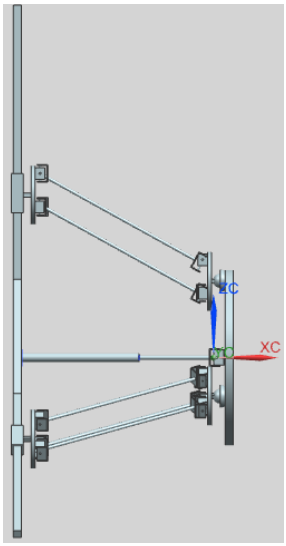

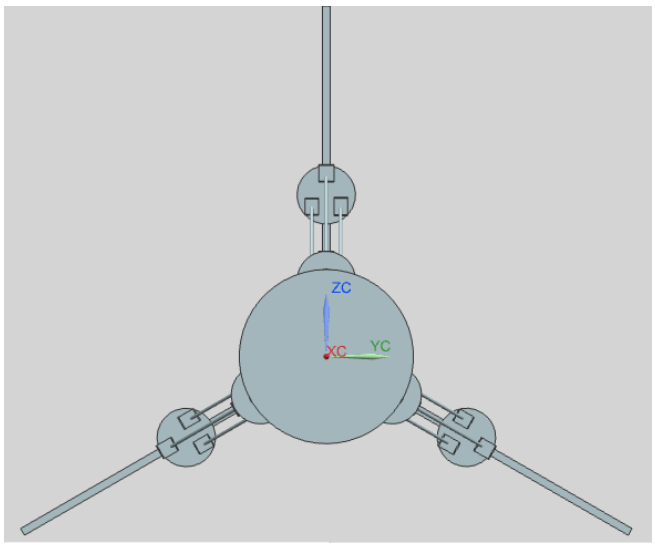

(b). XZ view (c). YZ view

Figure 3.1. Different views of 3PU*S-PU parallel manipulator

The novelty of the new proposed 3PU*S-PU manipulator can be concluded as follows: firstly, by employing the U* joint, the stiffness of this parallel manipulator can be greatly improved since the pure-translational universal joint (U* joint) is a type of parallelogram family. The structure of the U* joint, which is shown in Figure 3.2, consists of two main parts: one is two plates, and the other is three links which connect the two plates through

the universal joints, from which one can see that the loads on the plate can be distributed by three links. Therefore, the stiffness of the parallel manipulator by using the U* joint is higher than that of using normal leg. There are actually two purposes in using the U* joint: one is to increase the stiffness of the parallel manipulator, and the other is to increase the tilting angle or rotation capacity of the end-effector, because the performance of the U* joint resembles a parallelogram, and the parallelogram can increase the rotation capacity of the parallel manipulator [63, 116]. Secondly, by changing the structure of the middle passive leg, i.e. changing the degrees of freedom of the middle passive leg, the whole parallel manipulator can be reconfigured; for example, if one removes the middle passive leg, the three degrees of freedom mechanism will turn to six degrees of freedom.

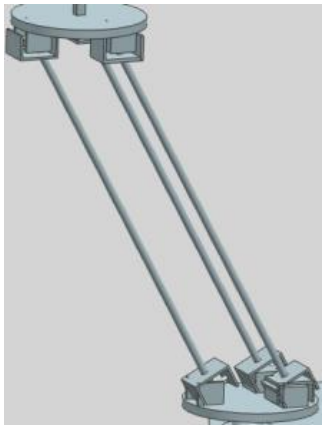

Figure 3.2. Pure-translational universal joint

Here the manipulator we proposed has only three degrees of freedom, so the second purpose of the U* joint mentioned is deactivated by the middle passive UP leg. In the machine tool design, we normally just need three degrees of freedom; i.e. one translational motion along the Z axis and two rotational motions about the X and Y axes.

However, if one wants to design some more than three degrees of freedom mechanisms based on the hybrid manipulator we proposed, one can remove the middle passive leg, then the whole structure will become a six degrees of freedom manipulator. Thus by changing the structure of the middle passive leg, i.e. changing the degrees of freedom of the middle passive leg, the whole parallel manipulator can be reconfigured.

3.3. Kinematic Analysis of the Mechanism

3.3.1. Inverse Kinematic of the Mechanism

The 3PU*S-PU mechanism is shown in Figure 3.3(a). The moving platform is connected to the base through three active legs and one passive leg. Each active leg has the same architecture P-U*-S. This U* joint is connected to the base and moving platform via a prismatic joint and a spherical joint, respectively. There is a passive leg in the middle, consisting of a universal joint attached to the moving platform and a passive link fixed to the base. There are two purposes in using this passive leg: one is to constrain the moving platform to have only three degrees of freedom as previously stated; and the other is to further increase the stiffness of this parallel manipulator [117]. By actuating these three prismatic joints on the guide ways, the moving platform can achieve the desired motions.

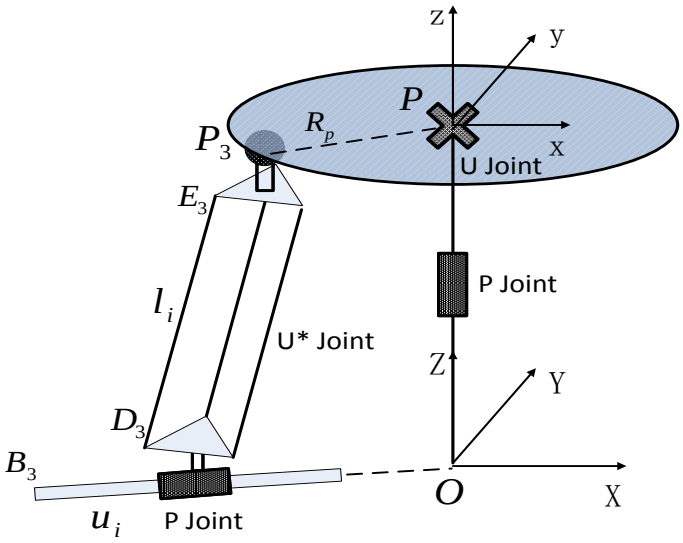

(a). Kinematic structures of 3PU*S-PU mechanism

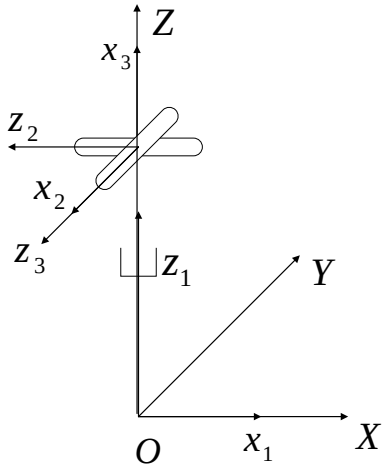

(b). Kinematic structures of central passive leg

Figure 3.3. Kinematic structures of 3PU*S-PU mechanism and central passive leg

The joints attached to the base and moving platform are denoted by B_1, B_2, B_3 and P_1, P_2, P_3, respectively. For the purpose of analysis, the fixed coordinate system $O(\mathrm{X},\mathrm{Y},\mathrm{Z})$ is attached to the center of the base, which coincides with the fixed point of the passive leg. The X axis points to the right and the Z axis is perpendicular to the base and points towards up. The moving coordinate system $P(\mathrm{x},\mathrm{y},\mathrm{z})$ is fixed at the center of the moving

platform. The x axis is parallel to the X axis and the z axis is perpendicular to the moving platform and points towards up. The guide ways intersect at the point O of the fixed coordinate system. $angle1$ is the angle between the X axis and line OB_1 and $angle2$ is the angle between the x axis and line PP_1. The radii of the base and moving platform are R_b and R_p, respectively.

$$\alpha_1 = angle1 \tag{6}$$

$$\alpha_2 = angle1 + 120^\circ \tag{7}$$

$$\alpha_3 = angle1 + 240^\circ \tag{8}$$

$$\theta_1 = angle2 \tag{9}$$

$$\theta_2 = angle2 + 120^\circ \tag{10}$$

$$\theta_3 = angle2 + 240^\circ \tag{11}$$

where $\alpha_i (i = 1,2,3)$ is the angle between the X axis and line OB_i and θ_i is the angle between the x axis and line PP_i. The coordinates of points B_1, B_2 and B_3 with respect to the fixed coordinate system are denoted as ${}^{o}B_i (i = 1,2,3)$; the coordinates of points P_1, P_2 and P_3 with respect to the moving coordinate system are denoted as ${}^{P}P_i$, and the coordinates of points P_1, P_2 and P_3 with respect to the fixed coordinate system are denoted as ${}^{o}P_i$. ${}^{o}P_i$ can then be written as follows:

$${}^{o}P_i = R_e \, {}^{P}P_i + {}^{o}P \tag{12}$$

where ${}^{o}P = \begin{bmatrix} 0 & 0 & z_e \end{bmatrix}^T$ is the coordinate of the center of the moving platform with respect to the fixed coordinate frame. R_e is the rotation matrix of the moving platform with respect to the base.

$$R_e = \begin{bmatrix} -\sin\theta_y & 0 & -\cos\theta_y \\ -\cos\theta_x \cos\theta_y & \sin\theta_x & \cos\theta_x \sin\theta_y \\ \cos\theta_y \sin\theta_x & \cos\theta_x & -\sin\theta_x \sin\theta_y \end{bmatrix} \tag{13}$$

where θ_x, θ_y and θ_z are the rotation angles of the moving platform with respect to the X, Y and Z axes of the fixed coordinate system. Thus,

$${}^{o}P_i = \begin{bmatrix} x_{pi}^o \\ y_{pi}^o \\ z_{pi}^o \end{bmatrix} = R_e \, {}^{P}P_i + {}^{o}P = \begin{bmatrix} -R_p \cos\theta_i \sin\theta_y \\ R_p \sin\theta_i \sin\theta_x - R_p \cos\theta_i \cos\theta_x \cos\theta_y \\ z_e + R_p \cos\theta_x \sin\theta_i + R_p \cos\theta_i \cos\theta_y \sin\theta_x \end{bmatrix} \tag{14}$$

Differentiate the above equation, and it has

$$\begin{bmatrix} \delta x_{pi}^o & \delta y_{pi}^o & \delta z_{pi}^o \end{bmatrix}^T = \begin{bmatrix} J_i \end{bmatrix} \begin{bmatrix} \delta\theta_x & \delta\theta_y & \delta\theta_z & \delta x & \delta y & \delta z_e \end{bmatrix}^T \tag{15}$$

and

$$\begin{bmatrix} J_i \end{bmatrix} = \begin{bmatrix} 0 & -R_p \cos\theta_i \cos\theta_y & 0 & 0 & 0 & 0 \\ R_p \sin\theta_i \cos\theta_x + R_p \cos\theta_i \sin\theta_x \cos\theta_y & R_p \cos\theta_i \cos\theta_x \sin\theta_y & 0 & 0 & 0 & 0 \\ -R_p \sin\theta_x \sin\theta_i + R_p \cos\theta_i \cos\theta_y \cos\theta_x & -R_p \cos\theta_i \sin\theta_y \sin\theta_x & 0 & 0 & 0 & 1 \end{bmatrix} \tag{16}$$

From the vector loop equation, the following equation can be obtained:

$${}^{o}P_i - {}^{o}B_i - \mathrm{u}_\mathrm{i}\, n_i = \mathrm{l}_\mathrm{i}\, s_i \tag{17}$$

where u_i is the actuated input; i.e. the length of B_iD_i; n_i is the unit vector pointing along the rails, which can be written as $n_i = \begin{bmatrix} -\cos\alpha_i & -\sin\alpha_i & 0 \end{bmatrix}^T$; l_i is the length of the U* link; i.e. the length of fixed link D_iE_i; s_i is the unit vector pointing along the link D_iE_i.

$$\mathrm{l_i}\, s_i = {}^{o}P_i - {}^{o}B_i - \mathrm{u_i}\, n_i$$

$$= \begin{bmatrix} -R_p \cos\theta_i \sin\theta_y \\ R_p \sin\theta_i \sin\theta_x - R_p \cos\theta_i \cos\theta_x \cos\theta_y \\ z_e + R_p \cos\theta_x \sin\theta_i + R_p \cos\theta_i \cos\theta_y \sin\theta_x \end{bmatrix} - \begin{bmatrix} R_b \cos\alpha_i \\ R_b \sin\alpha_i \\ 0 \end{bmatrix} - \mathrm{u_i} \begin{bmatrix} -\cos\alpha_i \\ -\sin\alpha_i \\ 0 \end{bmatrix} \quad (18)$$

$$= \begin{bmatrix} -R_p \cos\theta_i \sin\theta_y - R_b \cos\alpha_i + \mathrm{u_i} \cos\alpha_i \\ R_p \sin\theta_i \sin\theta_x - R_p \cos\theta_i \cos\theta_x \cos\theta_y - R_b \sin\alpha_i + \mathrm{u_i} \sin\alpha_i \\ z_e + R_p \cos\theta_x \sin\theta_i + R_p \cos\theta_i \cos\theta_y \sin\theta_x \end{bmatrix} = \begin{bmatrix} l_{ix} \\ l_{iy} \\ l_{iz} \end{bmatrix}$$

Dot multiplying equation (18) with itself yields the following:

$$\mathrm{l_i}^2 = ({}^{o}P_i - {}^{o}B_i - \mathrm{u_i}\, n_i)^T ({}^{o}P_i - {}^{o}B_i - \mathrm{u_i}\, n_i) = {l_{ix}}^2 + {l_{iy}}^2 + {l_{iz}}^2 \quad (19)$$

From equation (19), the following is achieved:

$$\mathrm{u_i} = \frac{-(2A\cos\alpha_i + 2B\sin\alpha_i) \pm \sqrt{(2A\cos\alpha_i + 2B\sin\alpha_i)^2 - 4(A^2 + B^2 + C^2 - \mathrm{l_i}^2)}}{2} \quad (20)$$

where

$A = -R_p \cos\theta_i \sin\theta_y - R_b \cos\alpha_i$,

$B = R_p \sin\theta_i \sin\theta_x - R_p \cos\theta_i \cos\theta_x \cos\theta_y - R_b \sin\alpha_i$,

$C = z_e + R_p \cos\theta_x \sin\theta_i + R_p \cos\theta_i \cos\theta_y \sin\theta_x$

3.3.2. Jacobian of the Mechanism

By combining equations (14) and (19), the following equation can be obtained:

$$\mathrm{l_i}^2 = (x_{pi}^o - R_b \cos\alpha_i + \mathrm{u_i} \cos\alpha_i)^2 + (y_{pi}^o - R_b \sin\alpha_i + \mathrm{u_i} \sin\alpha_i)^2 + (z_{pi}^o)^2 \quad (21)$$

Taking the derivative of equation (21) with respect to x_{pi}^o, yields:

$$\partial u_i(l_{ix}\cos\alpha_i + l_{iy}\sin\alpha_i) = -l_{ix}\partial x_{pi}^o \tag{22}$$

Taking the derivative of equation (21) with respect to y_{pi}^o, yields:

$$\partial u_i(l_{ix}\cos\alpha_i + l_{iy}\sin\alpha_i) = -l_{iy}\partial y_{pi}^o \tag{23}$$

Taking the derivative of equation (21) with respect to z_{pi}^o, yields:

$$\partial u_i(l_{ix}\cos\alpha_i + l_{iy}\sin\alpha_i) = -z_{pi}^o\partial z_{pi}^o \quad (z_{pi}^o = l_{iz}) \tag{24}$$

We set $k_{ip} = l_{ix}\cos\alpha_i + l_{iy}\sin\alpha_i$; the above three equations can then be written as:

$$\partial u_i = -\frac{l_{ix}}{k_{ip}}\partial x_{pi}^o,\ \partial u_i = -\frac{l_{iy}}{k_{ip}}\partial y_{pi}^o, \partial u_i = -\frac{l_{iz}}{k_{ip}}\partial z_{pi}^o \tag{25}$$

From equation (25), the following is obtained:

$$3\partial u_i = -\frac{l_{ix}}{k_{ip}}\partial x_{pi}^o - \frac{l_{iy}}{k_{ip}}\partial y_{pi}^o - \frac{l_{iz}}{k_{ip}}\partial z_{pi}^o \tag{26}$$

and

$$\partial u_i = \begin{bmatrix}\partial u_1\\ \partial u_2\\ \partial u_3\end{bmatrix}$$

$$= \frac{1}{3}\begin{bmatrix}-\frac{l_{ix}}{k_{ip}} & -\frac{l_{iy}}{k_{ip}} & -\frac{l_{iz}}{k_{ip}}\end{bmatrix}\cdot\begin{bmatrix}\partial x_{pi}^o\\ \partial y_{pi}^o\\ \partial z_{pi}^o\end{bmatrix}$$

$$= \frac{1}{3}\begin{bmatrix}-\frac{l_{ix}}{k_{ip}} & -\frac{l_{iy}}{k_{ip}} & -\frac{l_{iz}}{k_{ip}}\end{bmatrix}\cdot[J_i]\begin{bmatrix}\delta\theta_x\\ \delta\theta_y\\ \delta\theta_z\\ \delta x\\ \delta y\\ \delta z_e\end{bmatrix} = J_{parallel}\begin{bmatrix}\delta\theta_x\\ \delta\theta_y\\ \delta\theta_z\\ \delta x\\ \delta y\\ \delta z_e\end{bmatrix} \tag{27}$$

where $J_{parallel} = \frac{1}{3}\begin{bmatrix} \begin{bmatrix} -\frac{l_{1x}}{k_{1p}} & -\frac{l_{1y}}{k_{1p}} & -\frac{l_{1z}}{k_{1p}} \end{bmatrix}[J_1] \\ \begin{bmatrix} -\frac{l_{2x}}{k_{2p}} & -\frac{l_{2y}}{k_{2p}} & -\frac{l_{2z}}{k_{2p}} \end{bmatrix}[J_2] \\ \begin{bmatrix} -\frac{l_{3x}}{k_{3p}} & -\frac{l_{3y}}{k_{3p}} & -\frac{l_{3z}}{k_{3p}} \end{bmatrix}[J_3] \end{bmatrix}$

The twist of the moving platform is presented as $t = \begin{bmatrix} \delta\theta_x & \delta\theta_y & \delta\theta_z & \delta x & \delta y & \delta z_e \end{bmatrix}^T$, and

$$\begin{bmatrix} \delta l_1 \\ \delta l_2 \\ \delta l_3 \end{bmatrix} = \begin{bmatrix} \begin{bmatrix} \frac{l_{1x}}{l_1} & \frac{l_{1y}}{l_1} & \frac{l_{1z}}{l_1} \end{bmatrix}[J_1] \\ \begin{bmatrix} \frac{l_{2x}}{l_2} & \frac{l_{2y}}{l_2} & \frac{l_{2z}}{l_2} \end{bmatrix}[J_2] \\ \begin{bmatrix} \frac{l_{3x}}{l_3} & \frac{l_{3y}}{l_3} & \frac{l_{3z}}{l_3} \end{bmatrix}[J_3] \end{bmatrix} \cdot \begin{bmatrix} \delta\theta_x \\ \delta\theta_y \\ \delta\theta_z \\ \delta x \\ \delta y \\ \delta z_e \end{bmatrix} = J_{co} \cdot \begin{bmatrix} \delta\theta_x \\ \delta\theta_y \\ \delta\theta_z \\ \delta x \\ \delta y \\ \delta z_e \end{bmatrix} \quad (28)$$

The central passive leg can be viewed as a serial component. The kinematic structure of the central passive leg is illustrated in Figure 3.3 (b), from which the D-H parameters of the passive leg are obtained, as seen in Table 3.1.

Table 3.1. D-H parameters for the central passive leg

i	a_i	d_i	α_i	θ_i
0	0	0	0	0
1	0	z_e	90°	-90°
2	0	0	90°	θ_x
3	0	0	-90°	θ_y

Thus

$$Q_0 = \begin{bmatrix} 1 & 0 & 0 \\ 0 & 1 & 0 \\ 0 & 0 & 1 \end{bmatrix} \tag{29}$$

$$Q_1 = \begin{bmatrix} 0 & 0 & -1 \\ -1 & 0 & 0 \\ 0 & 1 & 0 \end{bmatrix} \tag{30}$$

$$Q_2 = \begin{bmatrix} \cos\theta_x & 0 & \sin\theta_x \\ \sin\theta_x & 0 & -\cos\theta_x \\ 0 & 1 & 0 \end{bmatrix} \tag{31}$$

$$Q_3 = \begin{bmatrix} \cos\theta_y & 0 & -\sin\theta_y \\ \sin\theta_y & 0 & \cos\theta_y \\ 0 & -1 & 0 \end{bmatrix} \tag{32}$$

where Q_i is the rotation matrix from the i^{th} frame to the $(i+1)^{th}$ frame of the passive leg. The following equations can then be obtained through equation (29) [118]:

$$e_{41} = Q_0 e_{40} \tag{33}$$

$$e_{42} = Q_0 Q_1 e_{40} \tag{34}$$

$$e_{43} = Q_0 Q_1 Q_2 e_{40} \tag{35}$$

where e_{4i} is the third column of the rotation matrix $Q_0 Q_1 \cdots Q_{i-1}$ and $e_{40} = \begin{bmatrix} 0 & 0 & 1 \end{bmatrix}^T$. The position vectors are expressed as follows:

$$r_{41} = Q_0 a_{41} + Q_0 Q_1 a_{42} + Q_0 Q_1 Q_2 a_{43} \tag{36}$$

$$r_{42} = Q_0 Q_1 a_{42} + Q_0 Q_1 Q_2 a_{43} \tag{37}$$

$$r_{43} = Q_0 Q_1 Q_2 a_{43} \tag{38}$$

where $a_{41} = \begin{bmatrix} 0 & 0 & z_e \end{bmatrix}^T$, $a_{42} = \begin{bmatrix} 0 & 0 & 0 \end{bmatrix}^T$ and $a_{43} = \begin{bmatrix} 0 & 0 & 0 \end{bmatrix}^T$. For the passive leg, we have:

$$J_{serial}\,\dot{\theta}_4 = t \tag{39}$$

where $\dot{\theta}_4 = \begin{bmatrix} \dot{z}_e & \dot{\theta}_x & \dot{\theta}_y \end{bmatrix}$. The Jacobian matrix of the passive limb of the manipulator J_{serial} can be expressed as follows:

$$J_{serial} = \begin{bmatrix} zeros(3,1) & e_{42} & e_{43} \\ e_{41} & e_{42} \times r_{42} & e_{43} \times r_{43} \end{bmatrix} \tag{40}$$

The Jacobian matrix of the whole mechanism can be written as [114]:

$$J = J_{parallel} J_{serial} \tag{41}$$

3.4. Compliance Modeling and Single-Objective Optimization

3.4.1. Kinetostatic Modeling

The general derivation process of the Cartesian compliance matrix is as follows. Based on the principle of virtual work [118], the following equation is obtained:

$$(J_{co} J_{serial})^T \tau = J_{serial}{}^T w \tag{42}$$

where τ is the vector of actuator forces, w is the force or torque applied to the moving platform. An actuator compliance matrix C is defined as:

$$C\tau = \Delta\rho \tag{43}$$

where $\Delta\rho$ is the joint displacement. Equation (42) can be rewritten as follows:

$$\Delta\rho = C(J_{co} J_{serial})^{-T} J_{serial}{}^T w \tag{44}$$

Further, for a small displacement vector $\Delta\rho$, one obtains:

$$\Delta\rho = J_{co}\Delta c \tag{45}$$

where Δc is a vector of small Cartesian displacement and rotation [118]. By plugging equation (45) into (44), and rearranging the equation, the following can be derived:

$$\Delta c = J_{serial}(J_{co}J_{serial})^{-1}C(J_{co}J_{serial})^{-T}J_{serial}{}^{T}w \tag{46}$$

Thus the Cartesian compliance matrix is naturally obtained as follows:

$$C_c = J_{serial}(J_{co}J_{serial})^{-1}C(J_{co}J_{serial})^{-T}J_{serial}{}^{T} \tag{47}$$

where C_c is a symmetric positive semi-definite (6×6) matrix. The reason why we use the compliance matrix rather than the stiffness matrix in the above derivation is that matrix C_c is not invertible, which is why it is more convenient to employ the compliance matrix [118].

3.4.2. Single-Objective Optimization

In order to implement the optimization process, the objective function should be first established. In order to minimize the compliance, the trace of the Cartesian compliance is used as the objective function.

(1). Objective function:

$$ObjF = \sum_{i=1}^{6} C_c(i,i) \tag{48}$$

(2). Design variables:

$$D = [R_P, R_b, L, angle1, angle2]$$

where L is the length of the fixed link on the U* joint. Here we assume that each U* joint is the same, i.e. $\mathrm{l}_1 = \mathrm{l}_2 = \mathrm{l}_3 = L$.

(3). Constraints:

Here we assume the following constraints for the purpose of analysis:

$$R_P \in [0.04, 0.15]m, R_b \in [0.4, 0.6]m, \mathrm{l}_\mathrm{i} \in [0.35, 0.5]m, angle1 \in [15^\circ, 45^\circ], angle2 \in [15^\circ, 45^\circ]$$

The optimization is performed under the following configuration:

$$\alpha_1 = angle1,\ \alpha_2 = angle1 + 120^\circ,\ \alpha_3 = angle1 + 240^\circ \tag{49}$$

$$\theta_1 = angle2,\ \theta_2 = angle2 + 120^\circ,\ \theta_3 = angle2 + 240^\circ \tag{50}$$

$$\theta_x = 90^\circ,\ \theta_y = -90^\circ,\ z_e = 0.3 \tag{51}$$

The following results are obtained by using a differential evolution (DE) optimization algorithm with the following parameters: population size: 75; maximum of generations: 100; crossover ratio: 1; mutation function: constraint dependent.

The optimal parameters are obtained after about 50 generations. The optimum value for the objective function is 0.08111. The result of the global compliance optimization is illustrated in Figure 3.4. In order to have the minimum global compliance for the mechanism, the moving platform's radius should be 0.15m, the radius of the base should be 0.57m, the length of the fixed link should be 0.35m, the angle between the X axis and line OB_i should be 0.27rad, and the angle between the x axis and line PP_i should be 0.29rad, as listed in Table 3.2. After running DE four times, we obtain the same results as shown in Figure 3.5.

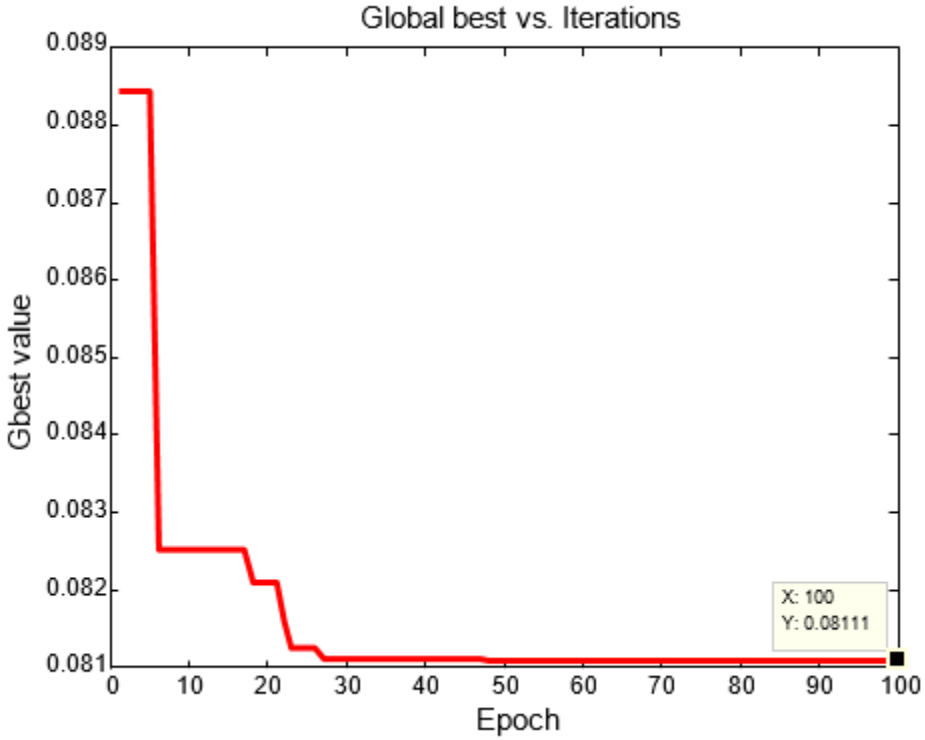

Figure 3.4. Optimization result of global compliance using DE

Table 3.2. The corresponding optimal parameters

R_P	R_b	L	$angle1$	$angle2$
0.15m	0.5716m	0.35m	0.274rad	0.2995rad

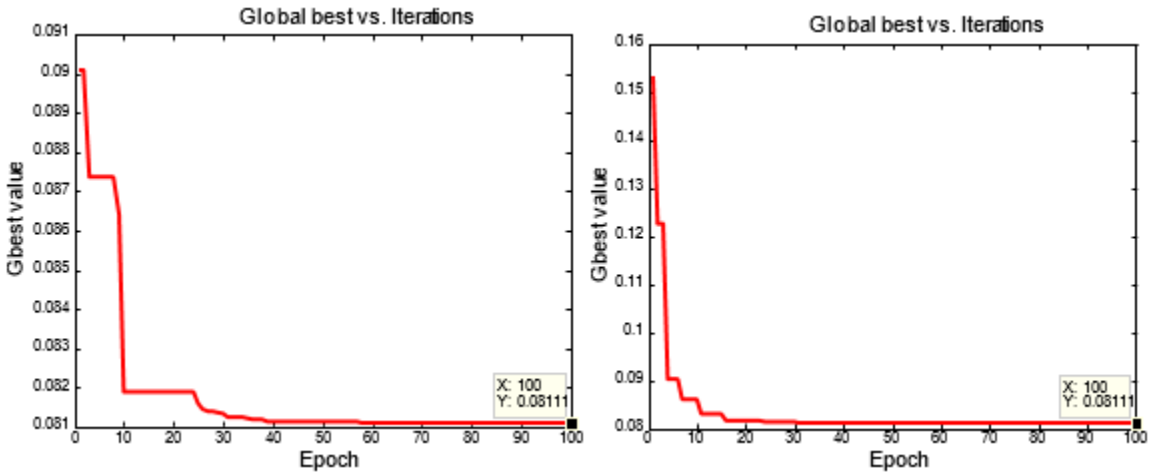

(a) First time run (b) Second time run

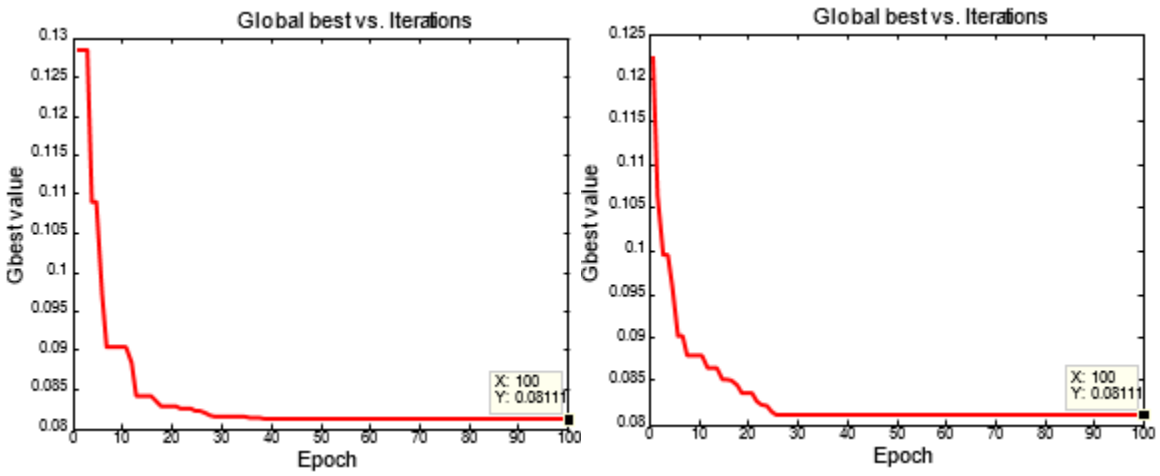

(c) Third time run (d) Fourth time run

Figure 3.5. Optimization result of global compliance

We can achieve the same results by using a genetic algorithm with the same tuning parameters. Figure 3.6 shows a plot of the best function values in each generation versus the iteration number. The black points (bottom points) represent the best fitness values and the blue points (top points) represent the mean fitness values in each generation. The optimal parameters are obtained after 51 generations.

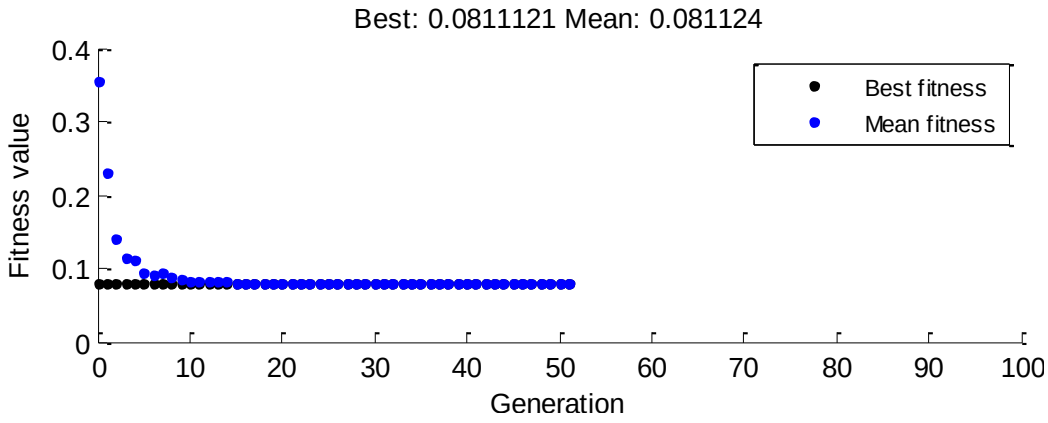

Figure 3.6. Optimization result of global compliance using GA

The optimum value for the objective function is 0.08. The results imply that, in order to obtain the minimum global compliance for the mechanism, the radius of the platform needs to be 0.15m, the radius of the base needs to be 0.57m, the length of the fixed link needs to 0.35m, the angle between the X axis and line OB_i should be 0.27rad, and the angle between the x axis and line PP_i should be 0.28rad, as listed in Table 3.3.

Table 3.3. The corresponding optimal parameters

R_P	R_b	L	$angle1$	$angle2$
0.15m	0.57m	0.35m	0.27rad	0.28rad

After optimization, we select the optimized solutions as above, and the compliance matrix is:

$$C_c = \begin{bmatrix} 0.0403 & 0 & 0 & 0 & 0 & 0 \\ 0 & 0.0403 & 0 & 0 & 0 & 0 \\ 0 & 0 & 0 & 0 & 0 & 0 \\ 0 & 0 & 0 & 0 & 0 & 0 \\ 0 & 0 & 0 & 0 & 0 & 0 \\ 0 & 0 & 0 & 0 & 0 & 0.0005 \end{bmatrix} \tag{52}$$

The compliance sum is 0.0811. Before optimization, $R_P = 0.1$, $R_b = 0.3$, $L = 0.4$, $angle1 = 30^\circ$, $angle2 = 30^\circ$, the compliance matrix is as follows:

$$C_c = \begin{bmatrix} 0.1185 & 0 & 0 & 0 & 0 & 0 \\ 0 & 0.1185 & 0 & 0 & 0 & 0 \\ 0 & 0 & 0 & 0 & 0 & 0 \\ 0 & 0 & 0 & 0 & 0 & 0 \\ 0 & 0 & 0 & 0 & 0 & 0 \\ 0 & 0 & 0 & 0 & 0 & 0.0006 \end{bmatrix} \tag{53}$$

The compliance sum is 0.2376. After optimization, the compliance sum has improved approximately 2.9 times.

3.4.3. Global Condition Index of the Mechanism

One of the disadvantages of parallel mechanisms is that they normally have a smaller workspace. As a result, many researchers tried to maximize the workspace to make it larger, but it was found that making the parallel manipulators to have the maximum workspace volume could sometimes lead to poor kinematic performances. The global condition index [119] was later proposed for workspace optimization in order to have a so-called "well-conditioned workspace". Here the index is used as an objective function for workspace optimization. The derivation process for the index is briefly described as follows: firstly, many points n_{total} are randomly picked in the possible workspace; secondly, one needs to determine if each point is inside of the workspace. This can be carried out by finding the inverse kinematic for each actuated input to identify if the prismatic joint is in the range of the guide ways. Thirdly, one determines the kinematics condition index KCI, which is the summation of the reciprocal of the condition number of the Jacobian matrix for each point that falls inside the workspace. Finally, the global condition index η can be obtained by multiplying KCI and the possible workspace volume(pwv), then dividing by the total number of previously selected points n_{total} :

$$\eta = pwv \cdot KCI / n_{total} \tag{54}$$

Therefore, the objective function for workspace optimization is η . The greater the value, the better the workspace of the mechanism. One can use GA, DE or PSO to single

optimize the global condition index to achieve a maximum well-conditioned workspace. However, rather than using this method, we are going directly to the multi-objective optimization for the stiffness and workspace due to the fact that these normally conflict with each other.

3.5. Multi-objective Optimization

3.5.1. Establishment of Objective Functions

Normally, when the stiffness of the parallel manipulator increases, its workspace will be decreased, and vice versa, i.e. these two conflict with one another. One should always compromise between these two and find an optimal solution based on specific design requirements and preferences.

1. Objective functions:

Here the objective functions for the compliance/stiffness and workspace are as follows, respectively. The objective function for stiffness can be written as the summation of the main leading diagonal elements of the compliance matrix, i.e. global compliance,

$$ObjF1 = \sum_{i=1}^{6} C_c(i,i) \tag{55}$$

Since lower compliance means higher level of stiffness, our purpose is to minimize the global compliance. As an alternative, we can use the sum of the mean value and standard deviation of the leading diagonal elements of the compliance matrix as the objective function. The mean value can represent the average compliance over the workspace, and the standard deviation indicates the compliance fluctuation. Generally, the smaller the

mean value, the less the deformation; the smaller the standard deviation, the more uniform the compliance distribution throughout the workspace [120].

The objective function for the workspace is the global condition index:

$$\eta = \frac{\pi \cdot R_P^2 \cdot (h_{\max} - h_{\min}) \cdot KCI}{n_{total}} \tag{56}$$

2. Design variables:

$$D = [R_P, R_b, L, angle1, angle2]$$

3. Constraints:

$$R_P \in [0.04, 0.15]m, R_b \in [0.4, 0.6]m, \mathrm{l_i} \in [0.35, 0.5]m, angle1 \in [15^\circ, 45^\circ], angle2 \in [15^\circ, 45^\circ]$$

3.5.2. Optimization Process

The problem was solved by using the gamultiobj solver in matlab with the following parameters, as listed in Table 3.4.

Table 3.4. Optimization parameters

Population size	75
Maximum of generations	100
Selection strategy	Tournament
Tournament size	2
Crossover type	Intermediate
Crossover ratio	1
Mutation function	constraint dependent
Pareto Front population fraction	0.35

After optimization, the Pareto Front of compliance and workspace is illustrated in Figure 3.7, from which can be seen the compliance sum and global condition index conflict. This means that if one wants to have a higher level of stiffness, one has to sacrifice the workspace, hence the results are compromised.

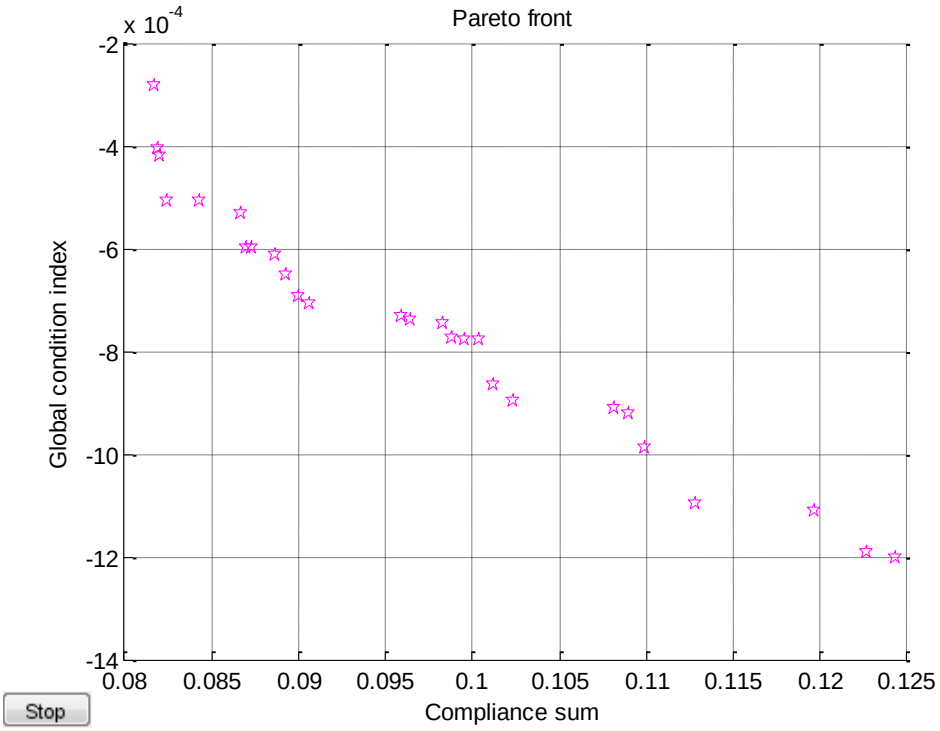

Figure 3.7. Pareto Front of compliance and workspace

One can see that there is no single optimum value. There is not just one optimal solution but rather several solutions, which are called non-dominated solutions. Based on our requirements, we can select from those results. Different requirements may cause one to select different values; i.e. if we want a higher level of stiffness and the workspace is not important, we can then select the larger value for stiffness and sacrifice some

workspace. Here, we give four typical results for the objective function and the corresponding design variables, as shown in Table 3.5.

Table 3.5. Typical results for objective functions and the corresponding design variables

R_P	R_b	L	$angle1$	$angle2$	Compliance Sum	Global condition index
0.1491	0.4153	0.3547	0.3721	0.3735	0.0843	-0.0005
0.1489	0.4174	0.3881	0.3997	0.3656	0.1012	-0.0008
0.1498	0.4162	0.3619	0.3795	0.3733	0.0870	-0.0005
0.1486	0.4192	0.4265	0.4237	0.3746	0.1227	-0.0012

3.5.3. Results Analysis

After optimization, R_P=0.1491, R_b=0.4153, L=0.3547, $angle1$=0.3721, $angle2$=0.3735 are selected, the compliance matrix is then as follows:

$$C_c = \begin{bmatrix} 0.0419 & 0 & 0 & 0 & 0 & 0 \\ 0 & 0.0419 & 0 & 0 & 0 & 0 \\ 0 & 0 & 0 & 0 & 0 & 0 \\ 0 & 0 & 0 & 0 & 0 & 0 \\ 0 & 0 & 0 & 0 & 0 & 0 \\ 0 & 0 & 0 & 0 & 0 & 0.0005 \end{bmatrix} \tag{57}$$

The compliance sum is 0.0843.

Before optimization, we select R_P=0.06, R_b=0.5, L=0.4, $angle1$=0.523, $angle2$ =0.523, thus the compliance matrix is as follows:

$$C_c = \begin{bmatrix} 0.3292 & 0 & 0 & 0 & 0 & 0 \\ 0 & 0.3292 & 0 & 0 & 0 & 0 \\ 0 & 0 & 0 & 0 & 0 & 0 \\ 0 & 0 & 0 & 0 & 0 & 0 \\ 0 & 0 & 0 & 0 & 0 & 0 \\ 0 & 0 & 0 & 0 & 0 & 0.0006 \end{bmatrix} \tag{58}$$

The compliance sum is 0.6590. One can see that after optimization the compliance is decreased, which means the stiffness has increased.

After optimization, the real path generated by the attachment point P_1 on the moving platform is shown in Figure 3.9. The reason we plotted the path generated by the attachment point P_1 on the moving platform, instead of the workspace, is because the definition of the workspace is normally the region to which the center of the moving platform can reach. However, this manipulator has two rotational motions about the X and Y axes and one translational motion along the Z axis. Due to the fact that the universal joint on the passive leg is fixed at the center of the moving platform, the path, to which the center of the moving platform can reach, is a straight line, as shown in Figure 3.8.

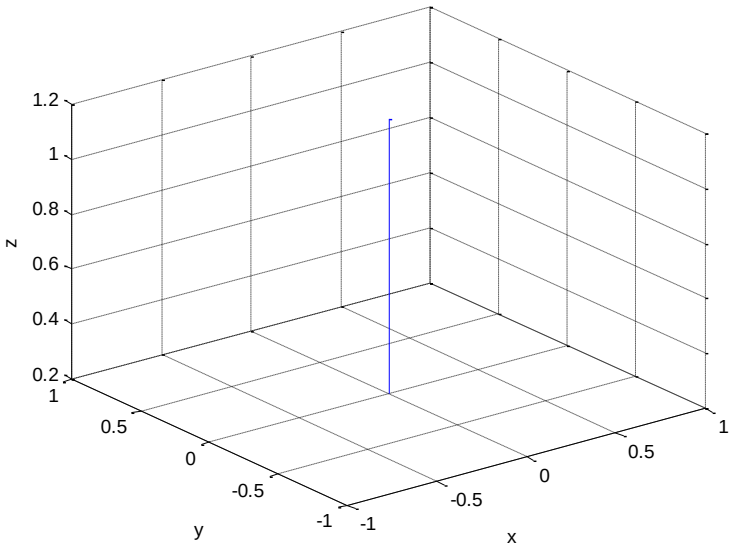

Figure 3.8. Path of the moving platform center

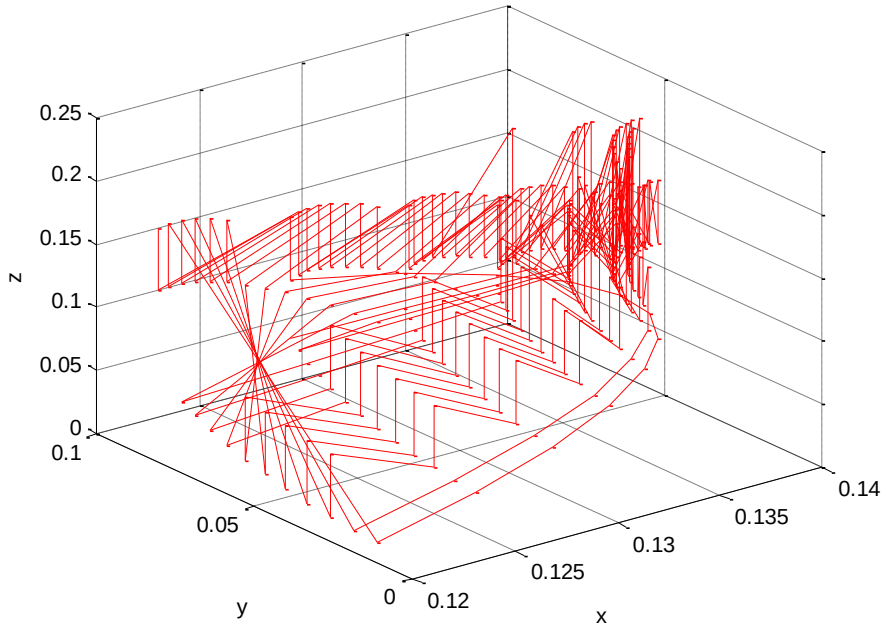

Figure 3.9. Path of point P_1 after optimization

Before optimization, the path that the attachment point P_1 on the moving platform generated is shown in Figure 3.10.

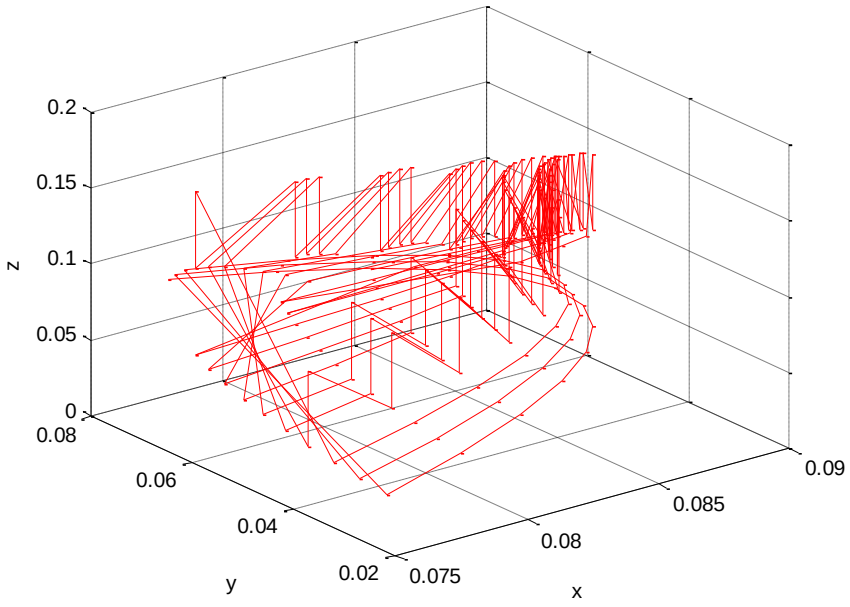

Figure 3.10. Path of point P_1 before optimization

The green path (right hand side) in Figure 3.11 represents the result after optimization, and the red path (left hand side) represents the result before optimization. It can be seen that the point P_1 on the moving platform can extend further after optimization.

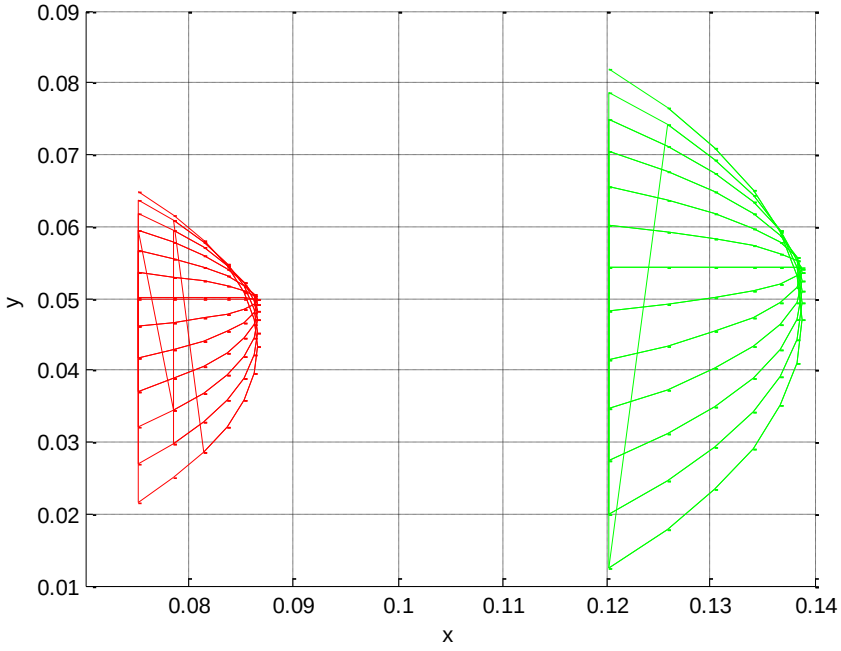

(a). XY view

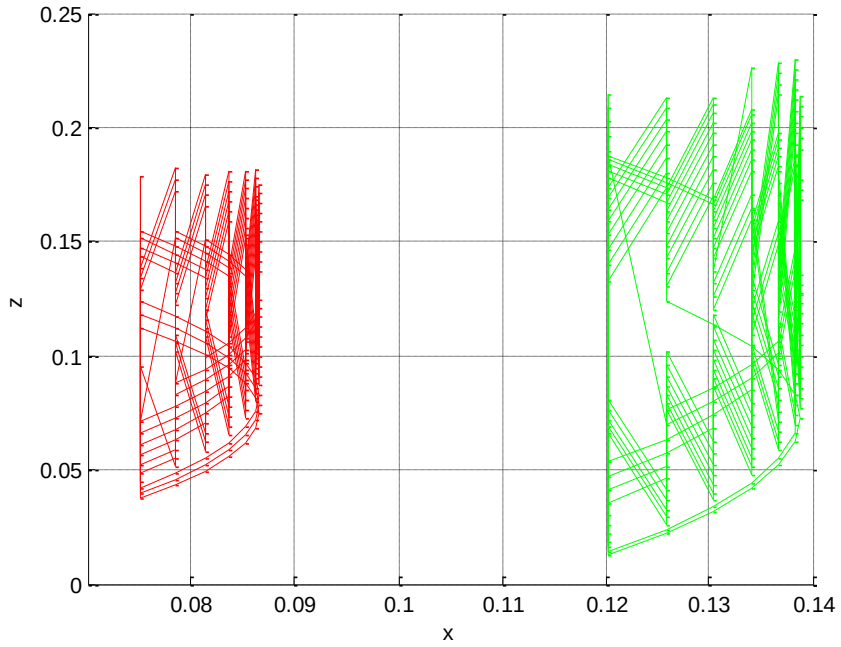

(b). XZ view

Figure 3.11. Path comparison of point P_1 before and after optimization

3.6. Dynamics of the Mechanism

In this section, the dynamics of the 3PU*S-PU hybrid manipulator are analyzed by resorting to the Lagrangian method, the results of which will be used as a guideline for controlling the manipulator. In this manipulator, u_1, u_2 and u_3 are the actuated joints. Normally, the Lagrangian equations are arranged into two sets [121]: the first set contains the Lagrange multiplier and the second set contains the actuator forces. The first set of equations can be written as follows:

$$\sum_{i=1}^{3} \lambda_i \frac{\partial \Delta_i}{\partial q_j} = \frac{d}{dt}\left(\frac{\partial L}{\partial \dot{q}_j}\right) - \frac{\partial L}{\partial q_j} - F_j \tag{59}$$

where F_j is the external applied force, λ_i is the Lagrangian multiplier, and Δ_i is the i^{th} constraint function. By writing equation (59) for θ_x, θ_y and z_e, one can have three equations, and these three equations can be solved for three Lagrangian multipliers. Once the multipliers are determined, the actuator forces can be solved from the second set of equations, given as follows:

$$Q_j = \frac{d}{dt}\left(\frac{\partial L}{\partial \dot{q}_j}\right) - \frac{\partial L}{\partial q_j} - \sum_{i=1}^{3} \lambda_i \frac{\partial \Delta_i}{\partial q_j} \tag{60}$$

where Q_j is the actuator force. The constraint equations can be obtained as follows:

$$\Delta_i = \left|D_i E_i\right|^2 - \mathrm{l_i}^2$$

$$\begin{aligned} &= (-R_p \cos\theta_i \sin\theta_y - R_b \cos\alpha_i + \mathrm{u_i} \cos\alpha_i)^2 \\ &+(R_p \sin\theta_i \sin\theta_x - R_p \cos\theta_i \cos\theta_x \cos\theta_y - R_b \sin\alpha_i + \mathrm{u_i} \sin\alpha_i)^2 \\ &+(z_e + R_p \cos\theta_x \sin\theta_i + R_p \cos\theta_i \cos\theta_y \sin\theta_x)^2 - \mathrm{l_i}^2 \end{aligned} \tag{61}$$

$$= 0$$

The total kinetic energy of the parallel manipulator is:

$$K = K_p + \sum_{i=1}^{3} K_{bi} + K_a \tag{62}$$

where K_p is the kinetic energy of the moving platform, K_{bi} is the kinetic energy of the U* link of limb i, and K_a is the kinetic energy of the middle passive limb. The total potential energy of the parallel manipulator is as follows:

$$U = U_p + \sum_{i=1}^{3} U_{bi} + U_a \tag{63}$$

where U_p is the potential energy of the moving platform, U_{bi} is the potential energy of the U* link of the i^{th} limb, and U_a is the potential energy of the middle passive leg.

The Lagrangian function L can be obtained as follows:

$$\begin{aligned} L = &\frac{1}{2} m_p \dot{z}_e^{\,2} + \frac{3}{2} m_b \dot{z}_e^{\,2} + \frac{1}{2} m_b (\dot{u}_1^{\,2} + \dot{u}_2^{\,2} + \dot{u}_3^{\,2}) + \frac{3}{2} m_a \dot{z}_e^{\,2} \\ &-m_p z_e g - 3 m_b z_e g - m_b R_p \cos\theta_x (\sin\theta_1 + \sin\theta_2 + \sin\theta_3) g \\ &-m_b R_p \cos\theta_y \sin\theta_x (\cos\theta_1 + \cos\theta_2 + \cos\theta_3) g - \frac{3}{2} m_a z_e g \end{aligned} \tag{64}$$

where m_p is the mass of the moving platform, m_b is the mass of the U* link, and m_a is the mass of the middle passive limb. Taking the derivatives of the Lagrangian function

with respect to the six generalized coordinates θ_x, θ_y, z_e, u_1, u_2 and u_3, one obtains the following:

$$\frac{\partial L}{\partial \theta_x} = m_b g R_p \sin\theta_x(\sin\theta_1 + \sin\theta_2 + \sin\theta_3) - m_b g R_p \cos\theta_y \cos\theta_x(\cos\theta_1 + \cos\theta_2 + \cos\theta_3);$$

$$\frac{d}{dt}(\frac{\partial L}{\partial \dot{\theta}_x}) = 0;\ \frac{\partial L}{\partial \theta_y} = m_b g R_p \sin\theta_y \sin\theta_x(\cos\theta_1 + \cos\theta_2 + \cos\theta_3);\ \frac{d}{dt}(\frac{\partial L}{\partial \dot{\theta}_y}) = 0;$$

$$\frac{\partial L}{\partial z_e} = -m_p g - 3m_b g - \frac{3}{2} m_a g;\ \frac{d}{dt}(\frac{\partial L}{\partial \dot{z}_e}) = m_p \ddot{z}_e + 3m_b \ddot{z}_e + 3m_a \ddot{z}_e;\ \frac{\partial L}{\partial u_1} = 0;$$

$$\frac{d}{dt}(\frac{\partial L}{\partial \dot{u}_1}) = m_b \ddot{u}_1;\ \frac{\partial L}{\partial u_2} = 0;\ \frac{d}{dt}(\frac{\partial L}{\partial \dot{u}_2}) = m_b \ddot{u}_2;\ \frac{\partial L}{\partial u_3} = 0;\ \frac{d}{dt}(\frac{\partial L}{\partial \dot{u}_3}) = m_b \ddot{u}_3$$

Taking the partial derivatives of Δ_i with respect to θ_x, θ_y, z_e, u_1, u_2 and u_3, one obtains the following:

$$\frac{\partial \Delta_i}{\partial \theta_x} = 2(R_p \sin\theta_i \sin\theta_x - R_p \cos\theta_i \cos\theta_x \cos\theta_y - R_b \sin\alpha_i + \mathrm{u_i} \sin\alpha_i)(R_p \sin\theta_i \cos\theta_x + R_p \cos\theta_i \sin\theta_x \cos\theta_y)$$
$$+2(z_e + R_p \cos\theta_x \sin\theta_i + R_p \cos\theta_i \cos\theta_y \sin\theta_x)(-R_p \sin\theta_x \sin\theta_i + R_p \cos\theta_i \cos\theta_y \cos\theta_x)$$

$$\frac{\partial \Delta_i}{\partial \theta_y} = 2(-R_p \cos\theta_i \sin\theta_y - R_b \cos\alpha_i + \mathrm{u_i} \cos\alpha_i)(-R_p \cos\theta_i \cos\theta_y)$$
$$+2(R_p \sin\theta_i \sin\theta_x - R_p \cos\theta_i \cos\theta_x \cos\theta_y - R_b \sin\alpha_i + \mathrm{u_i} \sin\alpha_i)(R_p \cos\theta_i \cos\theta_x \sin\theta_y)$$
$$+2(z_e + R_p \cos\theta_x \sin\theta_i + R_p \cos\theta_i \cos\theta_y \sin\theta_x)(-R_p \cos\theta_i \sin\theta_y \sin\theta_x)$$

$$\frac{\partial \Delta_i}{\partial z_e} = 2(z_e + R_p \cos\theta_x \sin\theta_i + R_p \cos\theta_i \cos\theta_y \sin\theta_x)$$

$$\frac{\partial \Delta_1}{\partial u_1} = 2(-R_p \cos\theta_1 \sin\theta_y - R_b \cos\alpha_1 + \mathrm{u_1} \cos\alpha_1)(\cos\alpha_1)$$
$$+2(R_p \sin\theta_1 \sin\theta_x - R_p \cos\theta_1 \cos\theta_x \cos\theta_y - R_b \sin\alpha_1 + \mathrm{u_1} \sin\alpha_1)\sin\alpha_1$$

$$\frac{\partial \Delta_i}{\partial u_1} = 0 \qquad (i = 2,3)$$

$$\frac{\partial \Delta_i}{\partial u_2} = 0 \qquad (i = 1,3)$$

$$\frac{\partial \Delta_2}{\partial u_2} = 2(-R_p \cos\theta_2 \sin\theta_y - R_b \cos\alpha_2 + \mathrm{u}_2 \cos\alpha_2)(\cos\alpha_2)$$
$$+2(R_p \sin\theta_2 \sin\theta_x - R_p \cos\theta_2 \cos\theta_x \cos\theta_y - R_b \sin\alpha_2 + \mathrm{u}_2 \sin\alpha_2)(\sin\alpha_2)$$

$$\frac{\partial \Delta_i}{\partial u_3} = 0 \qquad (i = 1,2)$$

$$\frac{\partial \Delta_3}{\partial u_3} = 2(-R_p \cos\theta_3 \sin\theta_y - R_b \cos\alpha_3 + \mathrm{u}_3 \cos\alpha_3)(\cos\alpha_3)$$
$$+2(R_p \sin\theta_3 \sin\theta_x - R_p \cos\theta_3 \cos\theta_x \cos\theta_y - R_b \sin\alpha_3 + \mathrm{u}_3 \sin\alpha_3)(\sin\alpha_3)$$

Plugging the obtained derivatives into equations (59) and (60), the following dynamic equations are obtained:

$$\begin{aligned} &2\sum_{i=1}^{3} \lambda_i [(R_p \sin\theta_i \sin\theta_x - R_p \cos\theta_i \cos\theta_x \cos\theta_y - R_b \sin\alpha_i + \mathrm{u}_i \sin\alpha_i)(R_p \sin\theta_i \cos\theta_x + R_p \cos\theta_i \sin\theta_x \cos\theta_y) \\ &+(z_e + R_p \cos\theta_x \sin\theta_i + R_p \cos\theta_i \cos\theta_y \sin\theta_x)(-R_p \sin\theta_x \sin\theta_i + R_p \cos\theta_i \cos\theta_y \cos\theta_x)] \\ &= -(m_b g R_p \sin\theta_x (\sin\theta_1 + \sin\theta_2 + \sin\theta_3) - m_b g R_p \cos\theta_y \cos\theta_x (\cos\theta_1 + \cos\theta_2 + \cos\theta_3)) - f_{px} \end{aligned} \tag{65}$$

$$\begin{aligned} &2\sum_{i=1}^{3} \lambda_i [(-R_p \cos\theta_i \sin\theta_y - R_b \cos\alpha_i + \mathrm{u}_i \cos\alpha_i)(-R_p \cos\theta_i \cos\theta_y) \\ &+(R_p \sin\theta_i \sin\theta_x - R_p \cos\theta_i \cos\theta_x \cos\theta_y - R_b \sin\alpha_i + \mathrm{u}_i \sin\alpha_i)(R_p \cos\theta_i \cos\theta_x \sin\theta_y) \\ &+(z_e + R_p \cos\theta_x \sin\theta_i + R_p \cos\theta_i \cos\theta_y \sin\theta_x)(-R_p \cos\theta_i \sin\theta_y \sin\theta_x)] \\ &= -m_b g R_p \sin\theta_y \sin\theta_x (\cos\theta_1 + \cos\theta_2 + \cos\theta_3) - f_{py} \end{aligned} \tag{66}$$

$$\begin{aligned} &2\sum_{i=1}^{3} \lambda_i (z_e + R_p \cos\theta_x \sin\theta_i + R_p \cos\theta_i \cos\theta_y \sin\theta_x) \\ &= m_p \ddot{z}_e + 3m_b \ddot{z}_e + 3m_a \ddot{z}_e - (-m_p g - 3m_b g - \frac{3}{2} m_a g) - f_{pz} \end{aligned} \tag{67}$$

Thus,

$$\begin{aligned} f_1 = m_b \ddot{u}_1 &- 2\lambda_1 (-R_p \cos\theta_1 \sin\theta_y - R_b \cos\alpha_1 + \mathrm{u}_1 \cos\alpha_1)(\cos\alpha_1) \\ &+2(R_p \sin\theta_1 \sin\theta_x - R_p \cos\theta_1 \cos\theta_x \cos\theta_y - R_b \sin\alpha_1 + \mathrm{u}_1 \sin\alpha_1) \sin\alpha_1 \end{aligned} \tag{68}$$

$$f_2 = m_b \ddot{u}_2 - 2\lambda_2(-R_p \cos\theta_2 \sin\theta_y - R_b \cos\alpha_2 + u_2 \cos\alpha_2)(\cos\alpha_2) \\ +2(R_p \sin\theta_2 \sin\theta_x - R_p \cos\theta_2 \cos\theta_x \cos\theta_y - R_b \sin\alpha_2 + u_2 \sin\alpha_2)\sin\alpha_2 \quad (69)$$

$$f_3 = m_b \ddot{u}_3 - 2\lambda_3(-R_p \cos\theta_3 \sin\theta_y - R_b \cos\alpha_3 + u_3 \cos\alpha_3)\cos\alpha_3 \\ +2(R_p \sin\theta_3 \sin\theta_x - R_p \cos\theta_3 \cos\theta_x \cos\theta_y - R_b \sin\alpha_3 + u_3 \sin\alpha_3)\sin\alpha_3 \quad (70)$$

The multipliers can be determined from equations (65) to (67). Actuator forces can then be determined from equations (68) to (70). The above three equations can be used as a guideline for controlling the hybrid manipulator. Future work will focus on the nonlinear control of this new parallel manipulator based on Lagrangian dynamics.

3.7. Conclusions

A novel 3-DOF hybrid manipulator 3PU*S-PU is proposed and analyzed. The advantages of this new type of manipulator are described, and the kinematic analysis is then conducted for the purpose of the subsequent performance analysis. Thirdly, the relatively most important kinematic performances, i.e. stiffness/compliance and workspace, are analyzed and optimized by resorting to the differential evolution and genetic algorithm. Fourthly, the multi-objective optimization for the compliance and workspace of the mechanism is implemented, based on the Pareto Front theory, and the results show that the two kinematic performances are improved after optimization. The dynamic analysis of the mechanism is finally conducted based on the Lagrangian method, which later sets a path for controlling the manipulator. The novelty of this proposed new GF set based manipulator is that by changing the original passive leg to PU type, the manipulator can therefore have the desired three degrees of freedom, and by applying U* joints as three

limbs instead of the conventional limbs, the stiffness of this hybrid manipulator can be greatly improved.

4

Dynamic Balancing Design

When mechanisms and parallel manipulators move, because the CoM is not fixed and angular momentum is not constant, vibration is produced in the system. The purpose of dynamic balancing is to make constant the CoM and the angular momentum of the system. Dynamic balancing is normally achieved by using extra devices (e.g. counterweights, counter-rotations) to counter-balance the shaking force and shaking moment that the original mechanism exerted to the base. However, the problem is that the whole system will become heavier and have more inertia when using those counter-balancing devices. Here, it is proposed to achieve dynamic balancing through reconfiguration, which can reduce the addition of mass and inertia. Furthermore, after designing a naturally dynamically balanced single leg, the legs will be combined to synthesize parallel mechanisms, and a spatial dynamically balanced grasper mechanism is designed and studied.

Two main contributions of this chapter can be concluded as follows: new reactionless parallel manipulators are derived and dynamic balancing through the reconfiguration concept is proposed for the first time. This research is important for manufacturing and space areas.

4.1. Dynamic Balance through Reconfiguration

4.1.1. SteadiCam

The SteadiCam uses counter-weights to achieve force balance. The mass relations are adjusted to achieve dynamic balance. Here, the concept of mass relationship is proposed. Two links at the bottom act as counter-weights to force balance the system. Now if one spins the system, it is dynamically balanced. If one moves up link 2 as shown in Figure 4.1, it is still force balanced, but no longer dynamically balanced. Thus the question is how one can rearrange the structure to regain the dynamic balance.

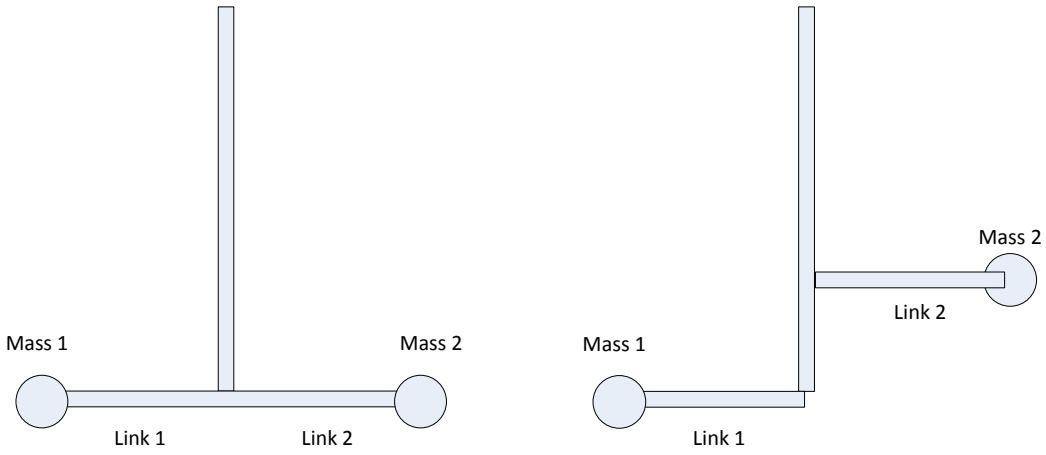

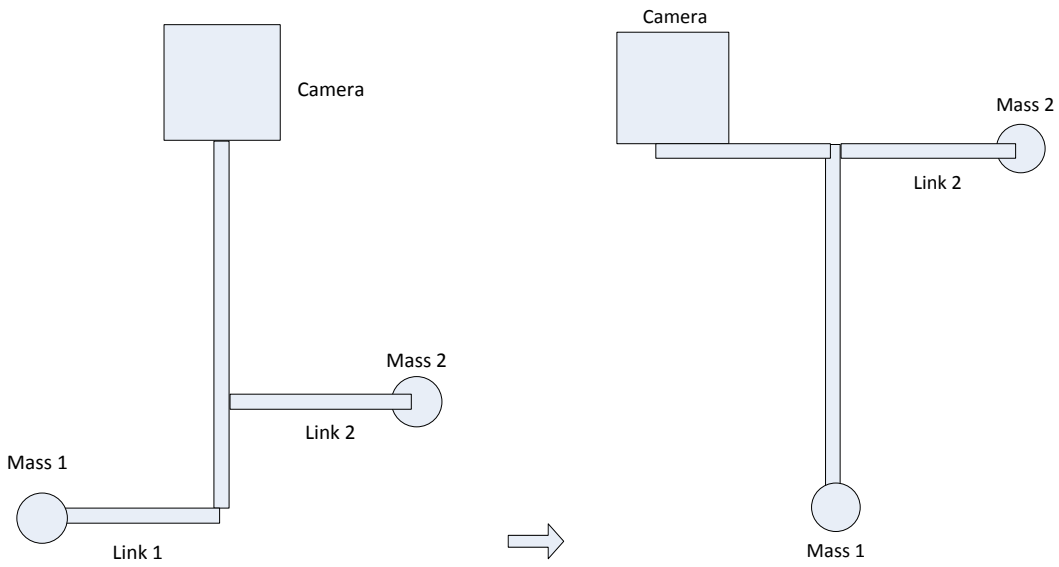

Figure 4.1. Simplified version of SteadiCam

Assuming that one moves an extreme case, i.e. move link 2 all the way to the top, it is obvious that if one wants to regain the dynamic balance, the camera needs to be moved in a counter-clockwise direction, as does mass 1. Hence the same situation is obtained with the difference that the two masses are at the top and one mass is at the bottom. In other words, if one slightly moves link 2 up, i.e. in a counter-clockwise direction, the camera also needs to be moved counter-clockwise as does mass 1, in order to regain the dynamic balance. It is all about mass relations. As long as those mass relations are maintained, dynamic balancing can be achieved. What is important is the relationship of these three masses.

Figure 4.2 can also be seen as dynamic balancing through reconfiguration, through moving link 2 and mass 2 to achieve dynamic balancing, i.e. adapting the position of link 2 and mass 2.

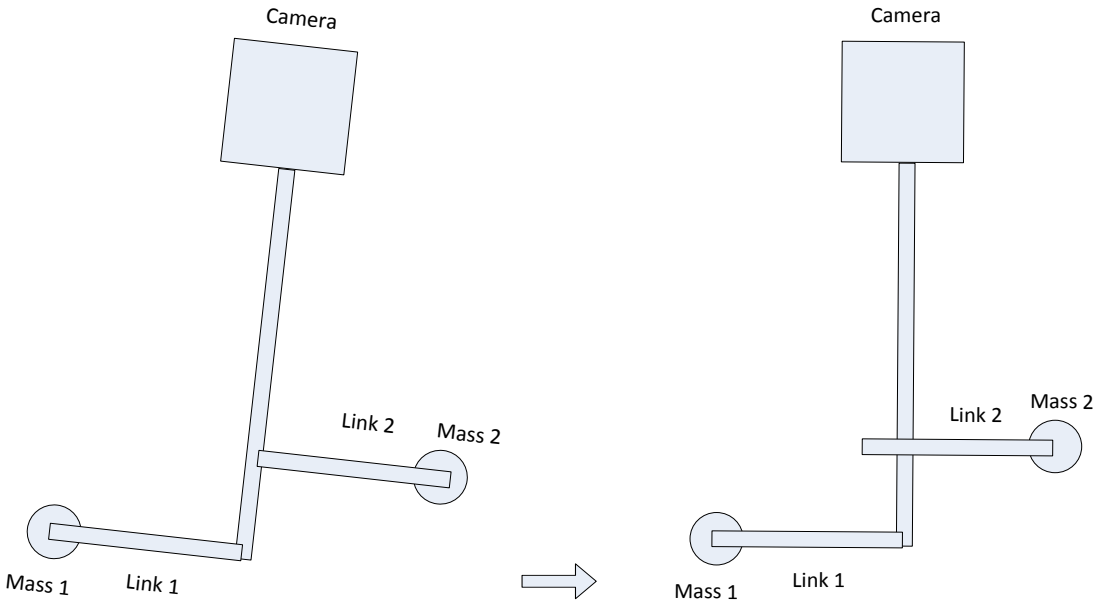

(a) Dynamic unbalance (b) Dynamic balance

Figure 4.2. Dynamic unbalance and balance of SteadiCam

4.1.2. 1-bar, 2-bar, 3-bar and 4-bar Linkages

Inspired by the above design, here balancing through the reconfiguration concept is proposed. For example, one can use a screw link as the link. The link can be moved so that the CoM of the link can be moved to the revolute joint point, then balanced. In this method, a counterweight is not used but the system is reconfigured by moving the screw link, so the system will not become heavy. Figure 4.3 shows such a concept of balancing through reconfiguration.

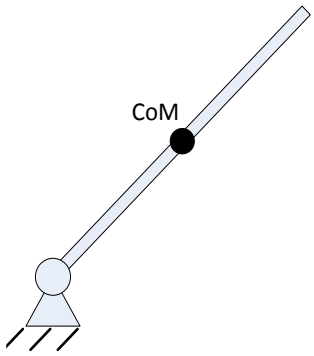

(a). Original unbalanced

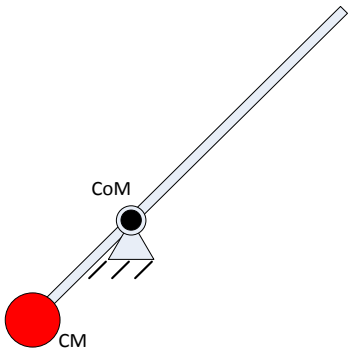

(b). Force balancing through CM

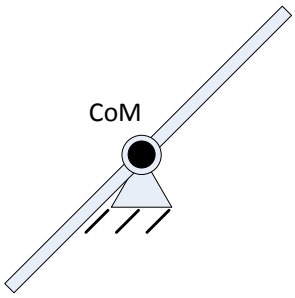

(c). Force balancing through reconfiguration

Figure 4.3. Concept of force balancing through reconfiguration

The coordinate of the CoM of the link with respect to the coordinate frame (x, y) is expressed as:

$$c_1 = \begin{bmatrix} x_1 \\ y_1 \end{bmatrix} = \begin{bmatrix} d_1 \cos\beta_1 \\ d_1 \sin\beta_1 \end{bmatrix} \tag{1}$$

where d_1 is the distance from the CoM of the link to the revolute joint, β_1 is the rotation angle of the link with respect to the x axis. The origin of the coordinate frame (x, y) coincides with the revolute joint, the x axis horizontally points towards right, and the y axis vertically points up. The linear momentum of the linkage is therefore:

$$m_1 \dot{c}_1 = m_1 \begin{bmatrix} \dot{x}_1 \\ \dot{y}_1 \end{bmatrix} = m_1 \begin{bmatrix} -d_1 \sin\beta_1 \\ d_1 \cos\beta_1 \end{bmatrix} \dot{\beta}_1 \tag{2}$$

where m_1 is the mass of the link. In order to have force balancing conditions, the linear momentum needs to be set constant. By observing the above equation, and since the mass cannot be set to zero, the only way to make it a constant is to set d_1 to zero, which means the CoM of the linkage is set to the revolute joint:

$$m_1 d_1 = 0 \rightarrow d_1 = 0 \tag{3}$$

The purpose of employing a counter-weight is to make the CoM move to the still point, so the question is whether one can achieve the same objective without using a counterweight. The link can be reconfigured so that the CoM is moved to the still point. One just wants to use the function of their links, and in this case it is the rotational function. For the two link scenario, as shown in Figure 4.4, it can now be seen that force balancing through reconfiguration does not add any counterweights, whereas for force balancing by adding a counterweight, the whole system becomes heavier.

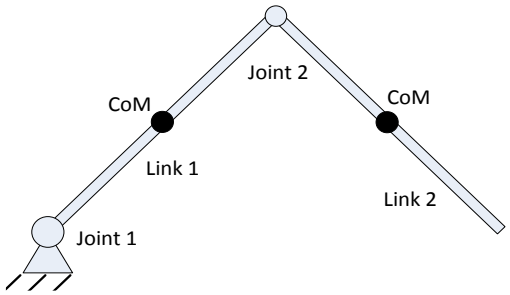

(a). Original unbalanced mechanism

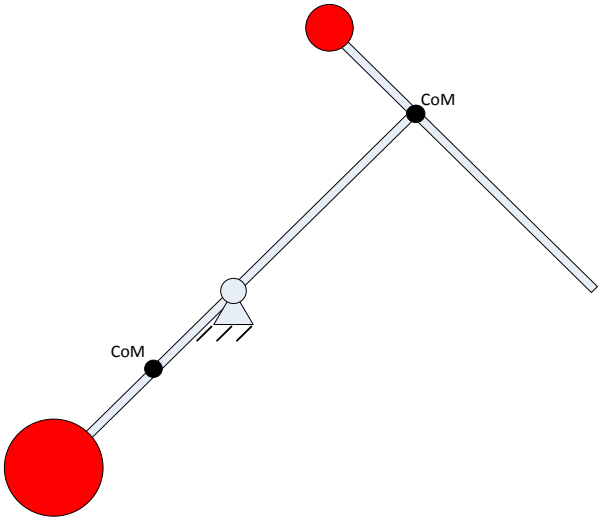

(b). Force balancing by adding CM

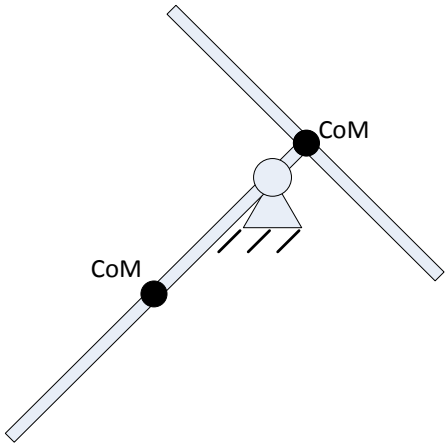

(c). Force balancing by reconfiguration

Figure 4.4. Force balancing of 2-DOF serially connected link through reconfiguration

The coordinate of the CoM of the link 2 with respect to the coordinate frame (x, y) is expressed as:

$$c_2 = \begin{bmatrix} x_2 \\ y_2 \end{bmatrix} = \begin{bmatrix} l_1 \cos\beta_1 + d_2 \cos\beta_2 \\ l_1 \sin\beta_1 + d_2 \sin\beta_2 \end{bmatrix} \tag{4}$$

where the mass and length of link 1 is denoted as m_1 and l_1, respectively, and the mass of link 2 is denoted as m_2 and l_2, respectively. d_2 is the distance from the CoM of link 2 to revolute joint 2, and β_2 is the rotation angle of link 2 with respect to the x axis. The linear momentum of the linkage is therefore:

$$\begin{aligned} m_1 \dot{c}_1 + m_2 \dot{c}_2 &= m_1 \begin{bmatrix} \dot{x}_1 \\ \dot{y}_1 \end{bmatrix} + m_2 \begin{bmatrix} \dot{x}_2 \\ \dot{y}_2 \end{bmatrix} \\ &= m_1 \begin{bmatrix} -d_1 \sin\beta_1 \\ d_1 \cos\beta_1 \end{bmatrix} \dot{\beta}_1 + m_2 \begin{bmatrix} -l_1 \sin\beta_1 \dot{\beta}_1 - d_2 \sin\beta_2 \dot{\beta}_2 \\ l_1 \cos\beta_1 \dot{\beta}_1 + d_2 \cos\beta_2 \dot{\beta}_2 \end{bmatrix} \\ &= \begin{bmatrix} m_1(-d_1 \sin\beta_1) + (-m_2 l_1 \sin\beta_1) \\ m_1(d_1 \cos\beta_1) + (m_2 l_1 \cos\beta_1) \end{bmatrix} \dot{\beta}_1 + \begin{bmatrix} -m_2 d_2 \sin\beta_2 \\ m_2 d_2 \cos\beta_2 \end{bmatrix} \dot{\beta}_2 \end{aligned} \tag{5}$$

In order to have the force balancing conditions, the linear momentum has to be constant. From observation of the above equation, in order to satisfy the above condition, the following force balancing conditions are therefore obtained:

$$\left.\begin{aligned} m_1 d_1 + m_2 l_1 = 0 \\ m_2 d_2 = 0 \end{aligned}\right\} \rightarrow \begin{cases} d_1 = -\dfrac{m_2 l_1}{m_1} \\ d_2 = 0 \end{cases} \tag{6}$$

From the above equation, the CoM of the link 2 is set to revolute joint 2 and the CoM of link 1 is at the point where the distance to revolute joint 1 is $\frac{m_2 l_1}{m_1}$.

For the three link case, as shown in Figure 4.5, if counterweights are used, the system becomes much heavier. For the unbalanced case, the CoM of the system is not fixed, as shown in Figure 4.5(a). By applying three counterweights, the CoM of the system is brought to a fixed point at the revolute joint on the base, as shown in Figure 4.5(b). It is obvious that the system becomes heavier and has more inertia.

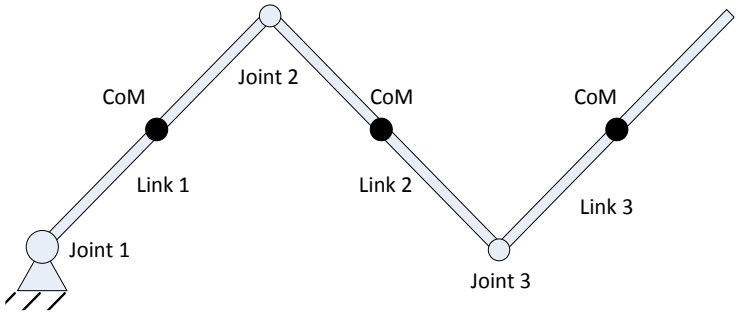

(a). Original unbalanced mechanism

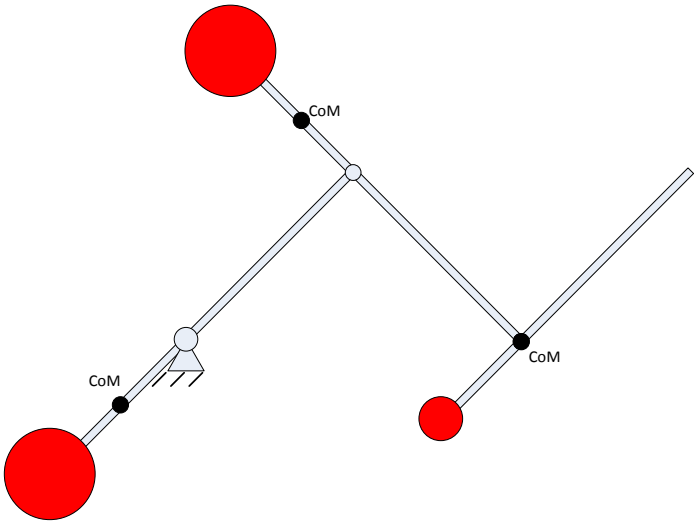

(b). Force balancing by adding CM

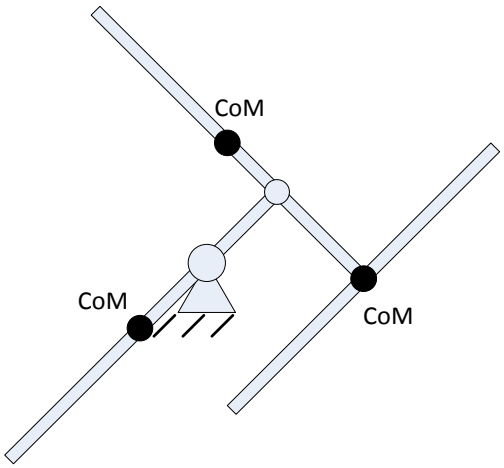

(c). Force balancing by reconfiguration

Figure 4.5. Force balancing of 3-DOF serially connected link through reconfiguration

The coordinate of the CoM of link 3 with respect to the coordinate frame (x, y) is expressed as:

$$c_3 = \begin{bmatrix} x_3 \\ y_3 \end{bmatrix} = \begin{bmatrix} l_1 \cos\beta_1 + l_2 \cos\beta_2 + d_3 \cos\beta_3 \\ l_1 \sin\beta_1 + l_2 \sin\beta_2 + d_3 \sin\beta_3 \end{bmatrix} \tag{7}$$

where d_3 is the distance from the CoM of link 3 to revolute joint 3, and β_3 is the rotation angle of link 3 with respect to the x axis. The linear momentum of the linkage system is therefore:

$$\begin{aligned} & m_1 \dot{c}_1 + m_2 \dot{c}_2 + m_3 \dot{c}_3 \\ &= m_1 \begin{bmatrix} \dot{x}_1 \\ \dot{y}_1 \end{bmatrix} + m_2 \begin{bmatrix} \dot{x}_2 \\ \dot{y}_2 \end{bmatrix} + m_3 \begin{bmatrix} \dot{x}_3 \\ \dot{y}_3 \end{bmatrix} \\ &= m_1 \begin{bmatrix} -d_1 \sin\beta_1 \\ d_1 \cos\beta_1 \end{bmatrix} \dot{\beta}_1 + m_2 \begin{bmatrix} -l_1 \sin\beta_1 \dot{\beta}_1 - d_2 \sin\beta_2 \dot{\beta}_2 \\ l_1 \cos\beta_1 \dot{\beta}_1 + d_2 \cos\beta_2 \dot{\beta}_2 \end{bmatrix} + m_3 \begin{bmatrix} -l_1 \sin\beta_1 \dot{\beta}_1 - l_2 \sin\beta_2 \dot{\beta}_2 - d_3 \sin\beta_3 \dot{\beta}_3 \\ l_1 \cos\beta_1 \dot{\beta}_1 + l_2 \cos\beta_2 \dot{\beta}_2 + d_3 \cos\beta_3 \dot{\beta}_3 \end{bmatrix} \\ &= \begin{bmatrix} m_1(-d_1 \sin\beta_1) + (-m_2 l_1 \sin\beta_1) + (-m_3 l_1 \sin\beta_1) \\ m_1(d_1 \cos\beta_1) + (m_2 l_1 \cos\beta_1) + (m_3 l_1 \cos\beta_1) \end{bmatrix} \dot{\beta}_1 + \begin{bmatrix} -m_2 d_2 \sin\beta_2 - m_3 l_2 \sin\beta_2 \\ m_2 d_2 \cos\beta_2 + m_3 l_2 \cos\beta_2 \end{bmatrix} \dot{\beta}_2 + \begin{bmatrix} -m_3 d_3 \sin\beta_3 \\ m_3 d_3 \cos\beta_3 \end{bmatrix} \dot{\beta}_3 \end{aligned} \tag{8}$$

Similarly, from observation of equation (8), the following force balancing conditions can be obtained by making the linear momentum constant:

$$\left.\begin{aligned} &m_1 d_1 + m_2 l_1 + m_3 l_1 = 0 \\ &m_2 d_2 + m_3 l_2 = 0 \\ &m_3 d_3 = 0 \end{aligned}\right\} \rightarrow \begin{cases} d_1 = -\dfrac{m_2 l_1 + m_3 l_1}{m_1} \\ d_2 = -\dfrac{m_3 l_2}{m_2} \\ d_3 = 0 \end{cases} \tag{9}$$

Thus the CoM of link 3 is set to revolute joint 3, the CoM of link 2 is at the point where the distance to the revolute joint 2 is $\frac{m_3 l_2}{m_2}$, and the CoM of link 1 is at the point where the distance to revolute joint 1 is $\frac{m_2 l_1 + m_3 l_1}{m_1}$.

From the above, it can be seen that when balancing by counterweight, the whole system becomes much heavier. The 4R four bar linkage has the following structure if the 4R four-bar linkage is seen as a three link open chain in series fashion, and the balancing solutions can be referred to equation (9). For the unbalanced 4R four bar linkage, as shown in Figure 4.6 (a), the CoM of the system is not fixed. By employing three counterweights, the CoM of the system is brought to a fixed point, as shown in Figure 4.6(b). If counterweights are used, the system becomes much heavier and has more inertia. Balancing through reconfiguration is illustrated in Figure 4.6(c-d). Instead of using counterweights, the system is reconfigured.

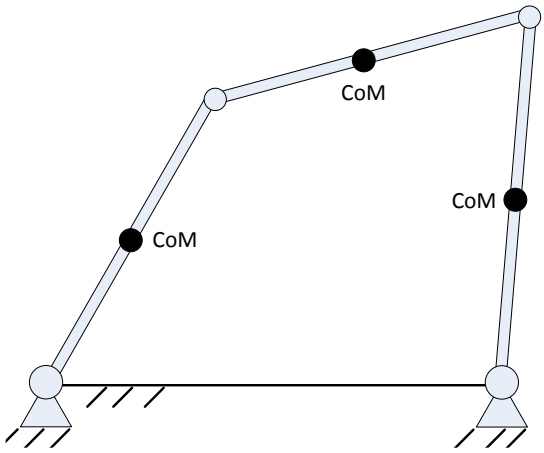

(a). Original unbalanced mechanism

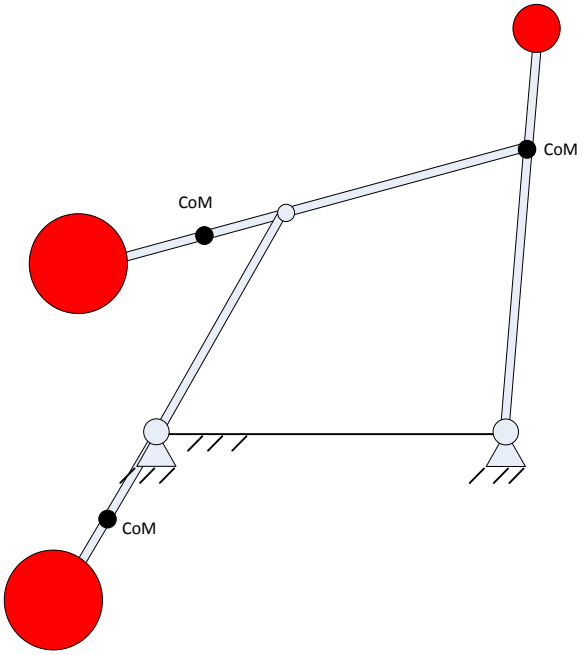

(b). Force balancing by adding CM

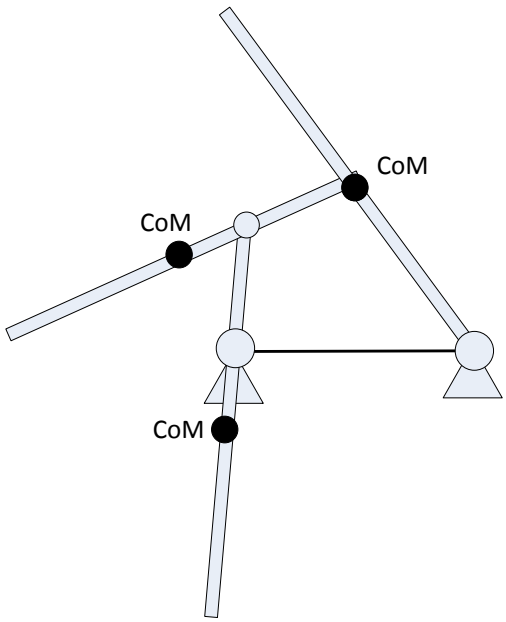

(c). Force balancing through reconfiguration

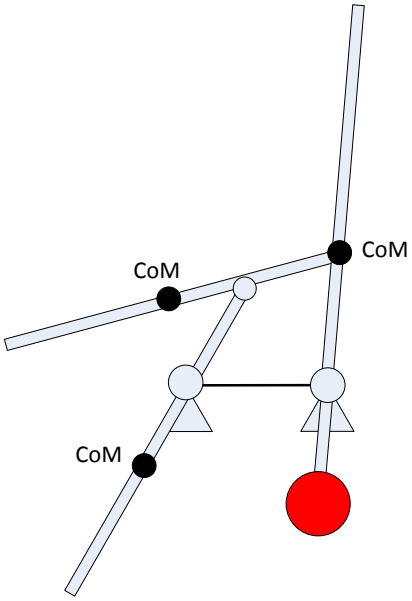

(d). Force balancing through reconfiguration & CM

Figure 4.6. Force balancing of 4R four-bar linkage through reconfiguration (case I)

If the 4R four-bar linkage is seen as a combination of a two link open chain in series fashion and a rotatable link, it has the following structure, and the balancing solutions can

be referred to equations (3) and (6). Similarly, for the unbalanced case, as shown in Figure 4.7(a), one can see that the CoM of the 4R four-bar linkage is not at a fixed point; the CoM of the system moves when the system is in motion. By using three counterweights, the CoM of the system can be made fixed at a revolute joint on the base, as shown in Figure 4.7(b). Instead of using the counterweights to move the CoM of the system to a fixed point, the system can be reconfigured, as illustrated in Figure 4.7(c). The addition of mass and inertia is therefore reduced.

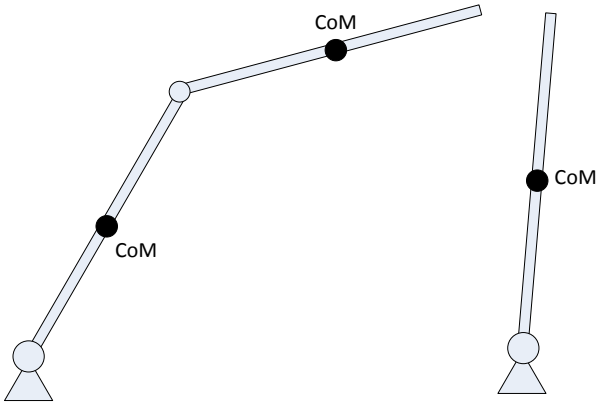

(a). Original unbalanced mechanism

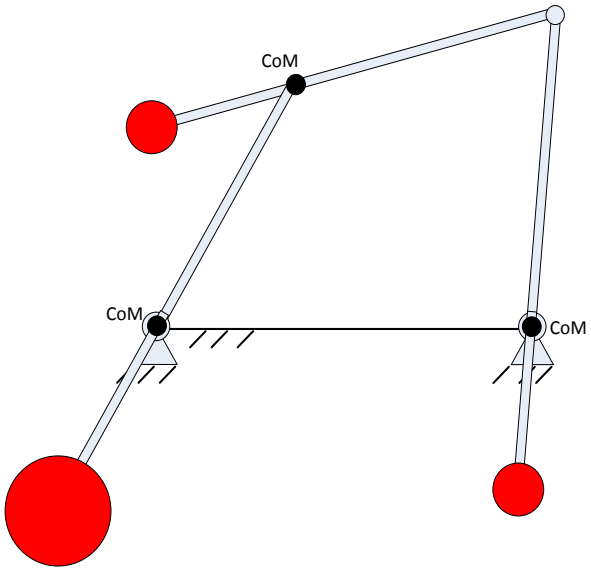

(b). Force balancing by adding CM

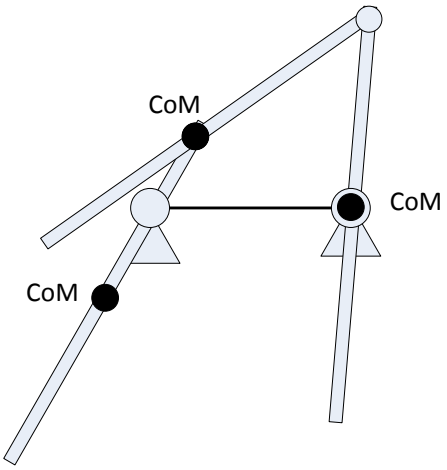

(c). Force balancing through reconfiguration

Figure 4.7. Force balancing of 4R four-bar linkage through reconfiguration (case II)

4.1.3. Crank-slider Linkage

The crank-slider mechanism is seen as a three link open chain in series fashion. The third link is a slider that will not rotate and will only translate. Because link 3 will not rotate, the CoM of link 3 will be at any point in link 3. Figure 4.8 illustrates the balancing through reconfiguration. One can see that force balancing through reconfiguration does not add counterweights and therefore the system will not become heavy after balancing.

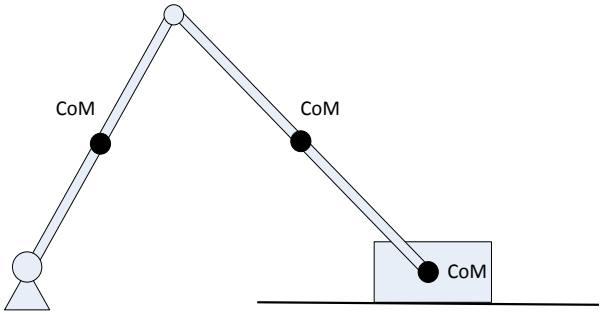

(a). Original unbalanced mechanism

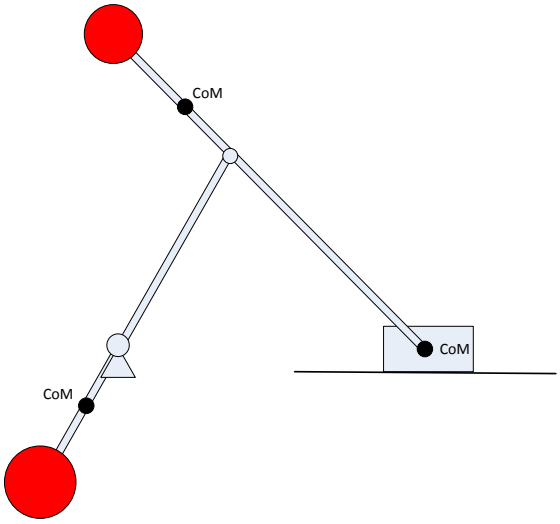

(b). Force balancing by adding CM

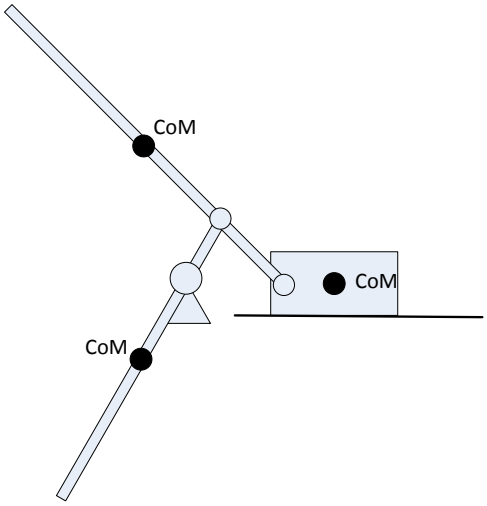

(c). Force balancing through reconfiguration

Figure 4.8. Force balancing of crank-slider mechanism through reconfiguration (if the links have the same length, the mechanism is also moment balanced)

Since the slider will only translate, equation (8) can be rewritten as:

$$
\begin{aligned}
& m_1 \dot{c}_1 + m_2 \dot{c}_2 + m_3 \dot{c}_3 \\
&= m_1 \begin{bmatrix} \dot{x}_1 \\ \dot{y}_1 \end{bmatrix} + m_2 \begin{bmatrix} \dot{x}_2 \\ \dot{y}_2 \end{bmatrix} + m_3 \begin{bmatrix} \dot{x}_3 \\ \dot{y}_3 \end{bmatrix} \\
&= m_1 \begin{bmatrix} -d_1 \sin\beta_1 \\ d_1 \cos\beta_1 \end{bmatrix} \dot{\beta}_1 + m_2 \begin{bmatrix} -l_1 \sin\beta_1 \dot{\beta}_1 - d_2 \sin\beta_2 \dot{\beta}_2 \\ l_1 \cos\beta_1 \dot{\beta}_1 + d_2 \cos\beta_2 \dot{\beta}_2 \end{bmatrix} + m_3 \begin{bmatrix} -l_1 \sin\beta_1 \dot{\beta}_1 - l_2 \sin\beta_2 \dot{\beta}_2 \\ l_1 \cos\beta_1 \dot{\beta}_1 + l_2 \cos\beta_2 \dot{\beta}_2 \end{bmatrix} \\
&= \begin{bmatrix} m_1(-d_1 \sin\beta_1) + (-m_2 l_1 \sin\beta_1) + (-m_3 l_1 \sin\beta_1) \\ m_1(d_1 \cos\beta_1) + (m_2 l_1 \cos\beta_1) + (m_3 l_1 \cos\beta_1) \end{bmatrix} \dot{\beta}_1 + \begin{bmatrix} -m_2 d_2 \sin\beta_2 - m_3 l_2 \sin\beta_2 \\ m_2 d_2 \cos\beta_2 + m_3 l_2 \cos\beta_2 \end{bmatrix} \dot{\beta}_2
\end{aligned}
\tag{10}
$$

Thus the following force balancing conditions can be obtained from equation (8) by making the linear momentum constant,

$$
\left.\begin{aligned} m_1 d_1 + m_2 l_1 + m_3 l_1 = 0 \\ m_2 d_2 + m_3 l_2 = 0 \end{aligned}\right\} \rightarrow \begin{cases} d_1 = -\dfrac{m_2 l_1 + m_3 l_1}{m_1} \\ d_2 = -\dfrac{m_3 l_2}{m_2} \end{cases} \tag{11}
$$

The CoM of the link 2 is at the point where the distance to revolute joint 2 is $\frac{m_3 l_2}{m_2}$, and the CoM of link 1 is at the point where the distance to revolute joint 1 is $\frac{m_2 l_1 + m_3 l_1}{m_1}$.

After designing a dynamically balanced single leg, the legs will be combined to synthesize parallel mechanisms. The above crank-slider mechanism, balanced through reconfiguration, can be used as a Scott-Russell mechanism, and can also be used to synthesize the planar 3-RPR parallel manipulator. One can see that balancing through reconfiguration does not add counterweights. If the links of the above crank-slider mechanism have the same length, then the mechanism is also moment balanced because of its symmetrical design [15].

Instead of the traditional Scott-Russell mechanism (i.e. an Assur group, a group that does not attach an additional DOF to the mechanism) [122], one can use the above balanced through reconfiguration crank-slider mechanism as a Scott-Russell mechanism and add it to each leg of the 3-RPR planar parallel manipulator, as shown in Figure 4.9. It is also expected that, if the passive balancing is changed to active balancing, the number of counter-rotations can then be reduced to only one counter-rotation, as shown in Figure 4.10.

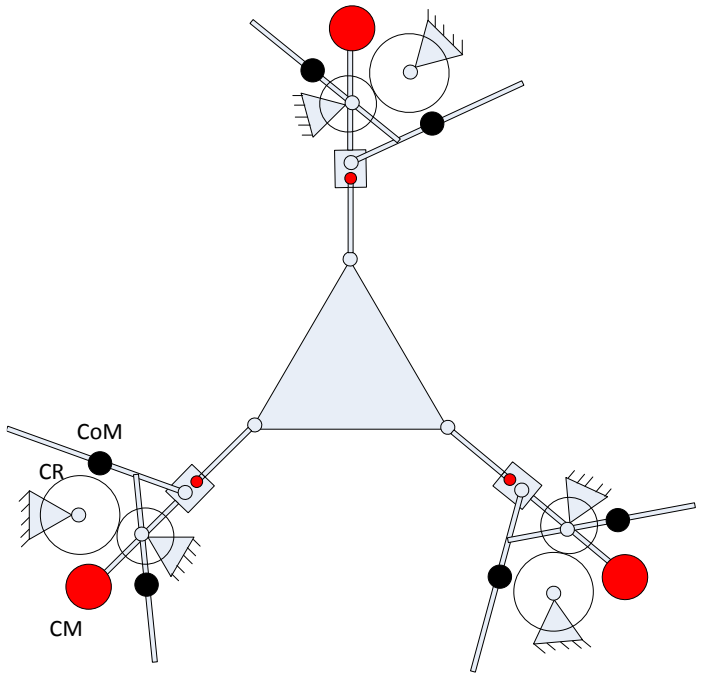

Figure 4.9. Dynamically balanced 3RPR planar parallel manipulator (passive balancing)

Only six counterweights and three counter-rotations are used if the system is passively balanced. One can see that by using the balance through reconfiguration crank-slider mechanism as a Scott-Russell mechanism (i.e. an Assur group [122]), no counterweight is

added. If one adheres to the original/traditional Scott-Russell mechanism, two counter-weights are added, which increases the weight.

The moving platform mass can be replaced by three point masses placed at three attachment points of the moving platform and the three legs. The three point masses are represented as m_{a1}, m_{a2}, and m_{a3}. If one satisfies the following, then the above condition can be obtained:

$$m_{ai} = \frac{m_p}{3} \tag{12}$$

$$I_a = 3m_{ai}R_p{}^2 \tag{13}$$

where m_p and R_p are the mass and radius of the moving platform, respectively. This replacement of the moving platform allows one to analyze the shaking force balancing and shaking moment balancing of each limb of the robotic system. By making the linear and angular momentum equal to 0, the shaking force and shaking moment can be balanced provided:

$$m_{cw1} = \frac{-m_1 r_1}{r_{cw1}} \tag{14}$$

$$m_{cw2} = -\frac{m_2 r_2 + m_{ai}}{r_{cw2}} \tag{15}$$

$$0 = I_4 + (m_4 r_4{}^2 + m_3)L_4{}^2 - I_3 - m_3 r_3{}^2 L_4{}^2 \tag{16}$$

$$\begin{aligned} I_{cr} = {} & (m_4 r_4{}^2 + m_3(1-r_3)^2)L_4{}^2 + I_4 + I_3 + I_2 + I_1 \\ & + (m_2 r_2{}^2 + m_{cw2} r_{cw2}{}^2 + m_1 r_1{}^2 + m_{cw1} r_{cw1}{}^2 + m_{ai})L_2{}^2 \end{aligned} \tag{17}$$

where m_{cw1} and m_{cw2} are the mass of counterweights 1 and 2. The CoM of link i is denoted as S_i. The mass and axial moment of inertia of link i are denoted as m_i and I_i,

respectively. r_1, r_{cw1} r_2 and r_{cw2} are dimensionless coefficients. The axial moment of inertia of the counter-rotations is denoted as I_{cr}. Hence, it is possible to design a reactionless planar parallel mechanism with only six counterweights and three counter-rotations.

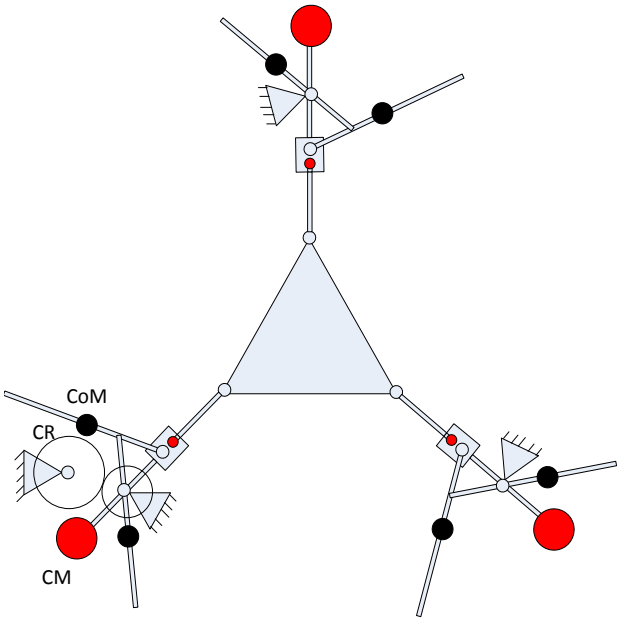

Figure 4.10. Dynamically balanced 3RPR planar parallel manipulator (active balancing)

Only six counterweights and one counter-rotation are used if the system is actively balanced. Based on the extension of [19], one can use the reconfiguration method to dynamically balance the 4-bar linkage with the Assur group [122] instead of adding the three counterweights, and use these through the reconfiguration balanced 4-bar linkage with the Assur group to construct the whole parallel robot; i.e. decompose first and integrate later. The above process illustrates the balancing through reconfiguration

method. Instead of adding counterweights, the purpose of which is to move the CoM, one can use the reconfiguration method to achieve the same goal.

4.2. Dynamically Balanced Spatial Grasper Mechanism Design

In this section, a dynamically balanced spatial grasper mechanism is proposed and designed based on the principal vector linkage. In the literature, no dynamically balanced spatial grasp mechanism can be found, thus a dynamically balanced spatial grasper mechanism is designed here. Through using the pantographs, the CoM of the grasper mechanism is fixed at a still point and through symmetrical structure design of the four fingers, it is also moment balanced. The advantages of the proposed dynamically balanced grasper mechanism and the design process are discussed in this chapter and the principal dimensions are derived.

4.2.1. Design of Grasper Mechanism

Grasper mechanisms can be used in many industrial areas. There are two main types of grasper mechanisms: planar grasper and spatial grasper. A planar grasper mechanism can be described as follows: the fingers are in the same plane or planes that are parallel with each other [123-126]. A spatial grasper mechanism can be described as follows: the fingers are not in the same plane. The purpose of the graspers is to grasp objects. Planar grasper and spatial grasper mechanisms can both grasp objects but, generally speaking, planar graspers can grasp regular shapes of objects, but for very complex shapes, spatial graspers are better than planar graspers in terms of steadiness and easiness. Most of the

graspers in use nowadays are not dynamically balanced, and some grasper mechanisms are medically based [127-129]; i.e. they can only be used in the medical arena, not in industry. Since the grasper mechanism is not dynamically balanced, the whole system will swing and vibrate when the grasper mechanism is grasping an object, which will severely affect the overall performance of the grasping process. For this reason, a dynamically balanced spatial grasper mechanism is developed, based on the pantograph and principal vector linkage. The pantographs are used to trace the CoM of the whole system and allow it to be fixed at a still point. The grasper mechanism is designed in such a way that the four fingers are symmetric so that the shaking moment of each opposite symmetrical finger can balance out each other. This will be the first dynamically balanced spatial grasper mechanism. The advantage of the grasper mechanism proposed here is firstly that it is dynamically balanced, and secondly, it can steadily grasp complex objects by using four symmetrical fingers.

This section will propose a spatial grasper mechanism that is dynamically balanced and also is geared towards the industry arena. It is known that the mechanism based on the principal vector linkage is force balanced and, through using the pantographs, the CoM of the grasper mechanism is fixed at a still point. Through symmetrical structure design of the four fingers, it is also moment balanced.

Figure 4.11 shows the dynamically balanced spatial grasper mechanism. Firstly, it is force balanced because the CoM of the whole system is at still point C by using the pantograph to trace the CoM. It is moment balanced because of its symmetrical design; the shaking moment of each opposite leg can balance out each other. The grasper

mechanism includes: eight principal links, 1, 2, 3, 4, and the other perpendicular parts 11, 12, 13, 14; and twenty four pantograph links, 5, 6, 7, 8, 9, 10, 16, 17, 18, 19, 20, 21 and their perpendicular counterparts, as shown in Figure 4.11. The links are all connected by a revolute joint, and the CoM of the grasper mechanism is at still point C, which is connected by link 15 to the ceiling. This link 15 can move along the guide ways to be able to operate at different locations of picking and placing, which will be illustrated in the application section.

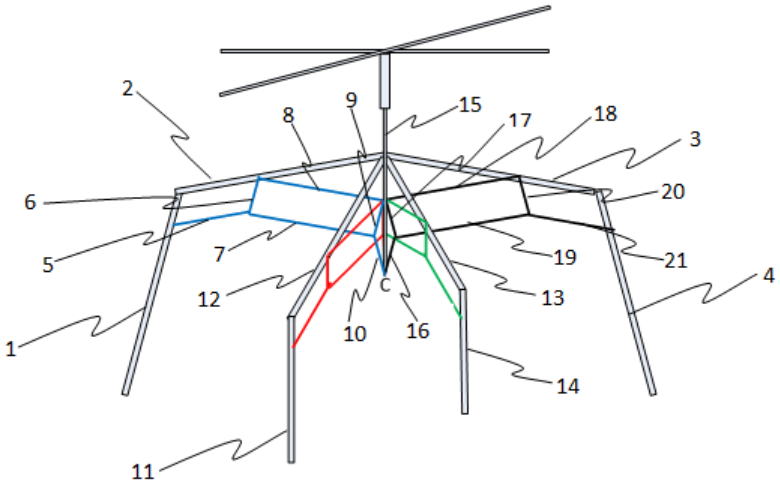

(a)

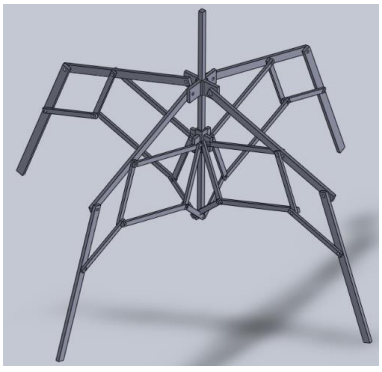

(b)

Figure 4.11. Dynamically balanced grasper mechanism

4.2.2. Principal Dimensions

The grasper mechanism can be decomposed into four segments, as shown in Figure 4.12. For the purpose of clearly showing the dimensions, the links are enlarged. One needs to first determine where to put the joint. In other words, the principal dimensions need to be determined, i.e. a_1, b_{21}, c_2 and the rest of the counterparts of the other segments. The principal dimensions can be determined from the force balancing condition [130], from which one can also obtain the fact that the leg should be opposite and symmetrical, as one intuitively designs the legs. In order to obtain the force balancing condition, the linear momentum needs to be determined and made equal to zero. The linear momentum of the motion of link 1 is expressed as follows, with respect to the coordinate frame x_0y_0, by fixing the links P_1B_1, B_1C_1 and C_1C [69]. Here it is assumed that the CoM of each link is on the line that connects the joints.

$$(m_2 + m_3 + m_4 + m_{18} + m_{19} + m_8 + m_{21} + m_{19} + m_{20})a_1 + m_6 p_6 + m_9 p_9 + m_{16} p_{16} - m_1 b_1 = 0 \quad (18)$$

where m_i is the mass of link i, and p_i is the distance from the CoM of link i to the connecting joint. From the above, the force balancing condition can be derived as follows:

$$(m_2 + m_3 + m_4 + m_{18} + m_{19} + m_8 + m_{21} + m_{19} + m_{20})a_1 + m_6 p_6 + m_9 p_9 + m_{16} p_{16} = m_1 b_1 \quad (19)$$

The dimension a_1 can be obtained as follows from the above force balancing condition:

$$a_1 = \frac{m_1 s_1 - m_{12} p_{12} - m_{13} p_{13} - m_{14} p_{14}}{m_1 + m_2 + m_3 + m_4 + m_{21} + m_{22} + m_{31} + m_{41} + m_{42} + m_{43}} \quad (20)$$

The dimensions b_{21} and c_2 can be determined by using the equivalent linear momentum system [69] and from the theory of principal vector linkage, the dimensions b_{21} and c_2 can be derived as follows:

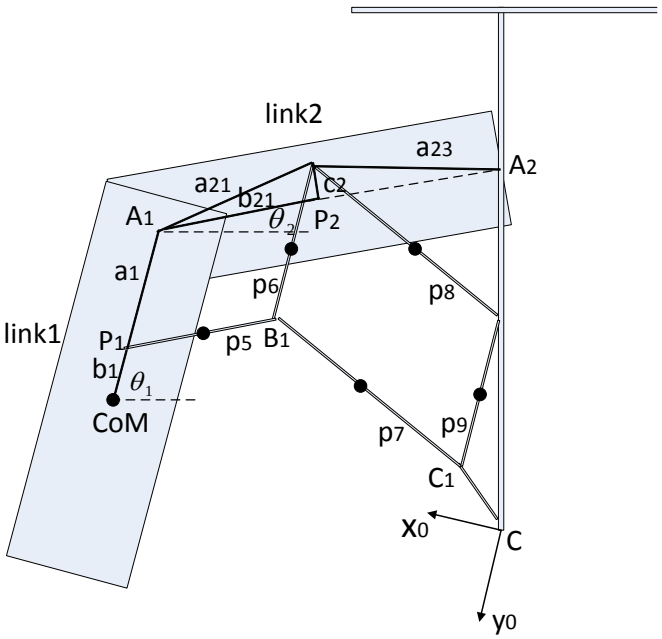

Figure 4.12. Segment of the grasper mechanism

$$b_{21} = \frac{(\frac{a_{21} + p_2^a}{a_{21}} + \frac{p_2^b}{a_{23}})(e_2 + \frac{p_2^b}{a_{23}} l_2)}{(\frac{a_{21} + p_2^a}{a_{21}} + \frac{p_2^b}{a_{23}})^2} \tag{21}$$

$$c_2 = \frac{(\frac{a_{21} + p_2^a}{a_{21}} + \frac{p_2^b}{a_{23}})(f_2 - \frac{q_2^b}{a_{23}} l_2)}{(\frac{a_{21} + p_2^a}{a_{21}} + \frac{p_2^b}{a_{23}})^2} \tag{22}$$

where

$a_{21} = \frac{m_2 p_2^a - m_5 p_5}{m_1}$,

$$a_{23} = \frac{m_2 p_2^b - m_{18} p_{18} - m_{19} p_{19}}{m_3 + m_4 + m_{21} + m_{20}},$$

and s_1 is the distance from the first joint A_1 to the CoM of link 1, e_2 is the distance from the first joint A_1 to the CoM of link 2 along the line that connects the joint A_1 and A_2, f_2 is the distance from the CoM of link 2 to the line that connects the joint A_1 and A_2, and l_2 is the opposite side of e_2. Because the system is symmetrical, the other principal dimension of the remaining segments can be calculated in the same manner.

4.2.3. Symmetrical Design

For moment balancing, one needs to first write the angular momentum. Figures 4.13(a) and (b) show the separate principal vector linkages. The angular momentum about the CoM of the grasper mechanism C can be written as follows:

$$\begin{aligned} A = {} & (I_1 + I_6 + I_9 + I_{16})\dot{\theta}_1 + (I_2 + I_5 + I_{18} + I_{19})\dot{\theta}_2 \\ & + (I_3 + I_7 + I_8 + I_{21})\dot{\theta}_3 + (I_4 + I_{10} + I_{18} + I_{20})\dot{\theta}_4 \\ & + m_1(r_1 \times \dot{r}_1) + m_2(r_2 \times \dot{r}_2) + m_3(r_3 \times \dot{r}_3) + m_4(r_4 \times \dot{r}_4) \\ & + m_5(r_5 \times \dot{r}_5) + m_6(r_6 \times \dot{r}_6) + m_9(r_9 \times \dot{r}_9) + m_{16}(r_{16} \times \dot{r}_{16}) \\ & + m_{18}(r_{18} \times \dot{r}_{18}) + m_{19}(r_{19} \times \dot{r}_{19}) + m_8(r_8 \times \dot{r}_8) + m_7(r_7 \times \dot{r}_7) \\ & + m_{21}(r_{21} \times \dot{r}_{21}) + m_{20}(r_{20} \times \dot{r}_{20}) + m_{17}(r_{17} \times \dot{r}_{17}) + m_{10}(r_{10} \times \dot{r}_{10}) \end{aligned} \quad (23)$$

where I_i is the inertia about its CoM of link i, r_i is the position vector of the CoM of link i relative to the CoM of grasper mechanism C, and $\dot{\theta}_i$ is the angle from the horizontal axis to the center line of link i.

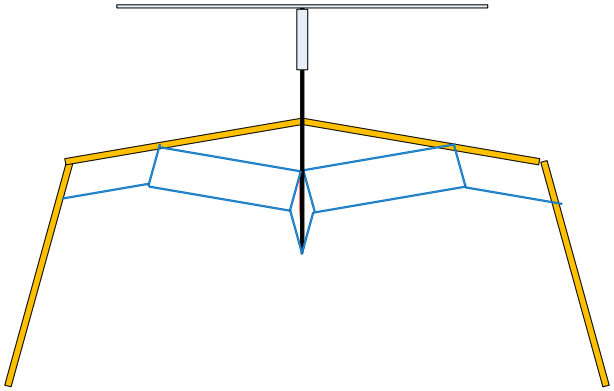

(a)

+

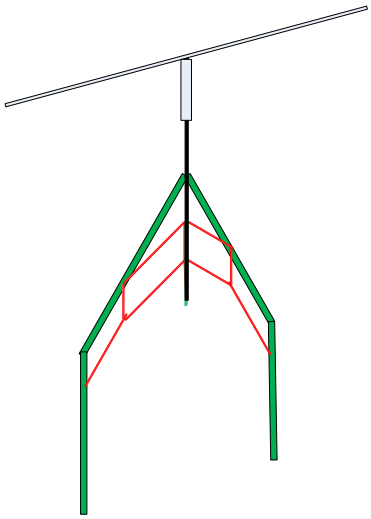

(b)

⇓

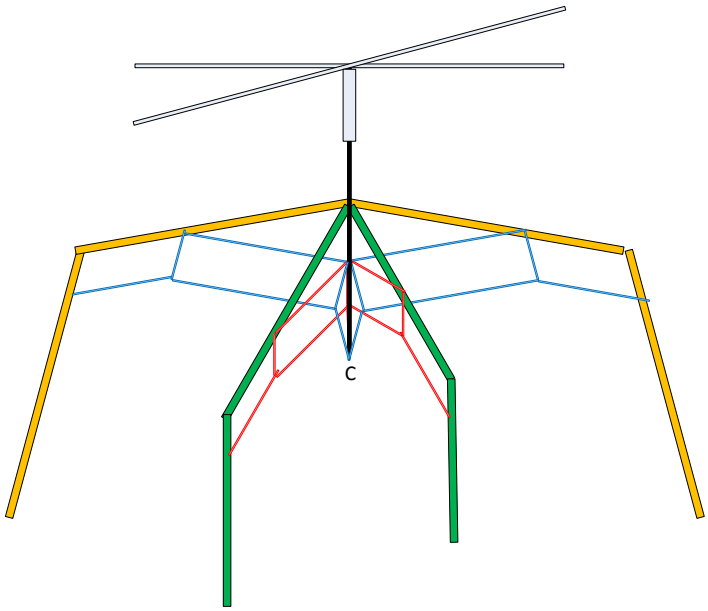

(c)

Figure 4.13. Principal vector linkages and symmetrical design

In the next step, in order to obtain the final form of the angular momentum, one substitutes the position vectors of the CoM of each link, relative to the CoM of the whole mechanism at point C, its position vector derivatives and the above force balancing conditions to the angular momentum equation. One then makes the angular momentum equal to zero to determine the moment balancing condition, from which one can derive that links 1 and 4 are symmetrical and have opposite motions, and links 2 and 3 are symmetrical and have opposite motions, as follows.

$$\dot{\theta}_1 + \dot{\theta}_4 = 0 \tag{24}$$

$$\dot{\theta}_2 + \dot{\theta}_3 = 0 \tag{25}$$

$$\theta_1 + \theta_4 = \pi \tag{26}$$

$$\theta_2 + \theta_3 = \pi \tag{27}$$

By vertically combining Figures 4.13(a) and (b), a symmetrical design can be derived, as shown in Figure 4.13(c).

4.2.4. Application

The proposed dynamically balanced grasper mechanism can be used in many areas, such as industrial picking and placing, and the space industry. Figure 4.14 shows the general concept of the grasping process in an industrial area. Because it is dynamically balanced, the whole system can be suspended by a single wire if the grasper is used in space, which can make the system lighter. Future work will include designing the proposed grasper mechanism to be foldable. When used in space, the grasper mechanism can be folded when it is sent into space and unfolded when it is in operation. Moreover, in some special situations, since it is dynamically balanced and there is no gravity in space, the grasper mechanism can be suspended by a single wire rather than a link.

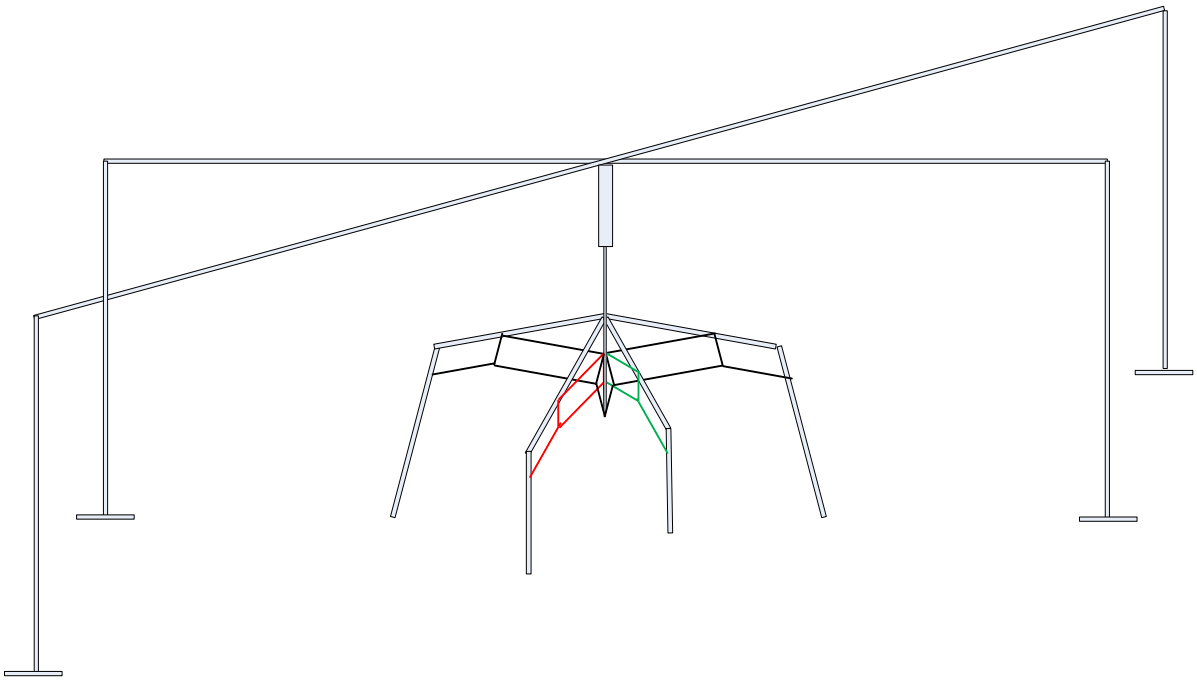

(a)

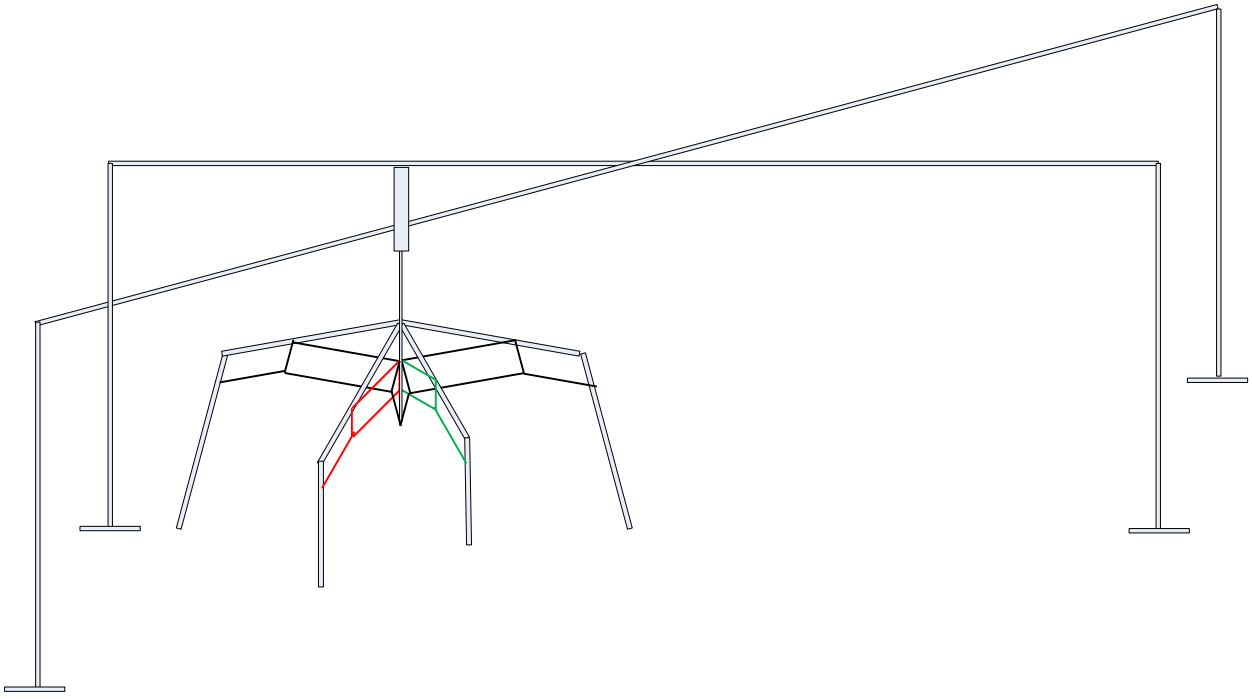

(b)

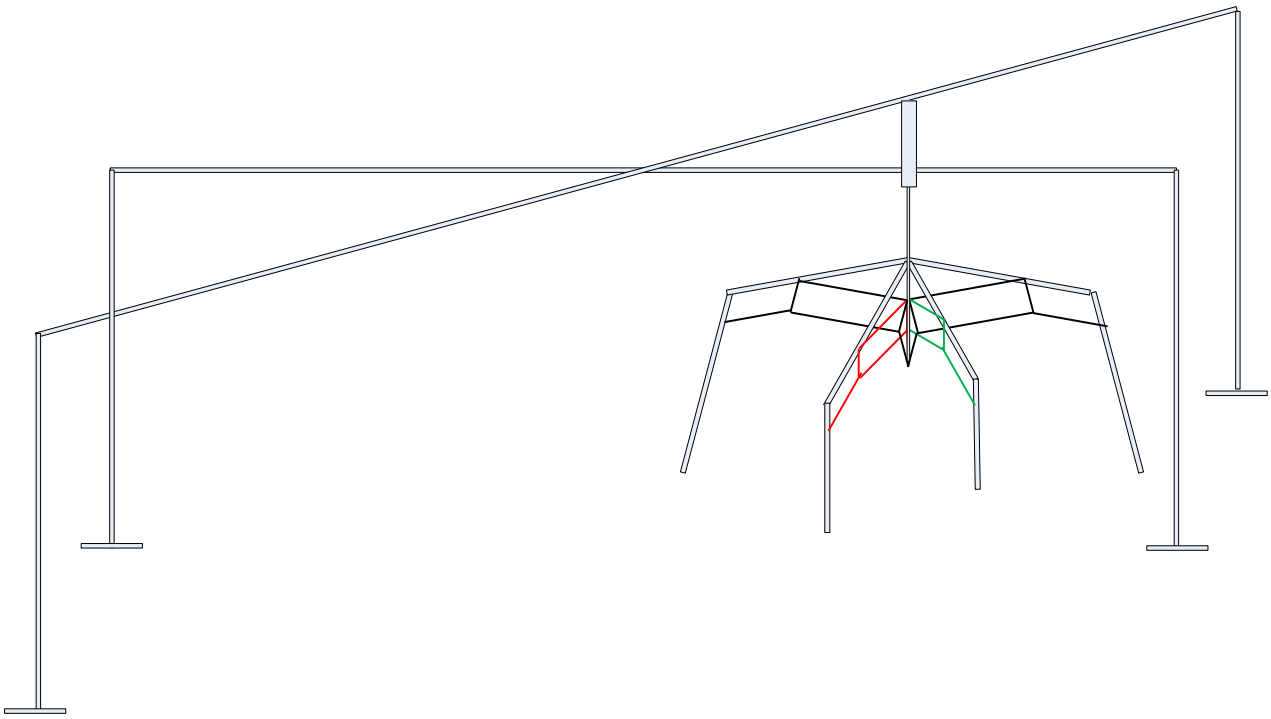

(c)

Figure 4.14. Grasper mechanism used in industrial arena

4.3. Testing

The testing is conducted by using Simulink and dSpace. Two motors (Pololu 12V, 19:1 gear motor w/encoder) and two motor controllers (Sabertooth dual 12A 6V-24V regenerative motor driver) are purchased, as shown in Figures 4.15 and 4.16. The technical specs of these two components are listed in Appendix A.

The Pololu 12V, 19:1 gear motor w/encoder is a 12 volt motor with a ratio of 19:1 gearbox and a quadrature encoder that can offer a resolution of 64 counts per revolution of the motor shaft, which agrees with 1216 counts per revolution of the gearbox's output shaft. These units have a 0.61 inch long, 0.24 inch diameter output

shaft. This motor is geared towards usage at 12 volt, and is able to start rotating at voltages as low as 1 volt.

The Sabertooth dual 12A 6V-24V regenerative motor driver is a recent development of the Sabertooth 2x10 motor controller. It is geared towards moderate powered robots and can be up to 100lbs for general purpose robotics. Sabertooth allows one to operate two motors with: analog voltage, radio control, serial and packetized serial, and it has separate and speed+direction operating patterns, which makes it an excellent choice for differential drive robots. The operating mode is set with onboard dual in-line package switches to avoid losing jumpers.

Figure 4.15. Pololu 12V 19:1 gear motor w/encoder

Figure 4.16. Sabertooth dual 12A 6V-24V regenerative motor driver

Here, a 2-DOF link manipulator is set up and built as an illustration. Instead of fixing the system to a frame, the system is suspended by strings in the air so that vibrations in the system can be easily observed. For the unbalanced 2-DOF link, when the manipulator moves from one position to another, as illustrated in Figure 4.17, the system will swing and vibrate, and lose balance. In the case of the balanced 2-DOF link case, when the manipulator moves from one position to another, as shown in Figure 4.18, the phenomenon of the unbalanced case is gone; the system will remain steady, and maintain the balanced condition.

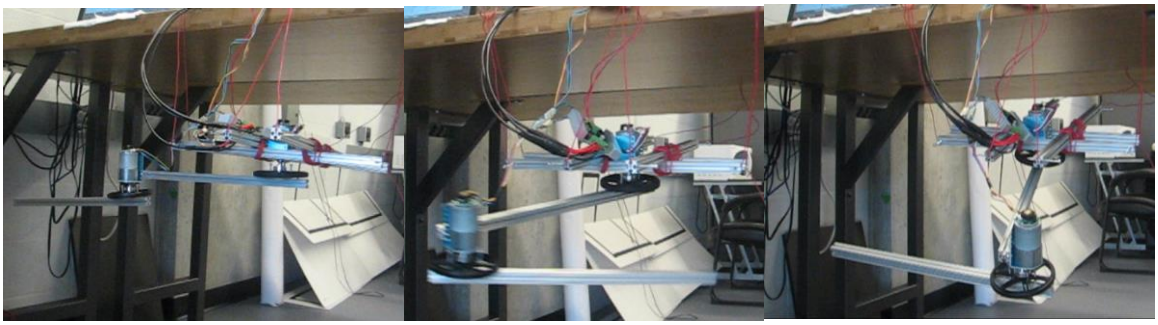

(a) First trial

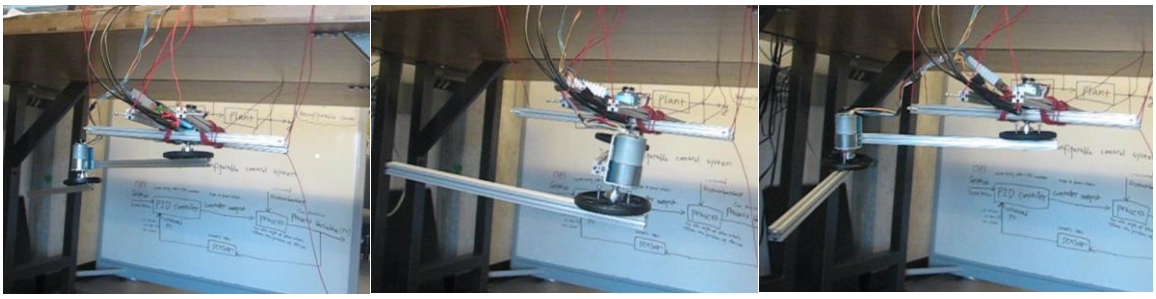

(b) Second trial

Figure 4.17. Unbalanced two-DOF link case

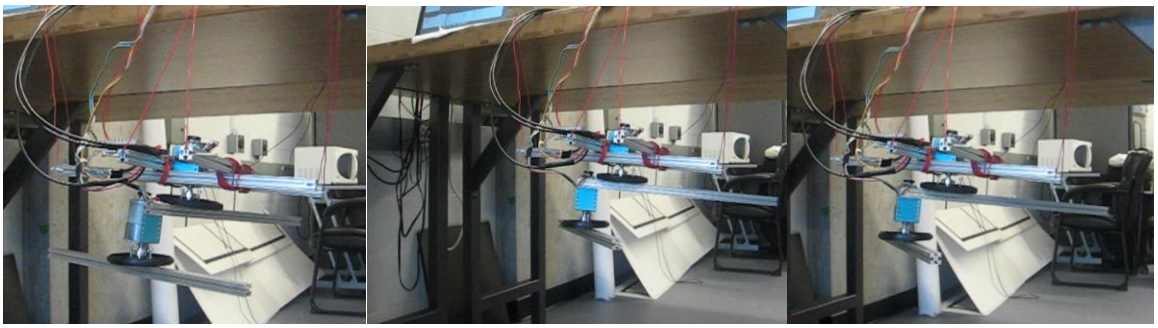

(a) Time step i (b) Time step i+1 (c) Time step i+2

Figure 4.18. Balanced two-DOF link case

4.4. Conclusions

The concept of dynamic balancing through reconfiguration, which can reduce the addition of mass and inertia, is proposed. In this method, a counterweight is not used but, through reconfiguring the system by moving the link, the system will not become heavy. Based on this idea, we first dynamically balance a single leg by the reconfiguration method (decomposition) and then combine the balanced legs to synthesize the whole parallel mechanism (integration); i.e. the decomposition and integration concept. New reactionless mechanisms and a dynamically balanced spatial grasper mechanism are

derived, based on the decomposition and integration concept and as well as by employing existing dynamically balanced structures.

5

Adaptive Control Design

When the end-effector of a robotic arm grasps different payload masses, the output of joint motion will vary, which will decrease the end-effector positioning accuracy of the robotic arm system. By using a model reference adaptive control approach, the payload variation effect can be solved. This chapter designs a joint motion controller for serial robotic manipulators. The convergence performance of the PID, MRAC and the PID+MRAC hybrid controllers for 1-DOF, 2-DOF and 3-DOF manipulators is compared. The comparison results show a higher convergence speed and better overall performance for the MRAC and the PID+ MRAC controllers than that of the PID controller, and a better convergence performance for the hybrid control compared to the MRAC control.

5.1. Introduction

Control of a serial manipulator can be divided into joint control and operational/task space control. Most robotic industries use a PID controller to control each robotic manipulator joint. The problem of not being able to compensate the payload variations results in using adaptive control, especially model reference adaptive control (MRAC). The MRAC method was first introduced by Whitaker et al. [22] in 1958, when they considered adaptive aircraft flight control systems, using a reference model to obtain error signals

between the actual and desired behavior. The MRAC was later further developed [131-134]. Dubowsky [96] was the first to apply the MRAC to the robotic manipulator. This approach follows the method in [97]. A steepest-descent method was used for updating the feedback gains, after which Horowitz applied the hyper-stability method and developed an adaptive algorithm [98] for a serial robotic arm.

The adaptive method proposed by Horowitz in [98] is different from Dubowsky's approach [96]. The two main differences are summarized as: firstly, in Horowitz's method, the overall control system has an inner loop model reference adaptive system controller and an outer loop position and velocity feedback loop, whereas the control system in Dubowsky's method is entirely based on the model reference adaptive controller; secondly, in Dubowsky's paper, the coupling among joints and nonlinear terms in the manipulator equations are ignored, whereas this is considered in Horowitz's method. The drawback of Horowitz's method is that the matrices M and N are assumed to be constant. An improved version of the method was later proposed in Sadegh [109]. The assumption that the inertia matrix and nonlinear term are constant during adaptation can be removed by modifying the control law and parameter adaptation law. Based on the MRAC control and by combining the PID control, a PID+MRAC hybrid controller is proposed for serial robotic manipulators. For the 1-DOF link, because the M and N matrices of the dynamic equation are constant, one can directly combine the PID and MRAC controllers to design the PID+MRAC controller. However, for more than 1-DOF cases, the above process is no longer applicable because the M and N matrices of the dynamic equation are not constant. On the positive side, however, Sadegh [109, 110] proposed an improved MRAC

that can remove the condition that the M and N matrices be constant. By using Sadegh's improved adaptive structure, and by combining the PID and MRAC controllers, a hybrid controller is designed for cases with more than 1-DOF. The convergence performance of the PID, MRAC, and PID+MRAC hybrid controllers for 1-DOF, 2-DOF and 3-DOF manipulators are compared.

5.2. PID, MRAC and Hybrid Control

5.2.1. PID Controller

The PID controller is illustrated in Figure 5.1. The output of the plant will be compared with the desired model rp and then will generally result in an error. This error will go through the PID control and through "error times control actions". The output of the PID controller will be the input to the plant model, and this circle will continue until the error between the actual output from the plant and the desired model converges to 0. This is the basic working principle of the PID control.

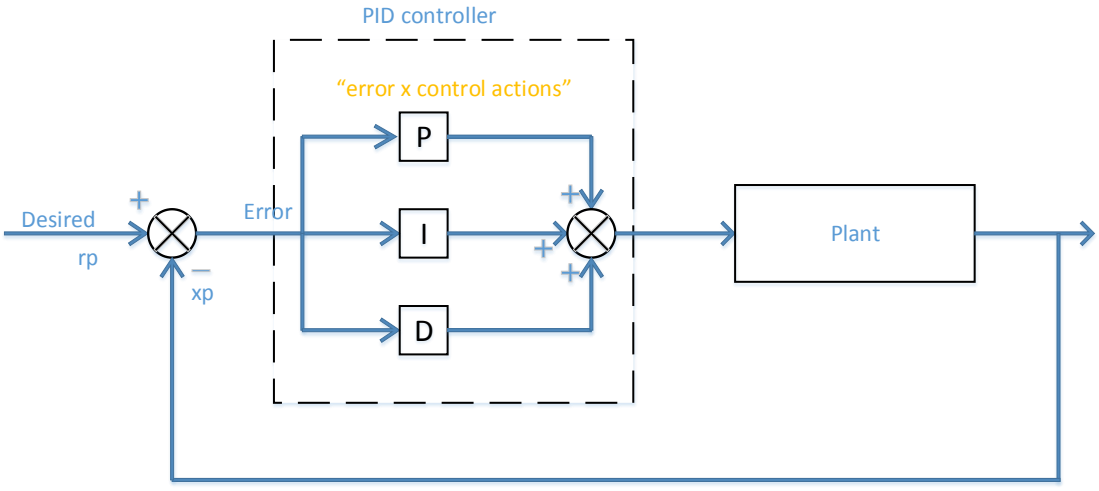

Figure 5.1. PID controller [135]

5.2.2. MRAC Controller

For the MRAC controller, Figure 5.2 shows such a system. One can see that this system does not contain any PID control. The output from the plant will be compared with the reference model, which will produce an error. This error will be used by the adaptive algorithm block and then produce the input elements to the plant. In the meantime, the output of the plant will compare with the desired model rp and will produce another error. This error will go through the integration action and then subtract the feedback processed position and velocity by the Kp and Kd elements. This process is very similar to the PID control, but is not a PID control. The output from this process, times the elements from the adaptive algorithm, plus the elements from the adaptive algorithm, will be the input to the plant. This process will continue until the error between the output of the plant and the reference model converges to 0. The ideal system is isolated from the plant, in the sense that the feedback values of the plant variables are not used to process the input to the reference model. The reference model input is processed from its own output variables by a “similar PID controller”. The ideal system is completely unaffected by the plant performance.

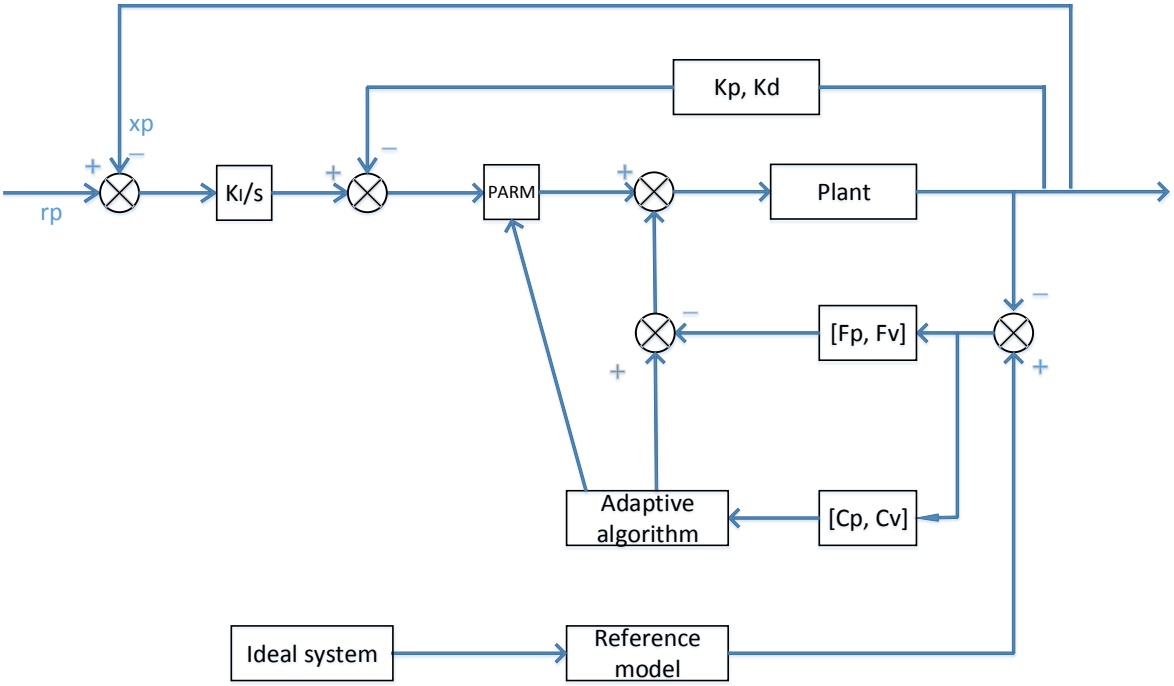

Figure 5.2. MRAC controller [98]

Sadegh's improved MRAC is illustrated in Figure 5.3. By modifying the control law (i.e. modeling the Coriolis and centripetal acceleration compensation controller into a bilinear function of the joint and model reference velocities rather than a quadratic function of the joint velocities) and parameter adaptation law (i.e. breaking down the nonlinear parameters in the dynamic equations into the result of the multiplication of two terms: one constant unknown term, which includes the masses, moments of inertia of the links, payload and link dimensions, and the other a known nonlinear function of the manipulator structural dynamics), the assumption that the inertia matrix and nonlinear term are constant during adaptation is removed.

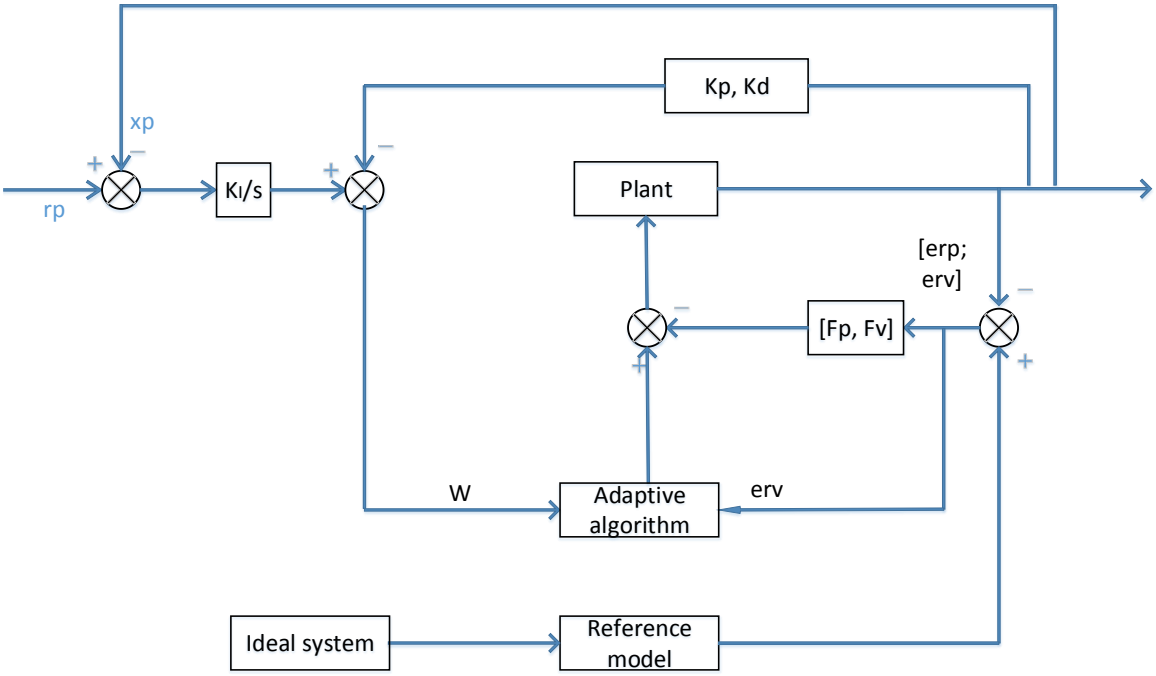

Figure 5.3. Improved MRAC controller [109]

5.2.3. PID+MRAC Hybrid Controller

By combining the PID and MRAC controllers, the PID+MRAC hybrid controller is obtained, as shown in Figure 5.4. As with the MRAC, the only difference between this hybrid PID+MRAC and MRAC is that the output of the plant will compare with the desired model rp and will produce an error. This error will go through the PID controller. The output of the PID controller, times the elements from the adaptive algorithm, plus the elements from the adaptive algorithm, will be the input to the plant. The authors [98] assume that M and N are constant during adaptation. For the 1-DOF link, because the M and N matrices of the dynamic equation are constant (M is constant, N is 0), one can directly combine the PID and MRAC controllers to design the PID+MRAC controller. However, for more than 1-DOF link, this is no longer applicable because the M and N matrices of the

dynamic equation are not constant. For the PID control, we need to use the Lagrange dynamic model, but for the MRAC, we need to use the Gibbs-Appell dynamic formulation. Since they are not compatible, we cannot combine the PID and MRAC in this case. On the positive side, however, Sadegh [109] proposed an improved MRAC that can remove the condition that the M and N matrices be constant, so that the Lagrange dynamic equation can be used. By using Sadegh's improved adaptive algorithm and structure, and by combining the PID and MRAC controllers, a hybrid controller is designed for cases of more than 1-DOF (e.g. 2-DOF and 3-DOF links). For the 2-DOF and 3-DOF link cases, the hybrid controller is shown in Figure 5.5.

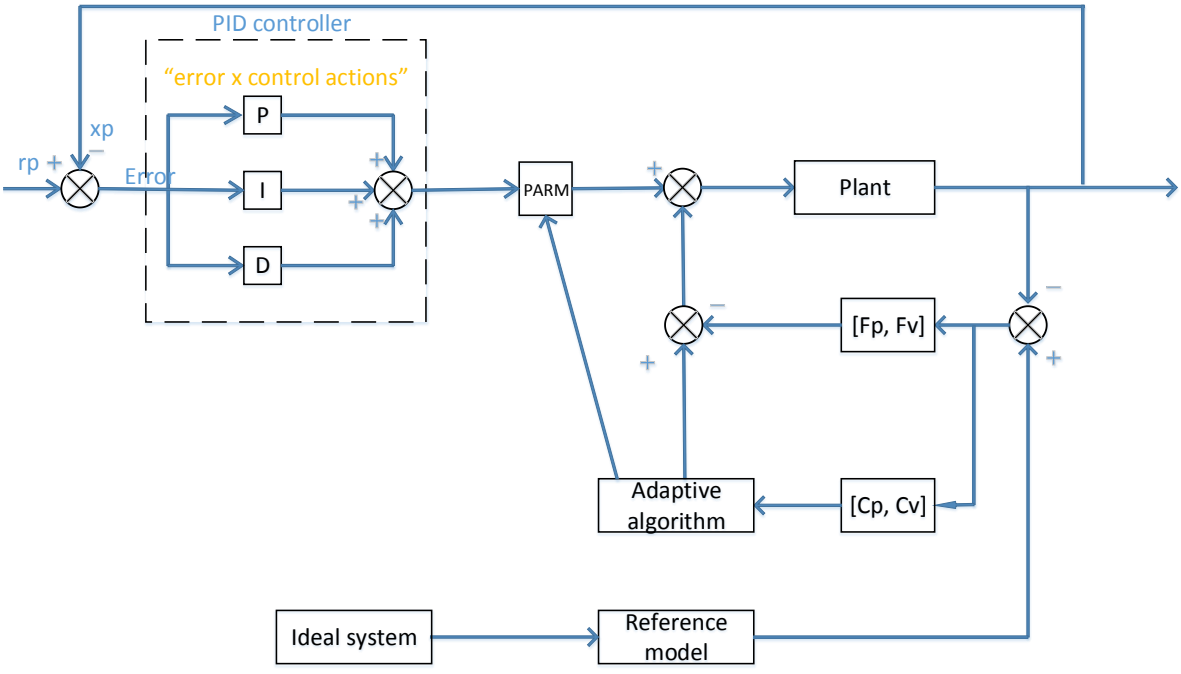

Figure 5.4. PID+MRAC hybrid controller for 1-DOF link

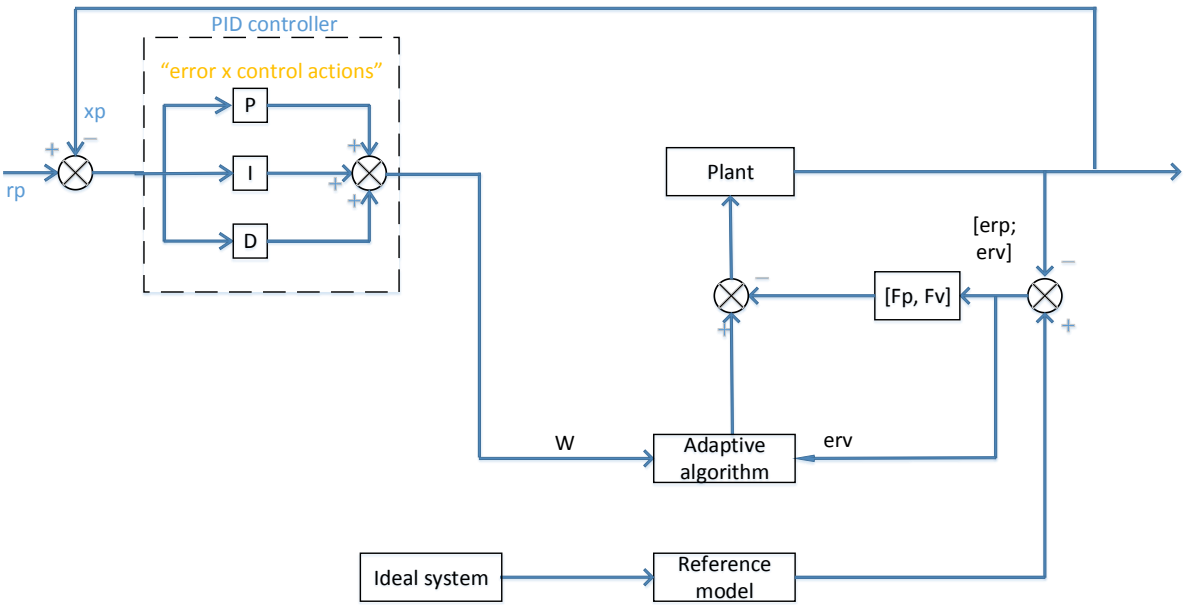

Figure 5.5. PID+MRAC hybrid controller for more than 1-DOF link

5.3. Dynamic Modeling and Re-parametrization

5.3.1. One-DOF Link Case

Here, the one-link manipulator will be used as an example, as shown in Figure 5.6. In order to implement PID control of the one link manipulator case, a dynamic equation has to be derived. By using the Lagrange method [135], the dynamic equation is presented as follows:

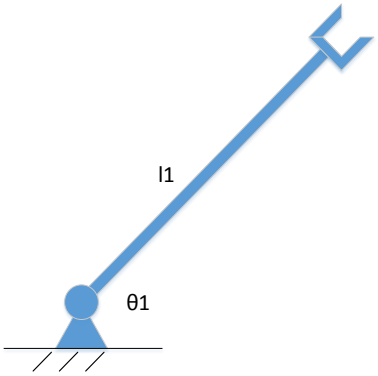

Figure 5.6. One link manipulator

The kinetic and potential energy of this link are as follows:

$$K_1 = \frac{1}{2} m_1 (l_1 \dot{\theta}_1)^2 \tag{1}$$

$$P_1 = m_1 g (l_1 \sin\theta_1) \tag{2}$$

The total kinetic and potential energy are:

$$K = K_1 = \frac{1}{2} m_1 (l_1 \dot{\theta}_1)^2 \tag{3}$$

$$P = P_1 = m_1 g (l_1 \sin\theta_1) \tag{4}$$

According to the Lagrange method:

$$\begin{aligned} L &= K - P \\ &= \frac{1}{2} m_1 (l_1 \dot{\theta}_1)^2 - m_1 g (l_1 \sin\theta_1) \end{aligned} \tag{5}$$

Thus the torque applied to the joint can be determined by:

$$\tau_1 = \frac{d}{dt} \frac{\partial L}{\partial \dot{\theta}_1} - \frac{\partial L}{\partial \theta_1} \tag{6}$$

where

$\frac{\partial L}{\partial \dot{\theta}_1} = m_1 l_1^{\,2} \dot{\theta}_1$,

$\frac{d}{dt} \frac{\partial L}{\partial \dot{\theta}_1} = m_1 l_1^{\,2} \ddot{\theta}_1$,

$\frac{\partial L}{\partial \theta_1} = -m_1 g l_1 \cos\theta_1$

Rewriting equation (6) results in:

$$\begin{aligned}\tau_1 &= (m_1 l_1^2)\ddot{\theta}_1 + (m_1 l_1 \cos\theta_1)g \\ &= M\ddot{\theta}_1 + 0 + (m_1 l_1 \cos\theta_1)g \\ &= M\ddot{\theta}_1 + 0 + Gg\end{aligned} \tag{7}$$

Through applying PID control, the controller output is the torque, i.e.

$$K_p e + K_i \int e dt + K_d \dot{e} = \tau_1 \tag{8}$$

where error $e = r_p - x_p$.

We know from the one-link manipulator M and N matrices, $M = m_1 l_1^2$, $N = 0$, the output from the manipulator (i.e. acceleration of the joint) can be determined as follows:

$$K_p e + K_i \int e dt + K_d \dot{e} = \tau_1 = (m_1 l_1^2)\ddot{\theta}_1 + (m_1 l_1 \cos\theta_1)g \tag{9}$$

Thus,

$$\Rightarrow \ddot{\theta}_1 = M^{-1}(K_p e + K_i \int e dt + K_d \dot{e}) \tag{10}$$

After deriving the acceleration of joint 1, one needs to take the integral with respect to time to obtain the velocity of joint 1 and take another integral to obtain the positon of joint 1.

$$\dot{\theta}_1 = \int \ddot{\theta}_1 dt \tag{11}$$

$$\theta_1 = \int \dot{\theta}_1 dt \tag{12}$$

For the MRAC, similarly with the PID control, the output from the controller can be determined as follows:

$$ControllerOut = \tau_1 = \hat{M} u + \hat{V} - F_p e - F_v \dot{e} \tag{13}$$

where $u = K_I \int (r_p - x_p) - K_p x_p - K_d x_v$

The manipulator dynamic equation is:

$$\tau_1 = (m_1 l_1^2)\ddot{\theta}_1 + (m_1 l_1 \cos\theta_1) g = Ma + 0 + Gg \tag{14}$$

Thus, the output from the manipulator (i.e. acceleration of the joint) is written as:

$$\hat{M}\, u + \hat{V} - F_p e - F_v \dot{e} = \tau_1 = Ma + V \tag{15}$$

Equation (15) results in:

$$\Rightarrow a = \ddot{\theta}_1 = M^{-1}(\hat{M}\, u + \hat{V} - F_p e - F_v \dot{e} - V) \tag{16}$$

Similarly, after deriving the acceleration of the joint, the time integral is taken to obtain the velocity of the joint and another integral is taken to obtain the positon of the joint.

$$\dot{\theta}_1 = \int \ddot{\theta}_1 dt \tag{17}$$

$$\theta_1 = \int \dot{\theta}_1 dt \tag{18}$$

Since $w(t) = -m(t)$ and $m(t) = (M - \hat{M})u(t) + (V - \hat{V}) = (M - \hat{M})u(t) + x_v{}^T (N_1 - \hat{N}_1(t)) x_v$,

$$\int_0^T y^T(t) w(t) dt = \int_0^T y^T(t)\, \tilde{\tilde{M}}\, u(t) dt + \int_0^T y_1(t) x_v{}^T (\hat{N}_1 - N_1) x_v dt \tag{19}$$

The first term is used to derive the adaptive algorithm for M, and the second term is used to derive the adaptive algorithm for N [136]. For the first term,

$$\int_0^T y^T(t)\, \tilde{\tilde{M}}\, u(t) dt = \int_0^T y_1\, \tilde{\tilde{m}}_{11} u_1 dt \tag{20}$$

Considering the first term in the above equation, we need to find $\frac{d}{dt}\hat{m}_{11}(t) = \frac{d}{dt}\tilde{\tilde{m}}_{11}(t)$,

so that

$$\int_0^T \tilde{m}_{11} y_1 u_1 dt \geq -\gamma^2 \tag{21}$$

From

$$\int_0^T z(t)^T \dot{z}(t)\, dt = \frac{z(T)^T z(T)}{2} - \frac{z(0)^T z(0)}{2} \geq -\frac{z(0)^T z(0)}{2} = -\gamma_0^{\,2} \tag{22}$$

By selecting $\frac{d}{dt}\hat{m}_{11}(t) = \frac{d}{dt}\tilde{m}_{11}(t) = k_{m11} y_1 u_1$,

$$\Rightarrow y_1 u_1 = \frac{\dot{\tilde{m}}_{11}(t)}{k_{m11}} \tag{23}$$

Then:

$$\int_0^T \tilde{m}_{11} y_1 u_1 dt = \int_0^T \tilde{m}_{11} \dot{\tilde{m}}_{11} \frac{1}{k_{m11}} dt = \frac{1}{k_{m11}} \int_0^T \tilde{m}_{11} \dot{\tilde{m}}_{11}\, dt \geq -\gamma^2 \tag{24}$$

5.3.2. Two-DOF Link Case

For the 2-DOF link case, as shown in Figure 5.7, the Lagrange method is applied to derive the dynamic equation for the PID control analysis.

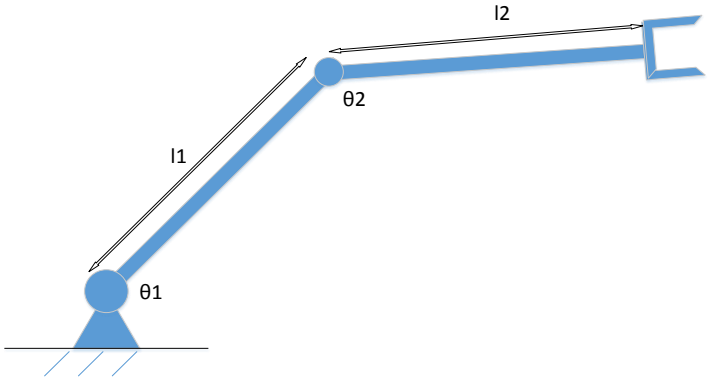

Figure 5.7. Two-link manipulator

The torques applied to the joints can be determined by:

$$\tau_1 = \frac{d}{dt}\frac{\partial L}{\partial \dot{\theta}_1} - \frac{\partial L}{\partial \theta_1} \tag{25}$$

$$\tau_2 = \frac{d}{dt}\frac{\partial L}{\partial \dot{\theta}_2} - \frac{\partial L}{\partial \theta_2} \tag{26}$$

The kinetic energy and potential energy for link 1 are expressed as:

$$K_1 = \frac{1}{2} m_1 (l_1 \dot{\theta}_1)^2 \tag{27}$$

$$P_1 = m_1 g (l_1 \sin\theta_1) \tag{28}$$

For link 2, we first write down the coordinates of the end of link 2, then differentiate them with respect to time in order to obtain the kinetic energy. The Cartesian coordinates of the end of link 2 are denoted as (x_2 , y_2):

$$x_2 = l_1 \cos\theta_1 + l_2 \cos(\theta_1 + \theta_2) \tag{29}$$

$$y_2 = l_1 \sin\theta_1 + l_2 \sin(\theta_1 + \theta_2) \tag{30}$$

One differentiates with respect to time:

$$\dot{x}_2 = -l_1 \dot{\theta}_1 \sin\theta_1 - l_2 (\dot{\theta}_1 + \dot{\theta}_2) \sin(\theta_1 + \theta_2) \tag{31}$$

$$\dot{y}_2 = l_1 \dot{\theta}_1 \cos\theta_1 + l_2 (\dot{\theta}_1 + \dot{\theta}_2) \cos(\theta_1 + \theta_2) \tag{32}$$

$$K_2 = \frac{1}{2} m_2 v_2^{\,2} \tag{33}$$

where $v_2^{\,2} = \dot{x}_2^{\,2} + \dot{y}_2^{\,2}$

Thus:

$$K_2 = \frac{1}{2} m_2 v_2^{\,2} = \frac{1}{2} m_2 l_1^{\,2} \dot{\theta}_1^{\,2} + \frac{1}{2} m_2 l_2^{\,2} (\dot{\theta}_1 + \dot{\theta}_2)^2 + m_2 l_1 l_2 \cos\theta_2 \, \dot{\theta}_1 (\dot{\theta}_1 + \dot{\theta}_2) \tag{34}$$

$$P_2 = m_2 g l_1 \sin\theta_1 + m_2 g l_2 \sin(\theta_1 + \theta_2) \tag{35}$$

The total kinetic and potential energy are therefore expressed as:

$$P = P_1 + P_2 = (m_1 + m_2) g l_1 \sin\theta_1 + m_2 g l_2 \sin(\theta_1 + \theta_2) \tag{36}$$

$$K = K_1 + K_2 = \frac{1}{2}(m_1 + m_2) l_1^{\,2} \dot{\theta}_1^{\,2} + \frac{1}{2} m_2 l_2^{\,2} (\dot{\theta}_1 + \dot{\theta}_2)^2 + m_2 l_1 l_2 \cos\theta_2 \, \dot{\theta}_1 (\dot{\theta}_1 + \dot{\theta}_2) \tag{37}$$

The Lagrange equation is obtained as:

$$L = K - P = \frac{1}{2}(m_1 + m_2) l_1^{\,2} \dot{\theta}_1^{\,2} + \frac{1}{2} m_2 l_2^{\,2} (\dot{\theta}_1 + \dot{\theta}_2)^2 + m_2 l_1 l_2 \cos\theta_2 \, \dot{\theta}_1 (\dot{\theta}_1 + \dot{\theta}_2) - (m_1 + m_2) g l_1 \sin\theta_1 - m_2 g l_2 \sin(\theta_1 + \theta_2) \tag{38}$$

Thus:

$$\tau_1 = \frac{d}{dt}\frac{\partial L}{\partial \dot{\theta}_1} - \frac{\partial L}{\partial \theta_1} = ((m_1 + m_2) l_1^{\,2} + m_2 l_2^{\,2} + 2 m_2 l_1 l_2 \cos\theta_2) \ddot{\theta}_1 + (m_2 l_2^{\,2} + m_2 l_1 l_2 \cos\theta_2) \ddot{\theta}_2 + (-2 m_2 l_1 l_2 \sin\theta_2) \dot{\theta}_1 \dot{\theta}_2 + (-m_2 l_1 l_2 \sin\theta_2) \dot{\theta}_2^{\,2} + ((m_1 + m_2) l_1 \cos\theta_1 + m_2 l_2 \cos(\theta_1 + \theta_2)) g \tag{39}$$

$$\tau_2 = \frac{d}{dt}\frac{\partial L}{\partial \dot{\theta}_2} - \frac{\partial L}{\partial \theta_2} = (m_2 l_2^{\,2} + m_2 l_1 l_2 \cos\theta_2) \ddot{\theta}_1 + (m_2 l_2^{\,2}) \ddot{\theta}_2 + (m_2 l_1 l_2 \sin\theta_2) \dot{\theta}_1^{\,2} + m_2 l_2 \cos(\theta_1 + \theta_2) g \tag{40}$$

If these are expressed in a matrix form, the following is obtained:

$$\begin{bmatrix}\tau_1\\ \tau_2\end{bmatrix} = M\ddot{\theta} + N$$
$$= \begin{bmatrix} m_{11} & m_{12} \\ m_{12} & m_{22}\end{bmatrix}\begin{bmatrix}\ddot{\theta}_1\\ \ddot{\theta}_2\end{bmatrix} + \begin{bmatrix} n_{11}\\ n_{21}\end{bmatrix} \quad (41)$$

where

$m_{11} = (m_1 + m_2)l_1^2 + m_2 l_2^2 + 2m_2 l_1 l_2 \cos\theta_2$,

$m_{12} = m_2 l_2^2 + m_2 l_1 l_2 \cos\theta_2$,

$m_{22} = m_2 l_2^2$

$n_{11} = 2(-m_2 l_1 l_2 \sin\theta_2)\dot{\theta}_1\dot{\theta}_2 + (-m_2 l_1 l_2 \sin\theta_2)\dot{\theta}_2^2$,

$n_{21} = m_2 l_1 l_2 \sin\theta_2 \dot{\theta}_1^2$

Applying the PID controller, the controller output is the torque, i.e.

$$K_p e + K_i \int e dt + K_d \dot{e} = \begin{bmatrix}\tau_1\\ \tau_2\end{bmatrix} \quad (42)$$

where error $e = r_p - x_p$. Because the two-link manipulator M and N matrices are known, the output from the manipulator (i.e. acceleration of joints 1 and 2) can be determined as follows:

$$\begin{bmatrix}\tau_1\\ \tau_2\end{bmatrix} = M\ddot{\theta} + N + Gg$$
$$= \begin{bmatrix} m_{11} & m_{12} \\ m_{12} & m_{22}\end{bmatrix}\begin{bmatrix}\ddot{\theta}_1\\ \ddot{\theta}_2\end{bmatrix} + \begin{bmatrix} n_{11}\\ n_{21}\end{bmatrix} + \begin{bmatrix} g_{11}\\ g_{21}\end{bmatrix} g \quad (43)$$

Thus:

$$K_p e + K_i \int e dt + K_d \dot{e} = \begin{bmatrix} \tau_1 \\ \tau_2 \end{bmatrix} = M \ddot{\theta} + N + Gg \tag{44}$$

Equation (44) results in:

$$\Rightarrow \begin{bmatrix} \ddot{\theta}_1 \\ \ddot{\theta}_2 \end{bmatrix} = M^{-1}(K_p e + K_i \int e dt + K_d \dot{e} - N) \tag{45}$$

After deriving the accelerations of joints 1 and 2, the time integral is taken to obtain the velocities of joints 1 and 2, and another integral is taken to obtain the positions of joints 1 and 2.

$$\begin{bmatrix} \dot{\theta}_1 \\ \dot{\theta}_2 \end{bmatrix} = \int \begin{bmatrix} \ddot{\theta}_1 \\ \ddot{\theta}_2 \end{bmatrix} dt \tag{46}$$

$$\begin{bmatrix} \theta_1 \\ \theta_2 \end{bmatrix} = \int \begin{bmatrix} \dot{\theta}_1 \\ \dot{\theta}_2 \end{bmatrix} dt \tag{47}$$

For the model reference adaptive control approach,

$$ControllerOut = \tau = \hat{M} u + \hat{V} - F_p e - F_v \dot{e} \tag{48}$$

where $u = K_I \int (r_p - x_p) - K_p x_p - K_d x_v$

The manipulator dynamic equation is:

$$\tau = Ma + V + Gg \tag{49}$$

Hence, the output from the manipulator (i.e. acceleration of joint) is:

$$\hat{M} u + \hat{V} - F_p e - F_v \dot{e} = \tau = Ma + V \tag{50}$$

Thus, the accelerations of the joints are as follows:

$$\Rightarrow \begin{bmatrix} a_1 \\ a_2 \end{bmatrix} = \begin{bmatrix} \ddot{\theta}_1 \\ \ddot{\theta}_2 \end{bmatrix} = M^{-1}(\hat{M}\, u + \hat{V} - F_p e - F_v \dot{e} - V) \tag{51}$$

After deriving the accelerations of the joints, the time integral is taken to obtain the velocities of joints 1 and 2, and another integral is taken to obtain the positions of joints 1 and 2.

Using the same approach, the adaptive algorithm is derived as follows:

$$\begin{aligned} \int_0^T y^T(t)\, \tilde{M}\, u(t) dt &= \int_0^T \begin{bmatrix} y_1 \\ y_2 \end{bmatrix}^T \begin{bmatrix} \tilde{m}_{11} & \tilde{m}_{12} \\ \tilde{m}_{12} & \tilde{m}_{22} \end{bmatrix} \begin{bmatrix} u_1 \\ u_2 \end{bmatrix} dt \\ &= \int_0^T [y_1, y_2] \begin{bmatrix} \tilde{m}_{11} & \tilde{m}_{12} \\ \tilde{m}_{12} & \tilde{m}_{22} \end{bmatrix} \begin{bmatrix} u_1 \\ u_2 \end{bmatrix} dt \\ &= \int_0^T \tilde{m}_{11} y_1 u_1 dt + \int_0^T \tilde{m}_{12}(y_1 u_2 + y_2 u_1) dt + \int_0^T \tilde{m}_{22} y_2 u_2 dt \end{aligned} \tag{52}$$

Considering the first term in the above equation, one needs to find $\frac{d}{dt}\hat{m}_{11}(t) = \frac{d}{dt}\tilde{m}_{11}(t)$, so that

$$\int_0^T \tilde{m}_{11} y_1 u_1 dt \geq -\gamma^2 \tag{53}$$

From

$$\int_0^T z(t)^T \dot{z}(t)\, dt = \frac{z(T)^T z(T)}{2} - \frac{z(0)^T z(0)}{2} \geq -\frac{z(0)^T z(0)}{2} = -{\gamma_0}^2 \tag{54}$$

Hence, by selecting $\frac{d}{dt}\hat{m}_{11}(t) = \frac{d}{dt}\tilde{m}_{11}(t) = k_{m11} y_1 u_1$,

$$\Rightarrow y_1 u_1 = \frac{\dot{\tilde{m}}_{11}(t)}{k_{m11}} \tag{55}$$

Thus:

$$\int_0^T \tilde{m}_{11} y_1 u_1 dt = \int_0^T \tilde{m}_{11} \dot{\tilde{m}}_{11} \frac{1}{k_{m11}} dt = \frac{1}{k_{m11}} \int_0^T \tilde{m}_{11} \dot{\tilde{m}}_{11} dt \geq -\gamma^2 \tag{56}$$

Using the same analysis on the other two terms, we obtain:

$$\frac{d}{dt}\hat{m}_{12}(t) = \frac{d}{dt}\tilde{m}_{12}(t) = k_{m12}(y_1 u_2 + y_2 u_1) \tag{57}$$

$$\frac{d}{dt}\hat{m}_{22}(t) = \frac{d}{dt}\tilde{m}_{22}(t) = k_{m22} y_2 u_2 \tag{58}$$

Derivation for M has now finished. Using the same approach, the adaptive algorithm for N can be obtained as follows:

$$\frac{d}{dt}\hat{n}_{12}(t) = \frac{d}{dt}\tilde{n}_{12}(t) = k_{n12}(2 y_1 x_{v1} x_{v2} - y_2 {x_{v1}}^2) \tag{59}$$

$$\frac{d}{dt}\hat{n}_{22}(t) = \frac{d}{dt}\tilde{n}_{22}(t) = k_{n22} y_1 {x_{v2}}^2 \tag{60}$$

For the MRAC approach, in order to combine the PID and MRAC, we need to re-parametrize the dynamic equation [112]:

$$\begin{bmatrix} (m_1+m_2)l_1^2 + m_2 l_2^2 + 2m_2 l_1 l_2 \cos\theta_2 & m_2 l_2^2 + m_2 l_1 l_2 \cos\theta_2 \\ m_2 l_2^2 + m_2 l_1 l_2 \cos\theta_2 & m_2 l_2^2 \end{bmatrix} \begin{bmatrix} u_1 \\ u_2 \end{bmatrix} + \begin{bmatrix} 2(-m_2 l_1 l_2 \sin\theta_2)\dot{\theta}_1\dot{\theta}_2 + (-m_2 l_1 l_2 \sin\theta_2)\dot{\theta}_2^2 \\ m_2 l_1 l_2 \sin\theta_2 \dot{\theta}_1^2 \end{bmatrix} \tag{61}$$
$$= W \cdot \begin{bmatrix} \Theta_1 \\ \Theta_2 \\ \Theta_3 \end{bmatrix}$$

By choosing

$\Theta_1 = (m_1 + m_2)l_1^2 + m_2 l_2^2$,

$\Theta_2 = m_2 l_2^2$,

$\Theta_3 = m_2 l_1 l_2$

$$\Rightarrow W = \begin{bmatrix} u_1 & u_2 & 2u_1\cos\theta_2 + u_2\cos\theta_2 - 2\dot{\theta}_1\dot{\theta}_2\sin\theta_2 - \dot{\theta}_2\dot{\theta}_2\sin\theta_2 \\ 0 & u_1 + u_2 & u_1\cos\theta_2 + \dot{\theta}_1\dot{\theta}_1\sin\theta_2 \end{bmatrix} \tag{62}$$

Since

$$\tau = W\begin{bmatrix}\Theta_1\\ \Theta_2\\ \Theta_3\end{bmatrix} - F_v \cdot erv - F_p \cdot erp \tag{63}$$

Substituting equation (41) into equation (63), the following equation results:

$$M\ddot{\theta} + N = \tau = W\begin{bmatrix}\Theta_1\\ \Theta_2\\ \Theta_3\end{bmatrix} - F_v \cdot erv - F_p \cdot erp \tag{64}$$

Thus equation (64) results in:

$$\Rightarrow \ddot{\theta} = (W\begin{bmatrix}\Theta_1\\ \Theta_2\\ \Theta_3\end{bmatrix} - F_v \cdot erv - F_p \cdot erp - N)/M \tag{65}$$

5.3.3. Three-DOF Link Case

For the 3-DOF link case, as shown in Figure 5.8, based on the Lagrange method, the dynamic equation is derived as follows.

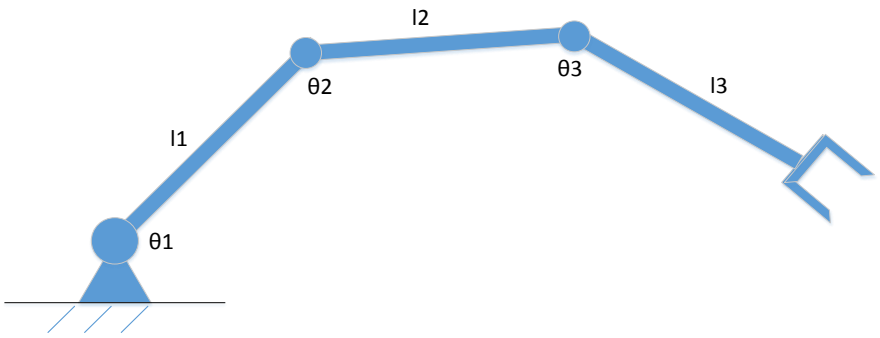

Figure 5.8. Three-link manipulator

The total kinetic energy of the system is:

$$K = \frac{1}{2}(m_1 v_1^{\,2} + m_2 v_2^{\,2} + m_3 v_3^{\,2} + I_1 \dot{\theta}_1^{\,2} + I_2 \dot{\theta}_2^{\,2} + I_3 \dot{\theta}_3^{\,2}) \tag{66}$$

where

$$v_1 = \sqrt{a^2 \dot{\theta}_1^{\,2}}$$

$$v_2 = \sqrt{r_1^2 \dot{\theta}_1^{\,2} + b^2 \dot{\theta}_2^{\,2} + 2 r_1 b \dot{\theta}_1 \dot{\theta}_2 \cos(\theta_2 - \theta_1)}$$

$$v_3 = \sqrt{r_1^2 \dot{\theta}_1^{\,2} + r_2^2 \dot{\theta}_2^{\,2} + c^2 \dot{\theta}_3^{\,2} + 2 r_1 r_2 \dot{\theta}_1 \dot{\theta}_2 \cos(\theta_2 - \theta_1)} + \sqrt{2 r_1 c \dot{\theta}_1 \dot{\theta}_3 \cos(\theta_1 + \theta_3) + 2 r_2 c \dot{\theta}_2 \dot{\theta}_3 \cos(\theta_2 + \theta_3)}$$

Substituting the above three equations into equation (66) results in:

$$\begin{aligned} K = {} & \frac{1}{2}(m_1 a^2 + m_2 r_1^2 + m_3 r_1^2 + I_1)\dot{\theta}_1^{\,2} + \frac{1}{2}(m_2 b^2 + m_3 r_2^{\,2} + I_2)\dot{\theta}_2^{\,2} \\ & + \frac{1}{2}(m_3 c^2 + I_3)\dot{\theta}_3^{\,2} + r_1(m_2 b + m_3 r_2)\cos(\theta_2 - \theta_1)\dot{\theta}_1 \dot{\theta}_2 \\ & + m_3 r_1 c \cos(\theta_1 + \theta_3)\dot{\theta}_1 \dot{\theta}_3 + m_3 r_2 c \cos(\theta_2 + \theta_3)\dot{\theta}_2 \dot{\theta}_3 \end{aligned} \tag{67}$$

The total potential energy of the system is:

$$P = m_1 g h_1 + m_2 g h_2 + m_3 g h_3 \tag{68}$$

where

$$h_1 = a \sin\theta_1$$

$$h_2 = r_1 \sin\theta_1 + b\sin\theta_2$$

$$h_3 = r_1 \sin\theta_1 + r_2 \sin\theta_2 + c\sin\theta_3$$

Substituting the above three equations into equation (68) results in:

$$P = (m_1 a + m_2 r_1 + m_3 r_1) g \sin\theta_1 + (m_2 b + m_3 r_2) g \sin\theta_2 + m_3 g c \sin\theta_3 \tag{69}$$

The Lagrange equation is thus:

$$\begin{aligned} L &= K - P \\ &= \frac{1}{2}(m_1 a^2 + m_2 r_1^2 + m_3 r_1^2 + I_1)\dot{\theta}_1^{\,2} + \frac{1}{2}(m_2 b^2 + m_3 r_2^{\,2} + I_2)\dot{\theta}_2^{\,2} + \frac{1}{2}(m_3 c^2 + I_3)\dot{\theta}_3^{\,2} \\ &\quad + r_1(m_2 b + m_3 r_2)\cos(\theta_2 - \theta_1)\dot{\theta}_1\dot{\theta}_2 + m_3 r_1 c\cos(\theta_1 + \theta_3)\dot{\theta}_1\dot{\theta}_3 + m_3 r_2 c\cos(\theta_2 + \theta_3)\dot{\theta}_2\dot{\theta}_3 \\ &\quad - (m_1 a + m_2 r_1 + m_3 r_1) g \sin\theta_1 - (m_2 b + m_3 r_2) g \sin\theta_2 - m_3 g c \sin\theta_3 \end{aligned} \tag{70}$$

Therefore:

$$\frac{\partial L}{\partial \theta_1} = r_1(m_2 b + m_3 r_2)\sin(\theta_2 - \theta_1)\dot{\theta}_1\dot{\theta}_2 - m_3 r_1 c\sin(\theta_1 + \theta_3)\dot{\theta}_1\dot{\theta}_3 - (m_1 a + m_2 r_1 + m_3 r_1) g\cos\theta_1 \tag{71}$$

$$\frac{\partial L}{\partial \theta_2} = -r_1(m_2 b + m_3 r_2)\sin(\theta_2 - \theta_1)\dot{\theta}_1\dot{\theta}_2 - m_3 r_2 c\sin(\theta_2 + \theta_3)\dot{\theta}_2\dot{\theta}_3 - (m_2 b + m_3 r_2) g\cos\theta_2 \tag{72}$$

$$\frac{\partial L}{\partial \theta_3} = -m_3 r_1 c\sin(\theta_1 + \theta_3)\dot{\theta}_1\dot{\theta}_3 - m_3 r_2 c\sin(\theta_2 + \theta_3)\dot{\theta}_2\dot{\theta}_3 - m_3 g c\cos\theta_3 \tag{73}$$

$$\frac{\partial L}{\partial \dot{\theta}_1} = (m_1 a^2 + m_2 r_1^2 + m_3 r_1^2 + I_1)\dot{\theta}_1 + r_1(m_2 b + m_3 r_2)\cos(\theta_2 - \theta_1)\dot{\theta}_2 + m_3 r_1 c\cos(\theta_1 + \theta_3)\dot{\theta}_3 \tag{74}$$

$$\frac{\partial L}{\partial \dot{\theta}_2} = (m_2 b^2 + m_3 r_2^{\,2} + I_2)\dot{\theta}_2 + r_1(m_2 b + m_3 r_2)\cos(\theta_2 - \theta_1)\dot{\theta}_1 + m_3 r_2 c\cos(\theta_2 + \theta_3)\dot{\theta}_3 \tag{75}$$

$$\frac{\partial L}{\partial \dot{\theta}_3} = (m_3 c^2 + I_3)\dot{\theta}_3 + m_3 r_1 c\cos(\theta_1 + \theta_3)\dot{\theta}_1 + m_3 r_2 c\cos(\theta_2 + \theta_3)\dot{\theta}_2 \tag{76}$$

$$\frac{d}{dt}\frac{\partial L}{\partial \dot{\theta}_1} = (m_1 a^2 + m_2 r_1^2 + m_3 r_1^2 + I_1)\ddot{\theta}_1$$
$$+r_1(m_2 b + m_3 r_2)\cos(\theta_2 - \theta_1)\ddot{\theta}_2 - r_1(m_2 b + m_3 r_2)\sin(\theta_2 - \theta_1)(\dot{\theta}_2 - \dot{\theta}_1)\dot{\theta}_2 \quad (77)$$
$$+m_3 r_1 c\cos(\theta_1 + \theta_3)\ddot{\theta}_3 - m_3 r_1 c\sin(\theta_1 + \theta_3)(\dot{\theta}_1 + \dot{\theta}_3)\dot{\theta}_3$$

$$\frac{d}{dt}\frac{\partial L}{\partial \dot{\theta}_2} = (m_2 b^2 + m_3 r_2^2 + I_2)\ddot{\theta}_2 + r_1(m_2 b + m_3 r_2)\cos(\theta_2 - \theta_1)\ddot{\theta}_1 \quad (78)$$
$$-r_1(m_2 b + m_3 r_2)\sin(\theta_2 - \theta_1)(\dot{\theta}_2 - \dot{\theta}_1)\dot{\theta}_1 + m_3 r_2 c\cos(\theta_2 + \theta_3)\ddot{\theta}_3 - m_3 r_2 c\sin(\theta_2 + \theta_3)(\dot{\theta}_2 + \dot{\theta}_3)\dot{\theta}_3$$

$$\frac{d}{dt}\frac{\partial L}{\partial \dot{\theta}_3} = (m_3 c^2 + I_3)\ddot{\theta}_3 + m_3 r_1 c\cos(\theta_1 + \theta_3)\ddot{\theta}_1 \quad (79)$$
$$-m_3 r_1 c\sin(\theta_1 + \theta_3)(\dot{\theta}_1 + \dot{\theta}_3)\dot{\theta}_1 + m_3 r_2 c\cos(\theta_2 + \theta_3)\ddot{\theta}_2 - m_3 r_2 c\sin(\theta_2 + \theta_3)(\dot{\theta}_2 + \dot{\theta}_3)\dot{\theta}_2$$

Thus:

$$\tau_1 = (m_1 a^2 + m_2 r_1^2 + m_3 r_1^2)\ddot{\theta}_1 + r_1(m_2 b + m_3 r_2)\cos(\theta_2 - \theta_1)\ddot{\theta}_2 + m_3 r_1 c\cos(\theta_1 + \theta_3)\ddot{\theta}_3 \quad (80)$$
$$-r_1(m_2 b + m_3 r_2)\sin(\theta_2 - \theta_1)\dot{\theta}_2^{\,2} - m_3 r_1 c\sin(\theta_1 + \theta_3)\dot{\theta}_3^{\,2} + (m_1 a + m_2 r_1 + m_3 r_1)g\cos\theta_1$$

$$\tau_2 = r_1(m_2 b + m_3 r_2)\cos(\theta_2 - \theta_1)\ddot{\theta}_1 + (m_2 b^2 + m_3 r_2^2)\ddot{\theta}_2 + m_3 r_2 c\cos(\theta_2 + \theta_3)\ddot{\theta}_3 \quad (81)$$
$$+r_1(m_2 b + m_3 r_2)\sin(\theta_2 - \theta_1)\dot{\theta}_1^{\,2} - m_3 r_2 c\sin(\theta_2 + \theta_3)\dot{\theta}_3^{\,2} + (m_2 b + m_3 r_2)g\cos\theta_2$$

$$\tau_3 = m_3 r_1 c\cos(\theta_1 + \theta_3)\ddot{\theta}_1 + m_3 r_2 c\cos(\theta_2 + \theta_3)\ddot{\theta}_2 + m_3 c^2\ddot{\theta}_3 \quad (82)$$
$$-m_3 r_1 c\sin(\theta_1 + \theta_3)\dot{\theta}_1^{\,2} - m_3 r_2 c\sin(\theta_2 + \theta_3)\dot{\theta}_2^{\,2} + m_3 g\cos\theta_3$$

Inserting the above equations in a matrix form, results in the following:

$$\begin{bmatrix}\tau_1\\ \tau_2\\ \tau_3\end{bmatrix} = M\ddot{\theta} + N$$

$$= \begin{bmatrix} m_{11} & m_{12} & m_{13} \\ m_{12} & m_{22} & m_{23} \\ m_{13} & m_{23} & m_{33} \end{bmatrix} \begin{bmatrix} \ddot{\theta}_1 \\ \ddot{\theta}_2 \\ \ddot{\theta}_3 \end{bmatrix} + \begin{bmatrix} n_{11} \\ n_{21} \\ n_{31} \end{bmatrix} \quad (83)$$

where

$$m_{11} = m_1 a^2 + m_2 r_1^2 + m_3 r_1^2$$

$$m_{12} = r_1(m_2 b + m_3 r_2)\cos(\theta_2 - \theta_1)$$

$$m_{13} = m_3 r_1 c \cos(\theta_1 + \theta_3)$$

$$m_{22} = m_2 b^2 + m_3 r_2^2$$

$$m_{23} = m_3 r_2 c \cos(\theta_2 + \theta_3)$$

$$m_{33} = m_3 c^2$$

$$n_{11} = -r_1(m_2 b + m_3 r_2)\sin(\theta_2 - \theta_1)\dot{\theta}_2^2 - m_3 r_1 c \sin(\theta_1 + \theta_3)\dot{\theta}_3^2$$

$$n_{21} = r_1(m_2 b + m_3 r_2)\sin(\theta_2 - \theta_1)\dot{\theta}_1^2 - m_3 r_2 c \sin(\theta_2 + \theta_3)\dot{\theta}_3^2$$

$$n_{31} = -m_3 r_1 c \sin(\theta_1 + \theta_3)\dot{\theta}_1^2 - m_3 r_2 c \sin(\theta_2 + \theta_3)\dot{\theta}_2^2$$

$$a = \frac{l_1}{2},\ b = \frac{l_2}{2},\ c = \frac{l_3}{2},\ r_1 = l_1,\ r_2 = l_2,\ r_3 = l_3$$

Applying the PID controller, the controller output is the torque,

$$K_p e + K_i \int e dt + K_d \dot{e} = \begin{bmatrix}\tau_1\\ \tau_2\\ \tau_3\end{bmatrix} \quad (84)$$

where error $e = r_p - x_p$. Knowing the 2-link manipulator M and N matrices, the output from the manipulator (i.e. acceleration of joints 1 and 2) can be determined as follows:

$$\begin{bmatrix} \tau_1 \\ \tau_2 \\ \tau_3 \end{bmatrix} = M\ddot{\theta} + N + Gg$$
$$= \begin{bmatrix} m_{11} & m_{12} & m_{13} \\ m_{12} & m_{22} & m_{23} \\ m_{13} & m_{23} & m_{33} \end{bmatrix} \begin{bmatrix} \ddot{\theta}_1 \\ \ddot{\theta}_2 \\ \ddot{\theta}_3 \end{bmatrix} + \begin{bmatrix} n_{11} \\ n_{21} \\ n_{31} \end{bmatrix} + \begin{bmatrix} g_{11} \\ g_{21} \\ g_{31} \end{bmatrix} g \tag{85}$$

Hence,

$$K_p e + K_i \int e dt + K_d \dot{e} = \begin{bmatrix} \tau_1 \\ \tau_2 \\ \tau_3 \end{bmatrix} = M\ddot{\theta} + N + Gg \tag{86}$$

Therefore, the accelerations of joints 1 and 2 are obtained as follows from equation (86):

$$\Rightarrow \begin{bmatrix} \ddot{\theta}_1 \\ \ddot{\theta}_2 \end{bmatrix} = M^{-1}(K_p e + K_i \int e dt + K_d \dot{e} - N) \tag{87}$$

After deriving the accelerations of joints 1 and 2, the time integral is taken to obtain the velocities of joints 1 and 2, and another integral is taken to obtain the positions of joints 1 and 2.

$$\begin{bmatrix} \dot{\theta}_1 \\ \dot{\theta}_2 \\ \dot{\theta}_3 \end{bmatrix} = \int \begin{bmatrix} \ddot{\theta}_1 \\ \ddot{\theta}_2 \\ \ddot{\theta}_3 \end{bmatrix} dt \tag{88}$$

$$\begin{bmatrix}\theta_1\\ \theta_2\\ \theta_3\end{bmatrix} = \int \begin{bmatrix}\dot{\theta}_1\\ \dot{\theta}_2\\ \dot{\theta}_3\end{bmatrix} dt \tag{89}$$

For the model reference adaptive control approach,

$$ControllerOut = \tau = \hat{M}\, u + \hat{V} - F_p e - F_v \dot{e} \tag{90}$$

where $u = K_I \int (r_p - x_p) - K_p x_p - K_d x_v$

The manipulator dynamic equation is: $\tau = Ma + V + Gg$, so the output from the manipulator (i.e. acceleration of joint) is:

$$\hat{M}\, u + \hat{V} - F_p e - F_v \dot{e} = \tau = Ma + V \tag{91}$$

From equation (91), the following is obtained:

$$\Rightarrow \begin{bmatrix}a_1\\ a_2\\ a_3\end{bmatrix} = \begin{bmatrix}\ddot{\theta}_1\\ \ddot{\theta}_2\\ \ddot{\theta}_3\end{bmatrix} = M^{-1}(\hat{M}\, u + \hat{V} - F_p e - F_v \dot{e} - V) \tag{92}$$

Similarly, after deriving the accelerations of the joints, the time integral is taken to obtain the velocities of the joints and another integral is taken to obtain the positions of the joints.

$$\begin{bmatrix}\dot{\theta}_1\\ \dot{\theta}_2\\ \dot{\theta}_3\end{bmatrix} = \int \begin{bmatrix}\ddot{\theta}_1\\ \ddot{\theta}_2\\ \ddot{\theta}_3\end{bmatrix} dt \tag{93}$$

$$\begin{bmatrix}\theta_1\\ \theta_2\\ \theta_3\end{bmatrix} = \int \begin{bmatrix}\dot{\theta}_1\\ \dot{\theta}_2\\ \dot{\theta}_3\end{bmatrix} dt \tag{94}$$

The adaptive algorithm is now derived as follows:

Since $w(t) = -m(t)$, and

$$\begin{aligned} m(t) &= (M - \hat{M})u(t) + (V - \hat{V}) \\ &= (M - \hat{M})u(t) + \begin{bmatrix} x_v^T (N_1 - \hat{N}_1(t)) x_v \\ x_v^T (N_2 - \hat{N}_2(t)) x_v \\ x_v^T (N_3 - \hat{N}_3(t)) x_v \end{bmatrix} \end{aligned} \tag{95}$$

Therefore:

$$w(t) = (\hat{M} - M)u(t) + \begin{bmatrix} x_v^T (\hat{N}_1(t) - N_1) x_v \\ x_v^T (\hat{N}_2(t) - N_2) x_v \\ x_v^T (\hat{N}_3(t) - N_3) x_v \end{bmatrix} \tag{96}$$

Note that:

$$\tilde{\tilde{M}} = \hat{M} - M \tag{97}$$

Hence,

$$\int_0^T y^T(t) w(t) dt = \int_0^T y^T(t) \tilde{\tilde{M}} u(t) dt + \sum_{i=1}^{3} \int_0^T y_i(t) x_v^T (\hat{N}_i - N_i) x_v dt \tag{98}$$

The first term is used to derive the adaptive algorithm for M, and the second term is used to derive the adaptive algorithm for N.

For the first term:

$$\int_0^T y^T(t)\,\tilde{M}\,u(t)dt = \int_0^T \begin{bmatrix} y_1 \\ y_2 \\ y_3 \end{bmatrix}^T \begin{bmatrix} \tilde{m}_{11} & \tilde{m}_{12} & \tilde{m}_{13} \\ \tilde{m}_{12} & \tilde{m}_{22} & \tilde{m}_{23} \\ \tilde{m}_{13} & \tilde{m}_{23} & \tilde{m}_{33} \end{bmatrix} \begin{bmatrix} u_1 \\ u_2 \\ u_3 \end{bmatrix} dt$$

$$= \int_0^T [y_1, y_2, y_3] \begin{bmatrix} \tilde{m}_{11} & \tilde{m}_{12} & \tilde{m}_{13} \\ \tilde{m}_{12} & \tilde{m}_{22} & \tilde{m}_{23} \\ \tilde{m}_{13} & \tilde{m}_{23} & \tilde{m}_{33} \end{bmatrix} \begin{bmatrix} u_1 \\ u_2 \\ u_3 \end{bmatrix} dt \tag{99}$$

$$= \int_0^T \tilde{m}_{11} y_1 u_1 dt + \int_0^T \tilde{m}_{12}(y_1 u_2 + y_2 u_1)dt + \int_0^T \tilde{m}_{13}(y_3 u_1 + y_1 u_3)dt$$
$$+ \int_0^T \tilde{m}_{22} y_2 u_2 dt + \int_0^T \tilde{m}_{23}(y_3 u_2 + y_2 u_3)dt + \int_0^T \tilde{m}_{33}\, y_3 u_3 dt$$

Considering the first term in the above equation, one needs to find $\frac{d}{dt}\hat{m}_{11}(t) = \frac{d}{dt}\tilde{m}_{11}(t)$,

(it is assumed that M is constant, i.e. $\dot{M} = 0$), so that

$$\int_0^T \tilde{m}_{11} y_1 u_1 dt \geq -\gamma^2 \tag{100}$$

From

$$\int_0^T z(t)^T\, \dot{z}(t)\, dt = \frac{z(T)^T z(T)}{2} - \frac{z(0)^T z(0)}{2} \geq -\frac{z(0)^T z(0)}{2} = -{\gamma_0}^2 \tag{101}$$

Thus, by selecting $\frac{d}{dt}\hat{m}_{11}(t) = \frac{d}{dt}\tilde{m}_{11}(t) = k_{m11} y_1 u_1$

$$\Rightarrow y_1 u_1 = \frac{\dot{\tilde{m}}_{11}(t)}{k_{m11}} \tag{102}$$

Then

$$\int_0^T \tilde{m}_{11} y_1 u_1 dt = \int_0^T \tilde{m}_{11} \dot{\tilde{m}}_{11} \frac{1}{k_{m11}} dt$$
$$= \frac{1}{k_{m11}} \int_0^T \tilde{m}_{11} \dot{\tilde{m}}_{11} dt \geq -\gamma^2 \quad (103)$$

Using the same analysis on the other two terms, we obtain:

$$\frac{d}{dt} \hat{m}_{12}(t) = \frac{d}{dt} \tilde{m}_{12}(t) = k_{m12}(y_1 u_2 + y_2 u_1) \quad (104)$$

$$\frac{d}{dt} \hat{m}_{13}(t) = \frac{d}{dt} \tilde{m}_{13}(t) = k_{m13}(y_3 u_1 + y_1 u_3) \quad (105)$$

$$\frac{d}{dt} \hat{m}_{22}(t) = \frac{d}{dt} \tilde{m}_{22}(t) = k_{m22} y_2 u_2 \quad (106)$$

$$\frac{d}{dt} \hat{m}_{23}(t) = \frac{d}{dt} \tilde{m}_{23}(t) = k_{m23}(y_3 u_2 + y_2 u_3) \quad (107)$$

$$\frac{d}{dt} \hat{m}_{33}(t) = \frac{d}{dt} \tilde{m}_{33}(t) = k_{m33} y_3 u_3 \quad (108)$$

For the derivation of N :

Since

$$\int_0^T y^T(t) w(t) dt$$
$$= \int_0^T y^T(t) \tilde{M} u(t) dt + \sum_{i=1}^{3} \int_0^T y_i(t) x_v^T (\hat{N}_i - N_i) x_v dt \quad (109)$$

The first term has been used to derive the adaptation algorithm for M . The second term is now used to derive the adaptation algorithm for N .

$$\sum_{i=1}^{3}\int_0^T y_i(t)x_v{}^T(\hat{N}_i - N_i)x_v dt$$

$$= \int_0^T y_1(t)x_v{}^T(\hat{N}_1 - N_1)x_v dt + \int_0^T y_2(t)x_v{}^T(\hat{N}_2 - N_2)x_v dt + \int_0^T y_3(t)x_v{}^T(\hat{N}_3 - N_3)x_v dt$$

$$= \int_0^T y_1(t)x_v{}^T \tilde{N}_1\, x_v dt + \int_0^T y_2(t)x_v{}^T \tilde{N}_2\, x_v dt + \int_0^T y_3(t)x_v{}^T \tilde{N}_3\, x_v dt$$

$$= \int_0^T y_1(t)\begin{bmatrix} x_{v1} & x_{v2} & x_{v3}\end{bmatrix}\begin{bmatrix} 0 & \tilde{n}_{12}^1 & \tilde{n}_{13}^1 \\ \tilde{n}_{12}^1 & \tilde{n}_{22}^1 & \tilde{n}_{33}^1 \\ \tilde{n}_{13}^1 & \tilde{n}_{33}^1 & \tilde{n}_{33}^1 \end{bmatrix}\begin{bmatrix} x_{v1} \\ x_{v2} \\ x_{v3}\end{bmatrix} dt + \int_0^T y_2(t)\begin{bmatrix} x_{v1} & x_{v2} & x_{v3}\end{bmatrix}\begin{bmatrix} -\tilde{n}_{12}^1 & 0 & 0 \\ 0 & 0 & \tilde{n}_{33}^2 \\ 0 & \tilde{n}_{33}^2 & \tilde{n}_{33}^2 \end{bmatrix}\begin{bmatrix} x_{v1} \\ x_{v2} \\ x_{v3}\end{bmatrix} dt$$

$$+\int_0^T y_3(t)\begin{bmatrix} x_{v1} & x_{v2} & x_{v3}\end{bmatrix}\begin{bmatrix} -\tilde{n}_{13}^1 & 0 & 0 \\ 0 & -\tilde{n}_{33}^2 & 0 \\ 0 & 0 & 0 \end{bmatrix}\begin{bmatrix} x_{v1} \\ x_{v2} \\ x_{v3}\end{bmatrix} dt$$

$$= \int_0^T \begin{bmatrix} y_1x_{v2}\,\tilde{n}_{12}^1 + y_1x_{v3}\,\tilde{n}_{13}^1 & y_1x_{v1}\,\tilde{n}_{12}^1 + y_1x_{v2}\,\tilde{n}_{22}^1 + y_1x_{v3}\,\tilde{n}_{33}^1 & y_1x_{v1}\,\tilde{n}_{13}^1 + y_1x_{v2}\,\tilde{n}_{33}^1 + y_1x_{v3}\,\tilde{n}_{33}^1 \end{bmatrix}\begin{bmatrix} x_{v1} \\ x_{v2} \\ x_{v3}\end{bmatrix} dt$$

$$+\int_0^T \begin{bmatrix} -y_2x_{v1}\,\tilde{n}_{12}^1 & y_2x_{v3}\,\tilde{n}_{33}^2 & y_2x_{v2}\,\tilde{n}_{33}^2 + y_2x_{v3}\,\tilde{n}_{33}^2 \end{bmatrix}\begin{bmatrix} x_{v1} \\ x_{v2} \\ x_{v3}\end{bmatrix} dt + \int_0^T \begin{bmatrix} -y_3x_{v1}\,\tilde{n}_{13}^1 & -y_3x_{v2}\,\tilde{n}_{33}^2 & 0 \end{bmatrix}\begin{bmatrix} x_{v1} \\ x_{v2} \\ x_{v3}\end{bmatrix} dt$$

$$= \int_0^T \left[y_1x_{v2}\,\tilde{n}_{12}^1 x_{v1} + y_1x_{v3}\,\tilde{n}_{13}^1 x_{v1} + y_1x_{v1}\,\tilde{n}_{12}^1 x_{v2} + y_1x_{v2}\,\tilde{n}_{22}^1 x_{v2} + y_1x_{v3}\,\tilde{n}_{33}^1 x_{v2} + y_1x_{v1}\,\tilde{n}_{13}^1 x_{v3} + y_1x_{v2}\,\tilde{n}_{33}^1 x_{v3} + y_1x_{v3}{}^2\,\tilde{n}_{33}^1 \right] dt \quad (110)$$

$$+\int_0^T \left[-y_2x_{v1}{}^2\,\tilde{n}_{12}^1 + y_2x_{v3}\,\tilde{n}_{33}^2 x_{v2} + y_2x_{v2}\,\tilde{n}_{33}^2 x_{v3} + y_2x_{v3}{}^2\,\tilde{n}_{33}^2 \right] dt + \int_0^T \left[-y_3x_{v1}{}^2\,\tilde{n}_{13}^1 - y_3x_{v2}{}^2\,\tilde{n}_{33}^2 \right] dt$$

$$= \int_0^T \tilde{n}_{12}^1(y_1x_{v2}x_{v1} + y_1x_{v1}x_{v2} - y_2x_{v1}^2)dt + \int_0^T \tilde{n}_{13}^1(y_1x_{v3}x_{v1} + y_1x_{v1}x_{v3} - y_3x_{v1}^2)dt + \int_0^T \tilde{n}_{22}^1(y_1x_{v2}^2)dt$$

$$+\int_0^T \tilde{n}_{33}^1(y_1x_{v3}x_{v2} + y_1x_{v2}x_{v3} + y_2x_{v3}^2)dt + \int_0^T \tilde{n}_{33}^2(y_2x_{v3}x_{v2} + y_2x_{v2}x_{v3} + y_2x_{v3}^2 - y_3x_{v2}^2)dt$$

Thus:

$$\frac{d}{dt}\hat{n}_{12}(t) = \frac{d}{dt}\tilde{n}_{12}(t) = k_{n12}(2y_1x_{v1}x_{v2} - y_2x_{v1}{}^2) \quad (111)$$

$$\frac{d}{dt}\hat{n}_{13}(t) = \frac{d}{dt}\tilde{n}_{13}(t) = k_{n13}(2y_1x_{v1}x_{v3} - y_3x_{v1}{}^2) \quad (112)$$

$$\frac{d}{dt}\hat{n}_{22}(t) = \frac{d}{dt}\tilde{n}_{22}(t) = k_{n22}y_1x_{v2}{}^2 \quad (113)$$

$$\frac{d}{dt}\hat{n}_{33}{}^1(t) = \frac{d}{dt}\tilde{n}_{13}{}^1(t) = k_{n33}^1(2y_1x_{v2}x_{v3} - y_1x_{v3}{}^2) \quad (114)$$

$$\frac{d}{dt}\hat{n}_{33}^{2}(t)=\frac{d}{dt}\tilde{n}_{13}^{2}(t)=k_{n33}^{2}(2y_2x_{v2}x_{v3}+y_2x_{v3}^{2}-y_3x_{v2}^{2}) \tag{115}$$

For the model reference adaptive control approach, in order to combine the PID and MRAC, by re-parametrizing the dynamic equation, we obtain:

$$\begin{bmatrix} m_1a^2+m_2r_1^2+m_3r_1^2 & r_1(m_2b+m_3r_2)\cos(\theta_2-\theta_1) & m_3r_1c\cos(\theta_1+\theta_3) \\ r_1(m_2b+m_3r_2)\cos(\theta_2-\theta_1) & m_2b^2+m_3r_2^2 & m_3r_2c\cos(\theta_2+\theta_3) \\ m_3r_1c\cos(\theta_1+\theta_3) & m_3r_2c\cos(\theta_2+\theta_3) & m_3c^2 \end{bmatrix}\begin{bmatrix} u_1 \\ u_2 \\ u_3 \end{bmatrix}+$$
$$\begin{bmatrix} -r_1(m_2b+m_3r_2)\sin(\theta_2-\theta_1)\dot{\theta}_2^{2}-m_3r_1c\sin(\theta_1+\theta_3)\dot{\theta}_3^{2} \\ r_1(m_2b+m_3r_2)\sin(\theta_2-\theta_1)\dot{\theta}_1^{2}-m_3r_2c\sin(\theta_2+\theta_3)\dot{\theta}_3^{2} \\ -m_3r_1c\sin(\theta_1+\theta_3)\dot{\theta}_1^{2}-m_3r_2c\sin(\theta_2+\theta_3)\dot{\theta}_2^{2} \end{bmatrix}=W\cdot\begin{bmatrix} \Theta_1 \\ \Theta_2 \\ \Theta_3 \\ \Theta_4 \\ \Theta_5 \\ \Theta_6 \end{bmatrix} \tag{116}$$

By choosing:

$$\Theta_1=m_1a^2+m_2r_1^2+m_3r_1^2$$

$$\Theta_2=r_1(m_2b+m_3r_2)$$

$$\Theta_3=m_3r_1c$$

$$\Theta_4=m_2b^2+m_3r_2^2$$

$$\Theta_5=m_3r_2c$$

$$\Theta_6=m_3c^2$$

The following is obtained:

$$\Rightarrow W=\begin{bmatrix} u_1 & u_2\cos(\theta_2-\theta_1)-\sin(\theta_2-\theta_1)\dot{\theta}_2^{2} & u_3\cos(\theta_1+\theta_3)-\sin(\theta_1+\theta_3)\dot{\theta}_3^{2} & 0 & 0 & 0 \\ 0 & u_1\cos(\theta_2-\theta_1)+\sin(\theta_2-\theta_1)\dot{\theta}_1^{2} & 0 & u_2 & u_3\cos(\theta_2+\theta_3)-\sin(\theta_2+\theta_3)\dot{\theta}_3^{2} & 0 \\ 0 & 0 & u_1\cos(\theta_1+\theta_3)-\sin(\theta_1+\theta_3)\dot{\theta}_1^{2} & 0 & u_2\cos(\theta_2+\theta_3)-\sin(\theta_2+\theta_3)\dot{\theta}_2^{2} & u_3 \end{bmatrix} \tag{117}$$

Since

$$\tau = W \begin{bmatrix} \Theta_1 \\ \Theta_2 \\ \Theta_3 \\ \Theta_4 \\ \Theta_5 \\ \Theta_6 \end{bmatrix} - F_v \cdot erv - F_p \cdot erp \tag{118}$$

Substituting equation (83) into equation (118) yields the following:

$$M \ddot{\theta} + N = \tau = W \begin{bmatrix} \Theta_1 \\ \Theta_2 \\ \Theta_3 \\ \Theta_4 \\ \Theta_5 \\ \Theta_6 \end{bmatrix} - F_v \cdot erv - F_p \cdot erp \tag{119}$$

Thus equation (119) results in:

$$\Rightarrow \ddot{\theta} = (W \begin{bmatrix} \Theta_1 \\ \Theta_2 \\ \Theta_3 \\ \Theta_4 \\ \Theta_5 \\ \Theta_6 \end{bmatrix} - F_v \cdot erv - F_p \cdot erp - N) / M \tag{120}$$

5.4. Simulation and Comparison between PID, MRAC and Hybrid Control

For the 1-DOF manipulator, after applying different masses, the joint motion output is illustrated in Figure 5.9. When the payload is 0, joint 1 motion is quite steady, but when the payload increases to 5 and 15, one can see that joint 1 motion is no longer the same, and also the joint output increases and decreases. By using the MRAC approach, we can

see from Figure 5.10 that under different payload masses, three lines coincide with each other under different payload masses. Joint 1 motion is the same, and the payload mass variation effect has been compensated.

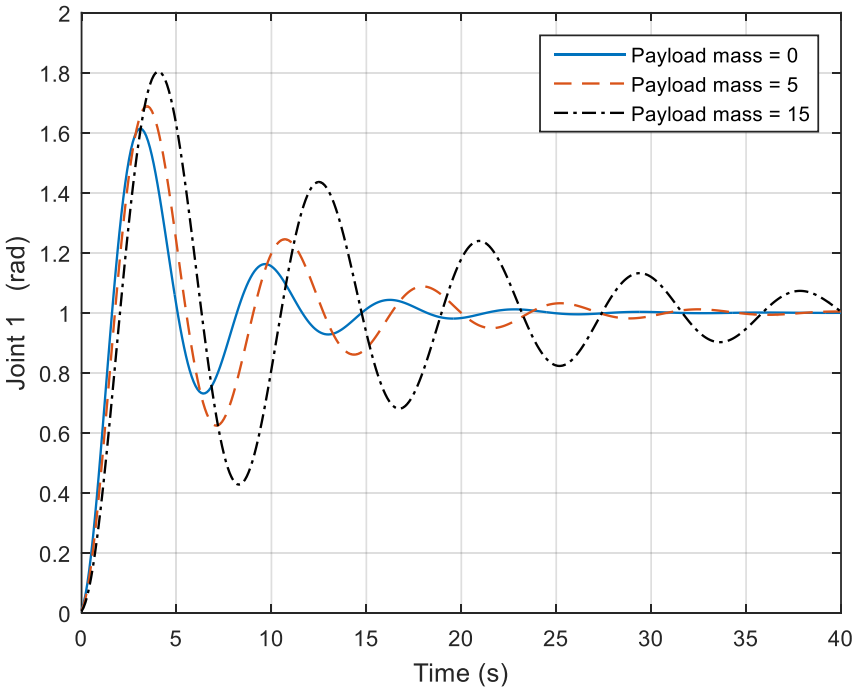

Figure 5.9. Joint 1 motion

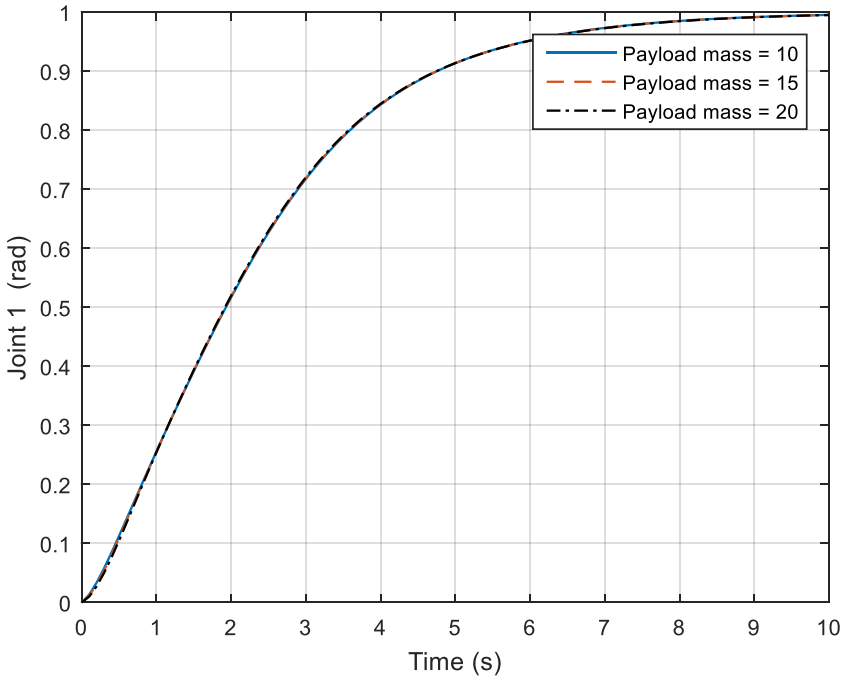

Figure 5.10. Joint 1 motion output

As shown in Figure 5.11, we can see that, for the PID control, it will take roughly 40 seconds to converge to 0. The MRAC control will take about 20 seconds to converge to the desired position, which is half the time of the PID control. Finally, the hybrid control takes about 10 seconds to converge to the desired position, which halves the time of the MRAC control. Another difference between the MRAC and the hybrid controls is that the MRAC control gradually converges to the desired position whereas the hybrid control first very quickly overshoots the desired position, to which it then gradually converges. After applying different masses, we found that the hybrid control is better than that of the PID and MRAC for all the mass cases. Here we list two of them (10kg and 15kg cases) as an illustration, as shown in Figures 5.11 and 5.12, respectively. From the above analysis, we can see that the convergence performance for the hybrid control is better than that of the MRAC control, and the MRAC control is better than the PID control.

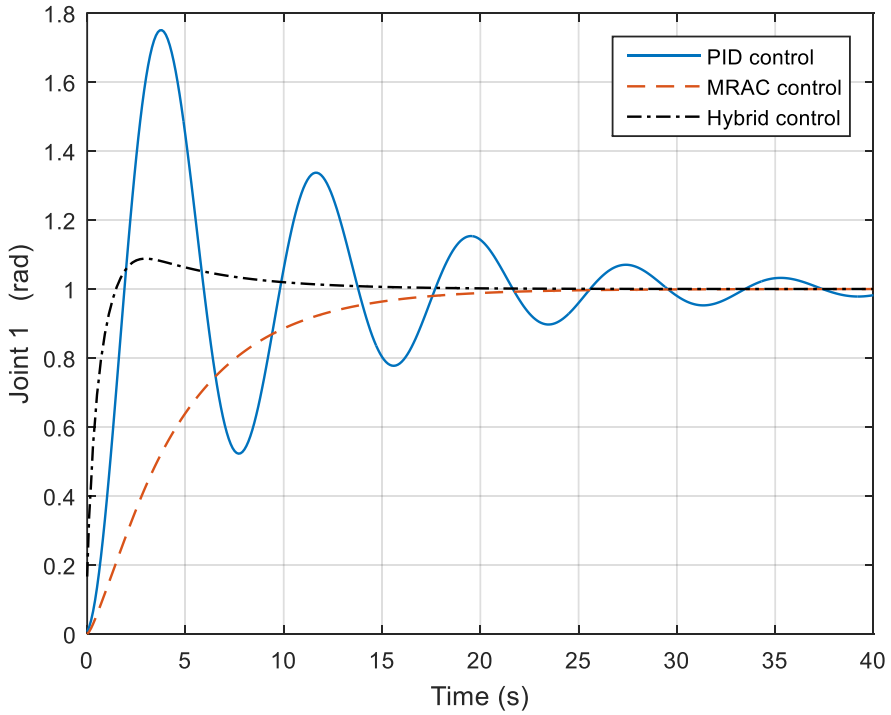

Figure 5.11. Joint output under PID, MRAC and hybrid control when payload is 10 kg

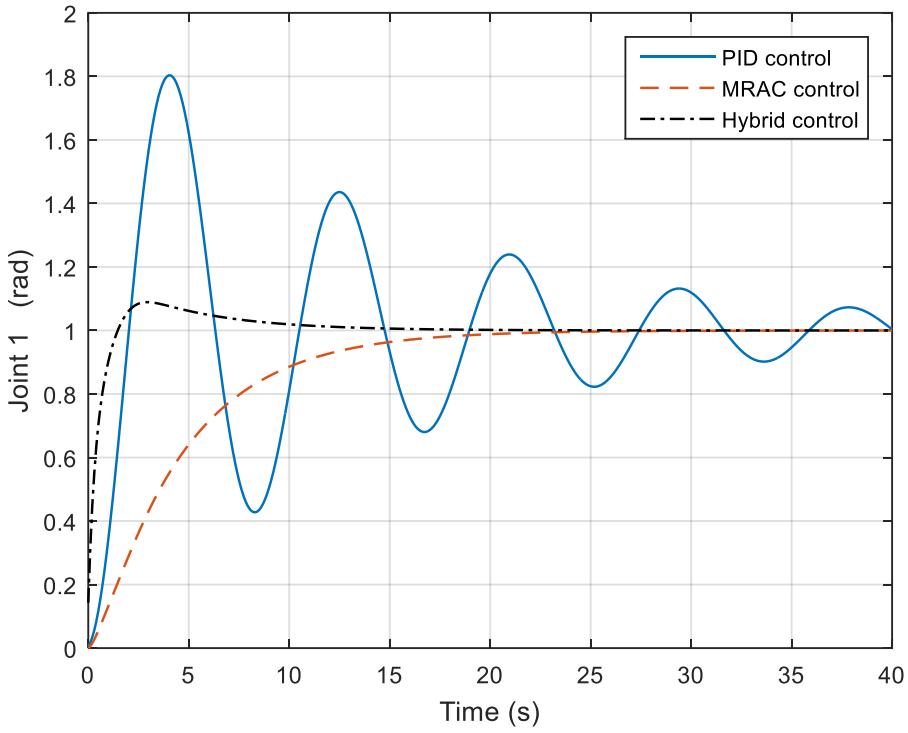

Figure 5.12. Joint output under PID, MRAC and hybrid control when payload is 15 kg

For the 2-DOF link case, after applying different payload masses, joint 1 motion output is illustrated in Figure 5.13(a) while joint 2 motion output is shown in Figure 5.13(b). For joint 1, when the payload is 0, the motion is quite steady, but when the payload increases to 5 and 15, one can see that joint 1 motion is no longer the same, as shown in Figure 5.13(a), and also the joint output increases and decreases. The same applies to joint 2, as seen in Figure 5.13(b). Figure 5.14(a) and (b) shows joints 1 and 2 output under different payload masses. By using the MRAC approach, three lines coincide with each other under different payload masses; i.e. the payload mass variation effect has been compensated.

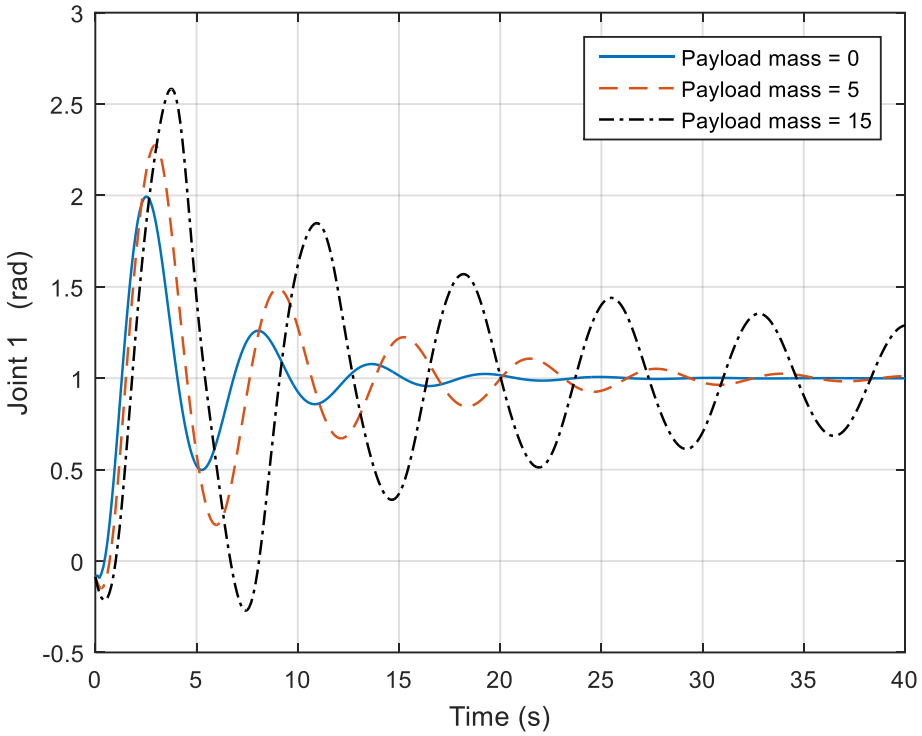

(a). Joint 1 output

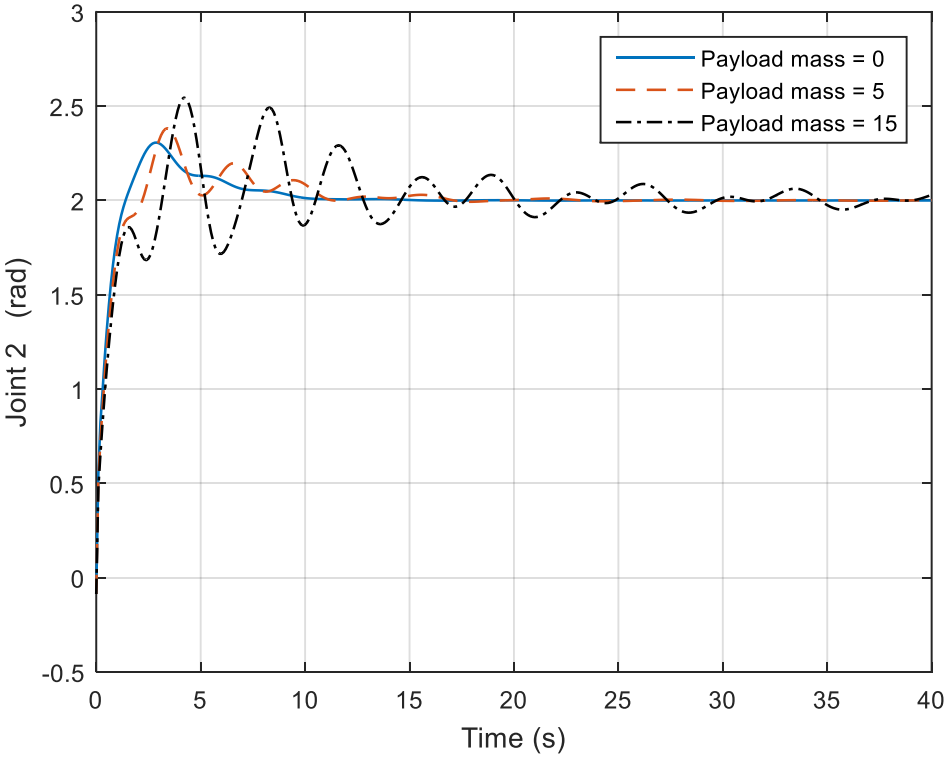

(b). Joint 2 output

Figure 5.13. Joints 1 and 2 output under PID

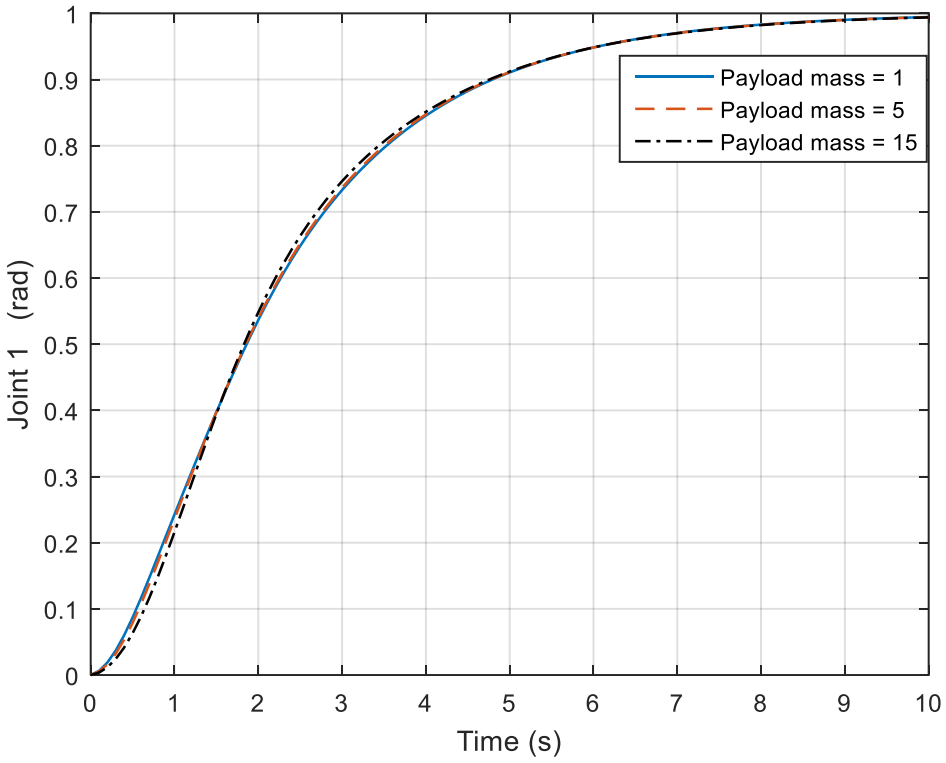

(a). Joint 1 output

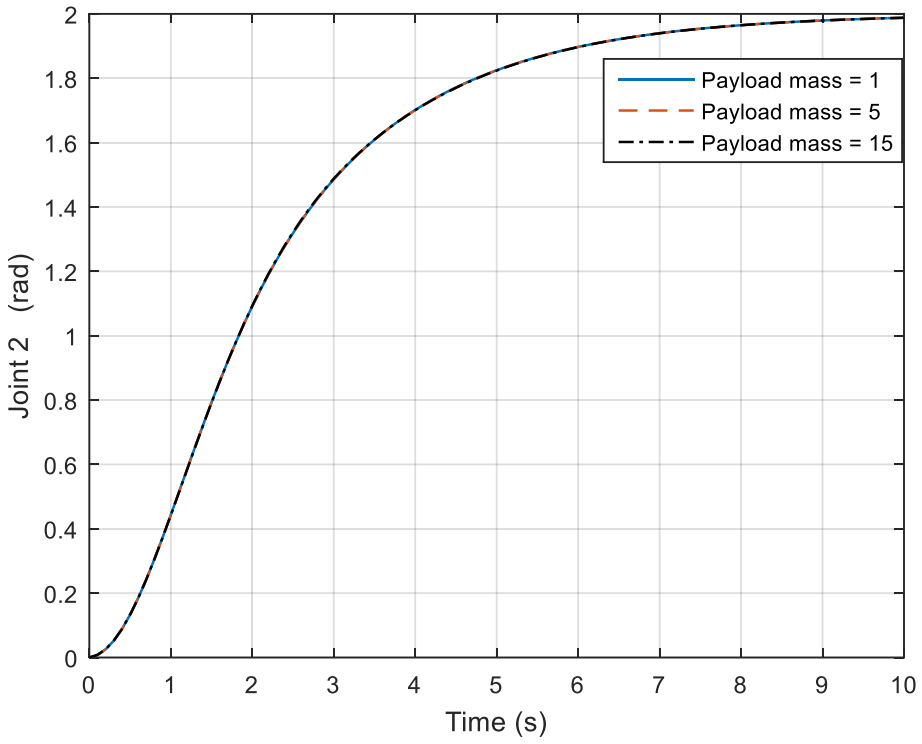

(b). Joint 2 output

Figure 5.14. Joints 1 and 2 output under MRAC

Furthermore, the convergence speed for the hybrid controller is faster than that of the MRAC controller, as shown in Figure 5.15. The hybrid and MRAC controllers are both better than that of the PID controller. After applying different masses, we found that hybrid control is better than that of the PID and MRAC for all the mass cases. Here we list two of them (1kg and 5kg cases) as an illustration, as shown in Figures 5.15 and 5.16. By using the same method, the process can be extended to multi-DOF serial manipulators.

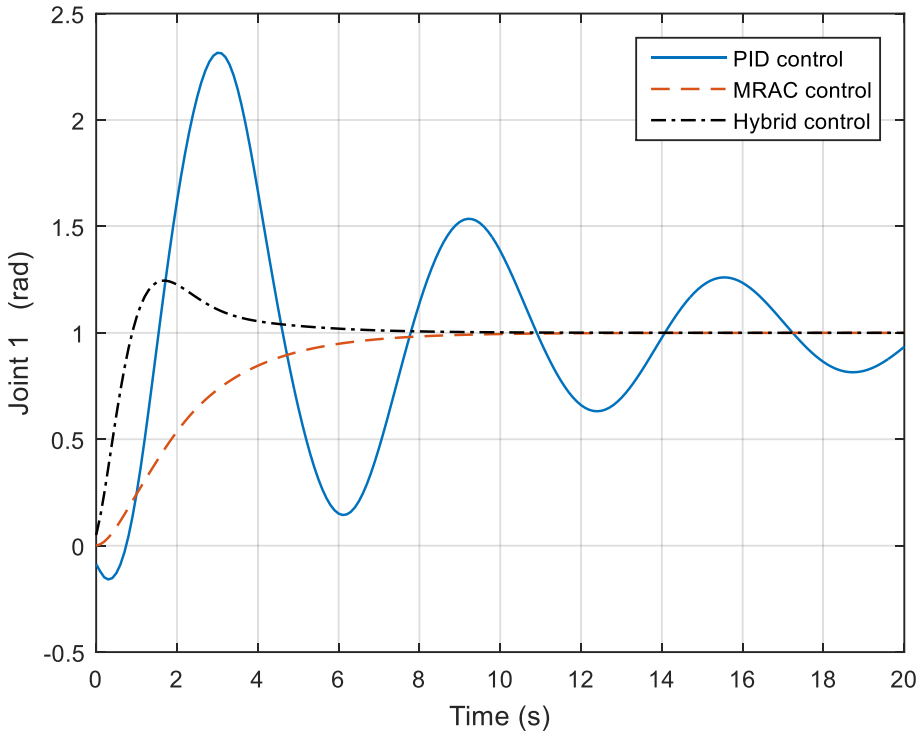

(a). Joint 1 output

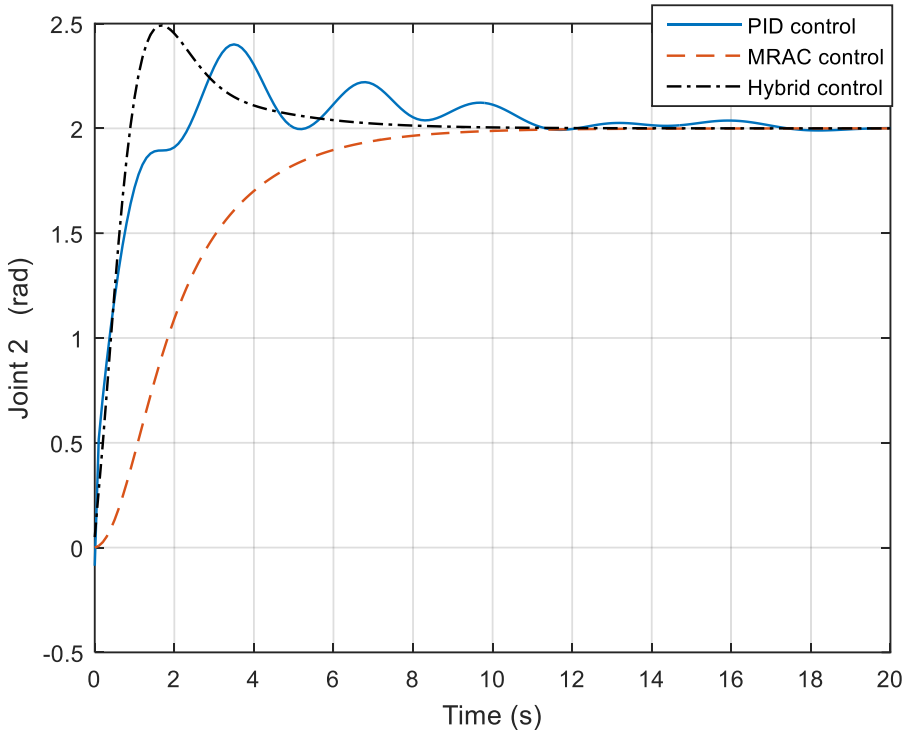

(a). Joint 2 output

Figure 5.15. Joints 1 and 2 output under PID, MRAC and hybrid control when payload is 1kg

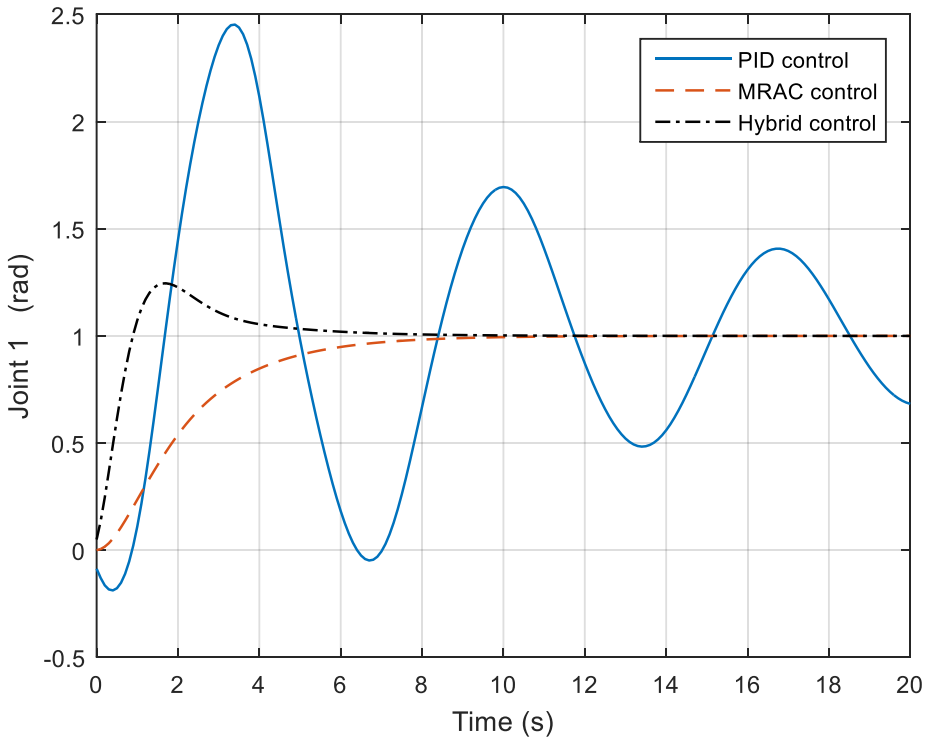

(a). Joint 1 output

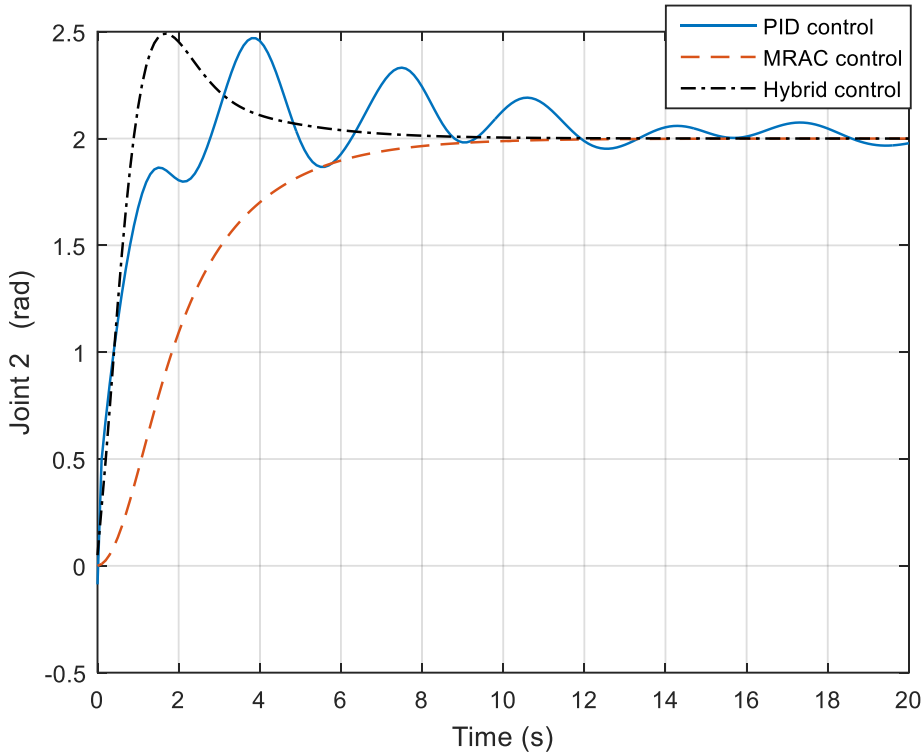

(b). Joint 2 output

Figure 5.16. Joints 1 and 2 output under PID, MRAC and hybrid control when payload is 5kg

For the 3-DOF case, after applying different payload masses, the joints motion output is illustrated in Figure 5.17. For joint 1, when the payload is 0, the motion is quite steady, but when the payload increases to 5 and 15, we can see that joint 1 motion is no longer the same. The same applies to joints 2 and 3. Figure 5.18 shows the joints output under different payload masses. By using the MRAC approach, the payload masses variation effect has been resolved. We can see that three lines coincide with each other under different payload masses; i.e. the payload mass variation effect has been compensated.

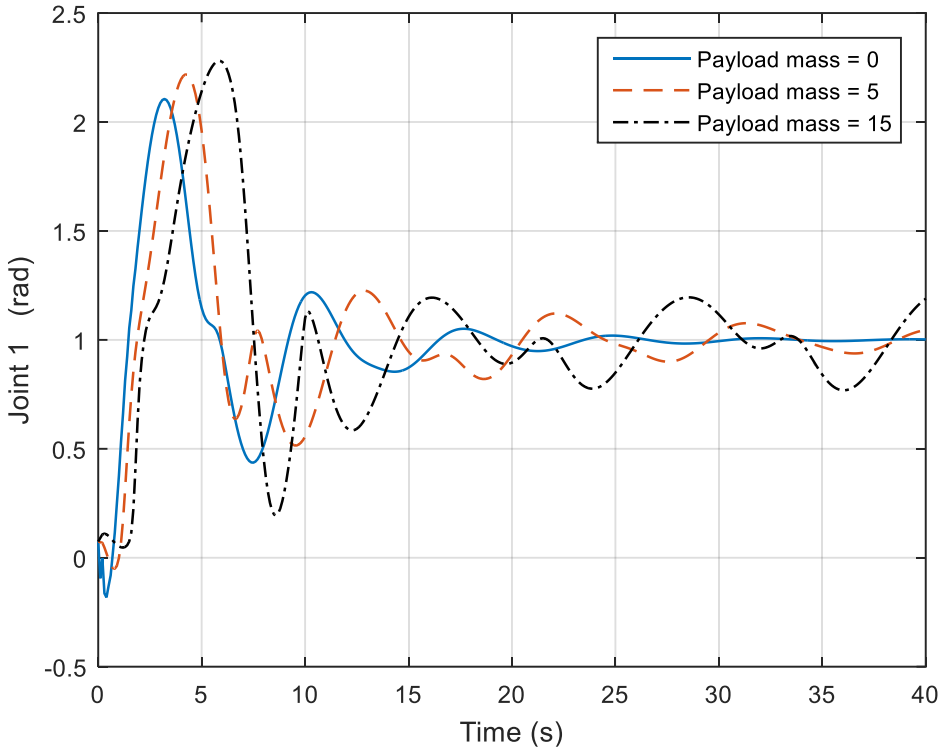

(a). Joint 1 output

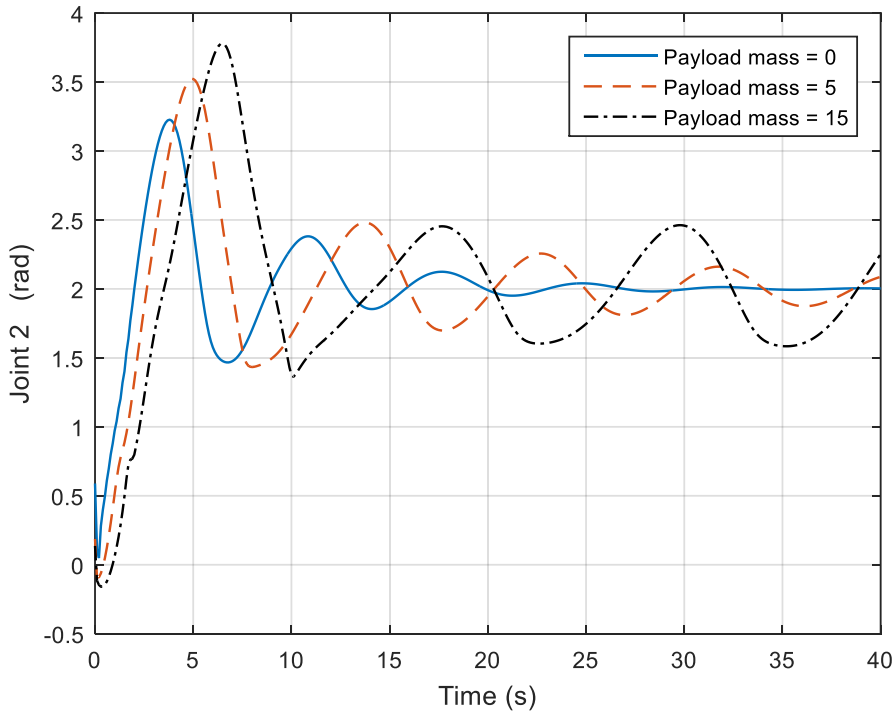

(b). Joint 2 output

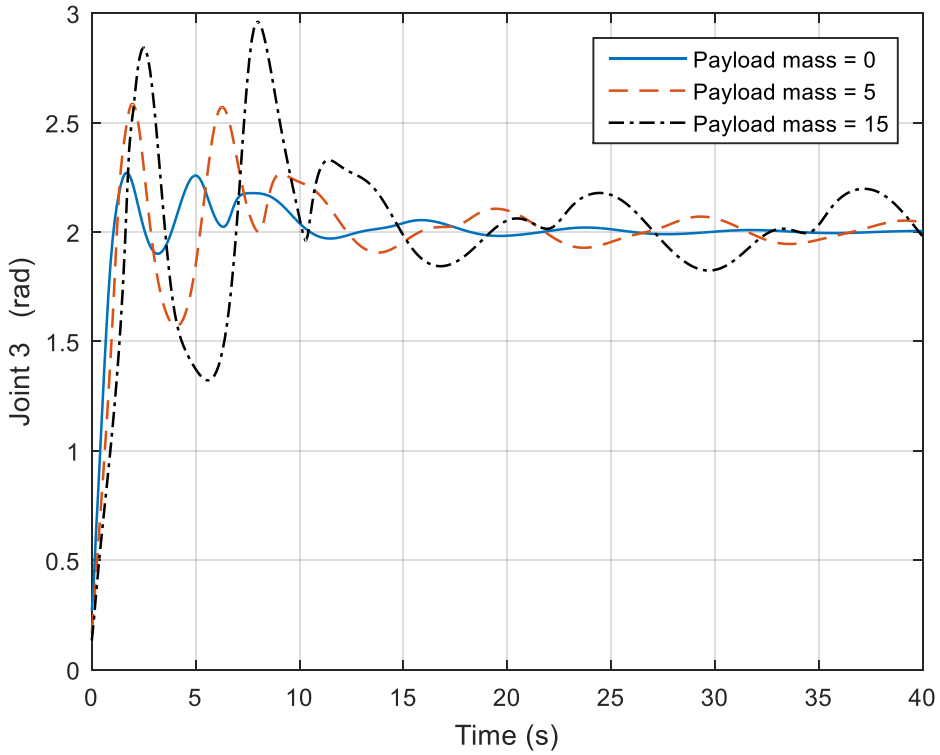

(c). Joint 3 output

Figure 5.17. Joints 1, 2, and 3 output

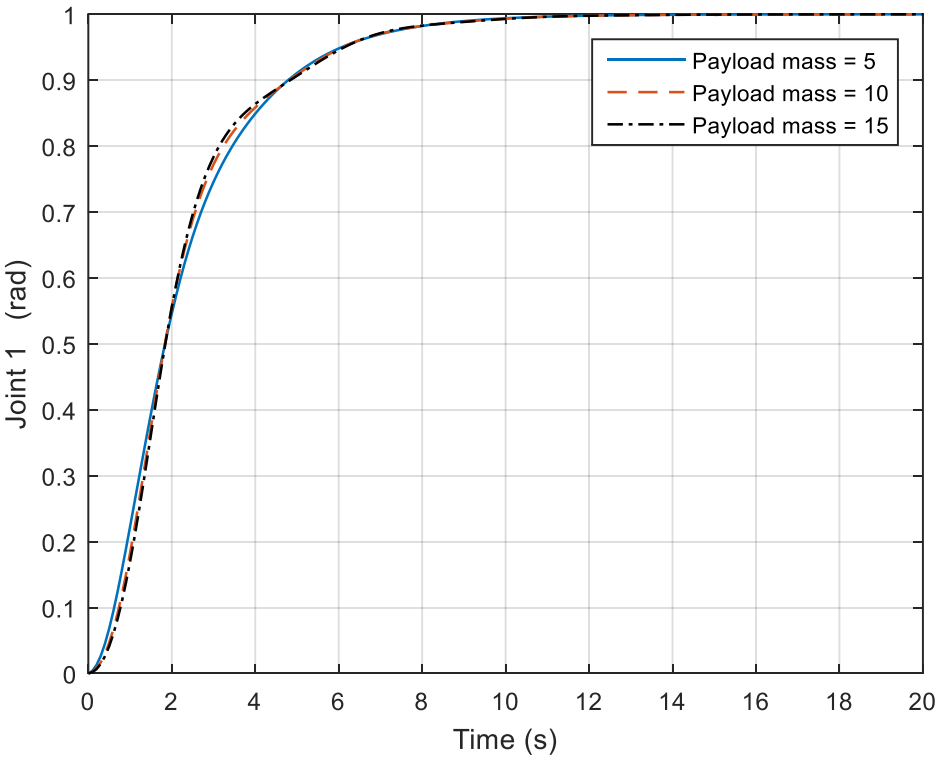

(a). Joint 1 output

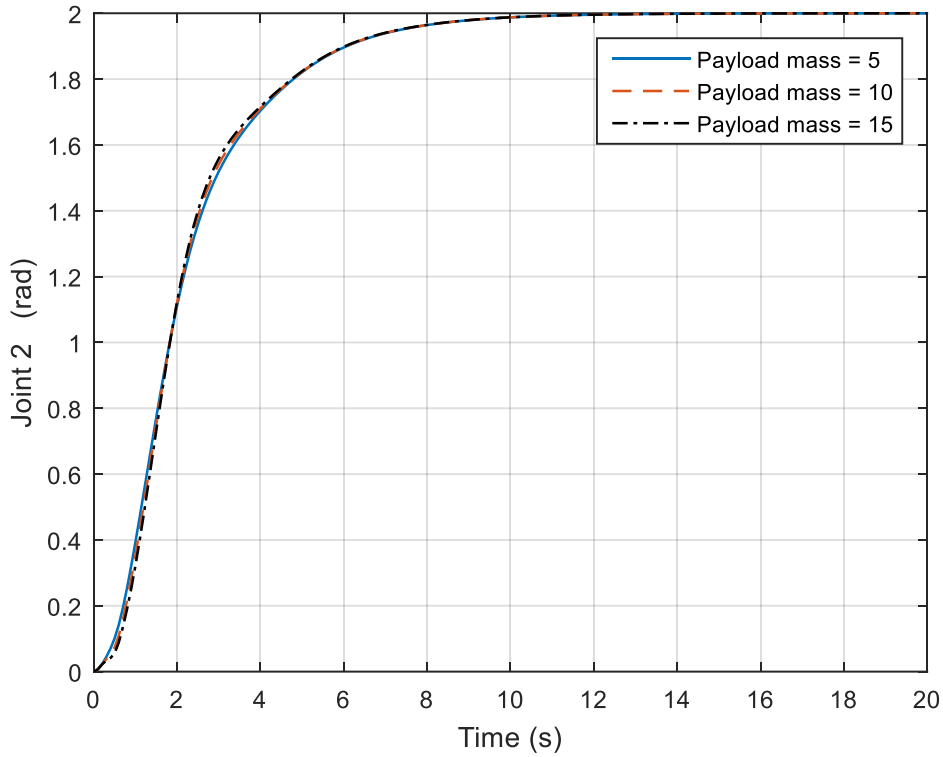

(b). Joint 2 output

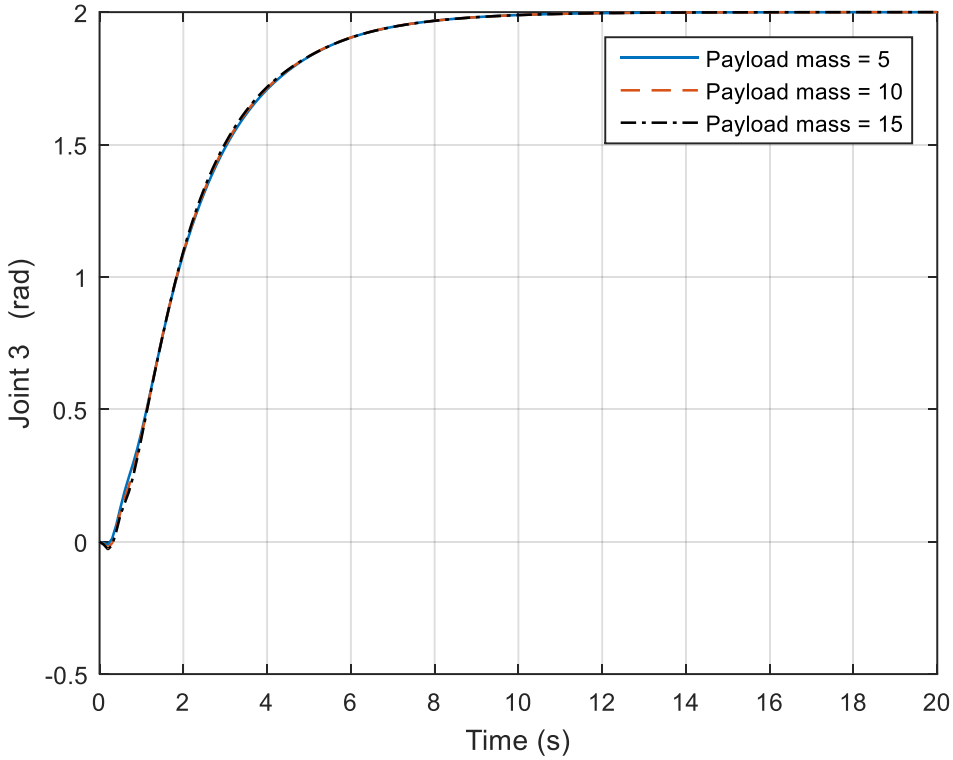

(c). Joint 3 output

Figure 5.18. Joints 1, 2, and 3 output

The convergence speed for the hybrid controller is faster than that of the MRAC controller, as shown in Figure 5.19. The hybrid and MRAC controllers are both better than that of the PID controller. After applying different masses, we found that hybrid control is better than that of the PID and MRAC for all the mass cases. Here we list two of them (5kg and 10kg cases) as an illustration, as shown in Figures 5.19 and 5.20.

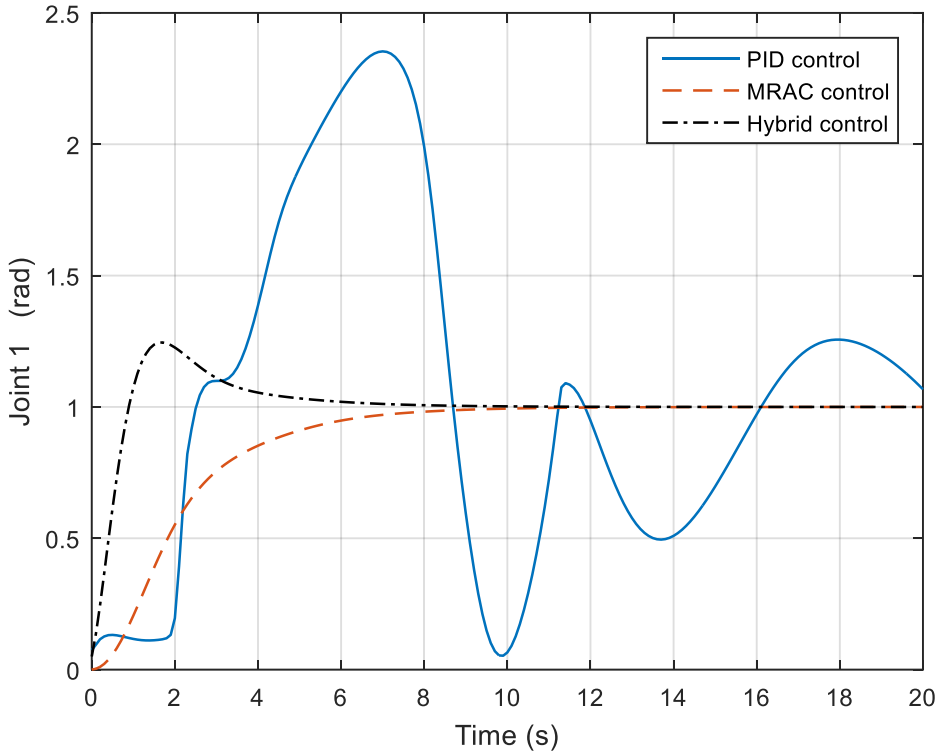

(a). Joint 1 output

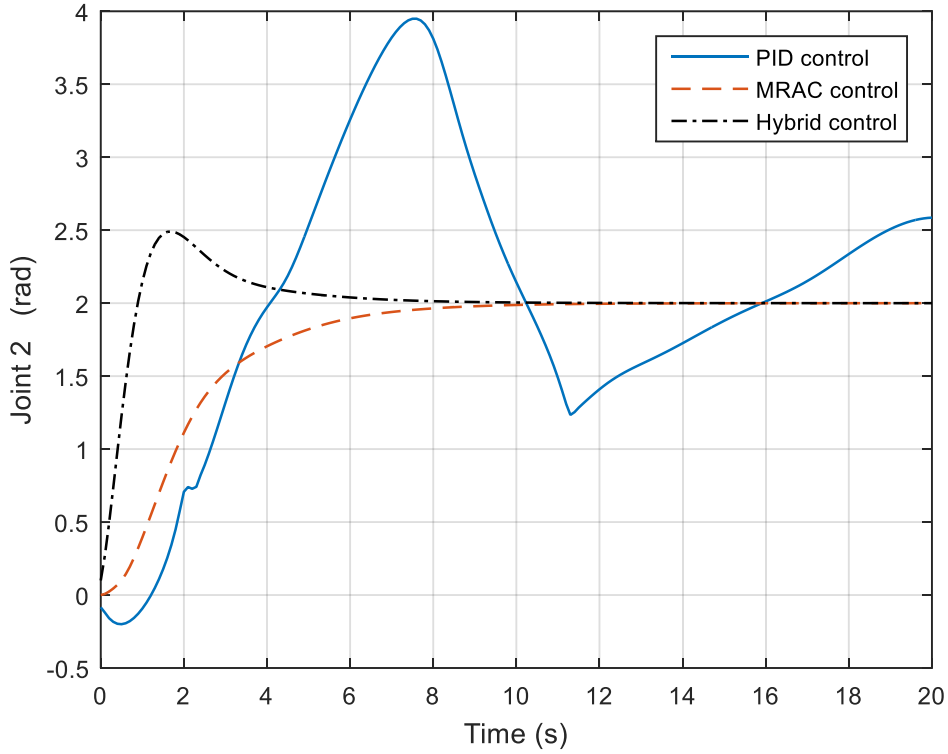

(b). Joint 2 output

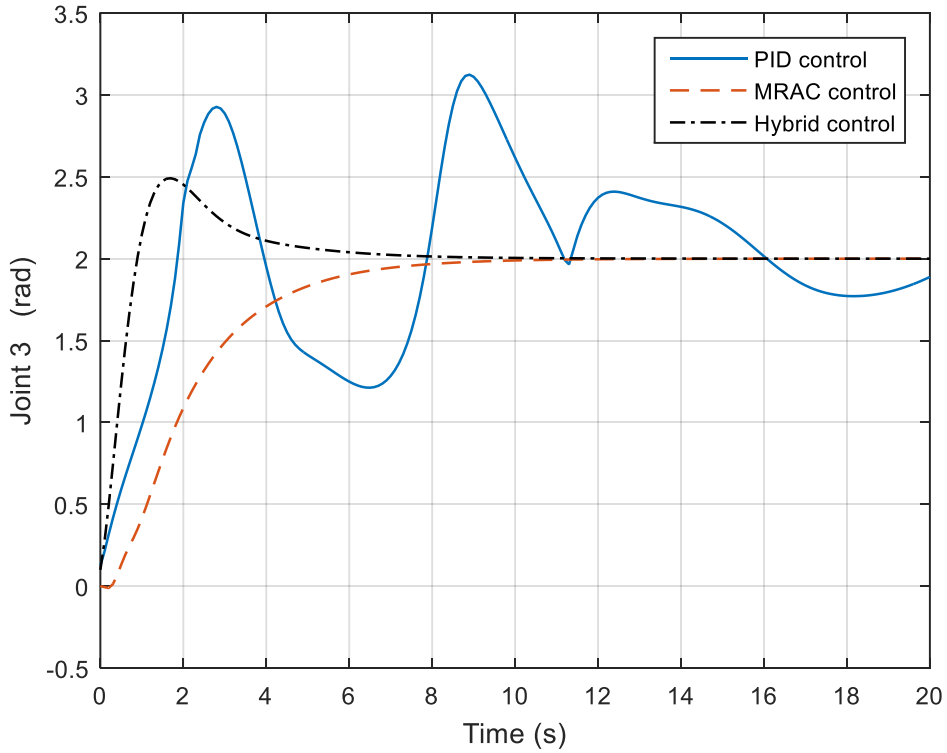

(c). Joint 3 output

Figure 5.19. Joints 1, 2 and 3 output under PID, MRAC and hybrid control when payload is 5kg

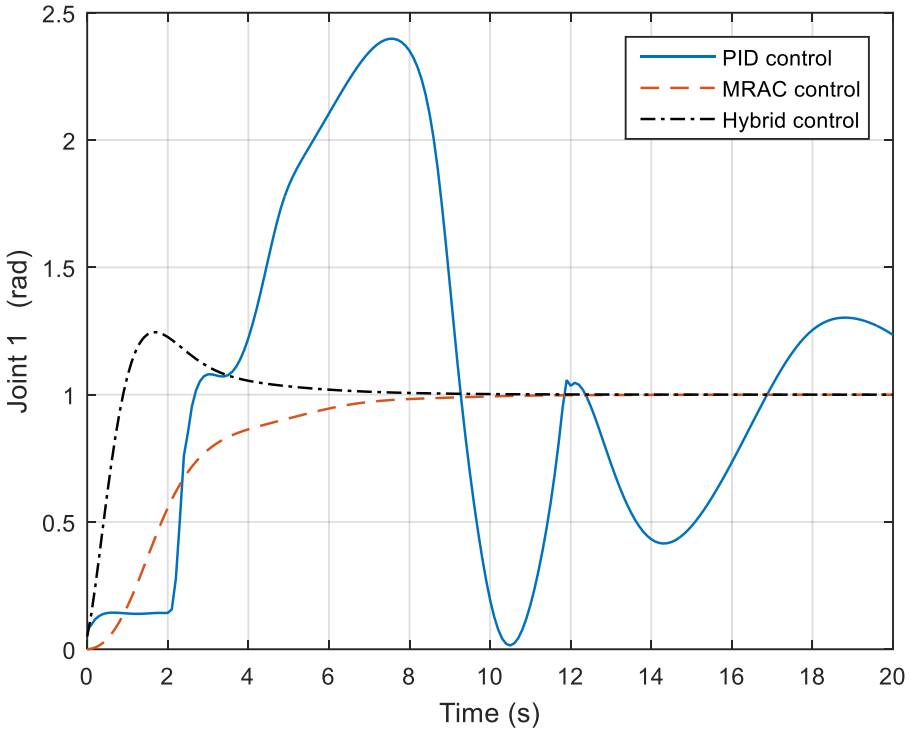

(a). Joint 1 output

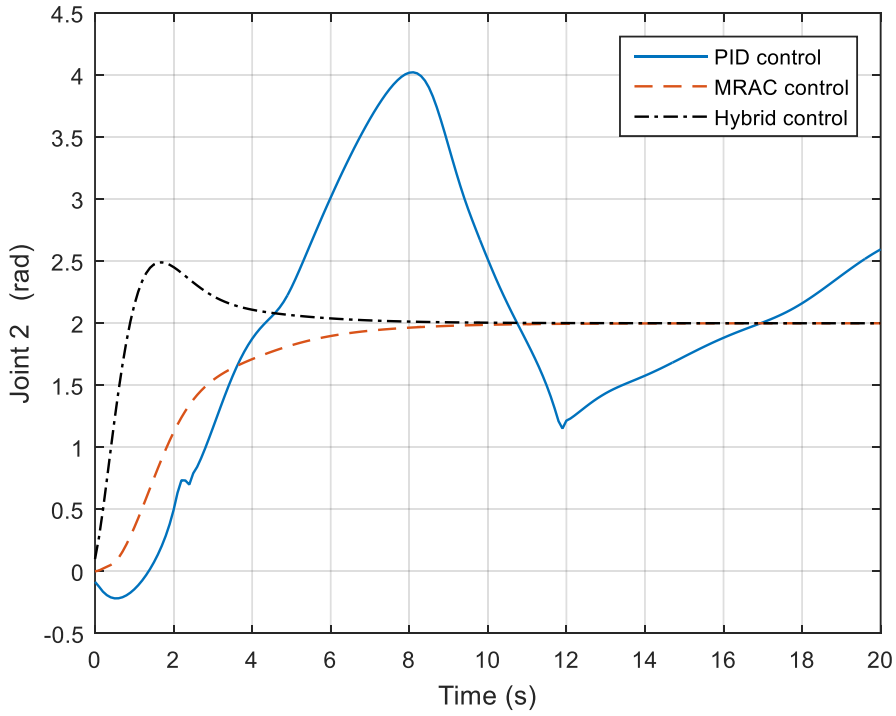

(b). Joint 2 output

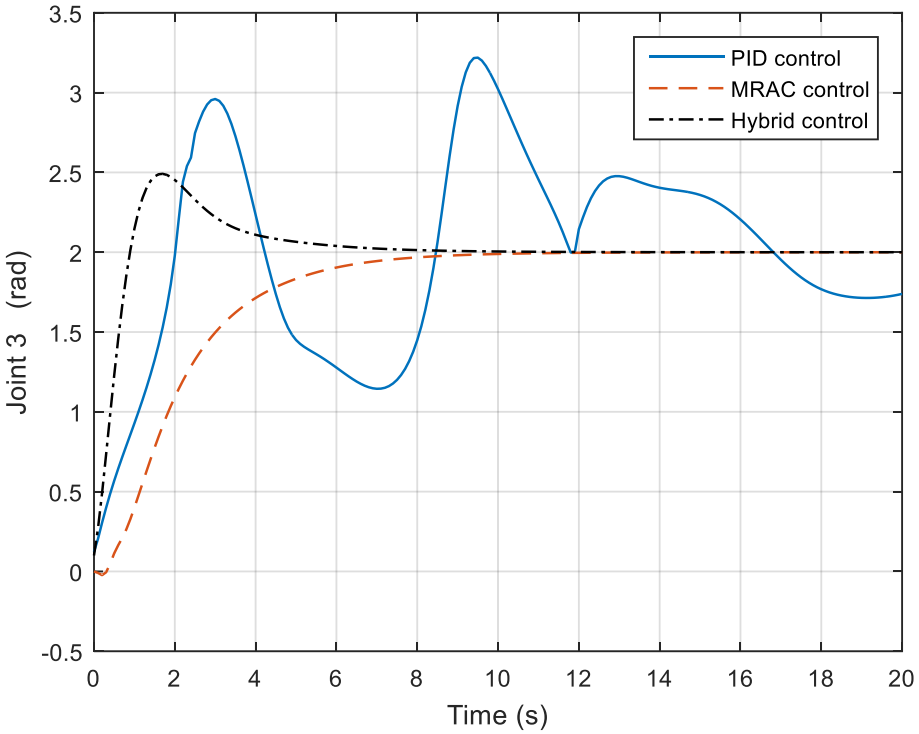

(c). Joint 3 output

Figure 5.20. Joints 1, 2 and 3 output under PID, MRAC and hybrid control when payload is 10kg

In conclusion, a hybrid controller is proposed by combining the PID and MRAC controllers, and also the convergence performance of the PID, MRAC, and PID+MRAC hybrid controllers is compared for 1-DOF, 2-DOF and 3-DOF manipulators. For the 1-DOF case, the results show that the convergence speed and its performance for the MRAC and PID+ MRAC controllers are better than that of the PID controller, whereas for the MRAC and PID+ MRAC controllers, the convergence performance for the hybrid control is better than that of the MRAC control. As shown in Figure 5.11, for the PID control, the joint takes roughly 40 seconds to converge to the desired position. The MRAC control takes about 20 seconds to converge to the desired position, which is half the time of the PID control. Finally, the hybrid control takes about 10 seconds to converge to the desired position,

which halves the time of the MRAC control. Similarly for more than 1-DOF cases, the results show that the convergence speed for the hybrid controller is faster than that of the MRAC controller. The hybrid and MRAC controllers are both better than that of the PID controller.

5.5. Experiments

The experiment is conducted by using Simulink and dSpace. The Pololu 12V 19:1 gear motor and Sabertooth dual 12A 6V-24V regenerative motor driver are used. The technical specs of the motor and controller are listed in Appendix A. Here, a two degrees of freedom serial robot manipulator is set up and built, as shown in Figure 5.21. A new robot has to be built, instead of using an already on the market robot, such as the model in the Robotics and Automation Laboratory at the University of Ontario Institute of Technology (UOIT), as shown in Figure 5.22, because the control system for most of these robots is built-in.

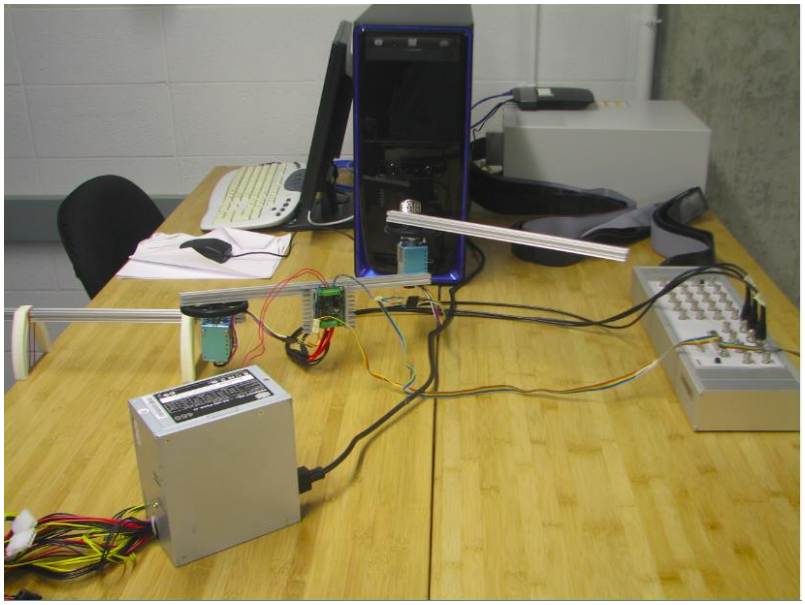

Figure 5.21. 2-DOF robot

Figure 5.22. 4-DOF robot

Under the PID control, when there is no payload at the end-effector of the robotic system, the joint 1 output motion is shown in Figure 5.23(a); after applying some payload masses, the joint output is shown in Figure 5.23(b). The upper line in the figures represents the joint current position after motion and the lower line represents the joint starting position. It can be seen that the joint 1 output motions are different under two different cases (i.e. with and without payload masses). Similarly for joint 2, when there is no payload, the joint 2 output motion is shown in Figure 5.24(a). After applying some payload masses, the joint output is shown in Figure 5.24(b). The joint 2 output motions are not the same under these two different cases. When some payload is loaded at the end-effector, the joint motion will change, which verifies the previous simulation.

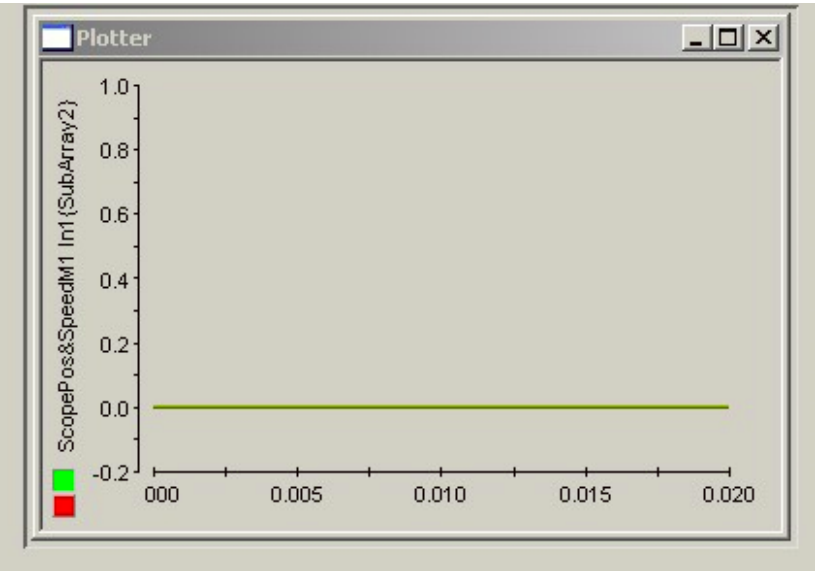

(a) Joint 1 output under PID control when there is no payload

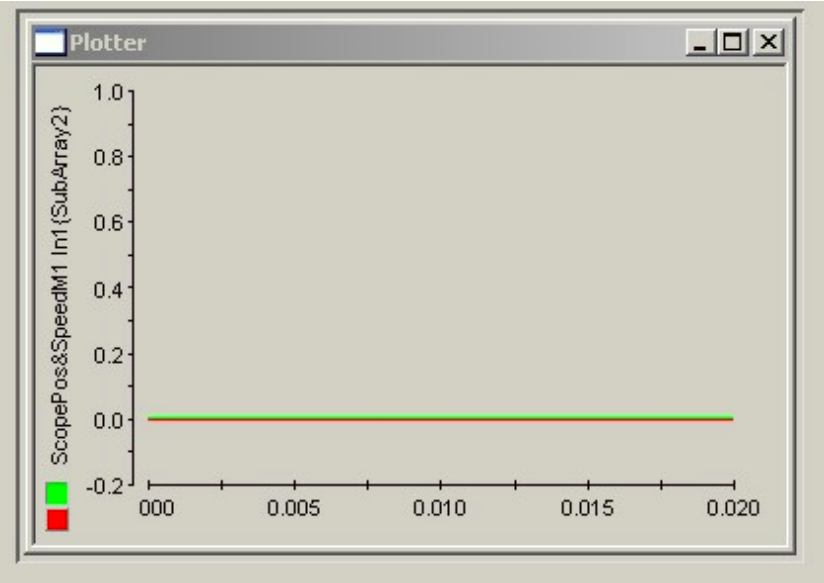

(b) Joint 1 output under PID control when there is payload

Figure 5.23. Joint 1 output under PID control with and without payload

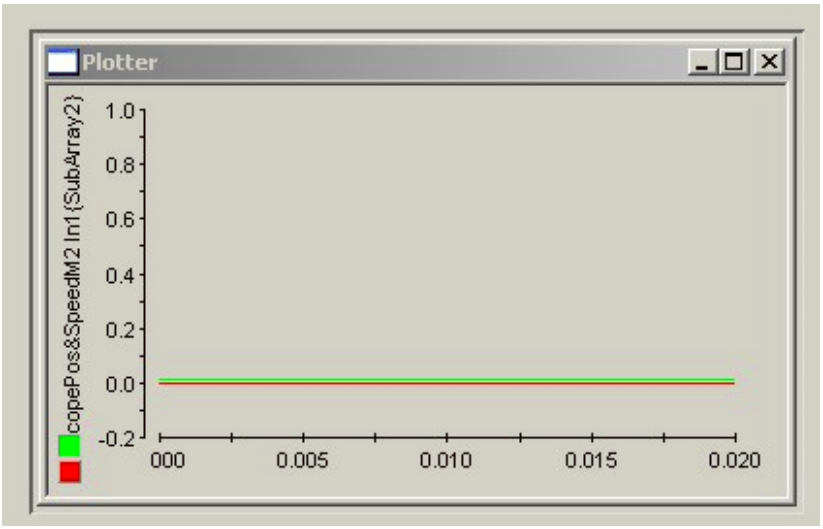

(a) Joint 2 output under PID control when there is no payload

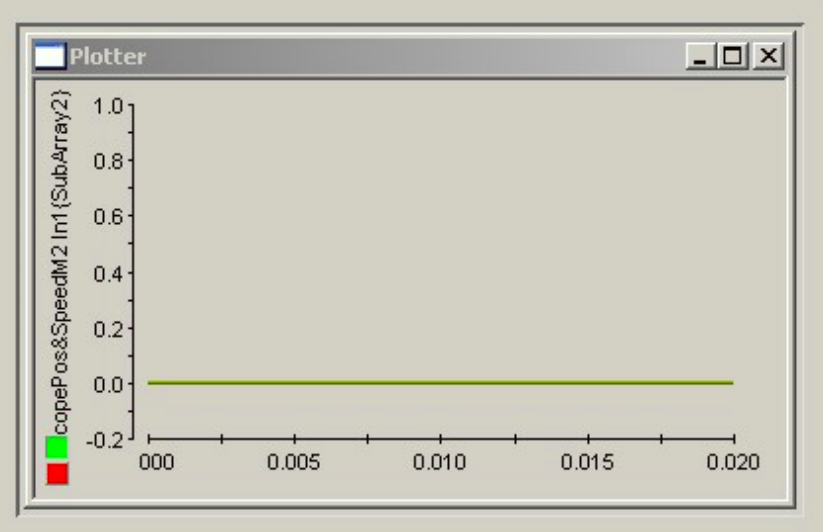

(b) Joint 2 output under PID control when there is payload

Figure 5.24. Joint 2 output under PID control with and without payload

For the hybrid control, we can see that the joint output motion is the same, no matter if the effector carries the payload or not. Figures 5.25 and 5.26 show the joints output under no payload and some payload masses. It can be seen that the joints outputs under two different cases (i.e. with and without payload masses) are the same. By using the hybrid control approach, the payload mass variation effect has been compensated. Furthermore, the convergence speed for the hybrid controller is faster than that of the MRAC controller.

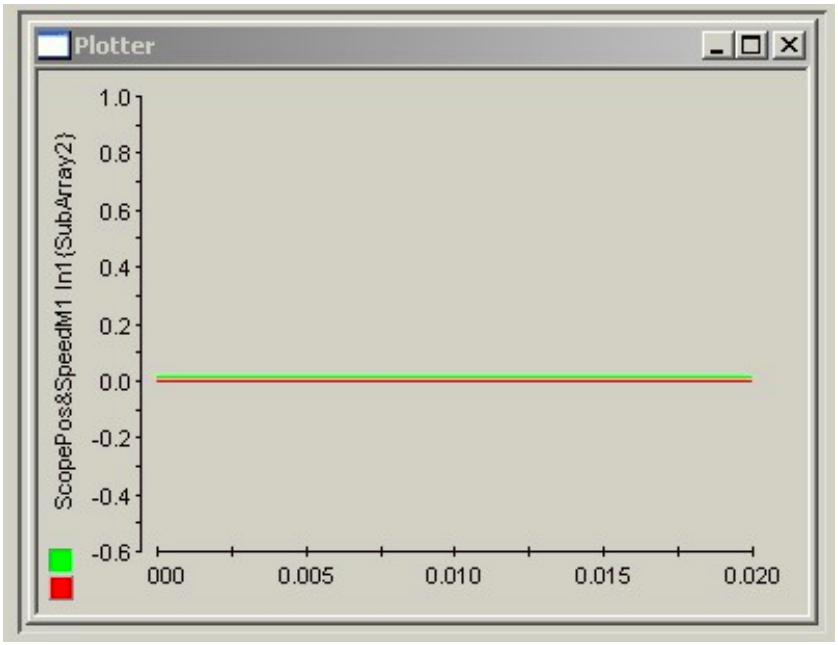

(a). Joint 1 output under hybrid control when there is no payload

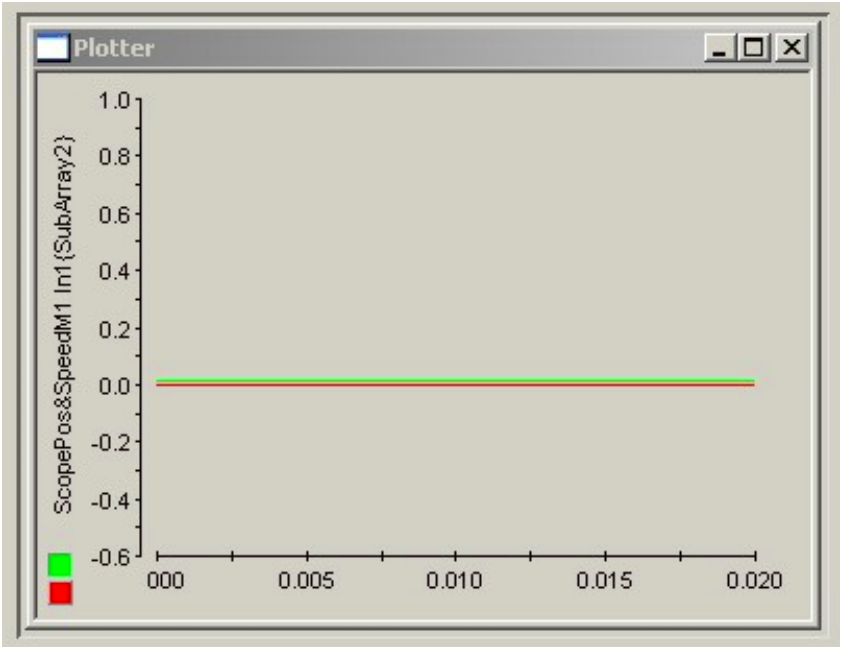

(b) Joint 1 output under hybrid control when there is payload

Figure 5.25. Joint 1 output under hybrid control with and without payload

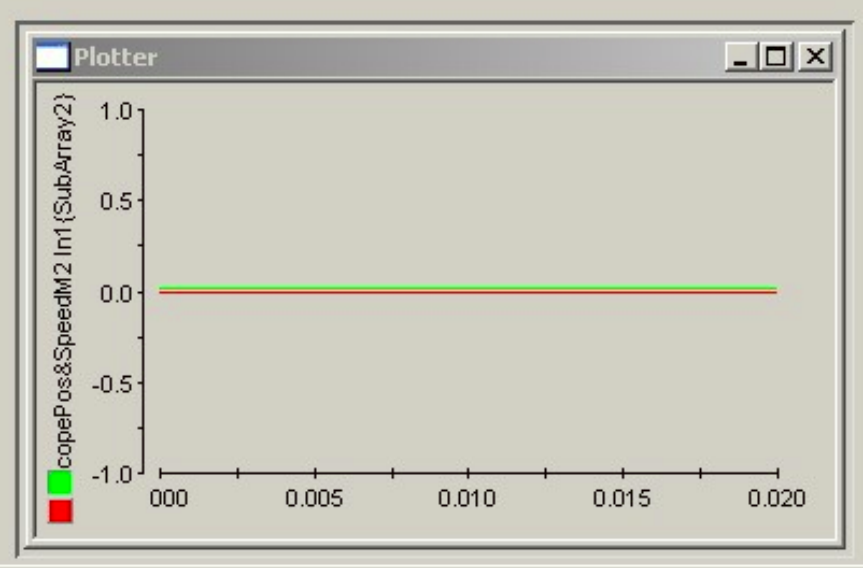

(a) Joint 2 output under hybrid control when there is no payload

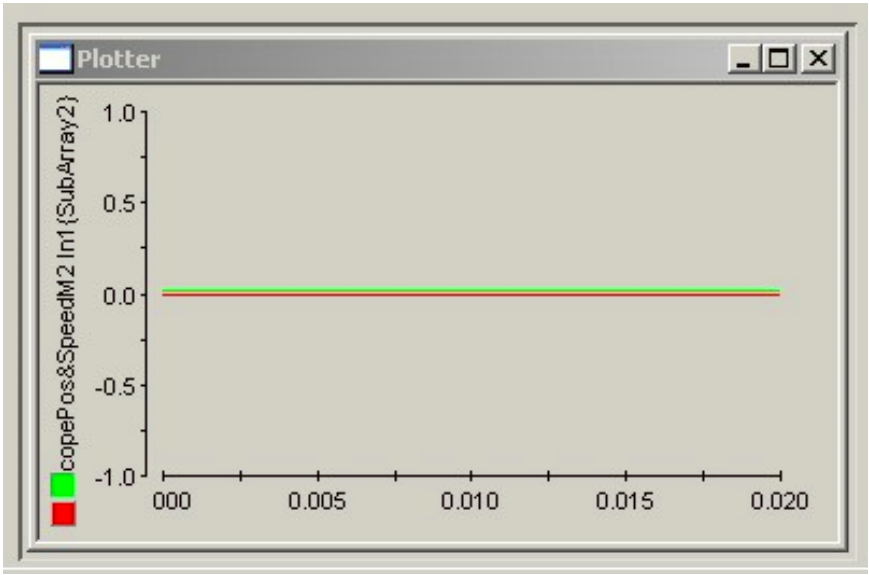

(b). Joint 2 output under hybrid control when there is payload

Figure 5.26. Joint 2 output under hybrid control with and without payload

5.6. Conclusions

A hybrid controller is proposed and designed by combining the PID and MRAC controllers. The convergence performance of the PID, MRAC, and PID+MRAC hybrid controllers is

compared for 1-DOF, 2-DOF and 3-DOF manipulators. For the 1-DOF case, the results show that the convergence speed and its performance for the MRAC and PID+ MRAC controllers is better than that of the PID controller, whereas for the MRAC and PID+ MRAC controllers, the convergence performance for the hybrid control is better than that of the MRAC control. For the MRAC, the joint output gradually goes towards the desired position, while for the PID+MRAC, the joint overshoots the desired position, to which it then gradually returns. For more than 1-DOF cases, the results show that the convergence speed for the hybrid controller is faster than that of the MRAC controller. The hybrid and MRAC controllers are both better than that of the PID controller. This study will provide a guideline for future research in the direction of new controller designs for manipulators in terms of convergence speed and other performances. Future research will focus on learning control design by simulating the human nervous system and internal control for robotic mechanisms.

6

Conclusions and Recommendations

6.1. Conclusions

(1). A novel 3-DOF hybrid manipulator 3PU*S-PU is proposed and analyzed.

The advantages of this new type of manipulator are first described, and the kinematic analysis is then conducted for the purpose of the subsequent performance analysis. Thirdly, the relatively most important kinematic performances, i.e. stiffness/compliance and workspace, are analyzed and optimized by resorting to the differential evolution and genetic algorithm. Fourthly, the multi-objective optimization of the compliance and workspace of the mechanism is implemented, based on the Pareto Front theory, and the results indicate that the two kinematic performances have been improved after optimization. The dynamic analysis of the mechanism, based on the Lagrangian method, is finally conducted, which sets a path for later controlling the manipulator.

The novelty of this proposed new GF set based manipulator is that, by changing the original passive leg to PU type, the manipulator can therefore have the desired three degrees of freedom and, by applying the U* joints as three limbs instead of conventional limbs, the stiffness of this hybrid/parallel manipulator can be greatly improved.

(2). Dynamic balancing through the reconfiguration concept is proposed, and a spatial dynamically balanced grasper mechanism is designed.

The concept of dynamic balancing through reconfiguration, which can reduce the addition of mass and inertia, is proposed for the first time. A screw link can be used and moved to the point where the CoM moves to the still point, and then balanced. In this method, a counterweight is not used but, through reconfiguration of the system by moving the screw link, the system will not become heavy. Based on this idea, one first dynamically balances a single leg by the reconfiguration method (decomposition) and then combines the balanced legs to synthesize the whole parallel mechanism (integration); i.e. the decomposition and integration concept, new reactionless mechanisms and a dynamically balanced spatial grasper mechanism are derived.

(3). A hybrid controller for multi degrees of freedom serial robotic manipulators is synthesized by combining a PID and a model reference adaptive controller in order to further improve the accuracy and joint convergence speed performance.

For the 1-DOF link case, because the inertia matrix and nonlinear term of the dynamic equation are constant, the PID and MRAC controllers can be directly integrated to design the hybrid controller. For more than 1-DOF link cases, since the inertia matrix and nonlinear term of the dynamic equation are not constant, the above procedure is no longer applicable. For the PID control, one needs to use the Lagrange dynamic model, whereas for the MRAC, the Gibbs-Appell dynamic formulation needs to be employed. Under this case, the PID and MRAC cannot be integrated to design the hybrid controller. An improved MRAC was earlier proposed; this can remove the condition that the inertia matrix and nonlinear term are constant. Therefore, the Lagrange dynamic equation can

be used. Thus, by integrating the improved MRAC and the PID controllers, a hybrid control system is designed for the more than 1-DOF link (e.g. 2-DOF and 3-DOF links) case.

The convergence performance of the PID, MRAC, and PID+MRAC hybrid controllers are compared for 1-DOF, 2-DOF and 3-DOF manipulators. For the 1-DOF case, the results show that the convergence speed and its performance for the MRAC and PID+ MRAC controllers is better than that of the PID controller, whereas for the MRAC and PID+ MRAC controllers, the convergence performance for the hybrid control is better than that of the MRAC control. For the MRAC, the joint output gradually goes towards the desired position, while for the PID+MRAC, the joint overshoots the desired position, to which it then gradually returns. For the more than 1-DOF case, the results show that the convergence speed for the hybrid controller is faster than that of the MRAC controller. The hybrid and MRAC controllers are both better than that of the PID controller.

6.2. Recommendations

This thesis employed the structure synthesis design approach, dynamic approach and control approach to improve the overall performance of robotic mechanisms. There are several areas that can be further developed. Future research can consider employing the mechatronics approach as a holistic design approach to further improve the performance (e.g. stiffness, workspace, operational accuracy and task adaptability) of robotic mechanisms.

In terms of the control approach, since the most reliable and intelligent control system ever encountered is the human internal control system, learning control design by

simulating human internal control and nervous systems for robotic mechanisms is worth exploring so as to make the control system more intelligent. The combination of the mechatronic design approach and learning control design approach for robotic mechanisms also has great potential for future enhancements. One of the applications of the learning control approach could be addressing safety issues such as those found in robotic based manufacturing industries.

Furthermore, new types of robotic mechanism synthesis and design, which are considered as one of the key transformative sectors for revolutionizing manufacturing in industries and further promoting performance-driven engineering platforms, still remain an open issue.

References

[1] D. Zhang, B. Wei, Single and multi-objective optimization issues and analysis of a 3UPU parallel manipulator, Proceedings of the ASME 2014 International Design Engineering Technical Conferences and Computers and Information in Engineering Conference, 2014, Buffalo, USA. doi:10.1115/DETC2014-34320, pp. 1-9.

[2] Z. Chi, D. Zhang, L. Xia, Z. Gao. Multi-objective optimization of stiffness and workspace for a parallel kinematic machine. International Journal of Mechanism and Materials in Design, Vol. 9, Issue 3, 2013, pp. 281-293.

[3] D. Zhang, B. Wei, Global stiffness and well-conditioned workspace optimization analysis of 3UPU-UPU robot based on Pareto Front theory. The 12th International Conference on Cooperative Design, Visualization and Engineering, Lecture Notes in Computer Science, Vol. 9320, 2015, pp. 124-133.

[4] D. Zhang, B. Wei. Kinematic analysis and optimization for 4PUS-RPU parallel mechanism. 2015 IEEE/ASME International Conference on Advanced Intelligent Mechatronics, Busan, Korea, 2015, pp. 330-335.

[5] D. Zhang, B. Wei, Force balance of mechanisms and parallel robots through reconfiguration method. 3rd IEEE/IFToMM International Conference on Reconfigurable Mechanisms and Robots, Beijing, China. Mechanisms and Machine Science, Vol. 36, 2015, pp. 351-361.

[6] Z. Bi, W. Zhang. Performance improvement of parallel robotics through flexible platform. Proceeding of the 6th International Symposium on Artificial Intelligence and Robotics and Automation in Space, St-Hubert, Canada, 2001, pp. 1-8.

[7] Q. Li, F. Wu, Control performance improvement of a parallel robot via the design for control approach. Mechatronics 14, 2004, pp. 947-964.

[8] L. Ren, J. Mills, D. Sun. Performance improvement of tracking control for a planar parallel robot using synchronized control. Proceedings of the 2006 IEEE/RSJ International Conference on Intelligent Robots and Systems, Beijing, China, 2006, pp. 2539-2544.

[9] A. Pott, H. Mutherich, W. Kraus, IPAnema: A family of cable-driven parallel robots for industrial applications. Mechanisms and Machine Science 12, 2013, pp. 119-134.

[10] C. Gosselin, J. Hamel, The agile eye: a high- performance three-degree-of-freedom camera-orienting device, IEEE International Conference on Robotics and Automation, San Diego, USA, 1994, pp. 781-786.

[11] D. Zhang, Z. Bi, B. Li, Design and kinetostatic analysis of a new parallel manipulator, Robotics and Computer-Integrated Manufacturing, Vol. 25, Issues 4, 2009, pp. 782-791.

[12] D. Zhang, Research activities on parallel robotic machines, Chinese Academy of Sciences, Research seminar, Beijing, August, 2011.

[13]http://mp.weixin.qq.com/s?__biz=MzA4NjY5NjQxNA==&mid=202511286&idx=1&sn=8786e652ba08b8975086041454b8cc98&scene=1&from=singlemessage&isappinstalled=0&key=7f2a50e6a9e3a33def8935c29a36d891fa9487f8546517400a8e24d3628ce1c6b10eadc09784bad3b7b0b13edd5e772b&ascene=0&uin=MTk0Mjg0MDA0NA%3D%3D&pa

ss_ticket=7uc6KWuuqIjzJi7kodj5axD3YmXElnRCaDDbqlVJ2sw4LgYgCQDuIZP1R6wy1J%2BC

[14] S. Foucault, C. Gosselin. Synthesis, design, and prototyping of a planar three degree-of-freedom reactionless parallel mechanism, ASME Journal of Mechanical Design, Vol. 126, Issue 6, 2005, pp. 992-999.

[15] V. Wijk, S. Krut, F. Pierrot, J. Herder. Design and experimental evaluation of a dynamically balanced redundant planar 4-RRR parallel manipulator, The International Journal of Robotics Research, 32, 2013, pp. 744–759.

[16] V. Arakelian, M. Smith. Design of planar 3-DOF 3-RRR reactionless parallel manipulators, Mechatronics, Vol. 18, Issue 10, 2008, pp.601-606.

[17] Y. Wu, C. Gosselin. Design of reactionless 3-DOF and 6-DOF parallel manipulators using parallelepiped mechanisms, IEEE Transactions on Robotics, Vol. 21, Issue 5, 2005, pp. 821-833.

[18] V. Wijk, B. Demeulenaere, J. Herder. Comparison of various dynamic balancing principles regarding additional mass and additional inertia, ASME Journal of Mechanisms and Robotics, Vol. 1, No. 4, 2009, pp. 041006-1-9.

[19] S. Briot, V. Arakelian. Complete shaking force and shaking moment balancing of in-line four bar linkages by adding a class-two RRR or RRP Assur group. Mechanism and Machine Theory, Vol. 57, 2012, pp. 13-26.

[20] V. Wijk, J. Herder. Dynamic Balancing of a single crank-double slider mechanism with symmetrically moving couplers. New Trends in Mechanism Science, Mechanisms and Machine Science, Vol. 5, 2010, pp 413-420.

[21] J. Sutherland, Model reference adaptive control of a two link manipulator, Master Thesis, Carleton University, 1987.

[22] H. Whitaker, J. Yamron, A. Kezer, Design of model reference adaptive control systems for aircraft, Report R-164, Instrumentation Laboratory, MIT Press, Cambridge, USA, 1958.

[23] D. Zhang, Parallel robotic machine tools. Springer, New York, NY, ISBN: 978-1-4419-1117-9, 2009.

[24] E. Bohez, Five-axis milling machine tool kinematic chain design and analysis. International Journal of Machine Tools and Manufacture, 42, 2002, pp. 505–520.

[25] Z. Gao, D. Zhang, Performance analysis, mapping, and multi-objective optimization of a hybrid robotic machine tool. IEEE Transactions on Industrial Electronics, Vol. 62, Issue 1, 2015, pp.423-433.

[26] G. Coppola, D. Zhang, K. Liu, A 6-DOF reconfigurable hybrid parallel manipulator. Robotics and Computer-Integrated Manufacturing, Vol. 30, Issue 2, 2014, pp. 99–106.

[27] D. Zhang, L. Wang, Z. Gao. An integrated approach for remote manipulation of a high-performance reconfigurable parallel kinematic machine. Journal of Manufacturing Systems. Vol. 29, Issue 4, 2010, pp.164-172.

[28] M. Tsai. Direct kinematic analysis of a 3-PRS parallel mechanism, Mechanism and Machine Theory, Vol. 38, No. 1, 2003, pp. 71-83.

[29] O. Company, F. Pierrot, Modeling and design issues of a 3-axis parallel machine tool, Mechanism and Machine Theory, Vol. 37, No. 11, 2002, pp. 1325-1345.

[30] D. Zhang, B. Wei. Design and optimization of a Tripod-based hybrid manipulator, ROMANSY-2014, CISM-IFToMM Symposium on Theory and Practice of Robots and Manipulators, Mechanisms and Machine Science 22, 2014, pp. 83-91.

[31] X. Hu. Design and analysis of a three degrees of freedom parallel kinematic machine. Master thesis. University of Ontario Institute of Technology, 2008.

[32] V. Nabat, M. Rodriguez, O. Company, Very high speed parallel robot for pick-and-place. 2005 IEEE/RSJ International Conference on Intelligent Robots and Systems, Edmonton, Canada, 2005, pp. 553-558.

[33] https://www.robots.com/applications/pick-and-place

[34] C. Connolly, ABB high-speed picking robots establish themselves in food packaging, Industrial Robot: An International Journal, Vol. 34, No. 4, 2007, pp. 281-284.

[35] E. Kljuno. R. Williams, Vehicle simulation system: controls and virtual reality based dynamics simulation. Journal of Intelligent and Robotic Systems, Vol. 52, Issue 1, 2008, pp. 79-99.

[36] L. Bruzzone, R. Molfino, R. Razzoli, Modelling and design of parallel robot for laser cutting applications, Proceedings of IASTED International Conference on Modelling, Identification and Control, Innsbruck, 2002, pp. 518-522.

[37] N. Plitea, D. Pisla, C. Vaida. On kinematics of a parallel robot used for the minimally invasive surgery. Proceedings in Applied Mathematics and Mechanics, 4010033–4010034, 2007, DOI 10.1002/pamm.200700850.

[38] M. Pan, Improved design of a three-degree of freedom hip exoskeleton based on biomimetic parallel structure. Master Thesis, University of Ontario Institute of Technology, Canada, 2011.

[39] G. Castelli, E. Ottaviano, Modeling and simulation of a cable based parallel manipulator as an assisting device. Proceedings of the 5th International Workshop on Computational Kinematics, Springer, 2010, pp. 17-24.

[40] S. Lessard, P. Bigras, I. Bonev, A new medical parallel robot and its static balancing optimization. Journal of Medical Devices. Vol. 1. 2007, pp. 272-278.

[41] C. Vaida, D. Pisla, P. Tucan. An innovative parallel robotic structure designed for transperineal prostate biopsy. The 14th IFToMM World Congress, Taipei, Taiwan, 2015. DOI: 10.6567/IFToMM.14TH.WC.OS2.049, pp. 1-8.

[42] Y. Li, Q. Xu, Design and development of a medical parallel robot for cardiopulmonary resuscitation. IEEE/ ASME Transactions on Mechatronics, Vol. 12, No. 3, 2007, pp. 265-273.

[43] G. Rosati, M. Andreolli, A. Biondi, P. Gallina, Performance of cable suspended robots for upper limb rehabilitation. Proceedings of the IEEE 10th International Conference on Rehabilitation Robotics, Noordwijk, Netherlands, 2007, pp. 385-392.

[44] J. Vazquez, Simulation of a parallel mechanical elbow with 3-DOF, Journal of Applied Research and Technology, Vol. 7, No. 2, 2009, pp. 113-123.

[45] N. Gorie, V. Dolga, Bio-mechatronics recovery systems for persons with disabilities. Proceedings of International Conference on Innovations, Recent Trends and Challenges in

Mechatronics, Mechanical Engineering and New High-Tech Products Development, Vol. 3, 2011, pp. 323-330.

[46] C. Kossowski, L. Notash, A novel wire actuated parallel robot with space applications, Proceedings of CCToMM Mechanisms, Machines and Mechatronics, Montreal, Canada, 2001, pp.1-2.

[47] F. Xi, A. Ross, S. Lang, Exploring a reconfigurable parallel robot for space applications, Proceeding of the 6th International Symposium on Artificial Intelligence and Robotics and Automation in Space, St-Hubert, Canada, 2001, pp. 1-8.

[48] T. Jones, G. Dunlop, Analysis of rigid-body dynamics for closed loop mechanisms-its application to a novel satellite tracking device. Journal of Systems & Control Engineering, Vol. 217, No. 4, 2003, pp. 285- 298.

[49] http://www.parallemic.org/Reviews/Review007.html

[50] L. Angel, J. Sebastian, R. Saltaren, R. Aracil, Robot tennis system part II: dynamics and control. Proceedings of the 44th IEEE Conference on Decision and Control, Seville, Spain, 2005, pp. 2030-2034.

[51]Y. Zhang, B. Wei, N. Wang, Kinematic performance analysis of 3-SPS-S spatial rotation parallel mechanism. Transactions of the Chinese Society for Agricultural Machinery, Vol. 43, Issue 4, 2012, pp. 212 -215.

[52] G. Cui, D. Zhang, H. Zhou, Y. Zhang. Operating dexterity optimization and analysis of a 3-DOF parallel manipulator for a tunnel segment assembly system. International Journal of Mechanics and Materials in Design, Vol. 11, Issue 3, 2015, pp. 277-285.

[53] Z. Sun, Bin Wei, Loading capacity analysis of a 3-SPS-S mechanism for segment assembly robots in shield tunneling machines. Proceedings of the 2011 International Conference on Advances in Construction Machinery and Vehicle Engineering, Shanghai, China, 2011, pp.99-101.

[54] Q. Liang, D. Zhang, Y. Wang, Y. Ge. Design and analysis of a miniature 4-dimensional force/torque sensor. 2012 IEEE International Conference on Robotics and Bio-mimetics, Guangzhou, China. pp. 148-153.

[55] Z. Gao, D. Zhang. Flexure parallel mechanism: configuration and performance improvement of a compact acceleration sensor. Journal of Mechanisms and Robotics, Vol. 4, Issue 3, 2012, doi:10.1115/1.4006660.

[56] D. Zhang, B. Wei. Design and analysis of a collision detector for hybrid robotic machine tools. Sensors & Transducers Journal, Vol. 193, Issue 10, 2015, pp. 67-73.

[57] D. Zhang, Z. Gao, I. Fassi, Design optimization of a spatial hybrid mechanism for micromanipulation. International Journal of Mechanism and Material in Design, Vol. 7, Issue 1, 2011, pp.55-70.

[58] D. Zhang, B. Li, J. Yang, Z. Gao, Conceptual design and kinematic analysis of a compliant parallel mechanism for micro/nano scale manipulation. Proceedings of ASME 2009 International Mechanical Engineering Congress and Exposition, Florida, USA, 2009. pp. 7-15.

[59] Z. Chi, M. Pan, D. Zhang. Design of a 3-DOF MEMS-based precision manipulator. Proceedings of 1st International Conference on Robot, Vision and Signal Processing. Kaohsiung, Taiwan. 2011, pp. 14-17.

[60] X. Liu, J. Jeong, J. Kim, A three translational DoFs parallel cube-manipulator. Robotica, Vol. 21, No. 6, 2003, pp. 645-653.

[61] https://en.wikipedia.org/wiki/Stewart_platform

[62] https://www.ieee.ca/millennium/canadarm/canadarm_technical.html

[63] X. Liu, J. Wang, G. Pritschow, A new family of spatial 3-DoF fully-parallel manipulators with high rotational capability, Mechanism and Machine Theory, 40, 2005, pp. 475-494.

[64] L. Tsai, Mechanism design: enumeration of kinematic structures according to function, CRC Press, 2001.

[65] O. Salgado, O. Altuzarra, V. Petuya, Type synthesis of a family of 3T1R fully-parallel manipulators using a group-theoretic approach, Proceedings of 12th IFToMM World Congress on the Theory of Machines and Mechanisms, Besancon, France, 2007, pp. 18-21.

[66] J. Angeles, S. Caro, W. Khan, The kinetostatic design of an innovative schonflies motion generator, Proceedings of the Institution of Mechanical Engineers, Part C, Journal of Mechanical Engineering Science 220, C7, 2006, pp. 935-944.

[67] R. Ricard, C.M. Gosselin. On the development of reactionless parallel manipulators. Proceedings of ASME Design Engineering Technical Conferences and Computers and Information in Engineering Conference, USA, 2000, pp. 1-10.

[68] V. Wijk, J. Herder. Dynamic balancing of Clavel's Delta robot. Computational Kinematics, 2009, pp 315-322.

[69] V. Wijk, Methodology for analysis and synthesis of inherently force and moment-balanced mechanisms - theory and applications. Doctoral Thesis, University of Twente, Netherlands, 2004.

[70] V. Wijk, J. Herder. On the development of low mass shaking force balanced manipulators. Advances in Robot Kinematics: Motion in Man and Machine, 2010, pp. 411-420.

[71] V. Wijk, J. Herder. Inherently balanced 4R four-bar based linkages. Latest Advances in Robot Kinematics, 2012, pp. 309-316.

[72] V. Wijk, J. Herder. Synthesis method for linkages with center of mass at invariant link point-Pantograph based mechanisms. Mechanism and Machine Theory, 48, 2012, pp. 15-28.

[73] V. Wijk, S. Krut, F. Pierrot, J. Herder. Generic method for deriving the general shaking force balance conditions of parallel manipulators with application to a redundant planar 4-RRR parallel manipulator, The 13th World Congress in Mechanism and Machine Science, Mexico, 2011, pp. 1-9.

[74] C. Gosselin, F. Vollmer, G. Cote, Y. Wu. Synthesis and design of reactionless three-degree of freedom parallel mechanisms, IEEE Transactions on Robotics and Automation, Vol. 20, No. 2, 2004, pp. 191-199.

[75] Y. Wu. Synthesis and analysis of reactionless spatial parallel mechanisms, Doctoral Thesis, Laval University, 2003.

[76] F. Gao. Complete shaking force and shaking moment balancing of four types of six-bar linkages, Mechanism and Machine Theory, Vol. 24, Issue 4, 1989, pp. 275–287.

[77] F. Gao. Complete shaking force and shaking moment balancing of 26 types of four-, five- and six-bar linkages with prismatic pairs, Mechanism and Machine Theory, Vol. 25, Issue 2,1990, pp. 183-192.

[78] F. Gao. Complete shaking force and shaking moment balancing of 17 types of eight-bar linkages only with revolute pairs, Mechanism and Machine Theory, Vol. 26, Issue 2, 1991, pp. 197-206.

[79] V. Arakelian, M. Smith. Complete shaking force and shaking moment balancing of linkages, Mechanism and Machine Theory, Vol. 34, Issue 8, 1999, pp. 1141-1153.

[80] S. Briot, I. Bonev, C. Gosselin, V. Arakelian. Complete shaking force and shaking moment balancing of planar parallel manipulators with prismatic pairs. Proceedings of the Institution of Mechanical Engineers -- Part K, Vol. 223, Issue 1, 2009, pp. 43-52.

[81] J. Herder, C. Gosselin. A counter-rotary counterweight (CRCM) for light-weight dynamic balancing, Proceedings of 2004 ASME Design Engineering Technical Conferences and Computers and Information in Engineering Conference, USA, 2004, pp. 1-9.

[82] J. Herder. Reaction-free systems, principles, conception and design of dynamically balanced mechanisms, Technical Report, Laval University, 2003.

[83] V. Wijk, B. Demeulenaere, C. Gosselin, J. Herder. Comparative analysis for low-mass and low-inertia dynamic balancing of mechanisms, ASME Journal of Mechanisms and Robotics, Vol. 4, No. 3, 2012, pp. 031008-1-8.

[84] V. Wijk, J. Herder. Synthesis of dynamically balanced mechanisms by using counter-rotary counter-mass balanced double pendula, ASME Journal of Mechanical Design, Vol. 131, No. 11, 2009, pp. 111003-1-8.

[85] V. Wijk, J. Herder. Dynamic balancing of mechanisms by using an actively driven counter-rotary counter-mass for low mass and low inertia, Proceedings of the Second International Workshop on Fundamental Issues and Future Research Directions for Parallel Mechanisms and Manipulators, France, 2008, pp. 241-251.

[86] V. Wijk, J. Herder. Active dynamic balancing unit for controlled shaking force and shaking moment balancing, ASME 2010 International Design Engineering Technical Conferences and Computers and Information in Engineering Conference, Canada, 2010, pp. 1515-1522.

[87] K. Wang, M. Luo, T. Mei. Dynamics analysis of a three-DOF planar serial-parallel mechanism for active dynamic balancing with respect to a given trajectory, International Journal of Advanced Robotic Systems, Vol. 23, Issue 10, 2013, doi: 10.5772/54201, pp.1-10.

[88] A. Valente, E. Carpanzano, M. Brusaferri, Design and implementation of distributed and adaptive control solutions for reconfigurable manufacturing systems, Proceedings of 2011 International Conference on Manufacturing Systems. 2011, pp. 1-6.

[89] Z. Bi, Y. Liu, B. Baumgartner, Reusing industrial robots to achieve sustainability in small and medium-sized enterprises, Industrial Robot: An International Journal, Vol. 42, Issue 3, 2015, pp. 264 – 273.

[90] E. Wilson, S. Rock, Reconfigurable control of a free-flying space robot using neural networks, Proceedings of 1995 American Control Conference, Vol.2, 1995, pp. 1355-1359.

[91] B. Jung, S. Jeong, D. Lee, Y. Kim, Adaptive reconfigurable flight control system using multiple model mode switching, Proceedings of the 16th IFAC World Congress, Vol. 16, Part 1, 2005, pp. 1-6.

[92] I. Landau, Introduction to adaptive control, Adaptive Control, Communications and Control Engineering, Springer, Verlag London Limited. 2011.

[93] A. Valentea, M. Mazzolinib, E. Carpanzanoa, An approach to design and develop reconfigurable control software for highly automated production systems, International Journal of Computer Integrated Manufacturing, Vol. 28, Issue 3, 2015, pp. 321-336.

[94] C. Neuman and H. Stone, MRAC control of robotic manipulators, 3rd Yale Workshop on Applications of Adaptive Systems Theory, Yale University, New Haven, CT, 1983, pp. 203-210.

[95] J. Amerongen, MRAS: model reference adaptive systems, Journal A, Vol. 22, No. 4, 1981, pp. 192-198.

[96] S. Dubowsky, D. Desforges, The application of model-referenced adaptive control to robotic manipulators, Journal of Dynamic Systems Measurement and Control, Vol. 101, 1979, pp. 193-200.

[97] D. Donalson, T. Leondes, A model referenced parameter tracking technique for adaptive control systems, IEEE Transactions on Applications and Industry, Vol. 82, Issue 68, 1963, pp. 241-252.

[98] R. Horowitz, M. Tomizuka, An adaptive control scheme for mechanical manipulators—compensation of nonlinearity and decoupling control, Journal of Dynamic Systems, Measurement, and Control, Vol. 108, Issue 2, 1986, pp. 1-9.

[99] T. Hsia, Adaptive control of robot manipulators – A review, Proceedings of 1986 IEEE International Conference on Robotics and Automation, 1986, pp. 183-189.

[100] R. Srinivasan, Adaptive control for robotic manipulators, Master Thesis, Carleton University, 1987.

[101] R. Horowitz, Model reference adaptive control of mechanical manipulators, Doctoral Thesis, University of California, 1983.

[102] Y. Landau, Adaptive control—the model reference approach, CRC Press. 1979.

[103] M. Tomizuka, R. Horowitz, G. Anwar, Adaptive techniques for motion controls of robotic manipulators, Proceedings of Japan - USA Symposium on Flexible Automation, 1986, Osaka, Japan.

[104] M. Tomizuka, R. Horowitz, Implementation of adaptive techniques for motion control of robotic manipulators, Journal of Dynamic Systems, Measurement, and Control, 110(1), 1988, pp. 62-69.

[105] R. Horowitz, M. Tsai, G. Anwar, M. Tomizuka, Model reference adaptive control of a two axis direct drive manipulator arm, Proceedings of 1987 IEEE International Conference on Robotics and Automation, pp. 1216 – 1222.

[106] M. Tomizuka, R. Horowitz, G. Anwar, Adaptive techniques for motion controls of robotic manipulators, Proceedings of Japan - USA Symposium on Flexible Automation, Japan, 1986, pp. 117-224.

[107] M. Tomizuka, R. Horowitz, C. Teo, Model reference adaptive controller and robust controller for positioning of varying inertia, Proceedings of Conference on Applied Motion Control, University of Minnesota, 1985, pp. 191-196.

[108] J. Hamadi, Adaptive control methods for mechanical manipulators: a comparative study, Master Thesis, Naval Postgraduate School, 1989.

[109] N. Sadegh, R. Horowitz, Stability analysis of an adaptive controller for robotic manipulators, Proceedings of 1987 IEEE International Conference on Robotics and Automation, pp. 1223-1229.

[110] N. Sadegh, R. Horowitz, Stability and robustness analysis of a class of adaptive controllers for robotic manipulators, International Journal of Robotics Research, Vol. 9, No. 3, 1990, pp. 74-92.

[111] N. Sadegh, Adaptive control of mechanical manipulators: stability and robustness analysis, Doctoral Thesis, University of California, 1987.

[112] J. Craig., P. Hsu. S. Sastry, Adaptive control of mechanical manipulators. Proceedings of the 1986 IEEE International Conference on Robotics and Automation, San Francisco, USA, 1986, pp. 190-195.

[113] F. Gao, J. Yang, Q. Ge, GF set theory for the type synthesis of parallel manipulators. Science Press, 2010.

[114] D. Zhang, Z. Gao, Hybrid head mechanism of the groundhog-like mine rescue robot, Robotics and Computer-Integrated Manufacturing, Vol. 27, Issue 2, 2011, pp. 460-470.

[115] W. Zhang, P. Ouyang, Z. Sun. A novel hybridization design principle for intelligent mechatronics systems, Proceedings of International Conference on Advanced Mechatronics, Osaka, Japan, 2010, pp. 4-6.

[116] X. Liu, J. Wang, Some new parallel mechanisms containing the planar four-bar parallelogram, The International Journal of Robotics Research, Vol. 22, No. 9, 2003, pp. 717-732.

[117] D. Zhang, Z. Bi, B. Li, Design and kinetostatic analysis of a new parallel manipulator, Robotics and Computer-Integrated Manufacturing, Vol. 25, Issues 4, 2009, pp. 782-791.

[118] D. Zhang, Kinetostatic analysis and optimization of parallel and hybrid architectures for machine tools, Doctoral Thesis, Laval University, 2000.

[119] R. Stamper, L. Tsai, G. Walsh, Optimization of a three DOF translational platform for well-conditioned workspace, Proceedings of IEEE International Conference on Robotics and Automation, 1997, pp. 3250-3255.

[120] D. Zhang, Global stiffness optimization of parallel robots using kinetostatic performance indices, In Robot Manipulators Trends and Development, ISBN: 978-953-307-073-5, 2010, pp. 125-138.

[121] L. Tsai, Robot analysis: the mechanics of serial and parallel manipulators, John Wiley and Sons, Inc., 1999.

[122] T. Leinonen, Terminology for the theory of machines and mechanisms, Mechanism and Machine Theory, Vol. 26, No. 5, 1991, pp. 435-539.

[123] A. Dollar, R. Howe. Design and evaluation of a robust compliant grasper using shape deposition manufacturing. Proceedings of ASME International Mechanical Engineering Congress and Exposition, USA, 2005. 74(2). DOI: 10.1115/IMECE2005-79791.

[124] A. Dollar, R. Howe. Towards grasping in unstructured environments: grasper compliance and configuration optimization. Advanced Robotics, Vol. 19, No. 5, 2005, pp. 523–543.

[125] G. Kragten. Under-actuated hands fundamentals, performance analysis and design. Doctoral Thesis, Delft University of Technology, 2011.

[126] R. Stavenuiter. Design of an under-actuated grasper with adjustable compliance. Master Thesis, Delft University of Technology, 2013.

[127] A. Remirez, R. Lathrop, P. Russell, R. Webster, Design of a stiff steerable grasper for sinus surgery. Proceedings of the 2014 Design of Medical Devices Conference, USA, 2014, pp. 1-2.

[128] H. Hanley, M. Rosario, Y. Chen, Design and testing of a three fingered flexural laparoscopic grasper. Proceedings of the 2011 Design of Medical Devices Conference, USA, 2011, pp. 1-9.

[129] R. Deshmukh, N. Mhala. Development of prototype laparoscopic grasper with haptic feedback. International Journal of Innovative Research in Advanced Engineering Vol. 1 Issue 5, 2014, pp. 175-178.

[130] D. Zhang, B. Wei, Design of a dynamic balanced spatial grasper mechanism. Proceedings of 27th Chinese Control and Decision Conference, Qingdao, China, 2015, pp. 4321-4324.

[131] C. Cao, N. Hovakimyan, Design and analysis of a novel L1 adaptive control architecture with guaranteed transient performance, IEEE Transactions on Automatic Control, Vol. 53, No. 2, 2008, pp. 586-591.

[132] P. Jain, M.J. Nigam. Design of a model reference adaptive controller using modified MIT rule for a second order system. Advance in Electronic and Electric Engineering, Vol. 3, No. 4, 2013, pp. 477-484.

[133] N. Nguyen, K. Krishnakumar, J. Boskovic. An optimal control modification to model reference adaptive control for fast adaptation. AIAA Guidance, Navigation and Control Conference and Exhibit, Honolulu, Hawaii, 2008, pp. 1-19.

[134] M. Idan, M. Johnson, A. Calise, A hierarchical approach to adaptive control for improved flight safety, AIAA Journal of Guidance, Control and Dynamics, Vol. 25, No. 6, 2002, pp. 1012-1020.

[135] J. Craig, Introduction to robotics: mechanics and control, 3rd ed., Pearson/Prentice Hall, 2005.

[136] Y. Landau, Adaptive control: the model reference approach, Marcel Dekker, New York, 1979.

Appendix A - Technical Specifications of the Motor and Motor Driver

Gear Motor

Dimensions

Size	37D x 64L mm
Weight	210g
Shaft diameter	6mm

General specifications

Gear ratio	19:1
Free-run speed @ 6V	256 rpm[1]
Free-run current @ 6V	250 mA[1]
Stall current @ 6V	2500 mA[1]
Stall torque @ 6V	42 oz·in[1]
Free-run speed @ 12V	500 rpm
Free-run current @ 12V	300 mA
Stall current @ 12V	5000 mA
Stall torque @ 12V	84 oz·in
Lead length	11 in

Motor Driver

Mounting hole configuration	1.5x2.0"
Size	2.3" x 3" x .7" (59mm x 75mm x 17mm)
Weight	2.2oz
Input voltage	6V-24V
Output current	12A/ch
Peak output current	25A/ch
Operating modes	Analog, R/C, Serial

Notes:
1: This motor will run at 6 V but is intended for operation at 12 V.

Appendix B - Publication List

Journal Publications

[J1] Dan Zhang, **Bin Wei** (2016). Convergence Performance Comparisons of PID, MRAC and PID-MRAC Hybrid Controllers. Frontiers of Mechanical Engineering. (Accepted)

[J2] Dan Zhang, **Bin Wei** (2015). Payload variation compensation for robotic arms through model reference control approach. International Journal of Robotics and Automation. 2015. (In Press)

[J3] Dan Zhang, **Bin Wei** (2015). Design and analysis of a collision detector for hybrid robotic machine tools. Sensors & Transducers Journal, Vol. 193, Issue10, 2015, pp. 67-73.

[J4] Dan Zhang, **Bin Wei** (2014). Design, kinematic and dynamic modeling of a novel tripod based manipulator. Robotica. DOI: 10.1017/S0263574714002835, January 2015, pp. 1-19.

[J5] **Bin Wei**, Dan Zhang (2014). Critical review on complete dynamic balancing of mechanisms and parallel robots. International Journal of Mechanisms and Robotic Systems. Vol.2, No.2, 2015, pp.122-143.

[J6] Q. Liang, W. Wu, Dan Zhang, **Bin Wei**, W. Sun, Y. Wang, Y. Ge (2015). Design and Analysis of a Micromechanical Three-Component Force Sensor for Characterizing and Quantifying Surface Roughness. Measurement Science Review, Volume 15, Issue 5, 2015, pp. 248-255.

[J7] G. Cui, **Bin Wei** (2013), Stiffness, workspace analysis and optimization for 3UPU parallel robot mechanism, *TELKOMNIKA Indonesian Journal of Electrical Engineering,* Volume 11, No 9. pp. 5253-5261.

[J8] G. Cui, **Bin Wei** (2013), Multi-objective optimization for 4UPS-PU mechanism considering compliance of the passive leg, *Advances in Information Sciences and Service Sciences*, Volume 5, No. 8, pp. 103-110.

[J9] **Bin Wei** (2013), Compliance analysis, optimization and comparison for a new 3PUS-PU mechanism, *International Journal of Automotive and Mechanical Engineering*. Volume 7, pp. 924-939.

[J10] **Bin Wei** (2013), Stiffness performance analysis and optimization of 3-DOF parallel manipulators based on kinetostatic model, *World Journal of Engineering*, Vol. 10, Number 1, pp. 85-94.

[J11] **Bin Wei** (2012), Stiffness, workspace and dynamic performance analysis of 4UPS-PU mechanism, *Rakenteiden Mekaniikka (Journal of Structural Mechanics),* Vol. 45, No 4, pp. 213-227.

[J12] **Bin Wei**, G. Cui(2012), The stiffness analysis of 4UPS-PU parallel mechanism based on conservative congruence transformation model, *Machine Design and Research*, Vol. 28, No. 6, pp. 33-36.

[J13] Y. Zhang, **Bin Wei**(2012), Local stiffness and dexterity analysis of a 3-SPS-S orientation fine-tuning manipulator for segment assembly robots in shield tunneling machines, *Applied Mechanics and Materials Vols*. 128-129, pp. 904-908.

[J14] Y. Zhang, **Bin Wei**(2012), Kinematic performance analysis of 3SPS-S spatial rotation parallel mechanism, *Transactions of the Chinese Society for Agricultural Machinery*, 43(4):212-215.

Conference Publications

[C1] Dan Zhang, **Bin Wei** (2016). Discussion and Analysis of Main Dynamic balancing Methods for Robotic Manipulators. *Proceedings of the ASME 2016 International Design Engineering Technical Conferences & Computers and Information in Engineering Conference (ASME* IDETC/CIE 2016), August 21-24, 2016, Charlotte, North Carolina, USA. (Accepted)

[C2] Dan Zhang, **Bin Wei** (2016). Synthesis Design and Analysis of a Hybrid Controller for Robotic Arms. *Proceedings of the ASME 2016 International Design Engineering Technical Conferences & Computers and Information in Engineering Conference (ASME* IDETC/CIE 2016), August 21-24, 2016, Charlotte, North Carolina, USA. (Accepted)

[C3] Dan Zhang, **Bin Wei** (2016). Analysis and a Case Study of Model Reference Adaptive Control for Robotic Mechanisms. *Proceedings of the ASME 2016 International Design Engineering Technical Conferences & Computers and Information in Engineering Conference (ASME* IDETC/CIE 2016), August 21-24, 2016, Charlotte, North Carolina, USA. (Accepted)

[C4] Dan Zhang, **Bin Wei** (2016). Design of a Joint Control System for Serial Mechanical Arms Based on PID and MRAC Control, *2016 IEEE Asia-Pacific Conference on Intelligent Robot Systems (ACIRS 2016)*, July 20-24, 2016, Tokyo, Japan. (Accepted)

[C5] Dan Zhang, **Bin Wei** (2016). Analysis and Comparative Study of Reference Based Adaptive Control System for Serial Mechanisms. *2016 2nd International Conference on Control Science and Systems Engineering (ICCSSE 2016),* July 27-29, 2016, Singapore. (Accepted)

[C6] Dan Zhang, **Bin Wei** (2016). Study on Payload Effects on the Joint Motion Accuracy of Serial Mechanical Mechanisms. *2016 3rd International Conference on Mechanics and Mechatronics Research (ICMMR 2016)*, June 15-17, 2016, Chongqing, China. (Accepted)

[C7] Dan Zhang, **Bin Wei** (2016). New Reactionless Spatial Grasper Design and Analysis. *2016 2nd International Conference on Mechatronics and Robotics Engineering (ICMRE 2016)*, February 18-22, 2016, Nice, France. (In press)

[C8] Dan Zhang, **Bin Wei** (2016). Stiffness Analysis and Optimization for a Bio-Inspired 3-DOF Hybrid Manipulator. *2016 2nd International Conference on Mechatronics and Robotics Engineering (ICMRE 2016)*, February 18-22, 2016, Nice, France. (In press)

[C9] Dan Zhang, **Bin Wei** (2016). Critical Review and Progress of Adaptive Controller Design for Robot Arms. *2016 2nd International Conference on Mechatronics and Robotics Engineering (ICMRE 2016)*, February 18-22, 2016, Nice, France. (In press)

[C10] Dan Zhang, **Bin Wei**, Marc A. Rosen (2016). Overview of an Engineering Teaching Module on Robotics Safety. *2016 2nd International Conference on Mechatronics and Robotics Engineering (ICMRE 2016)*, February 18-22, 2016, Nice, France. (In press)

[C11] Dan Zhang, **Bin Wei** (2015). Discussion on model reference adaptive control of robotic manipulators. *International Conference on Innovative Design and Manufacturing (ICIDM 2016)*, January 24-26, 2016, Auckland, New Zealand. (In press)

[C12] Dan Zhang, **Bin Wei** (2015). Dynamic Balancing of Parallel manipulators through Reconfiguration. *ASME 2015 Dynamic Systems and Control (DSC) Conference,* October 28-30, Columbus, Ohio, USA, doi:10.1115/DSCC2015-9669, pp. V003T43A001-9.

[C13] Dan Zhang, **Bin Wei** (2015). Advances and Issues on Dynamic Balancing of Parallel Mechanisms. *Proceedings of 2015 IEEE International Conference on Mechatronics and Automation (ICMA2015)* Beijing, China, August 2-5, 2015. pp. 1548-1554.

[C14] Dan Zhang, **Bin Wei** (2014), Design and optimization of a Tripod-based hybrid manipulator, *ROMANSY-2014,XX CISM-IFToMM SYMPOSIUM on Theory and Practice of Robots and Manipulators*, Advances on Theory and Practice of Robots and Manipulators, Mechanisms and Machine Science 22, pp. 83-91.

[C15] Dan Zhang, **Bin Wei** (2014), Single and multi-objective optimization issues and analysis of a 3UPU parallel manipulator, *Proceedings of the ASME 2014 International Design Engineering Technical Conferences & Computers and Information in Engineering Conference*, August, 2014, Buffalo, USA. doi:10.1115/DETC2014-34320, pp. 1-9.

[C16] Dan Zhang, **Bin Wei** (2014). Comparison and verification of several stiffness models for a family of parallel manipulators, *Proceedings of the International Conference of Control, Dynamic Systems, and Robotics*, Ottawa, Canada, May 15-16. Paper No. 73, pp. 1-9.

[C17] Dan Zhang, **Bin Wei** (2014). Comparison between Differential Evolution and Particle Swarm Optimization Algorithms. *Proceedings of 2014 IEEE International Conference on Mechatronics and Automation (IEEE ICMA 2014)*, August 3-6, Tianjin, China. DOI: 10.1109/ICMA, pp. 239-244.

[C18] Dan Zhang, **Bin Wei** (2014), Global stiffness and well-conditioned workspace optimization analysis of 3UPU-UPU robot based on Pareto Front theory, *The 12th International Conference on Cooperative Design, Visualization and Engineering(CDVE2015)*, Sept. 20-23, 2015, Spain. Volume 9320 of the series Lecture Notes in Computer Science, pp 124-133.

[C19] Dan Zhang, **Bin Wei** (2014). Design, analysis and modelling of a capacitive-based collision detector for 3-dof hybrid robotic manipulator. *SENSORDEVICES 2015, the*

Sixth International Conference on Sensor Device Technologies and Applications, pp. 31-36, August 23 - 28, 2015 - Venice, Italy.

[C20] Dan Zhang, **Bin Wei** (2014). Kinematic Analysis and Optimization for 4PUS-RPU Parallel Mechanism. *2015 IEEE/ASME International Conference on Advanced Intelligent Mechatronics* (AIM 2015), July 7-11, 2015, Busan, Korea, pp. 330-335, doi: 10.1109/AIM.2015.7222553.

[C21] Dan Zhang, **Bin Wei** (2014). Force Balance of Mechanisms and Parallel Robots through Reconfiguration Method. *3rd IEEE/IFToMM International Conference on Reconfigurable Mechanisms and Robots*, July 2015, Beijing, China. Volume 36 of the series Mechanisms and Machine Science, pp 351-361.

[C22] Dan Zhang, **Bin Wei** (2014). Design of a Dynamic Balanced Spatial Grasper Mechanism. *The 27th Chinese Control and Decision Conference*, Qingdao, China. May, 2015, pp. 4321-4324.

[C23] Dan Zhang, **Bin Wei** (2014). Critical Review on Complete Dynamic Balancing of Mechanisms. The Fourteenth International Federation for the Promotion of Mechanism and Machine Science World Congress (2015 IFToMM World Congress), October, 2015, Taipei, Taiwan. DOI Number: 10.6567/IFToMM.14TH.WC.OPS10.001.

[C24] Dan Zhang, **Bin Wei** (2015). Research on Basic Theory and Key Technology of Marmot-like Robotics for Mine Safety Detection and Rescuing. 7th International Conference on Mining Science and Technology, Xuzhou, China, April 26-29, 2015.

[C25] Dan Zhang, **Bin Wei** (2014). Dynamic Balancing through Reconfiguration Approach for Green Manufacturing System. Tongji University Workshop, 2014.

[C26] Z. Sun, **Bin Wei**(2011), Loading Capacity Analysis of a 3-SPS-S Mechanism for Segment Assembly Robots in Shield Tunneling Machines, *Proceedings of the 2011 International Conference on Advances in Construction Machinery and Vehicle Engineering*, Shanghai, China, pp.99-101.

Book chapter:

Dan Zhang, **Bin Wei**. Chapter 1 - Review of Recent Advances on Reactionless Mechanisms and Parallel Robots, in book "D. Zhang, B. Wei (eds.), Dynamic Balancing of Mechanisms and Synthesizing of Parallel Robots", DOI 10.1007/978-3-319-17683-3, Springer International Publishing Switzerland 2015.

Books

[B1] Dan Zhang, **Bin Wei** (2015) Dynamic Balancing of Mechanisms and Synthesizing of Parallel Robots, Springer, New York, N.Y. Springer International Publishing, eBook ISBN

978-3-319-17683-3, Hardcover ISBN 978-3-319-17682-6. DOI 10.1007/978-3-319-17683-3.
[B2] Dan Zhang, **Bin Wei** (2016) Advanced Mechatronics and MEMS Devices II, Springer, Springer International Publishing, eBook ISBN 978-3-319-32180-6, Hardcover ISBN 978-3-319-32178-3, DOI 10.1007/978-3-319-32180-6.
[B3] Dan Zhang, **Bin Wei** (2016) Mechatronics and Robotics Engineering for Advanced and Intelligent Manufacturing, Springer International Publishing, eBook ISBN 978-3-319-33581-0, Hardcover ISBN 978-3-319-33580-3.
[B4] Dan Zhang, **Bin Wei** (2016) Adaptive Control for Robotic Manipulators, CRC Press, Taylor & Francis Group, ISBN 9781498764872. (In press)

Appendix C - Copyright Permission Letters

Copyright Permission Letter

April 27, 2016

Dear Marta,

I am preparing my PhD thesis for submission to the Office of Graduate Studies at the University of Ontario Institute of Technology (UOIT) in Oshawa, Ontario, Canada. I am seeking your permission to include a manuscript version of the following papers in the thesis:

1. Dan Zhang, Bin Wei. "Review of Recent Advances on Reactionless Mechanisms and Parallel Robots", in book D. Zhang, B. Wei (eds.), Dynamic Balancing of Mechanisms and Synthesizing of Parallel Robots, DOI 10.1007/978-3-319-17683-3_1, Springer International Publishing, pp 1-19.

2. Dan Zhang, Bin Wei. "Force Balance of Mechanisms and Parallel Robots Through Reconfiguration Method", in book X. Ding, X. Kong, J. Dai (eds.), Advances in Reconfigurable Mechanisms and Robots II, Mechanisms and Machine Science, Volume 36, 2016, DOI 10.1007/978-3-319-23327-7, Springer International Publishing, pp. 351-361.

Canadian graduate theses are reproduced by the Library and Archives of Canada (formerly National Library of Canada) through a non-exclusive, world-wide license to reproduce, loan, distribute, or sell theses. I am also seeking your permission for the material described above to be reproduced and distributed by the LAC(NLC). Further details about the LAC(NLC) thesis program are available on the LAC(NLC) website (www.nlc-bnc.ca).

Full publication details and a copy of this permission letter will be included in the thesis.

Yours sincerely,
Bin Wei

Permission is granted for:
a) the inclusion of the material described above in your thesis.
b) for the material described above to be included in the copy of your thesis that is sent to the Library and Archives of Canada (formerly National Library of Canada) for reproduction and distribution.

Name: Marta Moldvai Title: Editor

Signature: Marta Moldvai [redacted] Date: 5/3/2016

Copyright Permission Letter

April 27, 2016

To whom it may concern,

I am preparing my PhD thesis entitled "Performance Improvement for Robotic Mechanisms by: Synthesis Design, Dynamic Balancing and Adaptive Control Techniques" for submission to the Office of Graduate Studies at the University of Ontario Institute of Technology (UOIT) in Oshawa, Ontario, Canada. I am seeking your permission to include a manuscript version of the following paper in the thesis:

Dan Zhang, Bin Wei. "Dynamic Balancing of Parallel Manipulators Through Reconfiguration", ASME 2015 Dynamic Systems and Control Conference, Columbus, Ohio, USA, October 28–30, 2015, Volume 3, Paper No. DSCC2015-9669, pp. V003T43A001; 9 pages, doi:10.1115/DSCC2015-9669.

Canadian graduate theses are reproduced by the Library and Archives of Canada (formerly National Library of Canada) through a non-exclusive, world-wide license to reproduce, loan, distribute, or sell theses. I am also seeking your permission for the material described above to be reproduced and distributed by the LAC(NLC). Further details about the LAC(NLC) thesis program are available on the LAC(NLC) website (www.nlc-bnc.ca).

Full publication details and a copy of this permission letter will be included in the thesis.

Yours sincerely,
Bin Wei

Permission is granted for:

a) the inclusion of the material described above in your thesis.
b) for the material described above to be included in the copy of your thesis that is sent to the Library and Archives of Canada (formerly National Library of Canada) for reproduction and distribution.

Name: _____ Title: _____

Signature: _____ Date: _____

From: Beth Darchi [mailto:DarchiB@asme.org]
Sent: Monday, May 9, 2016 12:01 PM
To: Bin Wei <Bin.Wei@uoit.ca>
Subject: RE: Copyright permission request

Dear Mr. Wei:

It is our pleasure to grant you permission to use **all or any part of the ASME** paper "Dynamic Balancing of Parallel Manipulators Through Reconfiguration," by Dan Zhang and Bin Wei, Paper No. DSCC2015-9669, cited in your letter for inclusion in a PhD thesis to include a manuscript version of the following paper to be published by Office of Graduate Studies at the University of Ontario Institute of Technology (UOIT).

Permission is granted for the specific use as stated herein and does not permit further use of the materials without proper authorization. Proper attribution must be made to the author(s) of the materials. **Please note**: if any or all of the figures and/or Tables are of another source, permission should be granted from that outside source or include the reference of the original source. ASME does not grant permission for outside source material that may be referenced in the ASME works.

As is customary, we request that you ensure full acknowledgment of this material, the author(s), source and ASME as original publisher. Acknowledgment must be retained on all pages printed and distributed.

Many thanks for your interest in ASME publications.

Sincerely,

Beth Darchi
Publishing Administrator
ASME
2 Park Avenue, 6th Floor
New York, NY 10016-5990
Tel 1.212.591.7700
darchib@asme.org